Neutrino Physics and Flavor Symmetries: some studies in view of nonzero θ_{13}

Biswajit Karmakar

A thesis
submitted for the degree of
Doctor of Philosophy

Supervisor:
Dr. Arunansu Sil

Department of Physics
Indian Institute of Technology Guwahati
Guwahati 781039, India

June 2017

Declaration

The work in this thesis is based on research carried out at the Department of Physics, Indian Institute of Technology Guwahati, India under the supervision of Dr. Arunansu Sil. No part of this thesis has been submitted elsewhere for award of any other degree or qualification. Works presented in the thesis are entirely my own unless referenced to the contrary in the text.

Signed:

Date:

Certificate

Dr. Arunansu Sil
Associate Professor
Department of Physics, IIT Guwahati
Email: asil@iitg.ernet.in

It is certified that the work contained in the thesis entitled **"Neutrino Physics and Flavor Symmetries: some studies in view of nonzero θ_{13}"** by Mr. Biswajit Karmakar, a PhD student of the Department of Physics, IIT Guwahati was carried out under my supervision and has not been submitted elsewhere for award of any degree.

Dr. Arunansu Sil

Acknowledgements

I am deeply thankful to my supervisor Dr. Arunansu Sil for his constant guidance and involvement throughout this Ph.D. work. His positive energy always motivated me in my research. He always welcomed me whenever I knocked his door for a discussion. I learnt various aspects of high energy physics from these discussions. His politeness and friendly behavior helped me a lot to interact with him. I am really privileged to work with him and once again express my gratitude to him.

I would also like to take this opportunity to thank doctoral committee members Prof. Poulose Poulose, Dr. Bipul Bhuyan and Dr. Dipankar Bandyopadhyay for reviewing my progress and for giving me valuable comments and suggestions. I specially thank my collaborators Dr. Subhaditya Bhattacharya and Dr. Narendra Sahu for their support and valuable suggestion. I also thank all the high energy faculty member, Dr. Debasish Borah, Dr. Sayan Chakrabarti, Dr. Sovon Chakraborty, Dr. Meduri C Kumar, Dr. Debaprasad Maity, Dr. Bibhas Ranjan Majhi, Dr. Soumitra Nandi and Dr. Udit Raha at IIT Guwahati for useful discussions and introducing me to various new topics in the journal club meetings. I also thank Prof. S. F. King for the opportunity to visit University of Southampton and fruitful discussions. I thank Basab Bijoy Purkayastha for helping me on issues related to linux systems. I also thank all the anonymous peer reviewers for helping me with their critical thoughts which improved the quality of my publications.

I thank Dr. Vindhyawasini Prasad, Dr. Satendra Kumar Dr. Deepanwita Dutta for helping me to understand particle physics in my early days of Ph.D. It is my pleasure to thank my colleague Abhijit Saha for our endless interaction on physics as well as non-physics stuff. I also thank Sujay Shil, Rishav Roshan and Amit Dutta Banik for various discussions. I thank Shibananda Sahoo again for discussion on many topics.

During my Ph.D. tenure I also got several friends. I thank all of them for being there during my ups and downs. I thank Ramesh, who was my local guardian at Guwahati and waste his precious time on me! Anabil (and Anupama) was always there to cheer me up. I also thank my good old friend Sudin for his wisdom. I thank KC for always being there for no reason. I thank Sunando da, Ashmita di, Krishnanjan, Srimoy and Basubendu for our talks on anything. I thank Asish, Sourav, Kallol, Ramiz for making fun of me and tolerating my bad jokes. I also Tapas and Bappa da. We sat next-to each other in our office and shared lots of thoughts. I thank my batch-mates Himansgu Obaidulla, Partha, Bhagaban, Upendra and I remember our political discussions. I also thank my colleagues Arindam da, Soumenda, Supriyada, Souvik Da, Noor, Purusottam, Sayan, Subhasish, Biswaranjan, Deepanjali, Kamal, Nitin for their help. I also thank Monojit, Sabyasachi and Dipankar. We became very good friends and attended several schools and conferences together. I thank my old friends Tamal, Somen, Sandip, Biplob, Rajib, Uttam, Mrinmayee for being there.

Last but not the least, I am extremely grateful to my parents Mr. Bhabendra Nath Karmakar and Mrs. Ashtami Karmakar and my brother Prosenjit for their love, support and encouragement throughout my career. I also thank Maya Mashi and didi (my grand mother) loving me throughout my life.

Abstract

In this thesis we explore the possibility of explaining neutrino masses and mixing from discrete, non-Abelian flavor symmetric scenarios and study their impacts in several aspects involving particle physics and cosmology. To elucidate the recent observation on reactor mixing angle θ_{13} by several experiments like Daya Bay, RENO, Double Chooz and T2K, we exploit A_4 flavor symmetry based models. We show that a minimal modification is sufficient to deviate from the widely popular tribimaximal mixing in the lepton sector to generate nonzero θ_{13} of observed amount and hence we study its several phenomenological consequences. In this regard, we have studied two models based on A_4 flavor symmetric type-I and type-I+II seesaw. Here we minimally modify the existing Altarelli-Feruglio A_4 model by incorporating a scalar singlet, transforming non-trivially under A_4. This contributes in the neutrino mass matrices to deviate it from its tribimaximal configuration, ensuring generation of nonzero θ_{13}. Here we also make predictions for absolute neutrinos masses, effective mass parameter appearing in the neutrinoless double beta decay, Dirac and/or Majorana phases. We also obtain interesting sum rules for neutrino masses. Furthermore, we successfully reproduce observed lepton asymmetry of the universe in such scenarios due to the presence of heavy right handed neutrinos and scalar triplet in the theory. We study the role of nonzero θ_{13} and flavor structures of the Yukawa couplings on leptogenesis. In the type-I+II seesaw we show that complex vev of a scalar field responsible for generating nonzero θ_{13} can correlate all the CP phases (Dirac and Majorana) involved in the theory. Next, we study an A_4 based inverse seesaw scenario and find that a typical flavor structure of the small lepton number violating term responsible in explaining neutrino mass can completely dictate lepton mixing. Due to the mixing between light and heavy neutrino states in the framework, we have also studied the non-unitarity effects which contribute to lepton flavor violating processes, neutrinoless double beta decay etc. Finally to establish a connection between two seemingly uncorrelated sector (Standard Model and dark matter sector), we extend the flavor symmetry to the dark matter sector as well. Here we find that a global $U(1)$ flavor symmetry establishes a correlation between the relic abundance of dark matter and nonzero θ_{13} which can be probed at various ongoing and future direct and collider search experiments.


भारतीय प्रौद्योगिकी संस्थान गुवाहाटी
Indian Institute of Technology Guwahati

List of Publications Included in the Thesis:

1. **B. Karmakar** and A. Sil, *"Nonzero θ_{13} and leptogenesis in a type-I seesaw model with A_4 symmetry"*, Phys. Rev. D **91**, 013004 (2015) [arXiv:1407.5826 [hep-ph]].
2. **B. Karmakar** and A. Sil, *"Spontaneous CP violation in lepton-sector: A common origin for θ_{13}, the Dirac CP phase, and leptogenesis"*, Phys. Rev. D **93**, no. 1, 013006 (2016) [arXiv:1509.07090 [hep-ph]].
3. S. Bhattacharya, **B. Karmakar**, N. Sahu and A. Sil, *"Unifying the flavor origin of dark matter with leptonic nonzero θ_{13}"*, Phys. Rev. D **93**, no. 11, 115041 (2016) [arXiv:1603.04776 [hep-ph]].
4. **B. Karmakar** and A. Sil, *"An A_4 realization of inverse seesaw: neutrino masses, θ_{13} and leptonic non-unitarity"*, Preprint - arXiv:1610.01909 [hep-ph] .
5. S. Bhattacharya, **B. Karmakar**, N. Sahu and A. Sil, *"Flavor origin of dark matter and its relation with leptonic nonzero θ_{13} and Dirac CP phase δ"*, JHEP **1705**, 068 (2017), [arXiv:1611.07419 [hep-ph]].

Contents

List of Figures

List of Tables

Chapter 1

Introduction

Understanding the laws of nature has always been a major endeavor of human civilization. In this process, practice of science enables us to dig into the very minute details of the universe both at microscopic and macroscopic levels. Modern science is constantly evolving, with incredible development from both theoretical and experimental point of view. Over the years we have achieved several breakthroughs in understanding our universe but still there are several puzzles to be understood. In theoretical and phenomenological scientific community we take it as a challenge and try to answer these questions in a mathematically aesthetic way. Hence the purpose of constructing a successful theory is such that it can explain the observed phenomenon or have predictions which can be tested by the future experiments.

In this regards particle physics made lot of progress in the last century. We now know that the universe is made up of few fundamental particles governed by four fundamental forces namely gravitational, electromagnetic, strong and weak forces. The Standard Model (SM) of particle physics, proposed and developed in 70s, stands as the most profound theory of elementary particles and their interactions, excluding gravity. It is an extremely successful theory in terms of its predictability and excellent agreement with experiments. For example, the existence of W, Z, Higgs bosons and top quark were postulated much earlier before their actual observation at the experiments. Recently on 4^{th} July 2012, both ATLAS [1] and CMS [2] collaborations at LHC (through independent analysis) simultaneously announced the discovery of a new Higgs boson like particle compatible with SM, finding out the last missing piece of SM. Along with these, we also find that the prediction for anomalous magnetic moment of electron precisely matches with experimental observation.

Thus SM turns out to be a well established theory of elementary particles. However despite of having tremendous success it is not the complete theory of the nature due to its incapability in explaining various observed phenomena. For example, the immediate consequence of observation of neutrino oscillation is that they have tiny nonzero mass. Hence SM needs to be extended in order to accommodate massive neutrinos. Solution to the hierarchy problem still remains an open problem of SM. On the other side, cosmology is the branch of science where we study the universe as a whole. So far the simplest model, which explains several cosmological observations, is known as ΛCDM (Λ-Cold Dark Matter) model. However within the framework of SM, some of the essential elements of ΛCDM model can not be explained. These are mainly related to existence of dark matter and observed matter-antimatter asymmetry of the Universe. Therefore it is extremely important to address the issues related to SM and particle cosmology on same footing and look for a common framework to answer them simultaneously. To achieve this, neutrinos can play an important role. Neutrinos are part of SM lepton family. These particles are electrically neutral and interact very weakly with matter making them the most elusive particle of SM. Neutrinos are one of the most abundant particle of the universe and reaches to the surface of earth from various celestial source having a wide spectrum of energy and intensity. The natural sources for neutrinos are - solar neutrinos, cosmic background neutrinos, supernovae neutrinos and atmospheric neutrinos etc., whereas the artificial or man made source of neutrinos include accelerators neutrinos, reactors etc.

Therefore along with neutrino mass these cosmological puzzles (matter-antimatter asymmetry, dark matter etc.) also demand an urgent extension of the SM. For last thirty years, lot of efforts have been given to address these issues in various beyond the SM (BSM) scenarios. This thesis is also devoted in this direction keeping the lepton sector of the SM in the center stage, to study neutrino masses, mixing and CP violation in various BSM scenarios and extending its regime into the dark matter sector. Hereafter analyzing various phenomenological issues related with neutrino physics we try to establish some connections between neutrinos and above mentioned cosmological aspects. We also look for the possibility of involving additional symmetries (in addition to the SM gauge symmetry) which might play a crucial role in understanding the connection between particle physics and cosmology.

In the history of neutrinos, it was believed that these are massless spin half particles, making them sharply different from other spin half fermions. Neutrino experiments around the globe (Super-Kamionade, LSND, MINOS, SNO, K2K, KamLAND [3] etc.) have confirmed that neutrinos oscillate among different flavors. Neutrino oscillation is basically manifestation of mixing between their flavor and mass eigenstates. It is observed that the flavor mixing in quarks and that in leptons are very different. In standard parametrization [4], the lepton mixing matrix contains three mixing angles namely $\theta_{12}, \theta_{23}, \theta_{13}$ and one CP violating Dirac Phase δ (two additional Majorana will be there if neutrinos are Majorana particle). The magnitude of the corresponding mixing angles in quark sector are $\theta^q_{12} \approx 13^\circ, \theta^q_{23} \approx 2.5^\circ, \theta^q_{13} \approx 0.21^\circ$ [4], whereas these angles in the lepton sector are $\theta_{23} \approx 45^\circ, \theta_{12} \approx 35^\circ, \theta_{13} \approx 9^\circ$ [5]. Such difference in the pattern of quark and lepton mixing angles (along with their different types of mass hierarchies) is known as flavor puzzle. To understand this flavor puzzle it is essential to study physics behind generation of neutrino masses and mixing with great care. Up to 2012, neutrino oscillation data from various experiments suggested that: $\sin^2\theta_{12} \approx 1/3$, $\sin^2\theta_{23} \approx 1/2$. Such pattern of lepton mixing matrix with $\sin^2\theta_{13} = 0$ is known as tribimaximal mixing (TBM) [6] pattern. Such a neutrino mixing matrix can be elegantly explained by incorporating discrete flavor symmetries. Out of all the discrete groups studied in the literature, A_4 (discrete group of even permutations of four objects) turned out to be a special one which can reproduce this TBM pattern in a most economic way [7]. It is the smallest group having three dimensional representation which helps in accommodating three flavors of leptons and can explain the textures of fermion mass matrices. As stated before, observation on the mixing angle θ_{13} ($\simeq 8^\circ - 9^\circ$) rules out the existence of tribimaximal mixing in lepton sector and hence demands a modification of it. One of the main focus of this thesis is to construct a theory which can successfully accommodate observed value of nonzero θ_{13} from a discrete flavor symmetric point of view.

Now to explain tiny neutrino mass, seesaw mechanism [8] is perhaps the simplest way where heavy particles are incorporated in the theory. There are several variants of seesaw mechanism, namely, type-I, II, III, inverse seesaw mechanism etc. In type-I, II and III we include SM gauge singlet heavy right handed neutrinos, $SU(2)_L$ scalar and fermionic triplets respectively whereas in inverse seesaw one includes two sets of fermionic gauge singlets to realize lightness associated with neutrino mass. However the seesaw scenarios in general does not explain why the mixing angles should be of right order as observed in experiments. Therefore, seesaw mechanism embedded in flavor symmetries have potential to explain neutrino masses and mixing simultaneously. After breaking of electoweak and the flavor symmetry considered, one can obtain the relevant flavor structures of mass matrices and hence it can explain neutrino mixing in an elegant way. Prior to 2012 [9] (*i.e.* with $\theta_{13} = 0$), seesaw models with discrete flavored symmetries were developed to explain TBM mixing in the lepton sector. With clear evidence of nonzero θ_{13}, in this thesis we extend such models to explain observed θ_{13} and find some predictions or constraints on Dirac and/or Majorana CP phases, absolute neutrino masses and effective neutrino mass parameter appearing in neutrinoless double beta decay. Predictions of these quantities make the model feasible to test in the current and near future neutrino experiments. Moreover in low energy seesaw scenarios (e.g. inverse seesaw), due to reachable new physics scale it is also important to explore the role of neutrino flavor structure in leptonic non-unitarity effect (arising from mixing between heavy and light neutrino states) and lepton flavor violation.

As far as our present knowledge is concerned, just after the Big Bang, the universe started with equal amount of baryons and antibaryons. But the present observation suggests that there is a huge deficit of antibaryons over baryons, and the process which creates such asymmetry is termed as baryogenesis [10]. Interesting feature of the seesaw models is that, from the out of equilibrium decay of heavy particles (right handed neutrinos or scalar triplet) a lepton asymmetry can be produced (known as leptogenesis [11]). This lepton asymmetry then can also be converted into baryon asymmetry by SM sphaleron process explaining the matter-antimatter asymmetry of the Universe. Since we embed the seesaw framework is a flavor symmetric scenario that leads to the prediction of lepton mixing angles, Dirac and/or Majorna phases, it would be interesting to study whether there exists any impact on leptogenesis from flavor symmetry itself.

From several cosmological observation we know that around 26% content of the Universe is dark matter (DM) [12]. So far we have several evidences regarding the presence of DM in our universe, although the understanding of particle nature of DM is still missing. For example, we don't know how they interact with visible matter, what is its mass etc.. It is perhaps intriguing to investigate whether the new physics responsible for massive neutrinos can also have any role in describing the nature of DM. Along this line we extend the flavor (continuous) symmetry in DM sector as well and look for possible correlation with lepton sector in the light of nonzero θ_{13} and Dirac CP phase.

This thesis is organized in the following manner. In the remaining part of Chapter 1, after presenting a very brief overview on SM a discussion on physics of neutrino masses and mixing is provided. Then basic understanding of discrete flavor symmetry (particularly A_4) and matter-antimatter asymmetry is presented. Chapter 2 and 3 are devoted to elaborate on neutrino masses and mixing in an A_4 based type-I and general type-II seesaw respectively. With the involvement of nonzero θ_{13} successful generation of observed lepton asymmetry is also shown in both chapters. In an inverse seesaw scenario embedded with A_4 flavor symmetry, implication for leptonic non-unitarity effect and lepton flavor violation is explored in Chapter 4 along with the realization of neutrino masses and mixing. Chapter 5 deals with involvement of flavor symmetry in dark sector along with neutrino sector to draw a correlation between these two sectors. Finally we draw conclusion in Chapter 6 and some explicit calculations are presented in the Appendices.

1.1 The Standard Model of Particle Physics

Any discussion on particle physics will be incomplete without the knowledge of SM. It is a quantum field theory of fundamental interactions which accommodates the three fundamental forces of nature namely, strong, weak and electromagnetic forces. SM gauge theory is based upon the symmetry group $SU(3)_C \times SU(2)_L \times U(1)_Y$. The symmetry group $SU(3)_C$ is associated to the strong force and governs the interaction between particles having 'color' (denoted by the subscript C) charge (for quarks) with $SU(2)_L$ is related with the weak isospin and $U(1)_Y$ stands for the weak hypercharge, Y. The electoweak symmetry is broken down to $U(1)_{em}$. It results to three massive vector particles $W^{\pm}$ and Z while the gauge boson associated with the unbroken $U(1)_{em}$ is the massless photon. The photons are responsible for electromagnetic interactions and the $W^{\pm}, Z$ take part in weak interactions. There are eight gluons which mediate the strong interaction. Now the fermionic fields in the SM can be broadly classified into two categories: leptons and quarks. Here leptons are categorized into two types, charged leptons: electron (e), muon (μ), tau (τ) and neutrinos (the neutral ones): electron neutrino (ν_e), muon neutrino (ν_μ) and tau neutrino (ν_τ). All the charged lepton have same electric charge ($Q = -1$ for leptons, $Q = 1$ for anti-leptons) whereas neutrinos have zero electric charge ($Q = 0$). On the other hand there are three up-type quarks (with $Q = 2/3$, for up-type anti-quarks $Q = -2/3$):

up (u), charm (c) top (t) and three types of down-type quarks (with $Q = -1/3$, for down-type anti-quarks $Q = 1/3$): down (d), strange(s) and bottom (b). The left-handed and right-handed fermions belong to different representations of SM. Left-handed fermions are part of $SU(2)_L$ doublet, whereas right-handed fermions are $SU(2)_L$ singlets as shown in Table 1.1.

Generation	Leptons	Quarks
1st Generation	$\begin{pmatrix} \nu_e \\ e^- \end{pmatrix}_L$; e_R	$\begin{pmatrix} u \\ d \end{pmatrix}_L$; u_R, d_R
2nd Generation	$\begin{pmatrix} \nu_\mu \\ \mu^- \end{pmatrix}_L$; μ_R	$\begin{pmatrix} c \\ s \end{pmatrix}_L$; c_R, s_R
3rd Generation	$\begin{pmatrix} \nu_\tau \\ \tau^- \end{pmatrix}_L$; τ_R	$\begin{pmatrix} t \\ b \end{pmatrix}_L$; t_R, b_R

TABLE 1.1: Fermionic field content in Standard Model, Here the subscripts L, R stands for the left-handed and right-handed particles.

Breaking of electroweak symmetry down to $U(1)_{em}$ is taken place wihin SM in presence of a scalar field (Φ) which transforms as a doublet under $SU(2)_L$ carrying hypercharge $Y = 1$. Therefore the electoweak part of the SM Lagrangian invariant under $SU(2)_L \times U(1)_Y$ gauge symmetry is given by

$$\mathcal{L}_{\mathbf{I}} = \mathcal{L}_{\text{kin, gauge}} + \mathcal{L}_{\text{kin,matter}} \quad , \tag{1.1}$$

with

$$\begin{aligned} \mathcal{L}_{\text{kin, gauge}} &= -\frac{1}{4} W^a_{\mu\nu} W^{a\mu\nu} - \frac{1}{4} B_{\mu\nu} B^{\mu\nu}; && (1.2) \\ W^a_{\mu\nu} &= \partial_\mu W^a_\nu - \partial_\nu W^a_\mu + g\epsilon^{abc} W^b_\mu W^c_\nu, && (1.3) \\ B_{\mu\nu} &= \partial_\mu B_\nu - \partial_\nu B_\mu, && (1.4) \end{aligned}$$

and

$$\begin{aligned} \mathcal{L}_{\text{kin,matter}} &= \overline{\Psi}_L i\gamma^\mu D_\mu \Psi_L + \overline{\Psi}_R i\gamma^\mu (\partial_\mu + ig' \frac{Y}{2} B_\mu) \Psi_R; && (1.5) \\ D_\mu &= \partial_\mu + \frac{1}{2} ig\tau^a W^a_\mu + \frac{1}{2} ig' Y B_\mu, && (1.6) \end{aligned}$$

where $\mathcal{L}_{\text{kin, gauge}}$ indicates the normalized kinetic part of the Lagrangian involving the gauge fields ($W^{a=1,2,3}_\mu$ for $SU(2)_L$ and B_μ for the $U(1)_Y$ part) and $\mathcal{L}_{\text{kin,matter}}$ corresponds to the kinetic part of the Lagrangian involving fermionic fields. Here g, g' stands for

$SU(2)_L$ and $U(1)_Y$ gauge couplings respectively. Ψ_L and Ψ_R in Eq. (1.5) stands for fermionic left-handed and right-handed fields respectively. In SM, in order to break the electoweak symmetry spontaneously, the Higgs field $\Phi = (\phi^+, \phi^0)^T$ is incorporated. The part the SM Lagrangian, involving the Higgs field can be written as

$$\mathcal{L}_{\mathbf{II}} = \mathcal{L}_\Phi + \mathcal{L}_{\text{Yukawa}}, \tag{1.7}$$

where

$$\mathcal{L}_\Phi = (D_\mu \Phi)^\dagger (D^\mu \Phi) - V(\Phi) \quad \text{with} \quad V(\Phi) = \mu^2 \Phi^\dagger \Phi + \lambda (\Phi^\dagger \Phi)^2, \tag{1.8}$$

and the $\mathcal{L}_{\text{Yukawa}}$ will be stated below in a while. The scalar potential of the Higgs, $V(\Phi)$, is responsible for spontaneous symmetry breaking (SSM) of $SU(2)_L \times U(1)_Y \longrightarrow U(1)_{em}$. With the condition $\lambda > 0$ and $\mu^2 < 0$, the neutral component of the scalar field (ϕ^0) develops acquires a nonzero vacuum expectation value (vev), $v/\sqrt{2}$, and hence

$$\langle \Phi \rangle = \frac{1}{\sqrt{2}} \begin{pmatrix} 0 \\ v + h \end{pmatrix}, \tag{1.9}$$

with $v = \sqrt{-\mu^2/\lambda}$. Due to the spontaneous breaking of the electroweak symmetry, mixing occurs between the gauge fields and hence we identify the three massive gauge bosons states as $W^\pm$ (with mass $M_W = \frac{1}{2} g v$) and Z (having mass $M_Z = \frac{1}{2}\sqrt{g^2 + g'^2 v}$), while one remains massless to be identified as the photon. There remains a single neutral Higgs boson along with mass $(m_h^2 = 2v^2\lambda)$ as a remnant of Higgs mechanism.

Interestingly lepton and quark masses can also be generated using the same scalar field Φ by introducing Yukawa interaction as written in Eq. (1.7). The relevant Lagrangian is given by

$$\mathcal{L}_{\text{Yukawa}} = -y_{\ell_{ij}} \bar{L}_i \Phi e_{R_j} - y_{d_{ij}} \bar{Q_L}_i \Phi d_{R_j} - y_{u_{ij}} \bar{Q_L}_i \widetilde{\Phi} u_{R_j} + \text{h.c.}, \tag{1.10}$$

where $\widetilde{\Phi} = i\tau_2 \Phi^*$ and L, Q_L represent the left-handed lepton and quark doublets respectively, e_R, d_R and u_R stands fo the right handed charged leptons, down and up type quarks, and i, j are the generation indices. From this interaction, when Φ gets vev, masses for charged lepton, down and up type quarks can be obtained as $m_\ell = \frac{y_\ell v}{\sqrt{2}}$, $m_d = \frac{y_d v}{\sqrt{2}}$ and $m_u = \frac{y_u v}{\sqrt{2}}$. In Eq. (1.10), $y_{\ell_{ij}}, y_{d_{ij}}$ and $y_{u_{ij}}$ are the complex Yukawa couplings for the charged leptons down and up type quarks respectively. Note that the Yukawa coupling matrices are of 3 × 3 and SM does not provide any understanding about the individual entries or textures. So generally one can dagonalize the Yukawa complex coupling matrices associated with the quark mass matrices (m_d for down quarks and m_u for up quarks) using the transformations

$$u_{L_i} = V_{u_{ij}} u'_{L_j} \text{ and } d_{L_i} = V_{d_{ij}} d'_{L_j}, \tag{1.11}$$

$$u_{R_i} = W_{u_{ij}} u'_{R_j} \text{ and } d_{R_i} = W_{d_{ij}} d'_{R_j}. \tag{1.12}$$

Here u_{L_i}, d_{L_i} (u_{R_i}, d_{R_i}) and u'_{L_i}, d'_{L_i} (u'_{R_i}, d'_{R_i}) are the fields in the interaction and mass bases respectively. V_u $(W_{u_{ij}})$ and V_d $(W_{d_{ij}})$ are 3 × 3 unitary matrices. Hence after this, charged current interaction between quarks and the $W^\pm$ bosons (followed from first term of Eq. (1.5)) can be written as

$$-\frac{g}{\sqrt{2}}(\bar{u}_L, \bar{c}_L, \bar{t}_L)\gamma^\mu W^+_\mu \begin{pmatrix} d_L \\ s_L \\ b_L \end{pmatrix} = -\frac{g}{\sqrt{2}}(\bar{u}'_L, \bar{c}'_L, \bar{t}'_L)\gamma^\mu W^+_\mu (V_u^\dagger V_d) \begin{pmatrix} d'_L \\ s'_L \\ b'_L \end{pmatrix}, \tag{1.13}$$

where the matrix $V_u^\dagger V_d$ is known as the Cabibbo-Kobayashi-Maskawa (CKM) matrix [13, 14], V_{CKM}, representative of the quark mixing matrix. The matrix V_{CKM} can be parameterized in terms of three mixing angle and one CP phase as [15]

$$V_{\text{CKM}} = \begin{pmatrix} c_{12}c_{13} & s_{12}c_{13} & s_{13}e^{-i\delta} \\ -s_{12}c_{23} - c_{12}s_{13}s_{23}e^{i\delta} & c_{12}c_{23} - s_{12}s_{13}s_{23}e^{i\delta} & c_{13}s_{23} \\ s_{12}s_{23} - c_{12}s_{13}c_{23}e^{i\delta} & c_{12}s_{23} - s_{12}s_{13}c_{23}e^{i\delta} & c_{13}c_{23} \end{pmatrix}, \tag{1.14}$$

where $s_{ij} = \sin\theta_{ij}$, $c_{ij} = \cos\theta_{ij}$ are the mixing angels and δ is the CP violating phase.

1.2 Neutrinos in the Standard Model

As discussed in the previous section, in SM, masses for all fermions are generated after SSB through introduction of a Yukawa term (see Eq. (1.10)). In a gauge invariant way, this Yukawa term in general, is written as $-y\overline{\psi}_L\psi_R\phi^0$. Here ψ_L and ψ_R are the left-handed and right-handed fermion fields and y is the Yukawa coupling (complex in general). Once ϕ^0 gets vev, corresponding mass for the fermion ψ is obtained. Therefore presence of both of left and right handed components in SM is essential to write down a mass term. Now from the particle content of the SM given in Section 1.1, it is evident that right-handed partners for neutrinos are absent in SM. Therefore one cannot write a gauge invariant mass term and hence neutrinos turn out to be massless in SM.

Now, in absence of the right-handed neutrinos, the only possible Yukawa coupling allowed in the framework of SM, involving leptons and Higgs is given by the first term as in Eq. (1.10). The associated Yukawa coupling then can be diagonalized using the bi-unitary transformation

$$y_\ell = U_\ell y_\ell^{diag} V_\ell^\dagger, \tag{1.15}$$

where y_ℓ^{diag} is the diagonal Yukawa coupling. U_ℓ and V_ℓ are two 3×3 unitary matrices. Hence we can redefine the lepton fields as

$$\ell_L \longrightarrow U_\ell \ell_L, \quad \nu_L \longrightarrow U_\ell \nu_L, \quad e_R \longrightarrow V_\ell e_R, \tag{1.16}$$

where ℓ_L, ν_L and e_R are the left-handed charged leptons, left-handed neutrinos and right-handed singlet charged leptons respectively. As both components of the lepton doublet in the first term of Eq. (1.10) transforms in the same way, all these unitary rotation matrices (U_ℓ, V_ℓ) essentially not reflected in the letonic interactions written in Eq. (1.5). This indicates that for massless neutrinos any transformation that can be performed on the neutrino flavor eigenstates leaves the $V_{\rm CKM}$ analogous matrix for lepton sector as basically identity.

However in BSM scenario, where neutrinos are massive, gives rise to a phenomena known as neutrino mixing. In such scenarios the flavor eigenstates are not necessarily same as the mass eigenstates. Here the transformation between neutrino flavor and mass eigenstates can be written as $\nu_\alpha \to U_\nu \nu_i$. We discuss these issues in Section 1.5 elaborately. Therefore in case of massive neutrinos, following the same process as discussed in Section 1.1, the charged current interaction in the lepton sector can be written as

$$\begin{aligned} -\mathcal{L}_{\rm CC} &= \frac{g}{\sqrt{2}} \sum_\alpha \overline{\ell'}_{\alpha L} \gamma^\mu \nu_{\alpha L} W_\mu^- + h.c. \qquad (1.17) \\ &= \frac{g}{\sqrt{2}} \sum_{\alpha, i} \overline{\ell}_{\alpha L} \gamma^\mu \left(U_\ell^\dagger U_\nu\right)_{\alpha i} \nu_{iL} W_\mu^- + h.c., \qquad (1.18) \end{aligned}$$

where for the charged leptons primed and un-primed notation indicate the fields are in non-physical and physical (mass eigenstate) bases while for neutrinos the Latin indices (i,j) corresponds to mass basis. The unitary matrix

$$U = U_\ell^\dagger U_\nu, \tag{1.19}$$

is the CKM analogoue mixing matrix in the lepton sector and is called Pontecorvo-Maki-Nakagawa-Sakata (PMNS) [16] mixing matrix.

1.3 Evidences for Neutrino Mass

As discussed above, SM predicts neutrinos as massless particle. But over the years there are several compelling evidences and hints towards nonzero neutrino mass. Firstly, observation of neutrino oscillation (discussed in details in section 1.5) by several experiments around the globe demands that at-least some of the neutrinos have nonzero mass. In this phenomenon, neutrino flavor eigenstates ($\nu_{\alpha L} = \nu_{e,\mu,\tau}$) are considered to be the superposition of the mass eigenstates ($\nu_{iL} = \nu_{1,2,3}$) as $\nu_{\alpha L} = \sum_{i=1}^{3} U_{\alpha i}\nu_{iL}$, where the mixing matrix U is called the PMNS matrix [16] (elaborated in Section 1.5). Neutrino oscillation probabilities depend on the mass squared differences and mixing angles. Hence neutrino oscillation confirms that massive neutrinos do exit. Although, one can't conclusively comment on the absolute mass scale of neutrinos from the result of neutrino oscillation experiments.

On the other hand, the strongest bound on the absolute mass scale of the neutrinos comes from cosmological observation indicating that neutrinos might have played an important role in the course of evolution of early universe. Current cosmological observations such as the distribution of large scale structures or the cosmic microwave anisotropies can provide an upper bound on the sum of the absolute neutrinos masses. From the observation by Planck collaboration (with external Cosmic Microwave Background and Baryon Acoustic Oscillation data), this upper bound is given by [12]

$$\sum_i m_i \lesssim 0.23 \ \text{ eV}. \tag{1.20}$$

In addition to this, one can also probe the absolute neutrino mass scale through their kinematic effects in tritium β-decay. Few years ago the Mianz [17] and Troistk [18] group already put an upper bound on the absolute mass of electron neutrino as $m_{\bar{\nu}_e} < 2.3$ eV and $m_{\bar{\nu}_e} < 2.05$ eV (both at 90% CL) respectively. Ongoing Karlsruhe Tritium Neutrino (KATRIN) experiment [19] is expected to reach a better sensitivity to measure neutrino mass in the sub-eV range.

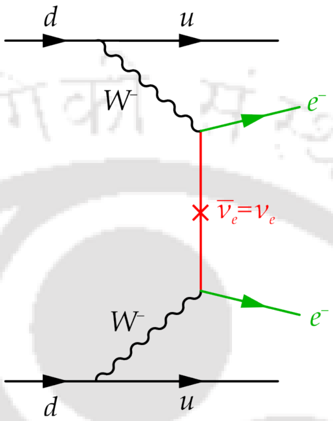

FIGURE 1.1: Feynman diagram for neutrinoless double beta decay [20].

Again, if neutrinos are considered to be Majorana particles (if they are their own anti-particles), then neutrino mass can be generated via a lepton number violating interaction (by two units, $|\Delta L| = 2$, see Section 1.4 for detailed discussion). This leads to a process known as neutrinoless double beta decay ($0\nu\beta\beta$) as shown in Fig. 1.1. In this decay process involving an atomic nucleus, two neutrons convert into two protons with the emission of two electrons :

$$(A, Z) \rightarrow (A, Z + 2) + 2e^-,$$

where A and Z stands for mass and atomic number respectively. In absence of any other lepton number violating interactions, the decay rate of such $0\nu\beta\beta$ process is directly proportional to the neutrino mass element and is given by [21],

$$|m_{ee}| = \left| \sum_i U_{ei}^2 m_i \right| . \tag{1.21}$$

Here $|m_{ee}|$ is known as the effective mass parameter, U is the PMNS matrix and m_i's are the neutrino mass. Present upper bound on this effective mass parameter from KamLAND-Zen [22] and EXO [23] Collaborations are $|m_{ee}| < (0.14 - 0.28)$ eV and

$|m_{ee}| < (0.19 - 0.45)$ eV respectively (both at 90% C.L.). Observation of $0\nu\beta\beta$ will establish that, (a) neutrinos are Majorana particle and lepton number conservation is not a symmetry of nature, (b) measurement of the effective mass parameter will help us understanding the neutrino mass hierarchy.

From the above discussion it is evident that neutrinos are massive and the absolute scale may range from eV to sub-eV. Therefore the obvious question that appears as a consequence of above discussion is that why neutrinos are much lighter then the other SM fermions and how we can explain the physics of these massive neutrinos. In Section 1.4, we will discuss issues related to the origin of neutrino mass.

1.4 Theory of Massive neutrinos

In the SM, due to the absence of $SU(2)_L$ singlet right handed singlet neutrinos, a Dirac mass term is absent and hence neutrinos are massless. However above mentioned evidences from wide range of physical phenomena hints towards massive neutrinos and it is important to introduce new physics scenarios in order to explain neutrino mass. Note that SM is a renormalizable theory and lepton number conservation turns out to be an accidental symmetry. Once we demand that the accidental lepton number conservation is only an approximate symmetry of SM, we can incorporate Majorana masses for the neutrinos through higher dimensional operators. Such a simple and economic way to incorporate neutrino mass via non-renormalizable dimension-5 operator (also known as Wienberg Operator [24]), constructed from lepton and Higgs doublets, is given by

$$\delta\mathcal{L}^{d=5} = \frac{1}{2} c_{ij} \frac{\left(\overline{L_i^c}\tilde{H}^*\right)\left(\tilde{H}^\dagger L_j\right)}{\Lambda}. \tag{1.22}$$

Here Λ is the new physics scale involved and c_{ij} is the dimensionless complex coefficient. Interestingly this is the only allowed dimension-5 operator invariant under SM gauge group, constructed from SM fields and also violates lepton number by two units. After electroweak symmetry breaking, neutrino mass obtained from Eq. (1.22) can be written as

$$m_{\nu_{ij}} = \frac{c_{ij}}{2\Lambda} v^2, \tag{1.23}$$

where v is the SM Higgs vev. Clearly the smallness of the neutrino mass m_ν is mainly dictated by largeness of the new physics scale Λ appearing in the dimension-5 operator. Such a dimension-5 operator always appears (as in Eq. (1.22)) in theories which incorporates neutrino mass as discussed below.

From the above discussion it is now obvious that, to explain neutrino mass we must go beyond the SM. Since the true nature of neutrinos is still elusive to us, we are left with two different possibilities: neutrinos are Dirac particles or they are Majorana particle. In the SM (Section 1.1) we have already talked about the Dirac fermions and we know that a mass term for such a particle can be written as

$$m_D\overline{\psi}_L\psi_R + h.c., \tag{1.24}$$

when there exists fields of both chirality. In the simplest extension of the SM, if we incorporate right-handed (RH) neutrinos in the theory, we can write a Dirac mass term for the neutrinos (similar to Eqs. (1.10, 1.24)). However to explain neutrino mass in the eV range, the associated Yukawa coupling becomes $\sim 10^{-11}$. Since there is no appealing reason for this extremely small coupling and hence the theory is considered to be 'unnatural'. Note that it is possible to introduce Majorana mass for RH neutrinos. We know the action of a particle-antiparticle conjugation operator (C) is defined as $\psi^c = C\bar{\psi}^T$ stands for charged conjugate of ψ with $C = i\gamma_2\gamma_0$. It can flip the chirality of a field, via $(\psi_L)^c = (\psi^c)_R$ and $(\psi_R)^c = (\psi^c)_L$. Now in case of Majorana fermions, the left and right-handed components are related by a C conjugation as $\psi = \psi_L + \psi_R = \psi_L + \eta(\psi_L)^c$ where η is a arbitrary phase factor ($\eta = e^{i\zeta}$) following $\psi^c = \eta^*\psi$. Now for these neutral fermions, the mass term can be written as

$$m_L\overline{(\psi^c)}_R\psi_L + M_R\overline{(\psi^c)}_L\psi_R, \tag{1.25}$$

In a nutshell, we must look for a mechanism which can provide tiny neutrino mass in a more natural way. Few such possibilities of neutrinos mass generation are: (i) Seesaw mechanisms (both high and low scale seesaw, some of these scenarios will be reviewed in this section). (ii) Loop mechanisms (also known as radiative mechanism) [25–28], (iii) R-parity violating supersymmetry [29, 30]. (iv) Extra Dimensions [31, 32] and String Theories [33]. In the following subsections we discuss mostly different seesaw mechanism of neutrino mass generation relevant for the landscape of the studies in this thesis.

1.4.1 Type-I Seesaw Mechanism

Perhaps the most elegant way to explain the small neutrino mass is the type-I seesaw mechanism [34–37]. In the minimal extension of the SM, gauge singlet RH Majorana (N_{R_i}, $i = 1, 2, 3$ for three generations) fermions, are included in the theory. Therefore in presence of both Dirac and Majorana fermions the Lagrangian responsible for neutrino mass can be written as

$$-\mathcal{L}_{\mathrm{Type-I}} = Y_D \bar{\ell} \widetilde{H} N_R + \frac{1}{2} M_R \overline{N_R^c} N_R + h.c., \tag{1.26}$$

and after electoweak symmetry breaking generates

$$-\mathcal{L}_{\mathrm{Type-I}} = m_D \overline{\nu_L} N_R + \frac{1}{2} M_R \overline{N_R^c} N_R + h.c.. \tag{1.27}$$

In Eq. (1.27), $m_D = Y_D v$ is the Dirac mass matrix for the neutrinos where Y_D is the coupling matrix. M_R is the symmetric mass matrix for the Majorana neutrinos. In the basis (ν_L, N_R^c), the effective neutrino mass matrix can be written as

$$M_\nu = \begin{pmatrix} 0 & m_D^T \\ m_D & M_R \end{pmatrix}. \tag{1.28}$$

For three generations of neutrinos, each entries in Eq. (1.28) are 3×3 matrices. Considering m_D to be much lighter than M_R ($m_D << M_R$), after block diagonalization, mass matrices for light and heavy neutrinos can be written as [38]

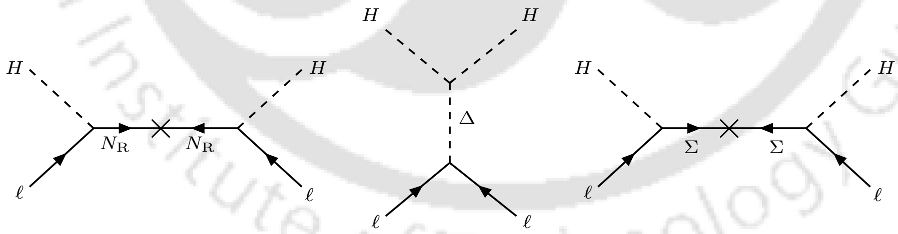

(a) Type-I (b) Type-II (c) Type-III

FIGURE 1.2: Feynman diagrams for Type-I, Type-II and Type-III seesaw.

$$m_\nu^I \simeq -m_D^T M_R^{-1} m_D \quad \text{and} \quad M_{\text{heavy}} \simeq M_R. \tag{1.29}$$

From Eq. (1.29) it is now clear that observed smallness of the light neutrinos can be explained form the heaviness of M_R. This is known as type-I seesaw mechanism of neutrino mass generation. A typical Feynman diagram for such process is given in the left panel of Fig. 1.2. Eq. (1.29) indicates that with $Y_D \sim \mathcal{O}(1)$, to generate neutrino mass of the order of 0.1 eV, makes $M_R \sim 10^{14}$ GeV[1]. Presence of these heavy neutrinos not only explains tiny neutrino mass, it can also play an important role in cosmology to explain the matter-antimatter asymmetry of the universe. Such possibility will be discussed in Section 1.7 and Chapter 2 is devoted in realizing a framework to establish a connection between neutrino masses, mixing and the matter-antimatter asymmetry of the universe in a type-I seesaw scenario.

1.4.2 Type-II Seesaw Mechanism

In type-II seesaw mechanism [40–43], SM model is extended by introducing $SU(2)_L$ scalar triplet field (Δ) having hypercharge 2. Combining with SM lepton doublets it can give rise to a Majorana mass term at renormalisable label provided Δ gets a vev. In its 2×2 matrix representation the scalar triplet can be written as

$$\Delta = \begin{pmatrix} \Delta^+/\sqrt{2} & \Delta^{++} \\ \Delta^0 & -\Delta^+\sqrt{2} \end{pmatrix}, \tag{1.30}$$

where Δ^0, Δ^+ and Δ^{++} are neutral, singly and doubly charged components of it. The Lagrangian relevant for neutrino mass can be written as

$$-\mathcal{L}_{\rm Type-II} = \left(Y_\Delta \ell^T C \Delta \ell + h.c.\right) + \left(\mu \widetilde{H}^T \Delta \widetilde{H} + h.c.\right) + M_\Delta^2 {\rm Tr}(\Delta^\dagger \Delta), \tag{1.31}$$

here Y_Δ is the complex coupling matrix responsible for providing Majorana masses to the neutrinos, μ is a dimensionful coupling constant associated with the lepton number violating term and M_Δ represents the mass of the scalar triplet. When the neutral component of the scalar gets vev ($\langle \Delta^0 \rangle = u_\Delta$), the neutrino mass matrix obtained via type-II seesaw can be written as

$$m_\nu^{II} \;=\; 2Y_\Delta u_\Delta \quad \text{with} \quad u_\Delta = \frac{\mu v^2}{M_\Delta^2}, \tag{1.32}$$

---

[1] Such a huge mass scale indicates that the origin of neutrino mass can also be related to some Grand Unified Theory (GUT) symmetry group like $SO(10)$ [39].

and hence neutrino mass gets the required seesaw suppression once we make the scalar triplets very heavy. In Eq. (1.32), $(v/M_\Delta)^2$ provides this suppression. Feynman diagram for type-II seesaw is illustrated in the middle panel of Fig. 1.2.

In presence of both RH neutrinos and scalar triplets, neutrino mass will get contribution from both type-I and type-II seesaw. In such a type-I+II scenario the effective mass matrix for neutrinos can be written as

$$m_\nu = m_\nu^{II} + m_\nu^{I} = m_\nu^{II} - m_D^T M_R^{-1} m_D. \tag{1.33}$$

In Chapter 3 of this thesis, we study interplay of both of these terms in explaining neutrino mass, mixing and its consequence in leptogenesis.

1.4.3 Type-III Seesaw Mechanism

In an alternate scenario, instead of fermionic singlet neutrinos as included in pure type-I seesaw, if we introduce $SU(2)_L$ fermionic triplet of zero (Σ) hypercharge :

$$\Sigma = \begin{pmatrix} \Sigma^0/\sqrt{2} & \Sigma^+ \\ \Sigma^- & -\Sigma^0\sqrt{2} \end{pmatrix}, \tag{1.34}$$

the Lagrangian relevant for neutrino mass can be written as [44]

$$-\mathcal{L}_{\text{Type}-\text{III}} = Y_\Sigma \bar{\ell}\Sigma\tilde{H} + \frac{1}{2} M_\Sigma \text{Tr}(\overline{\Sigma^c}\Sigma). \tag{1.35}$$

Here Y_Σ is the Yukawa coupling matrix whereas M_Σ represents the mass matrix for the fermionic triplet. The relevant Feynman diagram for this case is illustrated in the right panel of Fig. 1.2. Hence the neutrino mass matrix for type-III seesaw mechanism can be written as

$$m_\nu^{III} = -Y_\Sigma^T \frac{v^2}{M_\Sigma} Y_\Sigma. \tag{1.36}$$

Therefore, in the limit $M_\Sigma >> v$, *i.e.* when the fermionic triplets are heavy enough one can reproduce small neutrino mass using type-III seesaw mechanism also.

1.4.4 Inverse Seesaw Mechanism

Introducing heavy RH neutrinos N_{R_i} ($i = 1, 2, 3$ for three generations) in original type-I seesaw scenario one can explain tiny neutrino mass very easily. Here the energy of the lepton number violation responsible for generating neutrino is dictated by its mass, M_R. With the Yukawa couplings of order unity or so, we can obtain the light neutrino mass of observed magnitude, provided the new physics scale M_R is sufficiently high $\sim 10^{14}$ GeV or so. Though it suggests an interesting and natural explanation of why neutrinos are so light, such a high new physics scale is beyond the reach of present and future neutrino experiments. On the other hand, inverse seesaw [33, 45] turns out to be a potential alternate scenario where the new physics scale responsible for neutrino mass generation can be brought down near TeV scale at the expense of involving additional SM gauge singlet fermions S_i ($i = 1, 2, 3$ *i.e.* one per each generation of RH neutrinos). Therefore in presence of these two set of SM gauge singlets (having opposite lepton number), the inverse seesaw Lagrangian can be written as

$$-\mathcal{L}_{\text{ISS}} = Y_D \bar{L}\widetilde{H}N_R + M\overline{N_R^c}S + \frac{1}{2}\mu\overline{S^c}S + h.c.. \tag{1.37}$$

Here Y_D is the Dirac Yukawa coupling, M is the complex mass matrix for $N_R - S$ interaction. μ is a complex symmetric matrix originated from $\overline{S^c}S$ interaction and turns out to be the only source of lepton number violation in the theory with small μ. The lepton number conservation is an approximate symmetry of this model hence the $N_R - N_R$ term is not allowed as it provides a large lepton number violation. After electroweak symmetry breaking, the Lagrangian in Eq. (1.37) yields a 9×9 mass matrix M_ν in the basis (ν_L^c, N_R, S)

$$M_\nu = \begin{pmatrix} 0 & m_D & 0 \\ m_D^T & 0 & M \\ 0 & M^T & \mu \end{pmatrix}. \tag{1.38}$$

Now, with the assumption $\mu << m_D << M$, the effective mass matrix for the light neutrinos can be written as [46]

$$m_\nu = m_D M^{-1}\mu(M^T)^{-1}m_D^T = F\mu F^T, \tag{1.39}$$

where $m_D = Y_D v$ and $F = m_D M^{-1}$ which represents mixing between active and sterile neutrinos. Here we observe that, in Eq. (1.39), the neutrino mass is double suppressed by M. Hence to get the light neutrino mass in the eV range with Yukawa coupling of the order of unity, heavy neutrino mass M can be brought down to TeV scale once μ is at keV scale. In the limit $\mu \to 0$ the lepton number conservation of the theory is restored and we find the massless neutrinos just like SM. Therefore a small non-vanishing value of μ is more natural in 't Hooft sense [47]. Such a scenario have many important phenomenological consequences. It can lead to enhanced active-sterile neutrino mixing as well as make heavy neutrinos accessible to the direct search experiments at LHC. In Chapter 4 we explore one such scenario to study all the related phenomenological issues.

1.5 Origin of Lepton Mixing and Neutrino Oscillation

Evidences in favor of neutrino mass have changed our understanding (as elaborated in Section 1.3) regarding the neutrinos. An immediate consequence of neutrino mass is that they significantly contribute in lepton mixing and plays an important role in the phenomenon called neutrino oscillation. Before going to any further, here we present a very brief historical note on the neutrinos and then discuss neutrino mixing and oscillation.

Beta decay is the first physical process which motivated physicists to introduce a new particle called neutrino. In 1930 Wolfgang Pauli [48] first suggested the existence of a neutral particle with small mass to save the conservation laws in beta decay. Latter Enrico Fermi [49] published the theory of beta decay and named the particle as neutrino (*i.e.* little neutral one). In 1956, Clyde Cowan, Frederick Reines and their collaborators made history by detecting the electron (anti-)neutrinos ν_e [50] via inverse beta decay. Afterwards ν_μ [51] and ν_τ [52] were also discovered in two other experiments. These three flavors of neutrinos are part of SM and they interact weakly with $W^\pm$ and Z bosons through charged and neutral current interaction.

At the end of the last century striking observations were made by Sudbury Neutrino Observatory (SNO), Super-Kamiokande experiments observing neutrino oscillation with solar and atmospheric neutrinos respectively. But the story began many decades before this observation. Neutrinos plays an important role in the process of production of energy inside the core of the Sun. These are produced due to fusion of hydrogen into helium as (through the so-called pp-chain [54])

$$4p \to \alpha + 2e^+ + 2\nu_e + 28 \text{ MeV}. \tag{1.40}$$

As neutrinos interacts very weakly they can pass through the sun and reach to the earth. Ray Davis and his collaborators [55] made the earliest attempt to detect these solar neutrinos in 1968. The detecting material was perchloroethylene (rich in chlorine), kept in a huge tank under the Homestake mine in South Dakota, USA. Chlorine can absorb a neutrino and convert to argon via

$$\nu_e + {}^{37}Cl \to {}^{37}Ar + e. \tag{1.41}$$

They collected argon atoms for several months. These atoms were produced at a rate of about one atom every two days. Surprisingly, the total accumulation was only one third of what was predicted based on the Standard Solar Model [56]. This is known as the famous solar neutrino problem. Now on the other hand, neutrinos are also produced due to the hadronic showers produced by cosmic rays in the Earth's atmosphere following the chain reaction

$$\begin{aligned} \pi^\pm(K^\pm) &\longrightarrow \mu^\pm + \nu_\mu(\bar{\nu}_\mu), \\ \mu^\pm &\longrightarrow \nu_\mu(\bar{\nu}_\mu) + \nu_\mu(\bar{\nu}_\mu). \end{aligned}$$

From the above reactions, loosely one can expect that there will be twice atmospheric muon neutrinos over the electron neutrinos appearing at the detector. However experiments like Kamiokande [57], IMB [58] recorded much less events. This puzzle is known as atmospheric neutrino problem. These phenomenons indicated that some theoretical breakthrough is needed to answer these anomalies.

To solve the solar neutrino puzzle Bruno Pontecorvo first coined the beautiful idea of neutrino oscillation in 1957 [59]. He proposed that ν_e's produced at the Sun can actually transform into neutrino of another species (ν_e, anti-neutrinos etc.) during their journey to the Earth. Davis' experiment was insensitive to these neutrinos (other than ν_e) and hence the deficit. Neutrino oscillation is a quantum mechanical phenomenon where transition occurs among different neutrino flavors. There are several evidences for neutrino oscillation starting from atmospheric, solar neutrino experiments (e.g. Gallex [60], SAGE [61], SNO [62], Super-Kamiokande [63]) to nuclear reactors and particle accelerator (e.g. KamLAND [64], K2K [65], Minos [66] and T2K [67]) experiments. Experimental confirmations of neutrino oscillation are one of the most sensitive and important probe of nonzero neutrino mass. Therefore, if neutrinos have mass, the flavor eigenstates (say, $|\nu_\alpha\rangle$ dictated by specific charged current interaction) and mass eigenstates (say, $|\nu_i\rangle$) of neutrinos are not necessarily same. One can be expressed one as linear combination of other via

$$|\nu_\alpha\rangle = \sum_{i=1}^{3} U_{\alpha i}|\nu_i\rangle; \qquad \alpha = e, \mu, \tau \tag{1.42}$$

where U is an unitary lepton mixing matrix. The oscillation probability for a neutrino flavor ν_α to transform into a different flavor ν_β where traveling a distance L is given by

$$\begin{aligned} P(\nu_\alpha \to \nu_\beta) &= \delta_{\alpha\beta} - 4\sum_{k>j} \mathrm{Re}[U^*_{\alpha k}U_{\beta k}U_{\alpha j}U^*_{\beta j}]\sin\left(\frac{\Delta m^2_{kj}L}{4E}\right) \\ &\quad +2\sum_{k>j} \mathrm{Im}[U^*_{\alpha k}U_{\beta k}U_{\alpha j}U^*_{\beta j}]\sin\left(\frac{\Delta m^2_{kj}L}{2E}\right), \end{aligned} \tag{1.43}$$

where $\Delta m^2_{kj} = m^2_k - m^2_j$ is the mass splitting between k^{th} and j^{th} neutrinos, L is the distance traveled and E is the energy. Usually, for $\alpha \neq \beta$ the oscillation probability of the channel is known as 'transition probability' and for $\alpha = \beta$ it is called 'survival probability'. Eq. (1.43) indicates that the transition probabilities depends on (i) distance between source and detector (L), (ii) mixing angles (appearing in U), (iii) energy of the neutrinos E and (iv) mass squared difference $(\Delta m^2_{kj} = m^2_k - m^2_j)$ of the corresponding neutrinos. Therefore nonzero neutrino mass and mixing are extremely important parameters for neutrino oscillation. Below we present a summary of current status of neutrino oscillation parameters.

As stated in the discussion after Eq. (1.16), considering neutrinos to be massive, see that the charged current interaction between the charged lepton, neutrino and the W boson involves the CKM like mixing matrix $U = U^\dagger_\ell U_\nu$ called PMNS matrix, where U_ℓ is the diagonalizing matrix of the charged lepton mass matrix and U_ν is that for the neutrinos. Thus for diagonal charged lepton sector, U_ν turns out to be the only contribution in the lepton mixing matrix (in Eq. (1.19)) which appears in the neutrino oscillation. However in most general case U stands for the lepton mixing matrix and acts as the rotation matrix between flavor and mass eigenstates.

Provided U is a general $n \times n$ unitary matrix, it can be parameterized by n^2 real parameters. Such a mixing matrix can be constructed from $\frac{1}{2}n(n-1)$ mixing angles and $\frac{1}{2}n(n+1)$ phases. However out of $\frac{1}{2}n(n+1)$ only $\frac{1}{2}(n-1)(n-2)$ phases are physically relevant. These phases are called Dirac Phase. For three generations ($n = 3$), only one phase appears in the mixing matrix U. On the other hand, if neutrinos are considered to be Majorana particle, for n generation there will be extra $(n-1)$ CP violating phases. These additional phases are known as Majorana phases. The lepton mixing matrix U is generally known as Pontecorvo-Maki-Nakagawa-Sakata (PMNS) matrix [16] and is analogous to the Cabbibo-Kobayashi-Maskawa (CKM) matrix for the quarks. In the standard parametrization (for three generations of neutrinos), this PMNS matrix can be written as [53]

$$\begin{aligned} U_{\text{PMNS}} &= \begin{pmatrix} 1 & 0 & 0 \\ 0 & c_{23} & s_{23} \\ 0 & -s_{23} & c_{23} \end{pmatrix} \begin{pmatrix} c_{13} & 0 & s_{13}e^{-i\delta} \\ 0 & 1 & 0 \\ -s_{13}e^{i\delta} & 0 & c_{13} \end{pmatrix} \begin{pmatrix} c_{12} & s_{12} & 0 \\ -s_{12} & c_{12} & 0 \\ 0 & 0 & 1 \end{pmatrix} P \\ &= \begin{pmatrix} c_{12}c_{13} & s_{12}c_{13} & s_{13}e^{-i\delta} \\ -s_{12}c_{23} - c_{12}s_{13}s_{23}e^{i\delta} & c_{12}c_{23} - s_{12}s_{13}s_{23}e^{i\delta} & c_{13}s_{23} \\ s_{12}s_{23} - c_{12}s_{13}c_{23}e^{i\delta} & c_{12}s_{23} - s_{12}s_{13}c_{23}e^{i\delta} & c_{13}c_{23} \end{pmatrix} P, \end{aligned} \tag{1.44}$$

with

$$P = \begin{pmatrix} 1 & 0 & 0 \\ 0 & e^{i\alpha_{21}/2} & 0 \\ 0 & 0 & e^{i\alpha_{21}/2} \end{pmatrix}, \tag{1.45}$$

where $s_{ij} = \sin\theta_{ij}$, $c_{ij} = \cos\theta_{ij}$, δ is the Dirac CP violating phase. Also P is as diagonal phase matrix which contains two Majorana phases (α_{21} and α_{31}), if neutrinos are Majorana particles.

1.5.1 Neutrino Oscillation Parameters

As mentioned earlier, from enormous number of experiments around the globe it is now confirmed that neutrinos oscillate and we now have strong constraints on the oscillation parameters. For three flavor neutrino oscillation the involved parameters are[2]:

---

[2] Here, two Majorana phases appearing in the neutrino mixing matrix (Eq. 1.44), however have no consequence in the oscillation probabilities.

- Three mixing angles (θ_{12}, θ_{23} and θ_{13}).
- Dirac CP phase (δ).
- Two mass-squared differences, namely solar mass-squared difference ($\Delta m^2_{\odot}$) and atmospheric mass-squared difference (Δm^2_{atm}).

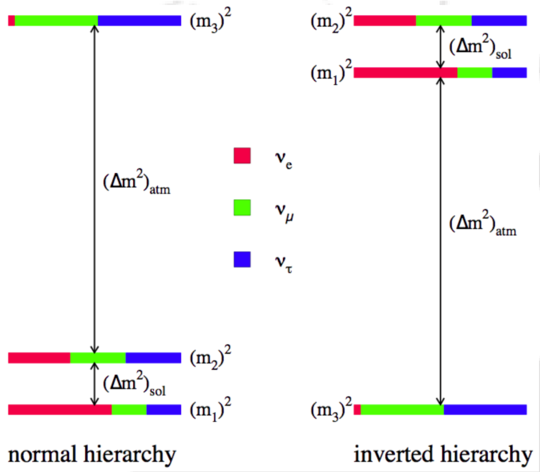

FIGURE 1.3: Schematic diagram form neutrino mass hierarchies. Left-panel represents normal hierarchy whereas right panel represents inverted hierarchy [68].

It turns out that scale associated with the two mass-squared differences are distinct and differs almost by two orders of magnitude. The 'small' mass-squared difference, $\Delta m^2_{\odot} = \Delta m^2_{21} = m^2_2 - m^2_1$ is involved in solar neutrino oscillation whereas the 'large' mass-squared difference, $\Delta m^2_{\text{atm}} = \Delta m^2_{32} = m^2_3 - m^2_2$ (or Δm^2_{31}) is involved in the atmospheric neutrino oscillation. From the present data the sign of Δm^2_{atm} is still unknown to us and this leads to two very different arrangement of the neutrino mass spectrum as shown in Fig. (1.3)[3]. Conventionally for $\Delta m^2_{\text{atm}} \approx \Delta m^2_{32} > 0$ it as called normal hierarchy (NH) and the the mass ordering is $m_1 < m_2 < m_3$. On the other hand for $\Delta m^2_{\text{atm}} \approx \Delta m^2_{31} < 0$ it is known as inverted hierarchy (IH) and the mass ordering follows the pattern $m_3 < m_1 < m_2$. Over the years neutrino oscillation parameters are being measured and we are now moving towards the precision measurement era of these parameters. The Super-Kamiokande experiment with atmospheric neutrinos first hinted a large mixing, close to maximal value ($\theta_{23} \simeq 45°$) and the atmospheric mass-squared difference to be

---

[3] In addition to this, quasi-degenerate spectrum of neutrino masses is possible with $m_1 \simeq m_2 \approx m_3$ with $m^2_{1,2,3} >> \Delta m^2_{\text{atm}}$.

$\Delta m^2_{\text{atm}} \simeq \mathcal{O}(10^{-3}\ \text{eV}^2)$ [69] providing a solution to the atmospheric neutrino problem stated earlier. Subsequently, SNO [62], KamLAND [64] suggested that $\sin^2\theta_{12} \simeq 1/3$ and solar mass-squared difference to be $\Delta m^2_{\odot} \simeq \mathcal{O}(10^{-5}\ \text{eV}^2)$ and solved the solar neutrino puzzle. Thus neutrino oscillation was confirmed by several oscillation experiments and the two mixing (θ_{12} and θ_{23}) angle were measured and found to be large. Afterwards several atmospheric and solar, neutrino oscillation experiments gathered plenty of data to achieve commendable precision. However the experiments aiming to measure the reactor mixing angle θ_{13} were sill in their evolutionary stage and prior to 2012 it was suggested that this mixing angle is small ($\sin^2\theta_{13} = 0.01^{+0.016}_{-0.011}$, best-fit vale with 1σ error)[9].

Now for complete understanding of neutrino mixing matrix it is essential to measure the third mixing angle θ_{13} as it can play an important role in theoretical model building of neutrino mass matrices. In addition to this, precise measurement of θ_{13} is extremely important for the design of the experiments aiming to measure the CP-violating phase δ. Further, neutrino mass hierarchy can be determined incorporating matter effect in neutrino oscillation which also depends on the magnitude of θ_{13}. Keeping this in mind several experiments were commissioned and in last ten years significant improvement have been made in measuring the size of θ_{13}. Earlier, the CHOOZ experiment [70–72] in France and Palo Verde experiment [73] in Arizona, USA both made attempts to measure θ_{13}. In each of these experiments the detector was placed roughly at a distance of 1 kilometer to study electron antineutrinos emitted (through inverse beta decay: $\bar{\nu}_e + p \to e^+ + n$) from nuclear reactors. However these two reactor experiments did not observe any positive hint for the mixing angle θ_{13} and was speculated to be very small. Upto 2003, these experiments only set an upper limit on θ_{13} and it is $\sin^2 2\theta_{13} < 0.14$ at 90% CL. Subsequently, several experiments started taking data to improve the measurement of θ_{13} with higher sensitivity.

In this regards three reactor experiment were set up to observe short baseline neutrino oscillation. These experiments are Double Chooz (in France), Daya Bay (in China) and RENO (in South Korea). By construction these experiments are very similar having both near and far detectors to measure un-oscillated and oscillated neutrino flux. Below we briefly discuss about these three short baseline experiments.

Double Chooz: This experiment is located at the same site of the earlier CHOOZ experiment in The Chooz Nuclear Power Plant, France. It is an upgraded version of CHOOZ with better statistical and systematic uncertainties. Also some development were made in the detection technique and material (the core target is made of transparent acrylic and holds Gadolinium-doped liquid scintillator). In this experiment, the near detector is placed at 400 meter away from the core for renormalization of the neutrino flux and to measure oscillation with any effect of θ_{13}. The far detector is placed at a distance of 1050 meter to study the oscillation. Comparing the data accumulated by both of these detectors an estimation for $\sin^2 2\theta_{13}$ is made. In 2012 this experiment reported the best fit value of θ_{13} with 1σ error as [74]

$$\sin^2 2\theta_{13} = 0.109 \pm 0.030(\text{stat.}) \pm 0.025(\text{syst.}), \tag{1.46}$$

with $\Delta m^2_{31} = 2.32 \times 10^{-3}$ eV^2 and discarded no oscillation assumption at 99.8% CL (2.9σ). After the announcement of first positive hint [75] on θ_{13} in 2011 by Double Chooz, two independent collaborations Daya Bay and RENO also started publishing their result.

Daya Bay: This experiment is situated at the Daya Bay Nuclear Plant in southern China. In this experiment six cores (two from Daya Bay Nuclear Plant and six from nearing LingAo Nuclear Plant) are used to study the antineutrino flux and relies on the basic principle of Double Chooz experiment. For Daya Bay reactor the near and far detectors are placed at a distance 350 meter and 2000 meter respectively. Whereas for LingAo reactor near and far detectors are located at a distance of 480 meter and 1600 meter respectively. Here the acrylic vessel filled with Gadolinium-doped liquid scintillators are used as detector. In 2012 Day Bay published its first result with positive hint of nonzero θ_{13} as [76]

$$\sin^2 2\theta_{13} = 0.089 \pm 0.010(\text{stat.}) \pm 0.005(\text{syst.}) \tag{1.47}$$

at 5.2σ. Afterwards more data was accumulated and a precise measurement was made in 2013 [77].

RENO: The RENO experiment [78] is located at the Hanbit Nuclear Power Plant (formerly Yeonggwang Nuclear Power Plant), Jeollanam-do province, South Korea. This experiment is also governed by Double Chooz concept. Two identical 16-ton Gadolinium-doped liquid scintillator detectors are placed roughly 294 meter (near detector) and 1383 meter (far detector) from the center of the six core reactor array. This experiment started taking data with both the detectors in August 2011 and after 229 day data-taking it reported

$$\sin^2 2\theta_{13} = 0.113 \pm 0.013(\text{stat.}) \pm 0.019(\text{syst.}) \tag{1.48}$$

at 4.9σ.

Apart from these short baseline experiments, few next generation long baseline experiments were built with an aim to measure θ_{13} using the same multiple detector concept. In these experiments θ_{13} is estimated from appearance of electron neutrino in a muon electron beam. In addition, these experiments aims to measure Dirac CP phase δ as well as the mass hierarchy considering matter effect. T2K (in Japan), MINOS and NOνA (both in USA) are examples of such long baseline experiments and typical baseline in these experiments ranges within few hundred kilometers.

Considering data obtained from various experiments a global analysis can be done to estimate the parameters appearing in the neutrino mass matrix as well as the mass squared differences [5]. In Table 1.2 we have summarized the neutrino oscillation parameters form a recent global analysis by Forero *et al*. Other similar analysis can be found in [79, 80].

Oscillation parameters	best fit	1σ range	3σ range
Δm^2_{21} $[10^{-5}$ eV$^2]$	7.60	7.42–7.79	7.11–8.18
$\|\Delta m^2_{31}\|$ $[10^{-3}$ eV$^2]$	2.48 (NH) 2.38 (IH)	2.41 – 2.53 2.32 – 2.43	2.30 – 2.65 2.20 – 2.54
$\sin^2\theta_{12}$	0.323	0.307–0.339	0.278–0.375
$\sin^2\theta_{23}$	0.567 (NH) 0.573 (IH)	0.439–0.599 0.530–0.598	0.392–0.643 0.403–0.640
$\sin^2\theta_{13}$	0.0234 (NH) 0.0240 (IH)	0.0214–0.0254 0.0221–0.0259	0.0177–0.0294 0.0183–0.0297

TABLE 1.2: Summary of neutrino oscillation parameters for normal and inverted neutrino mass hierarchies from the analysis of [5].

Currently the goal of present and future neutrino oscillation experiments involve determination of (*i*) octant of θ_{23}, *i.e.* whether $\theta_{23} < 45°$ or $\theta_{23} > 45°$. (*ii*) sign of $\Delta m^2_{\rm atm}$, which will determine the hierarchy of neutrino masses and (*iii*) magnitude of Dirac CP violating phase δ. Any theoretical model which have potential to address these issues can by verified by the upcoming experiments.

1.5.2 Patterns of Lepton Mixing

Understanding the pattern of fermion mixing still remains elusive to us. So far we only know that the quark mixing (dictated by the $V_{\rm CKM}$ matrix) is completely different from neutrino mixing (governed by the $U_{\rm PMNS}$ matrix). Numerical estimation shows that, the

CKM matrix is close to unity [4, 79] whereas PMNS matrix (U) is far from that and are given by

$$|V_{\rm CKM}| = \begin{pmatrix} 0.97427 \pm 0.00014 & 0.22536 \pm 0.00061 & 0.00355 \pm 0.00015 \\ 0.22522 \pm 0.00061 & 0.97343 \pm 0.00015 & 0.0414 \pm 0.0012 \\ 0.00886^{+0.00033}_{-0.00032} & 0.0405^{+0.0011}_{-0.0012} & 0.99914 \pm 0.00005 \end{pmatrix}, \tag{1.49}$$

and

$$|U_{\rm PMNS}| = \begin{pmatrix} 0.801 - 0.845 & 0.514 - 0.580 & 0.137 - 0.158 \\ 0.225 - 0.517 & 0.441 - 0.699 & 0.614 - 0.739 \\ 0.246 - 0.529 & 0.464 - 0.713 & 0.590 - 0.776 \end{pmatrix}, \tag{1.50}$$

respectively (without Majorana phases). Understanding the lepton mixing pattern still remains a challenge to the theorists. With the course of time, several proposals for explaining the mixing matrix have been proposed from symmetry point of view, which are compatible with the data to some extent. Suggested by the earlier data, if one considers maximal maxing for atmospheric sector (*i.e.* $\theta_{23} = 45°$) and no mixing for reactor sector (*i.e.* $\theta_{13} = 0°$) then the mixing is termed as 'bi-large' (BL) mixing (with $s_{12} = s_{23}$). The resulting mixing matrix is then given by

$$U_{\rm BL} = \begin{pmatrix} c_{12} & s_{12} & 0 \\ -s_{12}/\sqrt{2} & c_{12}/\sqrt{2} & -1/\sqrt{2} \\ -s_{12}/\sqrt{2} & c_{12}/\sqrt{2} & 1/\sqrt{2} \end{pmatrix}. \tag{1.51}$$

An interesting feature of this BL mixing is that any $\mu - \tau$ symmetric neutrino mass matrix of the form

$$m_\nu \Big|_{\mu \leftrightarrow \tau} = \begin{pmatrix} x & y & y \\ y & z & w \\ y & w & z \end{pmatrix} \tag{1.52}$$

can be diagonalized by $U_{\rm BL}$ with judicious choice of θ_{12}. Here x, y, w and z are in general complex quantities.

Following the measurement [62, 64], the solar mixing angle was very well approximated as, $\sin^2\theta_{12} = 1/3$. Therefore, all these three conditions can be put together ($\sin^2\theta_{23} = 1/2$, $\sin^2\theta_{12} = 1/3$ and $\sin\theta_{13} = 0$) which led to an interesting and experimentally viable scenario known as tribimaximal (TBM) mixing [6]. It is given by

$$U_{TB} = \begin{pmatrix} \sqrt{\frac{2}{3}} & \frac{1}{\sqrt{3}} & 0 \\ -\frac{1}{\sqrt{6}} & \frac{1}{\sqrt{3}} & -\frac{1}{\sqrt{2}} \\ -\frac{1}{\sqrt{6}} & \frac{1}{\sqrt{3}} & \frac{1}{\sqrt{2}} \end{pmatrix}. \tag{1.53}$$

From mass matrix in Eq. (1.52), TBM mixing is obtained for $x + y = w + z$. The name tribimaximal is derived due to trimaximal and bimaximal mixing pattern observed in the 2nd and 3rd columns of U_{TB} respectively. Such distinctive and unique structure of the TBM mixing matrix may indicate some special symmetry in the Lagrangian broken at high energy. Therefore the TBM structure of the neutrino mixing matrix got huge attention from model building point of view. To realize this TBM structure, models based on discrete flavor symmetries are widely popular due to simplicity and economic nature (this will be discussed in the next section in details).

However, current data no longer support exact TBM scenario in the lepton sector. As mentioned earlier, recent observation of θ_{13} from various experiments [75, 76, 78, 81] shows it has non-negligible contribution in the mixing matrix ($\theta_{13} = 8^\circ - 9^\circ$). In this thesis we start with the simple realization of TBM mixing and then look for the minimal extension to generate nonzero θ_{13}.

1.6 Role of Flavor Symmetry in Explaining Lepton Mixing

Up to the present day, we are yet to understand the data accumulated for lepton, quark masses and mixing. There still remains several unanswered questions within the framework of the SM, few of these are listed below:

1. Why there are three generations of quarks and leptons?
2. What is the origin of fermion mass hierarchies and why neutrinos are much lighter compared to the other SM fermions?
3. Why quark mixing pattern is quite different from the lepton mixing pattern?

All these questions together is known as flavor problem in particle physics. To address the issues related to the flavor problem we must go beyond SM. For this SM symmetries and particle content are often extended. For example, the mass hierarchies of quarks (both up and down type) and leptons can be explained once we impose an Abelian flavor symmetry $G_f = U(1)_{\rm FN}$, as suggested by Froggatt and Nielsen (FN) [82]. Unlike SM symmetries, under this symmetry, different generations of SM particles transform differently. Therefore, by introducing an additional scalar (also known as 'flavon', which is also charged under this additional symmetry) and considering spontaneous breaking of this symmetry, mass of the heaviest particle is generated. But masses of the lighter particles are generated from higher dimensional operators proportional to $\langle\theta\rangle/\Lambda \equiv \epsilon << 1$, where θ is the additional scalar introduced and Λ is the cut off scale of the theory. This process of generation of fermion mass hierarchy is called Froggatt-Nielsen mechanism. However Abelian symmetry like this suffers from few shortcomings. Firstly, they can not explain why there exits three generations. Secondly, certain mixing patterns like TBM mixing can't be predicted.

On the other hand a non-Abelian group G_f is usually much more predictive and there exits a wide range of such symmetries. The choice of a non-Abelian group can either be continuous or a discrete one. These exits large varieties of these groups. Example for non-Abelian continuous groups are: $SU(2), SU(3), SO(3)$ etc. whereas example for non-Abelian discrete groups are:

- Alternating groups A_n : A_4, A_5
- Symmetric groups S_n : S_3, S_4
- Dihedral groups D_n : D_4, D_5
- Binary Dihedral groups Q_n : Q_4, Q_6
- $\Delta(3n^2)$ and $\Delta(6n^2)$: $\Delta(27)$ and $\Delta(54)$
- T' : double covering group of A_4 etc.

For a brief review and breaking patterns of all these non-Abelain discrete groups, see [83]. Compared to Abelian groups, model building with non-Abelain discrete groups are much more interesting for two reasons: (a) non-Abelain discrete groups are well equipped in dealing with the flavor structures, (b) special attention is needed in constructing the scalar potential and hence realization of proper symmetry breaking pattern (as field content is often larger in the latter case) can be successful. Furthermore, non-Abelian discrete symmetries can be originated from profound fundamental theory such as string theory and extra dimension [84–91]. Therefore in the study of the patterns of lepton, quark mixing and masses, non-Abelian discrete flavor symmetries can play an important role in providing possible explanation for the experimental observations.

Out of all the non-Abelian discrete flavor symmetries found in the literature, due to its minimality, the group A_4 turns out to be most popular one in explaining fermion masses and mixing, particularly in lepton sector. The main advantage of using A_4 is that one can fully unify the three flavors of leptons $\ell_\alpha = (\ell_e, \ell_\mu, \ell_\tau)^T \sim 3$, as it is the smallest group which contains 3-dimensional representation. In this thesis, we have frequently used this symmetry to explain the observed lepton mixing. In the next subsection we now present a discussion on its representations and multiplication rules.

1.6.1 The A_4 Group

Non-Abelian discrete group A_4 is a group of even permutation of four objects. There are $4!/2 = 12$ elements in this group. It is symmetry group of a tetrahedron. Geometrically, these twelve elements are: one unit operator, three rotations by 180°, four clockwise rotations by 120° and four anti-clockwise rotations by 120°. The four irreducible representations of A_4 are 1 (one trivial singlet) , $1', 1''$ (two non-trivial one-dimensional representations are conjugate to each other) and 3 (triplet representation). Two generators, known as S and T can form all the 12 elements (through multiplications in all possible way) which satisfy

$$S^2 = T^3 = (ST)^2 = 1. \tag{1.54}$$

This relation dictates the ‘presentation’ of the group. Therefore, the three one dimensional representations are given by

$$1 \rightarrow (S = 1, T = 1), \tag{1.55}$$

$$1' \rightarrow (S = 1, T = \omega), \tag{1.56}$$

$$1'' \rightarrow (S = 1, T = \omega^2), \tag{1.57}$$

where $\omega = e^{2\pi i/3}$ is cubic root of unity. Now the multiplication rule for the singlets can be written as

$$1 \times 1 = 1, 1 \times 1' = 1', 1 \times 1'' = 1'', \tag{1.58}$$

$$1' \times 1' = 1'', 1' \times 1'' = 1 \text{ and } 1'' \times 1'' = 1'. \tag{1.59}$$

Now the basis for three dimensional representation can be written as

$$S = \frac{1}{3}\begin{pmatrix} -1 & 2 & 2 \\ 2 & -1 & 2 \\ 2 & 2 & -1 \end{pmatrix}, \quad T = \begin{pmatrix} 1 & 0 & 0 \\ 0 & \omega & 0 \\ 0 & 0 & \omega^2 \end{pmatrix}, \tag{1.60}$$

from which again all 12 matrices of the three dimensional representation of A_4 can be obtained and the product rule involving singlet and triplets are

$$1 \times 3 = 3, 1' \times 3 = 3, 1'' \times 3 = 3, \tag{1.61}$$

$$3 \times 3 = 1 + 1' + 1'' + 3_S + 3_A, \tag{1.62}$$

where subscripts S and A stands for 'symmetric' and 'asymmetric' combinations respectively. If we have two triplets having elements $a = (a_1, a_2, a_3)$ and $b = (b_1, b_2, b_3)$, their products are given by

$$(ab)_1 = a_1b_1 + a_2b_3 + a_3b_2, \tag{1.63}$$

$$(ab)_{1'} = a_3b_3 + a_1b_2 + a_2b_1, \tag{1.64}$$

$$(ab)_{1''} = a_2b_2 + a_3b_1 + a_1b_3, \tag{1.65}$$

$$(ab)_{3_S} = \frac{1}{3}\begin{pmatrix} 2a_1b_1 - a_2b_3 - a_3b_2 \\ 2a_3b_3 - a_1b_2 - a_2b_1 \\ 2a_2b_2 - a_1b_3 - a_3b_1 \end{pmatrix}, \tag{1.66}$$

$$(ab)_{3_A} = \frac{1}{2}\begin{pmatrix} a_2b_3 - a_3b_2 \\ a_1b_2 - a_2b_1 \\ a_3b_1 - a_1b_3 \end{pmatrix}. \tag{1.67}$$

Lastly, if c, d and e are three one dimensional representation transforming as $1, 1'$ and $1''$ respectively, their products with a triplet $a = (a_1, a_2, a_3)$ are given by

$$(ca)_3 = \begin{pmatrix} ca_1 \\ ca_2 \\ ca_3 \end{pmatrix}, \quad (da)_3 = \begin{pmatrix} da_3 \\ da_1 \\ da_2 \end{pmatrix} \quad (ea)_3 = \begin{pmatrix} ea_2 \\ ea_3 \\ ea_1 \end{pmatrix}. \tag{1.68}$$

Now A_4 has two subgroups G_S and G_T. G_S is the reflection subgroup generated by S whereas G_T (isomorphic to Z_3) is generated by T. Now when the A_4 flavor symmetry is broken by vev of a triplet scalar field, $\phi = (\phi_1, \phi_2, \phi_3)$ one can obtain two important breaking pattern $\langle\phi\rangle = (v_s, v_s, v_s)$ (when A_4 breaks down to G_S) and $\langle\phi\rangle = (v_T, 0, 0)$ (when A_4 breaks down to G_T). This symmetry breaking patterns plays a crucial role in obtaining fermion mass matrices.

As an illustrative purpose, here we show how A_4 can be responsible for flavor structures of the mass matrices. Let us consider the charged lepton mass matrix is being generated from a higher dimensional operator involving a scalar field ϕ_T (triplet under A_4 but singlet under SM gauge symmetry) having vev alignment $\langle\phi_T\rangle = (v_T, 0, 0)$. Now the three SM lepton doublets (L_e, L_μ, L_τ) can form a triplet under A_4 as $L = (L_e, L_\mu, L_\tau)$ and we consider RH charged leptons e_R, μ_R, τ_R are to be $1, 1''$ and $1'$ under A_4. Hence relevant Lagrangian can be written as

$$\mathcal{L}_l = \frac{y_e}{\Lambda}(\bar{L}\phi_T)He_R + \frac{y_\mu}{\Lambda}(\bar{L}\phi_T)'H\mu_R + \frac{y_\tau}{\Lambda}(\bar{L}\phi_T)''H\tau_R, \tag{1.69}$$

where we consider the SM Higgs doublet is a trivial singlet under A_4. Here Λ is the cutoff scale and y_e, y_μ and y_τ are the respective coupling constants. Terms in the first parenthesis represent products of two A_4 triplets, which further contracts with A_4 singlets 1, $1''$ and $1'$ corresponding to e_R, μ_R and τ_R respectively to make a true singlet under A_4. After breaking of A_4 symmetry in the direction $\langle\phi_T\rangle = (v_T, 0, 0)$, the lagrangian can be written as

$$\mathcal{L}'_l = \frac{v_T}{\Lambda}\left(y_e\bar{L}_eHe_R + y_\mu\bar{L}_\mu H\mu_R + y_\tau\bar{L}_\tau H\tau_R\right). \tag{1.70}$$

Finally after breaking of the electoweak symmetry we obtain the charged lepton mass matrix as

$$M_l = v\frac{v_T}{\Lambda}\begin{pmatrix} y_e & 0 & 0 \\ 0 & y_\mu & 0 \\ 0 & 0 & y_\tau \end{pmatrix}. \tag{1.71}$$

1.7 Neutrinos and its possible connection with matter antimatter asymmetry

So far we have discussed possible issues related to the mass and mixing of the neutrinos and how these can be understood by using symmetry argument. New physics which we incorporate to solve these puzzles might also play a crucial role in some other aspect of particle physics and cosmology. As mentioned earlier, till date one of the biggest mysteries in modern cosmology is why there is a huge predominance of matter over antimatter. This mismatch is usually represented in terms of baryon asymmetry, and is defined as

$$Y_B \equiv \left.\frac{n_B - n_{\bar{B}}}{s}\right|_0, \tag{1.72}$$

where $n_B, n_{\bar{B}}$ and s stands for number density for baryons, number density for antibaryons, entropy density and subscript 0 refers to at the present time respectively. According to recent observation by WMAP, this asymmetry (defined in Eq. (1.72)) is reported to be [92]

$$Y_B = (8.79 \pm 0.20) \times 10^{-11}. \tag{1.73}$$

The process by which this asymmetry can be dynamically generated is known as baryogenesis. In 1967, Sakharov [93] pointed out that three conditions must be satisfied in order to realize successful baryogenesis starting from a baryon symmetric universe:

1. Baryon number violation,
2. Combined C and CP violation,
3. Departure from thermal equilibrium.

Although SM can satisfy all the necessary conditions mentioned above, still SM alone can not explain observed baryon asymmetry. This is mainly due to two reasons, first, the CP violation in the SM is very small [94] and second, absence of strong first order electroweak phase transition [95, 96]. To overcome these difficulties many BSM scenarios have been suggested, e.g., leptogenesis [10], GUT baryogenesis [97], Affleck-Dine baryogenesis [98], electroweak baryogenesis [99, 100] etc. Out of all the scenarios proposed for baryogenesis, leptogenesis emerged as the most promising scenario due to its simplicity and intimate connection with physics of massive neutrinos. With the compelling evidences for neutrino masses, seesaw mechanism turns out to be the most elegant theory to explain neutrino mass as well as lepton asymmetry of the universe (leptogenesis) simultaneously. In seesaw scenarios lepton asymmetry is created through the out-of-equilibrium decay of heavy particles (e.g. RH neutrino, scalar or fermionic triplet(s) for type-I, II and III seesaw respectively) in the early Universe.

Now above mentioned three Sakharov conditions (now in terms of leptons instead of baryons) can easily be satisfied in an extended SM framework which accomodates neutrino mass through seesaw scenarios. For example in a type-I seesaw, where heavy RH neutrinos are included, the mass term violates lepton number. Then CP violation can occur through complex Yukawa coupling and the departure from thermal equilibrium condition can be satisfied once the interaction rate of the RH neutrinos are slower than the Hubble expansion rate. Therefore, in a nutshell, with complex CP phases in the Yukawa coupling, out-of-equilibrium decay of RH neutrinos can produce lepton asymmetry. Finally, sphaleron interactions [101–103] can convert this primordial lepton asymmetry into baryon asymmetry.

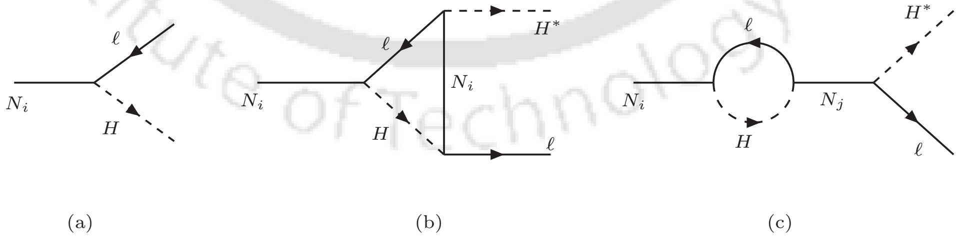

FIGURE 1.4: Feynman diagrams for decay of RH neutrinos into lepton and Higgs (a) tree level, (b) one-loop vertex level and (c) one-loop self energy level respectively. .

To illustrate the decay of heavy particle, we draw tree level and one loop vertex diagrams while RH neutrinos (in tyep-I seesaw), both RH neutrinos and scalar triplets (in type-I+II seesaw) are involved in Figs. 1.4-1.6. The CP asymmetry generated from the decay of only RH neutrinos to leptons and Higgs is given by

$$\epsilon_i \;=\; \frac{\Gamma(N_i \to \ell + H^*) - \Gamma(N_i \to \bar{\ell} + H)}{\Gamma(N_i \to \ell + H^*) + \Gamma(N_i \to \bar{\ell} + H)}. \tag{1.74}$$

Now due to interference of tree level decay with one-loop vertex and self energy diagrams (Fig. 1.4), this asymmetry (in the one flavor approximation regime [104–107]) can be written as [10, 108–113]

$$\epsilon_i = \frac{1}{8\pi} \sum_{j \neq i} \frac{\mathrm{Im}\left[\left((Y_\nu Y_\nu^\dagger)_{ji}\right)^2\right]}{(Y_\nu Y_\nu^\dagger)_{ii}} f\left(\frac{m_i}{m_j}\right), \tag{1.75}$$

in the basis where mass matrix for the RH neutrinos is diagonal. In SM the loop factor $f(x)$ in the above expression is defined as [109]

$$f(x) \equiv x\left[\frac{1}{1-x^2} + 1 - (1+x^2)\ln\left(\frac{1+x^2}{x^2}\right)\right], \tag{1.76}$$

whereas in the Minimal Supersymmetric Standard Model (MSSM) this loop factor can be written as [113]

$$f(x) \equiv -x\left[\frac{2}{x^2-1} + \ln\left(1 + \frac{1}{x^2}\right)\right], \tag{1.77}$$

with $x = m_i/m_j$. Here Y_ν is nothing but the complex Yukawa coupling (in the basis where RH neutrinos are diagonal) appearing in neutrino mass matrix (see Eq. (1.26)) and m_i's are real positive light neutrino mass eigenvalues (here we have replaced the heavy RH neutrino mass by the light neutrino mass using the type-I seesaw formula). The final

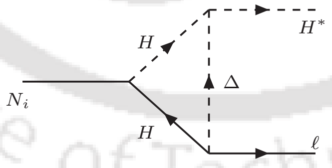

FIGURE 1.5: Feynman diagrams for decay of RH neutrinos into lepton and Higgs when scalar triplet is running in the loop. .

baryon asymmetry can be approximated as [11]

$$Y_B \approx 10^{-3} \sum_i \epsilon_i \eta_{ii}. \tag{1.78}$$

where η_{ii} is efficiency factor. It takes care of the possible washout effect which might wipe-out the produced asymmetry and can be obtained solving Boltzmann' equations [11, 110–113]. In Chapter 2, we study such a type-I seesaw scenario and discuss the relevance of flavor structures of the Yukawa coupling and nonzero θ_{13} in the lepton asymmetry parameter ϵ_i in details. Now if the RH neutrinos are nearly degenerate having mass differences comparable to their decay widths, the lepton asymmetry can be resonantly enhanced. This mechanism is known as resonant leptogenesis [114].

On the other hand, when both RH neutrino and scalar triplet (here we confine ourselves by considering only one triplet and hence one-loop self energy correction like diagram for scalar triplet is absent) are present, lepton asymmetry can be created from decay of RH neutrinos and/or scalar triplet [115]. In this case, the relevant tree level and one-loop higher order process are drawn in Fig. 1.5 and 1.6. Therefore when a single scalar triplet is involved, we have two different scenarios for generating the lepton asymmetry. First, when the RH Majorana neutrinos decay and heavy scalar triplet runs in the loop ($M_\Delta > M_R$). Second, when the single scalar triplet decays and heavy RH neutrinos runs in the loop ($M_\Delta > M_R$). In the first case, along with contribution from Fig. 1.4 additional contribution will be there due presence of the process as in Fig. 1.5. Whereas in the latter case, the lepton asymmetry is obtained due to interference of the tree level and one-loop vertex correction diagrams for decay of the scalar triplet as in Fig. 1.6. In Chapter 3, we explore one such case, where contributions form both decay of RH neutrinos and scalar triplets are important and study their effective contribution

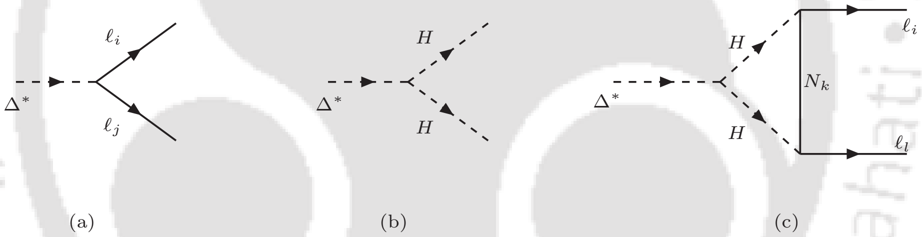

FIGURE 1.6: Feynman diagrams for decay of scalar triplet: (a), (b) tree level diagrams and (c) one-loop vertex correction diagram involving TH neutrinos in the loop. .

in lepton asymmetry in the proposed framework. Now, in an alternate scenario, instead of only one scalar triplet, if we introduce two scalar triplets (Δ_a, Δ_b), then leptogenesis from the decay of the scalar triplets is possible without involvement of RH neutrinos [116]. Here final lepton asymmetry is produced due to the interference between tree level and one-loop self energy contributions involving both Δ_a and Δ_b.

From the discussion presented in the previous section, it is now clear to us that there are several strong evidences and hints which motivates us to consider BSM scenarios to explain observed neutrino masses and mixing. Physics of neutrino mass brings neutrinos and quarks on equal footing, which can give a clue for the long standing flavor puzzle. CP violation in neutrinos sector and recently measured reactor mixing angle might play an instrumental role in cosmology. As shown in [132], the lepton asymmetry associated with a A_4 flavor structure indicating TBM mixing pattern is zero (or vanishingly small). Hence in this thesis with an attempt to realize deviation from TBM mixing would be natural to search for the possible generation of sizeable lepton asymmetry. In the proceeding chapters we present our attempts to explore such possibilities one by one, as Enrico Fermi once said, “It is no good to try to stop knowledge from going forward. Ignorance never is better than knowledge”.

Chapter 2

A_4 realization of type-I seesaw: Nonzero θ_{13} and leptogenesis

2.1 Introduction

In this chapter we aim to study lepton masses and mixing in a type-I seesaw based on A_4 discrete flavor symmetric scenario. We show that a minimal extension to the Altarelli-Feruglio (AF) [7] model, initially proposed to explain TBM mixing, helps deviating TBM mixing pattern and hence adequate θ_{13} of observed magnitude [5] can be generated. Interestingly, here we successfully constrain the Majorana phases from neutrino oscillation data and find a new sum rule for the light neutrinos. Further we show that a next-to-leading order contribution to the Yukawa coupling can generate the matter-antimatter asymmetry of the Universe and also study the of role Majorana phases and nonzero θ_{13} in this case. The analysis presented here is based on [117].

The measurement of non-vanishing value of the mixing angle θ_{13} from several experiments (Double Chooz[75], Daya Bay[76], RENO [78], T2K [81]), receives particular attention in these days since the precise determination of neutrino mixing would be crucial for better understanding the issues related to the flavor. In this context, it is important to study the neutrino mass matrix, m_ν, that can be structured from discrete flavor symmetry. The neutrino mass matrix m_ν, in general, can be diagonalized by the U_{PMNS} matrix (in the basis where charged leptons are diagonal) as

$$m_\nu = U^*_{PMNS} diag(m_1, m_2, m_3) U^\dagger_{PMNS}, \tag{2.1}$$

where m_1, m_2, m_3 are the real mass eigenvalues, U_{PMNS} is the unitary matrix which characterizes lepton mixing matrix involving three mixing angle θ_{12}, θ_{23}, θ_{13}, Dirac CP phase δ and two Majorana phases α_{21} and α_{31} as given in Eq. (1.44). Including θ_{13}, current status of all these parameters is summarized in Table 1.2. This clearly indicates a completely different pattern of mixing in the lepton sector compared to the quark sector (see Eq. 1.49 and Eq. (1.50)). Efforts therefore have been exercised for a long time in realizing the neutrino mixing pattern and among them patterns based on discrete flavor groups attract particular attention. A case of special mention is where $\sin^2\theta_{12} = 1/3$, $\sin^2\theta_{23} = 1/2$ along with $\sin\theta_{13} = 0$ resulted, called the tri-bimaximal (TBM) mixing pattern [6] and is given in Eq. 1.51. Note that all these mixing angles inclusive of vanishing θ_{13} were in the right ballpark of experimental findings before 2011. Many discrete groups have been employed [118] in realizing the TBM mixing pattern, and A_4 turned out to be a special one which can reproduce this pattern in a most economic way [7, 119, 120]. In this work, we mostly concentrate on Altarelli-Feruglio (AF) type of model [7] where the light neutrino masses are generated through type-I see-saw mechanism. So the right handed neutrinos (N^c) are introduced which transform as a triplet of A_4. Flavon fields transforming trivially and non-trivially under the A_4 are also introduced, whose vacuum expectation values break the A_4 flavor symmetry at some high scale. The framework is supersymmetric and based on the Standard Model gauge interactions. As it was argued in [7], the introduction of supersymmetry was instrumental to provide the correct vacuum alignment. Then the type-I see-saw leads to the TBM mixing in the light neutrinos while the charged lepton mass matrix is found to be diagonal.

However with the latest developments toward the nonzero value of θ_{13}, it is essential to modify the exact TBM pattern. Several attempts were made in this direction during last couple of years in the context of A_4-based flavor models [121–131]. It is to be noted from these analysis that inclusion of higher order terms only would not produce a sufficiently large θ_{13} as predicted by experiments. So a leading order deformation of the original A_4 model is required which we will study in this work.

Another important phenomenon that can not be realized in the context of the Standard Model is to explain the observed matter-antimatter asymmetry of the Universe.

However it is known that the standard weak interactions can lead to processes (mediated by sphaelerons) which can convert the baryons and leptons. So a baryon asymmetry can be effectively generated from a lepton asymmetry. The mechanism for generating the lepton asymmetry is called leptogenesis [11]. The discussion of it is of particular importance here, while explaining the generation of light neutrino mass through type-I see-saw mechanism. The inclusion of heavy right handed (RH) neutrinos in the framework provides the opportunity to discuss also the leptogenesis scenario through the CP-violating decay of it in the early Universe. Although the ingredients (RH neutrinos) are present, it is known that the see-saw models predicting the exact TBM structure can not generate the required lepton asymmetry [132], the reason being the term involved in the asymmetry related to the neutrino Yuwaka coupling matrix is proportional to the identity matrix and thus the lepton number asymmetry parameter vanishes. However it was shown in [132] that one can in principle consider higher dimensional operators in the neutrino Yukawa couplings of the model. The effect of this inclusion is to deviate the products of the Yukawa-terms in lepton asymmetry parameter from unity and thereby generating nonzero lepton asymmetry.

In this chapter, our aim is to produce nonzero θ_{13} as well as to realize leptogenesis in the same framework. We have extended the flavon-sector of AF [7] by introducing an extra flavon, ξ' which transforms as $1'$ under A_4. Similar sort of extensions have been considered in [122, 125]. However the analyses in those works are mostly related to the deviation over the final form of m_ν obtained from AF model, while here we consider modification of m_ν through the deviation from the RH neutrino mass matrix M_R. In [127, 133], a perturbative deviation from tri-bimaximal mixing is considered through M_R, though leptogenesis was not considered in that framework. This provides the opportunity to analyze M_R in detail and the effect on the Majorana phases can also be studied. Inclusion of Z_3 symmetry in the model forbids several unwanted terms and thus helps in constructing specific structure of the coupling matrices. While the charged lepton mass matrix is found to be in the diagonal form, the RH neutrino mass matrix has an additional structure originated from ξ'-related term. Due to this, the light neutrino diagonalizing matrix no longer remains in TBM form rather a deviation is resulted which leads to nonzero θ_{13}. In the RH neutrino mass matrix, three complex parameters a, b and d are present. We found that the low energy observables can be expressed in terms of two parameters $\lambda_1(=|d/a|)$, $\lambda_2(=|b/a|)$; relative phase between b and a (ϕ_{ba}) and $|a|$. The relative phase between d and a are assumed to be zero for simplicity. We have studied the dependence of θ_{13} on λ_1. The allowed range of θ_{13} restricts the range of the parameter space of λ_1. Then following the analysis [104], we are able to constrain also the Majorana phases (α_{21}, α_{31}) involved in the U_{PMNS} and study their dependence on the parameter λ_2 (for this we have fixed λ_1 to its value that corresponds to the best-fit value of $\sin^2\theta_{13}$) for both normal and inverted hierarchy cases. In this scenario, we obtain a general sum rule involving the light neutrino masses $m_{i=1,2,3}$ and the Majorana phases, α_{21}, α_{31}. The effective mass parameter involved in the neutrinoless double beta decay is also estimated. We then investigate the generation of lepton asymmetry from the decay of RH neutrinos within 'one flavor approximation' [104–107]. As previously stated, nonzero lepton asymmetry can be obtained once we include the next to leading order terms in the Yukawa sector. Note that this inclusion does not spoil the diagonal nature of charged lepton mass matrix. The explicit appearance of these Majorana phases in the CP-asymmetry parameter, ϵ_i, provides the possibility of studying the dependence of ϵ_i on λ_2. The expression of ϵ_i also involves the θ_{13} mixing angle in our set-up. Since θ_{13} depends on λ_1, we have also studied the variation of ϵ_i (or baryon asymmetry Y_B) against θ_{13} while λ_2 is fixed at a suitable value.

In section 2.2, we describe the structure of the model by specifying the fields involved and their transformation properties under the symmetries imposed. Then in section 2.3, we discuss the eigenvalues and phases involved in the RH neutrino sector. We also find the lepton mixing matrix and study the correlation between the mixing angles in terms of λ_1. Section 2.4 is devoted to study the Majorana phases, light neutrino masses, effective mass parameter involved in neutrinoless double beta decay. Leptogenesis is analysed in section 2.5 and following that, Chapter Summary in section 2.6.

2.2 Structure of The Model

We consider here an extension of the original Altarelli-Feruglio(AF) model [7] (with right-handed neutrinos) for generating lepton masses and mixing by introducing one additional flavon ξ' which transforms as $1'$ under A_4. We will find this modification turns out to be instrumental to have nonzero θ_{13}. The particle content and the symmetries of the model are provided in Table 2.1. The framework is supersymmetric and the gauge group is same as that of the Standard Model. All the left handed doublets $L_{i(=1,2,3)}$ transform as A_4 triplets, and the RH charged leptons e^c, μ^c, τ^c are A_4 singlets 1, $1''$, $1'$ respectively. In order to realize the type-I see-saw, three right handed neutrinos (N_i^c) are considered which are triplets of A_4. The flavor symmetry A_4 is accompanied by a discrete Z_3 symmetry, which forbids several unwanted terms. The A_4 multiplication rules are mentioned in Section 1.6. There are four flavons (ϕ_S, ϕ_T, ξ, ξ') in the model, which are SM gauge singlets. When the flavons (the scalar component of it) get vacuum expectation values (vev), $\langle\phi_S\rangle = (v_S, v_S, v_S)$, $\langle\phi_T\rangle = (v_T, 0, 0)$, $\langle\xi\rangle = u$, $\langle\xi'\rangle = u'$, the $A_4 \times Z_3$ symmetry is broken and generates the flavor structure of the sector. The fields ϕ_0^S, ϕ_0^T and ξ_0 are the driving fields, carrying two units of $U(1)_R$ charges, introduced to realize the vacuum alignments of the flavon fields, $\phi_S, \phi_T, \xi, \xi'$. Supersymmetry helps in realizing this vacuum alignment by setting the F-term to be zero. A brief discussion on the vacuum alignment is provided in appendix A. H_u and H_d are the two Higgs doublets present in the set-up transforming as singlets under A_4 with the vevs v_u and v_d respectively. With the above mentioned field configuration, the effective superpotential for the charged lepton sector contains the following terms in the leading order (LO),

	e^c	μ^c	τ^c	L_i	N_i^c	H_u	H_d	ϕ_S	ϕ_T	ξ	ξ'	ϕ_0^S	ϕ_0^T	ξ_0
A_4	1	$1''$	$1'$	3	3	1	1	3	3	1	$1'$	3	3	1
Z_3	ω	ω	ω	ω	ω^2	1	ω	ω^2	1	ω^2	ω^2	ω^2	1	ω^2
$U(1)_R$	1	1	1	1	1	0	0	0	0	0	0	2	2	2

TABLE 2.1: Fields content and transformation properties under the symmetries imposed on the model. Here ω is the third root of unity.

$$w_L = \left[y_e e^c(L\phi_T) + y_\mu \mu^c(L\phi_T)' + y_\tau \tau^c(L\phi_T)''\right]\left(\frac{H_d}{\Lambda}\right), \tag{2.2}$$

where Λ is the cut-off scale of the theory and y_e, y_μ, y_τ are the coupling constants. Terms in the first parenthesis represent products of two triplets (here L and ϕ_T for example) under A_4, each of these terms contracts with A_4 singlets 1, $1''$ and $1'$ corresponding to e^c, μ^c and τ^c respectively. Finally it sets the charged lepton coupling matrix as the diagonal one in the leading order,

$$Y_L = \frac{v_T}{\Lambda}\begin{bmatrix} y_e & 0 & 0 \\ 0 & y_\mu & 0 \\ 0 & 0 & y_\tau \end{bmatrix}, \tag{2.3}$$

once the flavon vevs as well as the Higgs vevs are inserted. The relative hierarchies between the charged leptons can be generated if one introduces global Froggatt-Nielsen ($U(1)_{FN}$)

flavor symmetry, under which RH charged leptons have different charges in addition to a FN field [82, 134].

In absence of the ξ' field, the neutrino sector would have the superpotential of the form

$$w_\nu = y(N^cL)H_u + x_A\xi(N^cN^c) + x_B(N^cN^c\phi_S), \tag{2.4}$$

which yields the Dirac (m_D) and Majorana (M_R) neutrino mass matrices at the LO as given by

$$m_D = yv_u \begin{bmatrix} 1 & 0 & 0 \\ 0 & 0 & 1 \\ 0 & 1 & 0 \end{bmatrix} \equiv Y_{\nu 0}v_u; \;\; M_R = \begin{bmatrix} a+2b/3 & -b/3 & -b/3 \\ -b/3 & 2b/3 & a-b/3 \\ -b/3 & a-b/3 & 2b/3 \end{bmatrix}, \tag{2.5}$$

where $a = 2x_Au, b = 2x_Bv_S$ and $Y_{\nu 0}$ can be taken as the LO neutrino Yukawa coupling matrix. Here y, x_A, and x_B are respective coupling constants. It has been known [7, 119, 120] that this kind of structure produces the exact TBM mixing, predicting $\theta_{13} = 0$. However in our setup, the inclusion of ξ' ensures the presence of another term in the superpotential w_ν, given by

$$x_N\xi'(N^cN^c), \tag{2.6}$$

at the LO, where x_N is another coupling constant. It introduces a modified Majorana mass matrix, compared to the one (M_R) in TBM case, having the form

$$M_{Rd} = \begin{bmatrix} a+2b/3 & -b/3 & -b/3 \\ -b/3 & 2b/3 & a-b/3 \\ -b/3 & a-b/3 & 2b/3 \end{bmatrix} + \begin{bmatrix} 0 & 0 & d \\ 0 & d & 0 \\ d & 0 & 0 \end{bmatrix}, \tag{2.7}$$

where $d = 2x_Nu'$. Since this additional term is also at the renormalizable level, we expect the term d to be of the order of a and b, in general. Inclusion of higher order terms in m_D would be very important in having leptogenesis as we will discuss it in section 2.5.

In general we expect the vevs of the flavon fields (v_S, v_T, u, u') are of same order of magnitude $\sim v$ (say). Therefore, the magnitude of light neutrino m_ν becomes $\sim (yv_u)^2/v$, generated through type-I see-saw mechanism. However there could be operators like $(LH_u)(LH_u)$, which can also contribute to the light neutrino mass. In our model such terms appear only in combination with ϕ_S, ξ and ξ' in quadrature $\left(LH_uLH_u\frac{1}{\Lambda^3}\left[\phi_S^2, \phi_S\xi, \phi_S\xi', \xi\xi', \xi'^2\right]\right)$, as LH_uLH_u is not an invariant under Z_3. Note that these terms contribute to the light neutrino mass of order $\frac{v_u^2}{v}\kappa^3$ where $\kappa = \frac{v}{\Lambda}\ell^{+}\ell^{-}1$. Hence they are relatively small compared to the neutrino mass generated from type-I see-saw by order of κ^3 with $y \sim \mathcal{O}(1)$ or so and therefore can be neglected in the subsequent analysis.

There are next-to-leading order (NLO) corrections present in the model which are suppressed by $1/\Lambda^n$ with $n \geq 1$. For the charged lepton, the leading order (LO) contribution $f^c(L\phi_T)\frac{H_d}{\Lambda}$ ($f^c = e^c, \tau^c, \mu^c$), is already $1/\Lambda$ suppressed. So possible NLO contributions are $f^c(L(\phi_T\phi_T)_A)\frac{H_d}{\Lambda^2}$ and $f^c(L(\phi_T\phi_T)_S)\frac{H_d}{\Lambda^2}$, where the suffixes A and S stand for anti-symmetric and symmetric triplet components from the product of two triplets in the first parenthesis under A_4. Now the first term essentially vanishes from the direction of vevs of ϕ_T and the contribution coming from the second term is again diagonal, similar to the one obtained from LO term. So a mere redefinition of y_e, y_μ, y_ν would keep the charged lepton matrix as a diagonal, even if NLO contributions are incorporated. This conclusion is in line of earlier observation [7, 132].

We could as well include higher order terms involving $1/\Lambda$ (which are allowed by all the symmetries imposed) to the neutrino Yukuwa coupling as $x_C(N^cL)_S\phi_T H_u/\Lambda + x_D(N^cL)_A\phi_T H_u/\Lambda$, with x_C and x_D as coupling constants. Therefore, at the next-to-leading order, the neutrino Yukuwa coupling matrix can be re-written as,

$$\begin{aligned} Y_\nu &= Y_{\nu 0} + \delta Y_\nu \\ &= y\begin{bmatrix} 1 & 0 & 0 \\ 0 & 0 & 1 \\ 0 & 1 & 0 \end{bmatrix} + \frac{x_C v_T}{\Lambda}\begin{bmatrix} 2 & 0 & 0 \\ 0 & 0 & -1 \\ 0 & -1 & 0 \end{bmatrix} + \frac{x_D v_T}{\Lambda}\begin{bmatrix} 0 & 0 & 0 \\ 0 & 0 & -1 \\ 0 & 1 & 0 \end{bmatrix}. \end{aligned} \tag{2.8}$$

This will not produce any significant effect on the light neutrino masses and mixing obtained through type-I see-saw mechanism primarily with leading order m_D and M_{Rd}, as those terms are suppressed by the cut-off scale Λ compared to the LO contribution. However these will have important role in leptogenesis, what we will discuss in section 2.5.

For RH Majorana neutrinos, the non-vanishing NLO corrections in the mass matrix arise from the following terms

$$\begin{aligned}\delta M_{Rd} &= C_1(N^cN^c)_S\phi_T\xi/\Lambda + C_2(N^cN^c)_A\phi_T\xi'/\Lambda + C_3(N^cN^c)(\phi_S\phi_T)/\Lambda \\ &+ C_4(N^cN^c)''(\phi_S\phi_T)'/\Lambda + C_5(N^cN^c)'(\phi_S\phi_T)''/\Lambda \\ &+ C_6(N^cN^c)_S(\phi_S\phi_T)_S/\Lambda + C_7(N^cN^c)_S(\phi_S\phi_T)_A/\Lambda. \end{aligned} \tag{2.9}$$

Here $C_{i=1,..,7}$ are the respective couplings and prefixes $'$ and $''$ correspond to the $1'$ and $1''$ singlets of A_4 produced from the multiplication of two triplets under A_4 within (...). Terms proportional to C_3 and C_4 can be absorbed in M_{Rd} and contributions from the remaining terms produce a deviation from M_{Rd} that can be written in a compact form as

$$\Delta M_{Rd} = \begin{bmatrix} 2X_D & X_B & -X_A \\ X_B & 2X_A & X_D \\ -X_A & X_D & X_B \end{bmatrix},$$

where $X_D = (3C_6v_s + C_7v_s + C_1u)\kappa$, $X_B = C_5v_s\kappa$ and $X_A = (2C_7v_s + C_2u_N)\kappa$. Almost similar type of conclusion was obtained in [104], apart from the fact that we have absorbed the term proportional to C_4 in LO contribution of M_{Rd} and a new contribution coming from C_2 (through ξ') is included in the definition of X_A.

2.3 Neutrino Masses and Mixing

Light neutrino mass matrix is obtained through the type-I see-saw mechanism as $m_\nu = m_D^TM^{-1}m_D$, where M is the Majorana mass matrix for RH neutrinos. Note that the Majorana mass matrix M, with the form M_R as in Eq.(2.5) (*i.e.* without ξ' field), can be diagonalized through $U_{TB}^TM_RU_{TB} = \text{diag}(M_{R1}e^{i\phi_1}, M_{R2}e^{i\phi_2}, M_{R3}e^{i\phi_3})$, where U_{TB} exhibits the TBM mixing pattern [6] (Eq. (1.51)) and $M_{R1,2,3}$ are given by $|b+a|$, $|a|$ and $|b-a|$ respectively. $\phi_{1,2,3}$ are the arguments of the eigenvalues respectively. It is found [127] that the light neutrino mass matrix m_ν $(= m_D^TM_R^{-1}m_D)$ in this case can also be diagonalized by a matrix U which is same as U_{TB} except the second and third rows of it are interchanged (apart from the phases involved), so as to have $U^Tm_\nu U = \text{diag}(m_1, m_2, m_3)$. The light neutrino mass eigenvalues m_i are given by $m_i = (yv_u)^2/M_{Ri}$, and they can be made real and positive since the phase of y can be absorbed due to redefinition of phases in lepton doublets and the phases ϕ_i can be included in the diagonal phase matrix of U. As previously discussed, this structure of M_R is not useful in explaining the nonzero θ_{13}, as seen while comparing the above form of U and U_{PMNS}. Since the measured value of θ_{13} is not very small, it is difficult to reconcile θ_{13} just by deforming m_ν from its above form with the introduction of small expansion parameter [135]. Rather we should have deformation parameter at the same order of the existing elements in m_ν. In our framework, we have introduced the ξ' field for this purpose.

2.3.1 RH Neutrinos

The new scalar singlet ξ' contributes to the heavy RH neutrino sector through the $x_N \xi'(N^c N^c)$ term and the Majorana neutrino mass matrix then takes the form of M_{Rd} as in Eq.(2.7). We note that after having a rotation by U_{TB}, the M_{Rd} takes the form as given by,

$$U_{TB}^T M_{Rd} U_{TB} = \begin{bmatrix} a+b-\frac{d}{2} & 0 & -\frac{\sqrt{3}}{2}d \\ 0 & a+d & 0 \\ -\frac{\sqrt{3}}{2}d & 0 & -a+b+\frac{d}{2} \end{bmatrix}. \tag{2.10}$$

Therefore a further rotation by U_1 (another unitary matrix) takes the matrix M_{Rd} to a diagonal one, $\text{diag}(M_1 e^{i\varphi_1}, M_2 e^{i\varphi_2}, M_3 e^{i\varphi_3}) = (U_{TB}U_1)^T M_{Rd} U_{TB} U_1$, where $M_{i=1,2,3}$ are given by,

$$M_1 = |b + \sqrt{a^2+d^2-ad}| = |a| \left| \lambda_2 e^{i\phi_{ba}} + \sqrt{1+\lambda_1^2 e^{2i\phi_{da}} - \lambda_1 e^{i\phi_{da}}} \right|, \tag{2.11}$$

$$M_2 = |a+d| = |a| \left| 1 + \lambda_1 e^{i\phi_{da}} \right|, \tag{2.12}$$

$$M_3 = |b - \sqrt{a^2+d^2-ad}| = |a| \left| \lambda_2 e^{i\phi_{ba}} - \sqrt{1+\lambda_1^2 e^{2i\phi_{da}} - \lambda_1 e^{i\phi_{da}}} \right|, \tag{2.13}$$

with $\lambda_1 = |d/a|$ and $\lambda_2 = |b/a|$. $\phi_{da} = \phi_d - \phi_a$ and $\phi_{ba} = \phi_b - \phi_a$ are the phase differences between (d,a) and (b,a) respectively. Phases associated with the above masses can be written as

$$\begin{aligned}
\varphi_1 &= \arg(b+\sqrt{a^2+d^2-ad}), && (2.14)\\
\varphi_2 &= \arg(a+d), && (2.15)\\
\varphi_3 &= \arg(b-\sqrt{a^2+d^2-ad}). && (2.16)
\end{aligned}$$

For simplicity, we will work with $\phi_{da}=0$. Hence above set of eigenvalues and phases can be rewritten as

$$\begin{aligned}
M_1 &= |a|\left|\lambda_2 e^{i\phi_{ba}}+\mathrm{K}\right| && \varphi_1=\arg(b+a\mathrm{K}), && (2.17)\\
M_2 &= |a|\,|1+\lambda_1| && \varphi_2=\arg(a+d), && (2.18)\\
M_3 &= |a|\left|\lambda_2 e^{i\phi_{ba}}-\mathrm{K}\right| && \varphi_3=\arg(b-a\mathrm{K}), && (2.19)
\end{aligned}$$

where $\mathrm{K}=\sqrt{1-\lambda_1+\lambda_1^2}$.

2.3.2 Light Neutrino Masses and Mixing Angles

Light neutrino masses obtained via type-I see-saw mechanism through $m_\nu = m_D^T M_{Rd}^{-1} m_D$ is now given by $m_D^T U_R U_m^* \left[\mathrm{diag}\left(M_1, M_2, M_3\right)\right]^{-1} U_m^* U_R^T m_D$ where $U_R = U_{TB}U_1$ and $U_m = \mathrm{diag}(e^{i\varphi_1/2}, e^{i\varphi_2/2}, e^{i\varphi_3/2})$. The special form of m_D (see in Eq.(2.5)) suggests that U_R, with the second and third rows interchanged, will be the diagonalizing matrix of the light neutrino mass matrix m_ν apart from the diagonal phase matrix. Since the charged lepton mass matrix is already diagonal, the lepton mixing matrix is given by [127]

$$U_\nu = \frac{m_D^T}{yv_u} U_{TB} U_1^* \mathrm{diag}(e^{i\varphi_1/2}, e^{i\varphi_2/2}, e^{i\varphi_3/2}), \tag{2.20}$$

so that $m_\nu = U_\nu^* \mathrm{diag}(m_i) U_\nu^\dagger$. Note that, the light neutrino masses $m_{1,2,3}$ (real and positive) are given by

$$m_i = \frac{(yv_u)^2}{M_i}, \tag{2.21}$$

where $M_{i=1,2,3}$ are taken from Eq.(2.17 - 2.19). We can now remove one common phase by setting $\varphi_1 = 0$. Hence, the final form of unitary matrix that diagonalizes m_ν is given by

$$U_\nu = \frac{m_D^T}{y v_u} U_{TB} \begin{bmatrix} \cos\theta & 0 & \sin\theta e^{-i\psi} \\ 0 & 1 & 0 \\ -\sin\theta e^{i\psi} & 0 & \cos\theta \end{bmatrix} \mathrm{diag}(1, e^{i\varphi_2/2}, e^{i\varphi_3/2}), \tag{2.22}$$

$$= \begin{bmatrix} \sqrt{\frac{2}{3}}\cos\theta & 1/\sqrt{3} & \sqrt{\frac{2}{3}}\sin\theta e^{-i\psi} \\ -\frac{\cos\theta}{\sqrt{6}} + \frac{\sin\theta}{\sqrt{2}} e^{i\psi} & 1/\sqrt{3} & -\frac{\cos\theta}{\sqrt{2}} - \frac{\sin\theta}{\sqrt{6}} e^{-i\psi} \\ -\frac{\cos\theta}{\sqrt{6}} - \frac{\sin\theta}{\sqrt{2}} e^{i\psi} & 1/\sqrt{3} & \frac{\cos\theta}{\sqrt{2}} - \frac{\sin\theta}{\sqrt{6}} e^{-i\psi} \end{bmatrix} \cdot \begin{bmatrix} 1 & 0 & 0 \\ 0 & e^{i\varphi_2/2} & 0 \\ 0 & 0 & e^{i\varphi_3/2} \end{bmatrix}, \tag{2.23}$$

where we have parametrized the extra U_1 matrix by θ and ψ and employed Eqs.(2.5) and (1.51). We identify the Majorana phases as

$$\varphi_2 = \alpha_{21} \quad \text{and} \quad \varphi_3 = \alpha_{31}. \tag{2.24}$$

In this type of model, using Eqs.(2.17 - 2.19) and Eq.(2.21) we find a general sum rule for light neutrino masses satisfying

$$\frac{1}{m_1} - \frac{2\mathrm{K} e^{i\alpha_{21}}}{m_2(1+\lambda_1)} = \frac{e^{i\alpha_{31}}}{m_3}. \tag{2.25}$$

Note that in the limit K→1 (*i.e.* with $\lambda_1 = 0$), the sum rule is reduced to the one found in [104, 136]. The Majorana phases α_{21} and α_{31} are therefore related to the light neutrino masses. They will play important role in leptogenesis, which we discuss in section 2.5. The sum rule may carry important consequence in neutrinoless double beta decay. A study with different sum rules in this direction can be found in [139].

The charged lepton mass-matrix being diagonal, the above form of U_ν leads to (see Eq. (1.44))

$$\sin\theta_{13} = \sqrt{\frac{2}{3}}\sin\theta, \qquad \delta = \psi; \tag{2.26}$$

$$\sin^2\theta_{12} = \frac{1}{3(1-\sin^2\theta_{13})} \quad \text{and} \quad \sin^2\theta_{23} = \frac{1}{2} + \frac{1}{\sqrt{2}}\sin\theta_{13}\cos\delta, \tag{2.27}$$

up to the order $\sin^2\theta_{13}$. The study of these correlations in presence of A_4 are available in the literature [127, 129, 140]. For rest of our analysis we will consider $\psi = 0$. The mixing angle θ is then given by

$$\tan 2\theta = \frac{\sqrt{3}\lambda_1}{(2-\lambda_1)}. \tag{2.28}$$

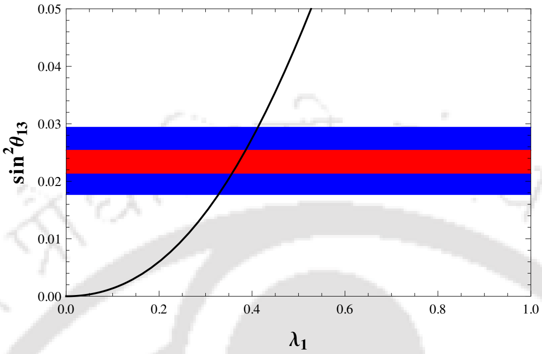

FIGURE 2.1: $\sin^2\theta_{13}$ vs λ_1 ($i.e.|d/a|$) plot. Horizontal blue shaded region stands for 3σ allowed range for $\sin^2\theta_{13}$ and the red shaded region inside represents 1σ range for $\sin^2\theta_{13}$ obtained from [5].

We have studied the variation of $\sin^2\theta_{13}$ against the parameter λ_1 in Fig.2.1, where the 1σ and 3σ allowed regions for $\sin^2\theta_{13}$ obtained from [5] are also indicated in the same by red and blue horizontal shaded regions respectively for both NH and IH. We observe that for NH, best fit [5] value of $\sin^2\theta_{13}$ (=0.0234) corresponds to $\lambda_1 = 0.37$ and that one for IH ($\sin^2\theta_{13}$ =0.024) corresponds to $\lambda_1 = 0.38$. We also note that the 3σ range of $\sin^2\theta_{13}$ covers a narrow interval of λ_1 that can be approximately expressed as $0.33 \lesssim \lambda_1 \lesssim 0.41$ as seen from Fig.2.1 for both NH and IH.

The other mixing angles θ_{12} and θ_{23} are also studied through the variation of $\sin^2\theta_{12}$ and $\sin^2\theta_{23}$ against λ_1, using Eq.(2.27). These findings are mentioned in Table 2.2 and they are well within the 3σ allowed regions of $\sin^2\theta_{12}$ and $\sin^2\theta_{23}$ [5]. So we conclude that this particular range of λ_1 ($0.33 \lesssim \lambda_1 \lesssim 0.41$) is consistent in producing all the three mixing angles successfully, and we will use this range of λ_1, while studying any other observables against λ_1 unless otherwise stated.

Range of λ_1 obtained from Fig.2.1	$\sin^2\theta_{12}$	$\sin^2\theta_{23}$
$0.36 \lesssim \lambda_1 \lesssim 0.39$	0.341-0.342	0.604-0.614
$0.33 \lesssim \lambda_1 \lesssim 0.41$	0.339-0.343	0.595-0.620

TABLE 2.2: Allowed regions of $\sin^2\theta_{12}$ and $\sin^2\theta_{23}$ for a restricted range of λ_1 (corresponding to Fig.2.1) in our set-up.

2.4 Constraints on parameters from neutrino oscillation data

Apart from λ_1, we have other parameters λ_2, $|a|$ and ϕ_{ba} (after setting $\phi_{da} = 0$) in the right handed neutrino sector. Note that λ_1, λ_2 and ϕ_{ba} can be constrained by neutrino oscillation data through the ratio of solar and atmospheric mass-squared differences ($\Delta m^2_\odot$ and $|\Delta m^2_A|$ respectively) defined by $r = \frac{\Delta m^2_\odot}{|\Delta m^2_A|}$ as exercised in [104, 136]. These mass-squared differences are defined as $\Delta m^2_\odot = \Delta m^2_{21} = m^2_2 - m^2_1$ and $|\Delta m^2_A| = |\Delta m^2_{31}| = m^2_3 - m^2_1 \approx |\Delta m^2_{32}| = m^2_3 - m^2_2$. Following [5], the best fit values of $\Delta m^2_\odot = 7.60 \times 10^{-5}\,\text{eV}^2$ (for both NH and IH) and $|\Delta m^2_A| = 2.48 \times 10^{-3}\,\text{eV}^2$ [NH] (and $|\Delta m^2_A| = 2.38 \times 10^{-3}\,\text{eV}^2$ [IH]) will be used in our analysis. Using Eqs.(2.17 - 2.19 and 2.21) we obtain r in terms of parameters involved in our framework as given by

$$r = \frac{[\lambda_2^2 + 2\lambda_2 \mathrm{K}\cos\phi_{ba} + \mathrm{K}^2 - (1+\lambda_1)^2](\lambda_2^2 - 2\lambda_2\mathrm{K}\cos\phi_{ba} + \mathrm{K}^2)}{4(1+\lambda_1)^2\lambda_2\mathrm{K}|\cos\phi_{ba}|}. \tag{2.29}$$

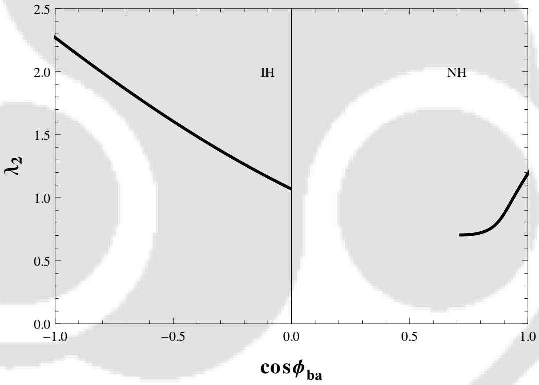

FIGURE 2.2: Variation of λ_2 with $\cos\phi_{ba}$. Here we have fixed λ_1=0.37 for NH and λ_1=0.38 for IH.

We recall that ϕ_{ba} is the relative phase between parameters b and a. Note that with $\lambda_1 = 0$, K becomes unity and the expression for r gets back the form in [136]. Considering $\lambda_1 < 1$ (as required for θ_{13} being in the acceptable range, see Fig.2.1) and as $\phi_{da} = 0$, K becomes real and considered to be positive. Then as is evident from Eq.(2.17 - 2.19) and Eq.(2.21), $\cos\phi_{ba} > 0$ for NH and $\cos\phi_{ba} < 0$ for IH. Using $r = 0.03$ [5], we can use Eq.(2.29) now to study the correlation between λ_2 and $\cos\phi_{ba}$ as shown in Fig.2.2. In doing so, we have set the value of λ_1 to be 0.37 (0.38) which corresponds to the best fit value of $\sin^2\theta_{13}$ for NH (IH) as stated before. Obviously the right panel of the plot corresponds to NH (as

$\cos\phi_{ba} > 0$) and left panel is for IH (as $\cos\phi_{ba} < 0$). We find that for NH, with $\lambda_1 = 0.37$, λ_2 is restricted to be in the range $0.71 - 1.2$ and for IH, with $\lambda_1 = 0.38$, λ_2 falls within[1] the range $1.1 - 2.3$. It will be further modified as we proceed after including the constraint on the sum of all the light neutrinos from the Planck data [12].

The light neutrino mass m_1 in this framework can be expressed as

$$m_1^2 = |\Delta m_A^2| r \frac{(1+\lambda_1)^2}{[\lambda_2^2 + 2\lambda_2 \mathrm{K}\cos\phi_{ba} + \mathrm{K}^2 - (1+\lambda_1)^2]}. \tag{2.30}$$

Now using the best fit value of $|\Delta m_A^2| = 2.48 \times 10^{-3}\mathrm{eV}^2$ [NH] ($2.38 \times 10^{-3}\mathrm{eV}^2$ [IH]), $r = 0.03$ and $\lambda_1 = 0.37$ (0.38), we can estimate m_1 from the above relation for NH (IH), shown in Fig.2.3, as a function of λ_2. Similarly m_2 and m_3 are also plotted in Fig.2.3.

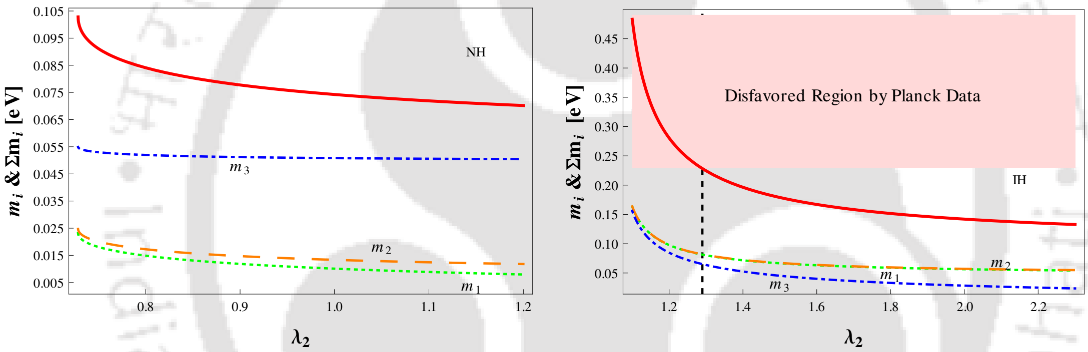

FIGURE 2.3: Light neutrino masses m_i's and their sum, $\sum m_i$, as a function of λ_2 for NH ($\lambda_1 = 0.37$) and IH ($\lambda_1 = 0.38$). Here in the right panel the shaded region indicates the disfavored values of $\sum m_i$. This makes allowed range for λ_2 more restricted for IH, indicated by the vertical black dashed line.

Note that in doing this, the correct sign of $\cos\phi_{ba}$ in Eq.(5.23) needs to be taken into account while NH and IH cases are considered. The lightest neutrino mass m_1 (m_3) falls in the range 0.008 eV $\lesssim m_1 \lesssim 0.02$ eV for NH (0.02 eV $\lesssim m_3 \lesssim 0.12$ eV for IH). In this plot we have also shown the sum of the light neutrino masses, $\sum m_i$. From Fig.2.3 , we conclude that it lies in the range 0.07 eV $\lesssim \sum m_i \lesssim 0.1$ eV for NH and 0.13 eV $\lesssim \sum m_i \lesssim 0.28$ eV for IH. The Planck data along with external CMB and BAO results [12] provide an upper bound as $\sum m_i \lesssim 0.23$ eV. Once this is considered, the range of $\sum m_i$ as obtained from our analysis for NH would not be affected. However in case of IH, it further restricts the range of λ_2 ($1.3 \lesssim \lambda_2 \lesssim 2.3$, indicated by vertical dashed line)

---

[1] Eq.(2.29) describes a quadratic equation of $|\cos\phi_{ba}|$ once other parameters are fixed. The range of λ_2 between 0 and 0.71 is excluded to keep the discriminant positive for λ_1=0.37 (for NH).

as observed from the shaded region of Fig.2.3, right panel. So the model's prediction for sum of all three light neutrino masses turns out to be,

$$0.07\ \text{eV} \lesssim \sum_{i=1}^{3} m_i \lesssim 0.1\ \text{eV}\,(\text{NH}) \;\;\&\;\; 0.13\ \text{eV} \lesssim \sum_{i=1}^{3} m_i \lesssim 0.23\ \text{eV}\,(\text{IH}). \tag{2.31}$$

In our analysis we can comment also on the relative magnitudes of heavy RH neutrinos. For NH we obtain $M_1 \simeq (1.1-1.5)M_2 \simeq (2.7-6.6)M_3$ and for IH we have $M_1 \simeq M_2 \simeq \frac{M_3}{1.2-2.3}$. So, in the present set-up Majorana neutrinos are not strongly hierarchical.

Two Majorana phases α_{21} and α_{31} can be investigated in the set-up in a similar way as done in [104]. Here in the model under consideration, we find Majorana phases α_{21} and α_{31} in terms of λ_1, λ_2 and ϕ_{ba} as given by

$$\tan\alpha_{21} = -\frac{\lambda_2 \sin\phi_{ba}}{\text{K} + \lambda_2\cos\phi_{ba}}, \tag{2.32}$$

$$\tan\alpha_{31} = \frac{2\text{K}\lambda_2 \sin\phi_{ba}}{\lambda_2^2 - \text{K}^2}. \tag{2.33}$$

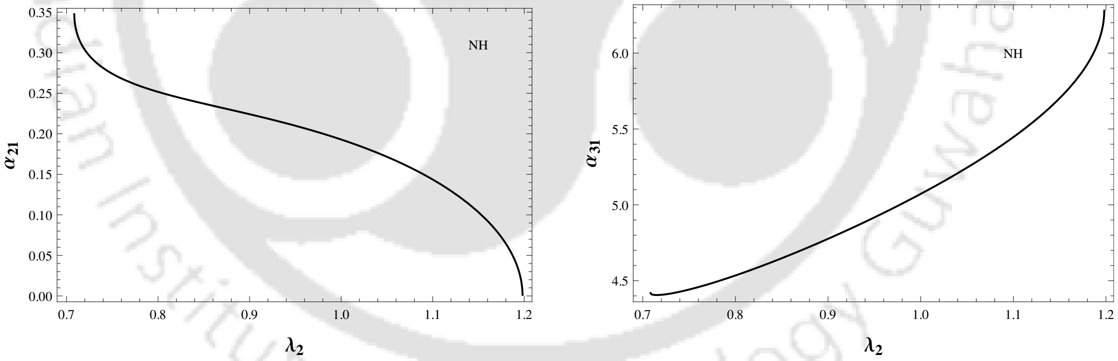

FIGURE 2.4: Variation of Majorana phases (α_{21}: left panel; α_{31}: right panel) with λ_2 for NH.

Note that there exists a relative sign between $\sin\alpha_{21}$ and $\sin\alpha_{31}$ as observed from the neutrino mass sum rule in Eq.(2.25). For NH, $\cos\phi_{ba} > 0$ as discussed before and $\sin\phi_{ba} < 0$ is considered in order to produce correct sign of baryon asymmetry [104]. Similarly, for IH we have $\cos\phi_{ba} < 0$ and $\sin\phi_{ba} < 0$. Taking all this into consideration, Eqs.(2.32) and (2.33) can successfully correlate Majorana phases (α_{21} and α_{31}) with parameters λ_1 and λ_2. We have plotted variation of α_{21} and α_{31} with λ_2 for both NH and IH in Fig.2.4 and

Fig.2.5 respectively. As before we have fixed $\lambda_1 = 0.37$ for NH ($\lambda_1 = 0.38$ for IH). This study of Majorana phases will be particularly useful when we will study the dependence of CP-violating parameter ϵ_i in our model on λ_2. Effective neutrino mass parameter, $|\langle m\rangle|$, is an important quantity which controls the neutrinoless double beta decay. In our model, the effective neutrino mass parameter is obtained as [53, 141]

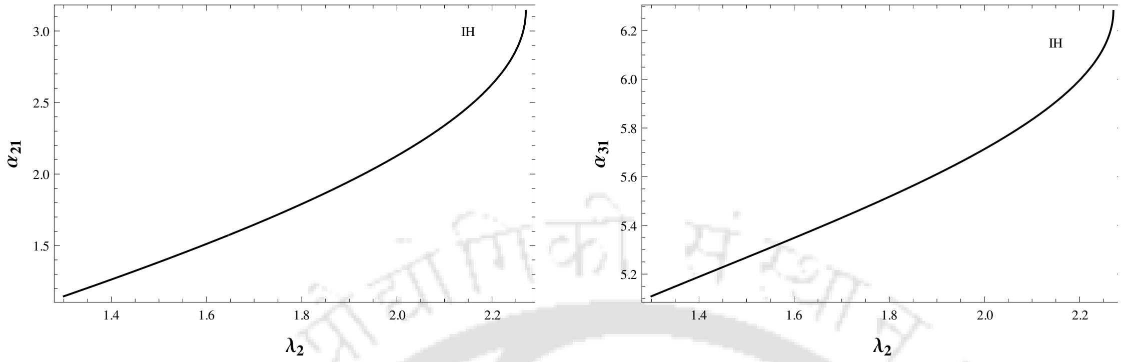

FIGURE 2.5: Variation of Majorana phases (α_{21}: left panel; α_{31}: right panel) with λ_2 for IH.

$$|\langle m\rangle| = \left|\frac{2}{3}m_1\cos^2\theta + \frac{1}{3}m_2 e^{i\alpha_{21}} + \frac{2}{3}m_3\sin^2\theta e^{i\alpha_{31}}\right|. \tag{2.34}$$

Since the dependence of m_i and $\alpha_{21,31}$ on λ_2 (for fixed λ_1) is known (from Fig.2.3, 2.4 and 2.5), we plot $|\langle m\rangle|$ as a function of λ_2 with $\lambda_1 = 0.37$ for NH and $\lambda_1 = 0.38$ for IH in Fig.2.6. We found the range for the $|\langle m\rangle|$ as 0.01 eV $< |\langle m\rangle| <$ 0.02 eV for NH and 0.015 eV $< |\langle m\rangle| <$ 0.067 eV for IH. The current upper limit on $|\langle m\rangle|$ however varies

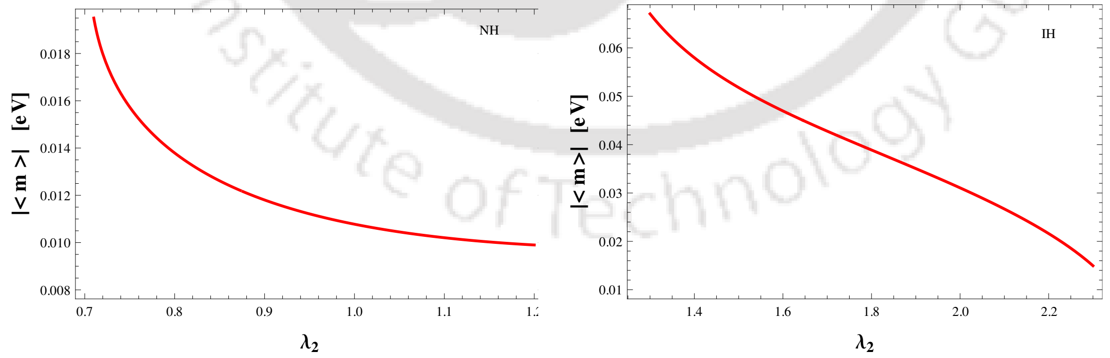

FIGURE 2.6: Variation of $|\langle m\rangle|$ with λ_2 for NH (left panel) and IH (right panel) respectively.

between 0.177 eV and 0.339 eV taking into account the different choices of nuclear matrix elements [142].

2.5 Leptogenesis

The presence of see-saw realization of light neutrino mass in the model under consideration gives the opportunity to study leptogenesis as the heavy RH neutrinos are already present in the model. It allows the generation of lepton asymmetry through the out-of-equilibrium decay of heavy RH neutrinos in the early Universe. This lepton asymmetry can be converted into baryon asymmetry of the Universe with the help of sphaleron process. With the consideration that the generation of lepton asymmetry happens at a temperature of the Universe $T \sim M_i \gtrsim (1+\tan^2\beta)10^{12}$ GeV (where $\tan\beta = v_u/v_d$), it does not distinguish between flavors, the so called 'one-flavor approximation' regime [104–107] is achieved. The CP-asymmetry generated by the out-of-equilibrium decay of each RH neutrinos (and sneutrinos) is given by [10, 108–113]

$$\epsilon_i = \frac{1}{8\pi}\sum_{j\neq i}\frac{\text{Im}\left[\left((\hat{Y}_\nu\hat{Y}_\nu^\dagger)_{ji}\right)^2\right]}{(\hat{Y}_\nu\hat{Y}_\nu^\dagger)_{ii}} f\left(\frac{m_i}{m_j}\right), \tag{2.35}$$

where $\hat{Y}_\nu$ is the effective Yukawa coupling matrix for neutrinos in the basis where RH neutrino mass matrix M_{Rd} is diagonal [2]. In the present set-up, $\hat{Y}_\nu = \text{diag}(1, e^{-i\alpha_{21}/2}, e^{-i\alpha_{31}/2})U_R^T Y_\nu$, where $U_R = U_{TB}U_1$. The loop factor $f(x)$ in the above expression (the model being supersymmetric) is defined as follows [113]

$$f(x) \equiv -x\left[\frac{2}{x^2-1} + \ln\left(1+\frac{1}{x^2}\right)\right], \tag{2.36}$$

with $x = m_i/m_j$. The total lepton asymmetry receives contribution from the decay of all three RH neutrinos (and sneutrinos).

It has been observed that at LO, (*i.e.* when $Y_\nu = Y_{\nu 0}$) product of the effective Yukawa coupling matrices $\hat{Y}_{\nu 0}\hat{Y}_{\nu 0}^\dagger$ is proportional to a unit matrix, hence lepton asymmetry parameter ϵ_i vanishes [132]. However considering NLO corrections to the Yukawa, we have

---

[2] Here Eq.(2.21) is used to express the loop factor f in terms of the ratio of light neutrino masses.

obtained Eq.(2.8). Therefore using Eq.(2.8), $\hat{Y}_\nu \hat{Y}_\nu^\dagger$ becomes

$$\hat{Y}_\nu \hat{Y}_\nu^\dagger = y^2\mathbf{I} + \begin{bmatrix} \cos 2\theta & \sqrt{2}e^{\frac{i\alpha_{21}}{2}} \cos\theta & e^{\frac{i\alpha_{31}}{2}} \sin 2\theta \\ \sqrt{2}e^{-\frac{i\alpha_{21}}{2}} \cos\theta & 0 & \sqrt{2}e^{\frac{i(\alpha_{31}-\alpha_{21})}{2}} \sin\theta \\ e^{\frac{-i\alpha_{31}}{2}} \sin 2\theta & \sqrt{2}e^{\frac{-i(\alpha_{31}-\alpha_{21})}{2}} \sin\theta & -\cos 2\theta \end{bmatrix} (2\mathrm{Re}(x_C)\kappa y) \tag{2.37}$$
$$+ \begin{bmatrix} -\frac{\sin 2\theta}{\sqrt{3}} & \sqrt{\frac{2}{3}}e^{i\frac{i\alpha_{21}}{2}} \sin\theta & \frac{1}{\sqrt{3}}e^{\frac{i\alpha_{31}}{2}} \cos 2\theta \\ \sqrt{\frac{2}{3}}e^{-i\frac{i\alpha_{21}}{2}} \sin\theta & 0 & -\sqrt{\frac{2}{3}}e^{\frac{i(\alpha_{31}-\alpha_{21})}{2}} \cos\theta \\ \frac{1}{\sqrt{3}}e^{\frac{-i\alpha_{31}}{2}} \cos 2\theta & -\sqrt{\frac{2}{3}}e^{\frac{-i(\alpha_{31}-\alpha_{21})}{2}} \cos\theta & \frac{1}{\sqrt{3}} \sin 2\theta \end{bmatrix} (2\mathrm{Re}(x_D)\kappa y)\,.$$

Note that having origin related to a NLO correction term, κ in general is expected to be small, $\kappa = v_T/\Lambda\ell^+\ell^-1$. Hence the expression of Eq. (2.37) is kept up to first order in κ. Finally in our framework the CP-asymmetry parameters corresponding to all three RH neutrinos, $\epsilon_{1,2,3}$ take the form as

$$\epsilon_1 = \frac{-\kappa^2}{2\pi}\left[\sin\alpha_{21}\left(2\mathrm{Re}(x_C)^2\cos^2\theta + \frac{2\mathrm{Re}(x_D)^2}{3}\sin^2\theta + \frac{2\mathrm{Re}(x_C)\mathrm{Re}(x_D)}{\sqrt{3}}\sin 2\theta\right) f\left(\frac{m_1}{m_2}\right)\right.$$
$$\left. + \sin\alpha_{31}\left(\mathrm{Re}(x_C)^2\sin^2 2\theta + \frac{\mathrm{Re}(x_D)^2}{3}\cos^2 2\theta + \frac{\mathrm{Re}(x_C)\mathrm{Re}(x_D)}{\sqrt{3}}\sin 4\theta\right) f\left(\frac{m_1}{m_3}\right)\right], \tag{2.38}$$

$$\epsilon_2 = \frac{\kappa^2}{2\pi}\left[\sin\alpha_{21}\left(2\mathrm{Re}(x_C)^2\cos^2\theta + \frac{2\mathrm{Re}(x_D)^2}{3}\sin^2\theta + \frac{2\mathrm{Re}(x_C)\mathrm{Re}(x_D)}{\sqrt{3}}\sin 2\theta\right) f\left(\frac{m_2}{m_1}\right)\right.$$
$$\left. - \sin(\alpha_{31}-\alpha_{21})\left(2\mathrm{Re}(x_C)^2\sin^2\theta + \frac{2\mathrm{Re}(x_D)^2}{3}\cos^2\theta - \frac{2\mathrm{Re}(x_C)\mathrm{Re}(x_D)}{\sqrt{3}}\sin 2\theta\right) f\left(\frac{m_2}{m_3}\right)\right], \tag{2.39}$$

$$\epsilon_3 = \frac{\kappa^2}{2\pi}\left[\sin\alpha_{31}\left(\mathrm{Re}(x_C)^2\sin^2 2\theta + \frac{\mathrm{Re}(x_D)^2}{3}\cos^2 2\theta + \frac{\mathrm{Re}(x_C)\mathrm{Re}(x_D)}{\sqrt{3}}\sin 4\theta\right) f\left(\frac{m_3}{m_1}\right)\right.$$
$$\left. + \sin(\alpha_{31}-\alpha_{21})\left(2\mathrm{Re}(x_C)^2\sin^2\theta + \frac{2\mathrm{Re}(x_D)^2}{3}\cos^2\theta - \frac{2\mathrm{Re}(x_C)\mathrm{Re}(x_D)}{\sqrt{3}}\sin 2\theta\right) f\left(\frac{m_3}{m_2}\right)\right]. \tag{2.40}$$

Lepton asymmetry in this scenario therefore depends on light neutrino masses m_i (through loop factor), Majorana phases $\alpha_{21,31}$, couplings $\mathrm{Re}(x_{C,D})$, κ (coming from the NLO correction terms in Yukawa) and interestingly on θ (and hence on λ_1). Recall that θ was originated from the deviation from the exact tri-bimaximal mixing and therefore leads to nonzero $\sin\theta_{13}$. We will come back to discuss it, before that let us discuss how this lepton asymmetry parameter is connected with observed baryon asymmetry of the Universe.

Lepton asymmetry can be linked to the baryon asymmetry [11, 143–145] as

$$Y_B = -1.48 \times 10^{-3} \sum_i \epsilon_i \eta_{ii}. \tag{2.41}$$

Here η_{ii} stands for the efficiency factor [113]. We consider the efficiency factor to be given by

$$\frac{1}{\eta_{ii}} \approx \frac{3.3 \times 10^{-3}\ \mathrm{eV}}{\tilde{m}_i} + \left(\frac{\tilde{m}_i}{0.55 \times 10^{-3}\ \mathrm{eV}}\right)^{1.16}, \tag{2.42}$$

with $\tilde{m}_i$ as the washout mass parameter, $\tilde{m}_i = \frac{(\hat{Y}_\nu \hat{Y}_\nu^\dagger)_{ii} v_u^2}{M_i} \simeq m_i$ to the leading order. The above expression is valid for $M_i < 10^{14}$ GeV [146]. This upper bound on M_i is also consistent in keeping the lepton number violating decays within the experimental limit[146, 147]. As we already have a lower bound on M_i from the 'one-flavor approximation', it turns out that low values of $\tan\beta$ are favored for this scenario to work[3]. Interestingly in [148], the authors have shown that if the scale of supersymmetry breaking (m_s) in MSSM is sufficiently large (say ~ 10 TeV or so) the low $\tan\beta$ region $\tan\beta \lesssim (3-5)$ is consistent with the results of LHC so far. Such large value of m_s on the other hand can in principle reduce the branching ratio for the LFV processes. However the details of this conjecture is beyond the scope of the present study.

2.5.1 Leptogenesis with fixed λ_1 and varying λ_2

In this section we will study the range of the parameters involved in Y_B expression so as to reproduce the correct amount of matter-antimatter asymmetry of the Universe. The observed value of Y_B is reported to be [92]

$$Y_B = (8.79 \pm 0.20) \times 10^{-11}. \tag{2.43}$$

As the efficiency factor (η_{ii}) is found to be $\sim \mathcal{O}(10^{-2})$, ϵ_i should be of order $\mathcal{O}(10^{-6})$ in order to reproduce the correct amount of baryon asymmetry of the Universe. As discussed earlier, we have kept λ_1 to be fixed at 0.37 for NH (0.38 for IH) which correspond to the best fit value of $\sin^2\theta_{13}$ [5]. We further note that the expression of Y_B involves θ which in tern is related to θ_{13}. So once λ_1 is fixed it would correspond to a particular value of θ. The expansion parameter $\kappa = v_T/\Lambda$ is taken to be $\sim 10^{-2}$. The variation of $\alpha_{21,31}$ and

---

[3] y is expected to be $\sim \mathcal{O}(10^{-1})$ in order to reproduce correct m_i for this range of M_i.

m_i's with λ_2 (for $\lambda_1 = 0.37$, 0.38 for NH and IH respectively) are already studied. Using those information, we can study the dependence of Y_B on λ_2 for fixed values of Re(x_C) and Re(x_D). The first bracketed expression in Eqs.(2.38 - 2.40) therefore serves merely as constant factor.

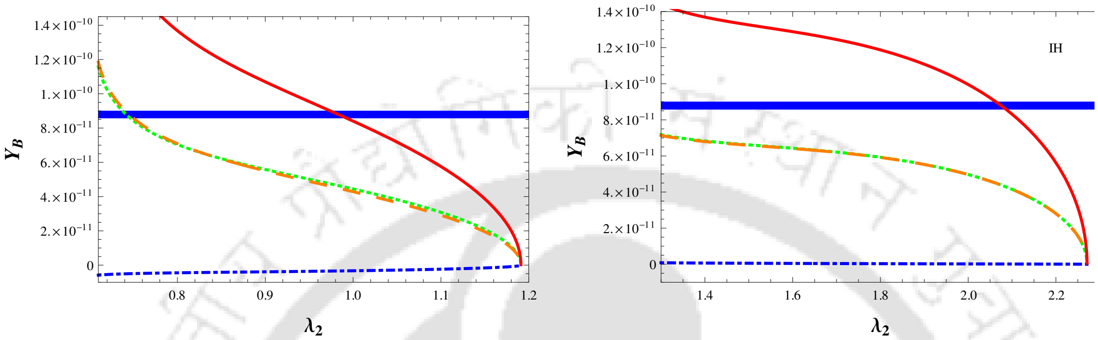

FIGURE 2.7: Baryon asymmetry of the Universe as function of λ_2 for NH (with $\lambda_1 = 0.37$, left panel) and IH (with $\lambda_1 = 0.38$, right panel). Here, red continuous line, orange large dashed line, green dotted line and blue dot-dashed line stand for total Y_B, $Y_{B1,2,3}$ respectively. The horizontal blue patch represents allowed range for total baryon asymmetry. For NH we have taken Re(x_C) = Re(x_D)=0.2 and for IH we have Re(x_C) = Re(x_D)=0.05. For both cases we have fixed κ at 0.01.

In Fig.2.7 (left panel), we have plotted total baryon asymmetry Y_B (red continuous line) along with individual $Y_{B1,2,3}$ (orange large dashed, green dotted and blue dot-dashed lines respectively) against λ_2 for Re(x_C)=Re(x_D) = 0.2 in case of NH. Note that the range of λ_2 $0.71 - 1.2$ for NH and $1.3 - 2.3$ for IH was already fixed (from Fig. 2.2 and 2.3) for $\lambda_1 = 0.37$ (for NH) and $\lambda_1 = 0.38$ (for IH) respectively. The relative sign between $\sin\alpha_{21}$ and $\sin\alpha_{31}$ is fixed from the sum rule, Eq.(2.25). Their dependence on λ_2 is depicted in Fig.2.4. In producing these plots, we recall that $\cos\phi_{ba} > 0$ for NH and $\cos\phi_{ba} < 0$ for IH. Also $\sin\phi_{ba} < 0$ is considered to produce correct sign of Y_B. In ϵ_1, $f(m_1/m_2)$ is of positive sign and remains dominant over $|f(m_1/m_3)|$ throughout the range of λ_2 by orders of magnitude. So an overall negative sign for ϵ_1 results when combined with $\sin\alpha_{21} > 0$ and $\sin\alpha_{31} < 0$ for the range of λ_2 inferred from Fig.2.7. Similar conclusion can be drawn for ϵ_2. In this case $f(m_2/m_1)$ is negative and its magnitude is sufficiently large compared to $|f(m_2/m_3)|$ so that differences between magnitude of $\sin\alpha_{21}$ and $\sin(\alpha_{31} - \alpha_{21})$ can not produce any sizable effect between the two terms (one is the set of terms proportional to $\sin\alpha_{21}$ and other is the similar set proportional to $\sin(\alpha_{31} - \alpha_{21})$) involved. So ϵ_2 is effectively dominated by the first term and overall it gives negative contribution. In ϵ_3, however both the terms involved contribute almost equally and overall ϵ_3 contributes with opposite sign (also seen in the Fig.2.7 terms of Y_{B3} which is negative, left panel) compared to $\epsilon_{1,2}$. As shown in Fig.2.7 (left panel), contribution from Y_{B3} is suppressed (and of opposite sign). This is due to the fact that the corresponding washout is larger though in magnitude $|\epsilon_3| \lesssim |\epsilon_{1,2}|$. A horizontal patch in Fig.2.7 is provided to indicate the allowed Y_B range [92]. It shows that for this specific choice of Re($x_{C,D}$)=0.2, correct amount of baryon asymmetry can be generated in our framework for $\lambda_2 \sim \mathcal{O}(1)$. Note that we can achieve this Y_B for not so large value of Re($x_{C,D}$) in comparison to the findings of [104]. To check the possible values of Re(x_C) and/or Re(x_D) we have drawn a contour plot in Fig.2.8 (left panel) between Re(x_D) and λ_2, while Re(x_C)=Re(x_D) is assumed as an example. The pattern of Y_B plot is also different from what was obtained in [104]. This is due to the involvement of nonzero θ.

In Fig.2.7 (right panel), we then plot Y_B, $Y_{B1,2,3}$ vs. λ_2 in case of IH with Re(x_C) = Re(x_D) = 0.05. As it was found in section 2.4, λ_2 ranges between 1.3 and 2.3 and $\cos\phi_{ba} < 0$ and $\sin\phi_{ba} < 0$ in this case. The Majorana CP-violating phases α_{21} and α_{31} are obtained in section 2.4 as function of λ_2 (see Fig.2.5, with $\lambda_1 = 0.38$). Here m_1 and m_2 are much closer to each other leading to large enhancement in the magnitude of loop factors $f(m_1/m_2)$ and $f(m_2/m_1)$. Their magnitudes are even larger than their counterpart in NH. Variation of these loop factors with λ_2 shows that $f(m_1/m_2) \simeq -f(m_2/m_1) gg f(m_3/m_{1,2})$ and $f(m_1/m_2) \simeq -f(m_2/m_1) gg -f(m_{2,1}/m_3)$. Overall nonzero CP-violating phases α_{21} and α_{31} are required to have leptogenesis but it appears that the final asymmetry is dominated by the loop factors. Though Y_{B1} and Y_{B2} face relatively large washout effect, still they generate sizable contribution and Y_{B3} gives sub-dominant contribution as shown in Fig.2.7. Here also we have plotted a contour between Re(x_D) and λ_2, assuming Re(x_C) = Re(x_D) with Y_B fixed at its central value, as shown in Fig.2.8 (right panel). We find that in this case, smaller values of Re(x_C) = Re(x_D) are favored compared to the ones in NH case.

Since the RH Majorana neutrino masses (in IH case particularly) are close to each other, we need to check the possibility of satisfying condition for resonant leptogenesis [114]. In our model, the quantity related to the mass degeneracy has been computed and found to be

$$\frac{M_2}{M_1} - 1 \approx (10^{-2} - 10^{-3}), \tag{2.44}$$

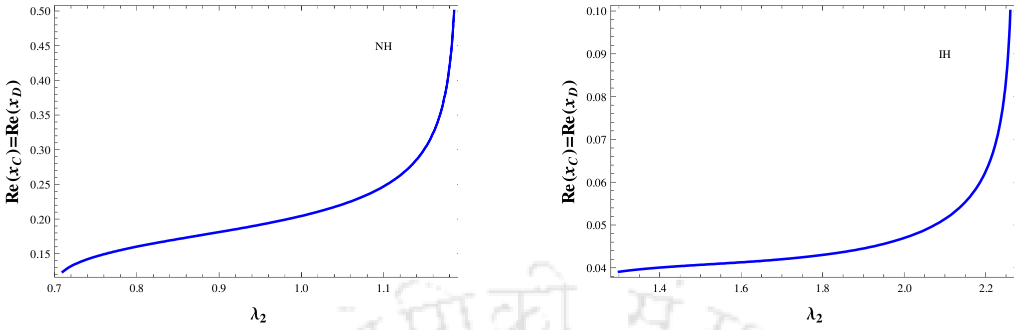

FIGURE 2.8: Contour plot of Re(x_C)(=Re(x_D)) and λ_2, with Y_B fixed at its central value.

after scanning over the full range of λ_2 ($1.3 \lesssim \lambda_2 \lesssim 2.3$). We find that the resonance condition,

$$\left|\frac{M_2}{M_1} - 1\right| \sim \left|\frac{\left(\hat{Y}_\nu \hat{Y}_\nu^\dagger\right)_{12}}{16\pi}\right|,$$

is not satisfied in our model. This is because the term in the right-hand-side of the resonance condition turns out to be of order $5 \times 10^{-2}\kappa y[\mathrm{Re}(x_C)\cos\theta + \mathrm{Re}(x_D)\sin\theta]$. As $\kappa \sim 10^{-2}$, $y \sim 10^{-1}$ and θ is expected to produce correct θ_{13},

$$\frac{\left(\hat{Y}_\nu \hat{Y}_\nu^\dagger\right)_{12}}{16\pi} \sim 10^{-5} - 10^{-6}.$$

Hence, in the present model, the resonant condition is not satisfied.

2.5.2 Leptogenesis with fixed λ_2 and varying λ_1

In this case we have taken a different approach by keeping λ_2 fixed at certain value, $\lambda_2 = 1$ for NH and $\lambda_2 = 2.1$ for IH [4]. Then we can study the variation of Y_B with λ_1. The range of λ_1 ($0.33 \lesssim \lambda_1 \lesssim 0.41$) is of course restricted from Fig.2.1 in section 2.3. By using Eq.(2.29) and taking $r = 0.03$, we can now investigate the variation of $\cos\phi_{ba}$ vs. λ_1. This is shown in Fig.2.9. We find that $\cos\phi_{ba}$ does not vary much with λ_1 in the specified range. Similar to the one discussed in section 2.4, we can also set the Majorana phases α_{21} and α_{31} as a function of λ_1 and finally we plot Y_B against $\sin^2\theta_{13}$ in Fig.2.10 as $\sin^2\theta_{13}$'s dependence on λ_1 is known. Note that, here also we have used the values $\mathrm{Re}(x_{C,D}) = 0.2$ for NH and

---

[4] From Fig.2.2 and Planck limit on $\sum m_i$, note that there is no such common value of λ_2 exists for which both NH and IH cases can be considered.

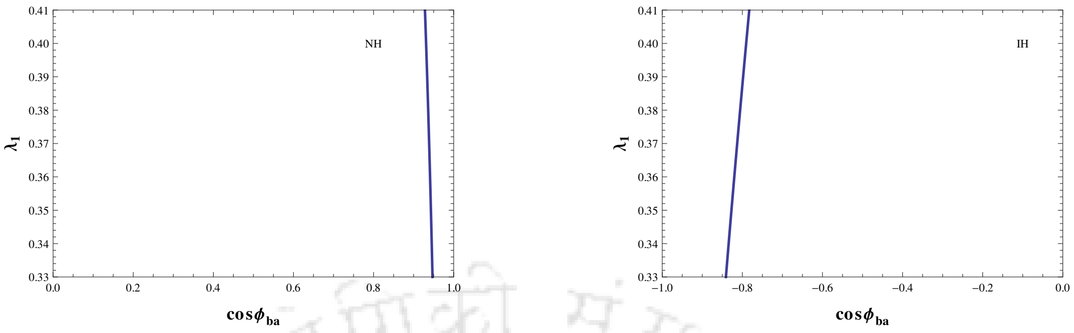

FIGURE 2.9: $\cos\phi_{ba}$ vs λ_1 for $\lambda_2 = 1$ NH and $\lambda_2 = 2.1$ for IH.

0.05 for IH as before. The maximum value of the effective neutrino mass parameter turns out to be $|\langle m\rangle| \sim 0.01$ eV for NH (0.025 eV for IH).

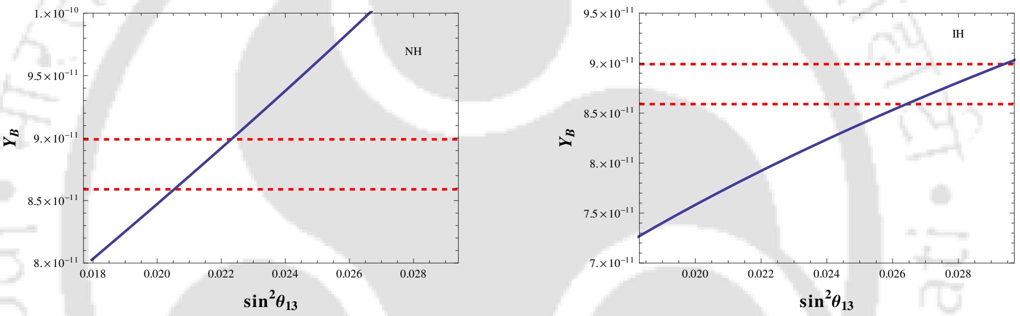

FIGURE 2.10: Baryon asymmetry Y_B vs $\sin^2\theta_{13}$ for NH (left panel) and IH (right panel). Here the region between horizontal dashed lines represent observed value for Y_B from [92].

2.6 Chapter Summary

In this Chapter, we have studied the generation of nonzero θ_{13} in a A_4 symmetric framework. For this, we have extended the particle content of the AF model by adding one flavon, ξ'. In doing so, we consider the generation of light neutrino masses and mixing through the type-I see-saw mechanism. The addition of ξ' leads to a deformed structure for the right handed neutrino mass matrix as compared to the one obtained in case of tri-bimaximal mixing pattern. The explicit structure of the right handed neutrino mass matrix as well as the neutrino Yukawa matrices dictated by the flavor symmetry imposed $(A_4 \times Z_3)$, helps in studying the mixing angles involved in the U_{PMNS} matrix. We find that our framework can reproduce all the mixing angles consistent with recent experimental findings for a restricted range of parameter space for λ_1 involved in the theory.

We find a modified sum rule for this particular set-up. Also the effective neutrino mass parameter $|\langle m\rangle|$ is studied. Since the structure of right handed neutrino sector is known, it also opens up the possibility to study leptogenesis in this framework and particularly the involvement of Majorana phases in the setup can be utilized. Following [104], we then study the Majorana phases α_{21} and α_{31} involved in U_{PMNS} and their dependence on parameter λ_2, while keeping λ_1 fixed at a value that could reproduce the best fit value of $\sin^2\theta_{13}$. This is done while constraints on neutrino parameters like the ratio of Δm^2_{21} and Δm^2_{31} is considered in conjugation with the sum rule obtained. It is known that this sort of model will not generate lepton asymmetry due to the special form of neutrino Yukawa matrix involved. The same conclusion holds here also and we need to consider the next-to-leading order effect to the neutrino Yukawa sector in order to realize nonzero lepton asymmetry. We have calculated the next-to-leading order terms in our setup and their involvement in the expression for the CP-asymmetry parameter ϵ_i. Then we have shown that within 'one flavor approximation', our setup is able to generate sufficient amount of lepton asymmetry through the decay of the right handed neutrinos (and sneutrinos) without assigning large values to the parameters involved. In obtaining this result, we fed the information obtained on the Majorana phases α_{21}, α_{31} as function of the parameters involved. As the baryon asymmetry can be linked with the generated lepton asymmetry finally we have studied the variation of baryon asymmetry parameter Y_B with λ_2. The effect of having nonzero θ_{13} is also studied.

It can also be noted that the framework restricts the RH neutrino masses in a narrow range between $(1+\tan^2\beta)10^{12}$ GeV and 10^{14} GeV as evident from the discussion below Eq.(2.42). This in turn can be used to estimate the scales involved in the theory. With our consideration that all the vevs of the new scalars involved in the set-up to be of similar order of magnitude, v, the RH neutrino masses are of order $M_i \sim 2xv$ as seen from Eq.(2.17-2.19). With coupling constants $x \sim \mathcal{O}(1)$, it further tells that v is of order 10^{13} GeV with $\tan\beta \sim 3$. Therefore the new flavons (whose masses are proportional to v as seen from Eq.(A.1)) are found to be as heavy as RH neutrinos, while the couplings involved are considered to be of order 1. So although the RH neutrinos have other interactions with the new scalars of the set-up (from Eq.(2.4)), its decay mode is essentially dominated by the Yukawa interactions with the lepton and higgs doublets only. This justifies our consideration of employing Eq.(2.35) which is the standard expression of leptogenesis for the decay of RH neutrinos through Yukawa interaction. Now, in order to produce correct amount of lepton asymmetry, we require to have $\kappa = \frac{v}{\Lambda}$ to be of order 10^{-2}. This value is also consistent with the tau lepton mass as appeared in Eq.(2.2) with the coupling $y_\tau \sim \mathcal{O}(1)$. This sets the typical value of the cut-off scale Λ to be 10^{15} GeV. The close proximity of Λ with the grand unification scale turns out to be an intriguing feature of the model.


भारतीय प्रौद्योगिकी संस्थान गुवाहाटी
Indian Institute of Technology Guwahati

Chapter 3

A_4 realization of type-II seesaw: a common origin for θ_{13}, Dirac CP phase and leptogenesis

3.1 Introduction

This chapter provides a possible interplay between the two terms of the general type-I+II seesaw formula, which leads to the generation of nonzero θ_{13}. The specific flavor structure of the model, guided by the $A_4 \times Z_4 \times Z_3$ symmetry and accompanied with the Standard Model singlet flavons, yields the conventional seesaw contribution to produce the TBM lepton mixing which is further corrected by the presence of the $SU(2)_L$ triplet contribution to accommodate θ_{13}. We consider the CP symmetry to be spontaneously broken by the complex vacuum expectation value (vev) of a singlet field S. While the magnitude of its complex vev is responsible for generating θ_{13}, its phase part induces the low energy CP violating phase (δ) and the CP violation required for leptogenesis. Hence the triplet contribution, although sub-dominant, plays crucial role in providing a common source for non-zero θ_{13}, δ and CP-violation required for leptogenesis. We also discuss the generation of lepton asymmetry in this scenario. The analysis presented here is based on [149].

CP violation in particle physics is an important phenomenon as it has a deep connection with the observed matter-antimatter asymmetry of the universe [93]. Along with this, CP violation is also related to our basic understanding of quark and lepton sector. CP violation in quark sector is a well established phenomenon [150–152] whereas we are yet to observe CP violation in lepton sector. Therefore it natural to ask the question: what would be the origin of CP violation? We first note that in a theory, CP can be violated in two ways: (a) explicit and (b) spontaneous. In SM explicit CP violation occurs due to the presence of complex Yukawa couplings in the Lagrangian. In an alternate scenario, where the original Lagrangian is CP symmetric, CP violation can be induced through spontaneous breaking by the vacuum. To realize spontaneous CP violation (SCPV), in the minimal extension, we can include complex scalar gauge singlet (say, S) which acquires complex by

$$\langle S \rangle = v_S e^{i\alpha_S}, \tag{3.1}$$

where v_S is the magnitude of the vev which can be much larger electroweak scale and α_S is a phase. Thus in such scenario SCPV can be achieved at a much larger scale. In literature, several BSM model of SCPV have proposed to find its connection with quark and lepton sector. Earlier it has been shown that the idea of SCPV [171] can be used to solve strong CP problem [172, 173]. Latter it has been successfully applied on models based on $SO(10)$[174, 175] and other extensions of Standard Model [176–178].

In the previous chapter, we have seen that Type-I seesaw mechanism [34–37] provides the simplest possibility by extending the SM with three RH neutrinos. An introduction of discrete symmetries into it may reveal the flavor structure of the neutrino and charged lepton mass matrix. For example, a type-I seesaw in conjugation with A_4 explains TBM lepton mixing pattern [6] in presence of SM singlet flavon (charged under A_4) fields which get vacuum expectation values (vev)[7, 119, 120]. However the original approach fails to accommodate the recent observation of non-zero θ_{13}[75, 76, 78, 81]. In Chapter 2, we have shown that an extension of the AF [7] by one additional flavon field can be employed to have a nonzero θ_{13} consistent with the present experimental results. The set-up also constraints the two Majorana phases involved in the lepton mixing matrix. The deviation of the TBM pattern is achieved through a deformation of the RH neutrino mass matrix compared to the original one. On the other hand, within the framework of a general type-I+II seesaw mechanism (where both RH neutrinos and $SU(2)_L$ triplet Higgs are present), light neutrino mass depends upon comparative magnitude of the pure type-I (mediated by heavy RH neutrinos) and triplet contributions. This interplay is well studied in the literature [153–162]. In recent years keeping in mind that θ_{13} is nonzero, efforts have been given to realize leptogenesis [163–169] and linking it with θ_{13} in models based on type-II seesaw[170].

In this chapter, we focus on the generation of light neutrino mass matrix through a type-II seesaw mechanism [40–43]. The fields content of the SM is extended with three right-handed neutrinos, one $SU(2)_L$ triplet and a set of SM singlet flavon fields. A flavor symmetry $A_4 \times Z_4 \times Z_3$ is considered. The type-II seesaw mechanism therefore consists of the conventional type-I seesaw contribution (m_ν^I) along with the triplet contribution (m_ν^{II}) to the neutrino mass matrix. Here we find the type-I contribution alone can generate the TBM mixing pattern, where the charged lepton mass matrix is a diagonal one. Then we have shown that the same flavor symmetry allows us to have a deviation from the conventional type-I contribution, triggered by the $SU(2)_L$ triplet's vev. We have found that this deviation is sufficient enough to keep θ_{13} at an acceptable level[5, 79, 80]. We mostly consider the triplet contribution to the light neutrino mass is subdominat compared to the conventional type-I contribution.

We further assume that apart from the flavons (SM singlets charged under A_4) involved, there is a A_4 singlet (as well as SM gauge singlet) field S, which gets a complex vacuum expectation value and thereby responsible for spontaneous CP violation at high scale [179–184]. All other flavons have real vevs and all the couplings involved are considered to be real. It turns out that the magnitude of this complex vacuum expectation value of S is responsible for the deviation of TBM by generating nonzero value of θ_{13} in the right ballpark. On the other hand, the phase associated with it generates the Dirac CP violating phase in the lepton sector. So in a way, the triplet contribution provides a unified source for CP violation and nonzero θ_{13}. In lepton sector, the other possibilities where CP violation can take place, involves complex vev of Higgs triplets[185, 186], or when a Higgs bi-doublet (particularly in left-right models) gets complex vev[187] or in a mixed situation [188–190]. However, we will concentrate in a situation where a scalar singlet S present in the theory gets complex vev as in [180]. We have also studied the lepton asymmetry production through the decay of the heavy triplet involved. The decay of the triplet into two leptons contributes to the asymmetry where the virtual RH neutrinos are involved in the loop. This process is effective when the triplet is lighter than all the RH neutrinos. It turns out that sufficient lepton asymmetry can be generated in this way. On the other hand if the triplet mass is heavier than the RH neutrino masses, the lightest RH neutrino may be responsible for producing lepton asymmetry where the virtual triplet is contributing in the one loop diagram.

In [180], authors investigated a scenario where the triplet vevs are the sole contribution to the light neutrino mass and a single source of spontaneous CP violation was considered. There, it was shown that the low energy CP violating phase and the CP violation required for leptogenesis both are governed by the argument of the complex vev of that scalar field. The nonzero value of θ_{13} however followed from a perturbative deformation of the vev alignment of the flavons involved. Here in our scenario, the TBM pattern is realized by the conventional type-I contribution. Therefore in the TBM limit, θ_{13} is zero in our set-up. Also there is no CP violating phase in this limit as all the flavons involved in m_ν^I are carrying real vevs, and hence no lepton asymmetry as well. Now once the triplet contribution (m_ν^{II}) is switched on, not only the θ_{13} , but also the leptonic CP violation turn out to be nonzero. For generating lepton asymmetry, two triplets were essential in [180], while we could explain the lepton asymmetry by a single triplet along with the presence of RH neutrinos. In this case, the RH neutrinos are heavier compared to the mass of the triplet involved.

The Chapter is organized as follows. In section 3.2, we describe the set-up of the model followed by constraining the parameter space of the framework from neutrino masses and mixing in section 3.3. In section 3.4, we describe how one can obtain lepton asymmetry out of this construction. Finally we conclude in section 3.5.

3.2 The Model

Our starting point is the conventional type-I seesaw mechanism to explain the smallness of light neutrino masses which further predicts a tribimaximal mixing (TBM) pattern in the lepton sector. For this part, we use the original AF model [7] by introducing a discrete A_4 symmetry and A_4 triplet flavon fields ϕ_S, ϕ_T along with a singlet ξ field. Of course three right handed neutrinos (N_R) are also incorporated. In addition, we include a $SU(2)_L$ triplet field (Δ) with hypercharge unity, the vev of which produces an additional contribution (hereafter called the triplet contribution) to the light neutrino mass. So our set-up basically involves a general type-II seesaw,

$$m_\nu = m_\nu^{II} + m_\nu^{I} = m_\nu^{II} - m_D^T M_R^{-1} m_D, \tag{3.2}$$

where m_ν^I is the typical type-I term and m_ν^{II} is the triplet contribution. To realize both, the relevant Lagrangian for generation of m_ν can be written as,

$$-\mathcal{L} = Y_D \bar{L}\widetilde{H} N_R + \frac{1}{2} M_R \overline{N_R^c} N_R + (Y_\Delta)_{ij} L_i^T C \Delta L_j, \tag{3.3}$$

so that $m_\nu^{II} = 2Y_\Delta u_\Delta$ and $m_D = Y_D v$, where u_Δ and v are the vevs of the triplet Δ and SM Higgs doublet (H) respectively. Y_D and Y_Δ correspond to the Yukawa matrices for the Dirac mass and triplet terms respectively, the flavor structure of which are solely determined by the discrete symmetries imposed on the fields involved in the model. M_R is the Majorana mass of the RH neutrinos. In the following subsection, we discuss in detail how the flavor structure of Y_D, Y_Δ and M_R are generated with the flavon fields. A discrete symmetry $Z_4 \times Z_3$ is also present in our model and two other SM singlet fields ξ' and S are introduced. These additional fields and the discrete symmetries considered play crucial role in realizing a typical structure of the triplet contribution to the light neutrino mass matrix as we will see below. Among all these scalar fields present, only the S field is assumed to have a complex vev while all other vevs are real. The framework is based on the SM gauge group extended with the $A_4 \times Z_4 \times Z_3$ symmetry. The field contents and charges under the symmetries imposed are provided in Table 3.1.

Field	e_R	μ_R	τ_R	L	N_R	H	Δ	ϕ_S	ϕ_T	ξ	ξ'	S
A_4	1	$1''$	$1'$	3	3	1	1	3	3	1	$1'$	1
Z_4	-1	-1	-1	i	i	1	$-i$	-1	$-i$	-1	i	-1
Z_3	ω	ω	ω	ω	ω	1	ω^2	ω	1	ω	ω^2	1

TABLE 3.1: Fields content and transformation properties under the symmetries imposed on the model.

With the above fields content, the charged lepton Lagrangian is described by,

$$\mathcal{L}_l = \frac{y_e}{\Lambda}(\bar{L}\phi_T)He_R + \frac{y_\mu}{\Lambda}(\bar{L}\phi_T)'H\mu_R + \frac{y_\tau}{\Lambda}(\bar{L}\phi_T)''H\tau_R, \tag{3.4}$$

to the leading order, where Λ is the cut-off scale of the theory and y_e, y_μ and y_τ are the respective coupling constants. Terms in the first parenthesis represent products of two A_4 triplets, which further contracts with A_4 singlets 1, $1''$ and $1'$ corresponding to e_R, μ_R

and τ_R respectively to make a true singlet under A_4. Once the flavons ϕ_S and ϕ_T get the vevs along a suitable direction as (u_S, u_S, u_S) and $(u_T, 0, 0)$ respectively[1], it leads to a diagonal mass matrix for charged leptons, once the Higgs vev v is inserted. Below we will first summarize how the TBM mixing is achieved followed by the triplet contribution in the next subsection. The requirement of introducing SM singlet fields will be explained subsequently while discussing the flavor structure of neutrino mass matrix in detail.

3.2.1 Type-I Seesaw and Tribimaximal Mixing

The relevant Lagrangian for the type-I seesaw in the neutrino sector is given by,

$$\mathcal{L}_{\mathcal{I}} = y\bar{L}\widetilde{H}N_R + x_A\xi\overline{N_R^c}N_R + x_B\phi_S\overline{N_R^c}N_R, \tag{3.5}$$

where y, x_A and x_B are the coupling constants. After the ξ and ϕ_S fields get vevs and the electroweak vev v is included, it yields the following flavor structure for Dirac (m_D) and Majorana (M_R) mass matrices,

$$m_D = Y_D v = yv\begin{pmatrix} 1 & 0 & 0 \\ 0 & 0 & 1 \\ 0 & 1 & 0 \end{pmatrix} \quad \text{and} \quad M_R = \begin{pmatrix} a+2b/3 & -b/3 & -b/3 \\ -b/3 & 2b/3 & a-b/3 \\ -b/3 & a-b/3 & 2b/3 \end{pmatrix}, \tag{3.6}$$

with $a = 2x_A\langle\xi\rangle = 2x_A u_\xi, b = 2x_B u_S$. The A_4 multiplication rules that results to this flavor structure can be found in [117]. Therefore the contribution toward light neutrino mass that results from the type-I seesaw mechanism is found to be,

$$\begin{aligned} m_\nu^I &= -m_D^T M_R^{-1} m_D, \\ &= -v^2y^2\begin{pmatrix} \frac{3a+b}{3a(a+b)} & \frac{b}{3a(a+b)} & \frac{b}{3a(a+b)} \\ \frac{b}{3a(a+b)} & -\frac{b(2a+b)}{3a(a^2-b^2)} & \frac{3a^2+ab-b^2}{3a(a^2-b^2)} \\ \frac{b}{3a(a+b)} & \frac{3a^2+ab-b^2}{3a(a^2-b^2)} & -\frac{b(2a+b)}{3a(a^2-b^2)} \end{pmatrix}. \end{aligned} \tag{3.7}$$

---

[1] The typical vev alignments of ϕ_S and ϕ_T are assumed here. We expect the minimization of the potential involving ϕ_S and ϕ_T can produce this by proper tuning of the parameters involved in the potential. However the very details of it are beyond the scope of this paper.

Now, we introduce two parameters $\alpha = b/a$ and $k = v^2y^2/a$ which are real and positive as they are part of the type-I contribution only. Therefore, Eq. (3.7) now takes the form

$$m_\nu^I = -k \begin{pmatrix} \frac{3+\alpha}{3(1+\alpha)} & \frac{\alpha}{3(1+\alpha)} & \frac{\alpha}{3(1+\alpha)} \\ \frac{\alpha}{3(1+\alpha)} & -\frac{\alpha(2+\alpha)}{3(1-\alpha^2)} & \frac{3+\alpha-\alpha^2}{3(1-\alpha^2)} \\ \frac{\alpha}{3(1+\alpha)} & \frac{3+\alpha-\alpha^2}{3(1-\alpha^2)} & -\frac{\alpha(2+\alpha)}{3(1-\alpha^2)} \end{pmatrix}. \tag{3.8}$$

Note that this form of m_ν^I indicates that the corresponding diagonalizing matrix would be nothing but the TBM matrix [6] of as given in Eq. (1.51).

As a characteristic of typical A_4 generated structure, the RH neutrinos mass matrix is as well diagonalized by the U_{TB}. In order to achieve the real and positive mass eigenvalues, the corresponding rotation U_R is provided on M_R as $U_R^T M_R U_R = M_R^{\text{diag}} = \text{diag}(a + b, a, a - b)$ with $U_R = U_{TB}\text{diag}(1, 1, e^{-i\pi/2})$ once $a > b$ is considered. On the other hand for $a < b$; through $U_R = U_{TB}$ itself, the real and positive eigenvalues of M_R $[M_R^{\text{diag}} = \text{diag}(a + b, a, b - a)]$ can be obtained. This would be useful when we will consider the decay of the RH neutrinos for leptogenesis in Section 3.4.

3.2.2 Triplet Contribution and Type-II seesaw

The leading order Lagrangian invariant under the symmetries imposed, that describes the triplet contribution to the light neutrino mass matrix (m_ν^{II}), is given by,

$$\mathcal{L}_{\mathcal{II}} = \frac{1}{\Lambda^2}\Delta L^T L(x_1 S + x_1' S^*)\xi', \tag{3.9}$$

where x_1 and x_1' are the couplings involved. Here ξ' develops a vev u_χ and the singlet S is having a complex vev $\langle S\rangle = v_S e^{i\alpha_S}$. As we have mentioned before, the vev of S provides the unique source of CP violation as all other vevs and couplings are assumed to be real. CP is therefore assumed to be conserved in all the terms involved in the Lagrangian. Similar to [180], CP is spontaneously broken by the complex vev of the S field. After plugging all these vevs, the above Lagrangian in Eq. (3.9) contributes to the following

Yukawa matrix for the triplet Δ as given by,

$$Y_\Delta = h \begin{pmatrix} 0 & 0 & 1 \\ 0 & 1 & 0 \\ 1 & 0 & 0 \end{pmatrix}, \quad h = \frac{1}{\Lambda^2} u \chi v_S (x_1 e^{i\alpha_S} + x_1' e^{-i\alpha_S}). \tag{3.10}$$

This specific structure follows from the A_4 charge assignments of various fields present in Eq. (3.9) and is instrumental in providing nonzero θ_{13} as we will see shortly.

Before discussing the vev of the Δ field, let us describe the complete scalar potential V, including the triplet Δ obeying the symmetries imposed, is given by,

$$V = V_S + V_H + V_\Delta + V_{SH} + V_{S\Delta} + V_{\Delta H}, \tag{3.11}$$

where

$$\begin{aligned} V_S &= \mu_S^2(S^2 + S^{*2}) + m_S^2 S^* S + \lambda_1(S^4 + S^{*4}) + \lambda_2 S^* S(S^2 + S^{*2}) + \lambda_3 (S^* S)^2, \\ V_H &= m_H^2 H^\dagger H + \lambda_4 (H^\dagger H)^2, \\ V_\Delta &= M_\Delta^2 \mathrm{Tr}(\Delta^\dagger \Delta) + \lambda_5 [\mathrm{Tr}(\Delta^\dagger \Delta)]^2, \\ V_{SH} &= \lambda_6 (S^* S) H^\dagger H + \lambda_7 (S^2 + S^{*2})(H^\dagger H), \\ V_{S\Delta} &= \mathrm{Tr}(\Delta^\dagger \Delta)[\lambda_8 (S^2 + S^{*2}) + \lambda_9 S^* S], \\ V_{\Delta H} &= \lambda_{10} (H^\dagger H) \mathrm{Tr}(\Delta^\dagger \Delta) + \lambda_{11} (H^\dagger \Delta^\dagger \Delta H) + \left(-\frac{\mu}{\Lambda} \widetilde{H}^T \Delta \widetilde{H} \phi_S \phi_T + h.c. \right). \end{aligned} \tag{3.12}$$

The above potential contains several dimensionful (denoted by $\mu_S, m_{S,H}, M_\Delta$) and dimensionless parameters (as $\lambda_{i=1,2,..11}$ and μ), which are all considered to be real. Similar to [180], here also it can be shown that the S field gets a complex vev for a choice of parameters involved in V_S as $m_S^2 < 0, \mu_S \simeq 0$ and $\lambda_3 > 2\lambda_1 > 0$. However contrary to [180], here we have only a single triplet field Δ. Once the ϕ_S, ϕ_T get vevs, the last term of $V_{\Delta H}$ results into an effective ΔHH interaction which would be important for leptogenesis. The vev of the triplet Δ is obtained by minimizing the relevant terms[2] from V after plugging the vevs of the flavons and is given by

$$\langle \Delta^0 \rangle \equiv u_\Delta = \eta \frac{v^2}{M_\Delta^2} \quad \text{and} \quad \eta = \frac{\mu}{\Lambda} u_S u_T. \tag{3.13}$$

---

[2] We consider couplings $\lambda_{8,9} << 1$.

Using Eqs.(3.10) and (3.13), the triplet contribution to the light neutrino mass matrix follows from the Lagrangian $\mathcal{L}_{\mathcal{II}}$ as

$$m_\nu^{II} = \begin{pmatrix} 0 & 0 & d \\ 0 & d & 0 \\ d & 0 & 0 \end{pmatrix}, \tag{3.14}$$

where

$$d = 2hu_\Delta = 2h\eta\frac{v^2}{M_\Delta^2}. \tag{3.15}$$

Note that only the triplet contribution (d) involves the phase due to the involvement of $\langle S \rangle$ in h, while the entire type-I contribution m_ν^I remains real. Therefore the term d serves as the unique source of generating all the CP-violating phases involved in neutrino as well as in lepton mixing. This will be clear once we discuss the neutrino mixing in the subsequent section. Now we can write down the entire contribution to the light neutrino mass as,

$$m_\nu = m_\nu^I + m_\nu^{II} = -k\begin{pmatrix} \frac{3+\alpha}{3(1+\alpha)} & \frac{\alpha}{3(1+\alpha)} & \frac{\alpha}{3(1+\alpha)} \\ \frac{\alpha}{3(1+\alpha)} & -\frac{\alpha(2+\alpha)}{3(1-\alpha^2)} & \frac{3+\alpha-\alpha^2}{3(1-\alpha^2)} \\ \frac{\alpha}{3(1+\alpha)} & \frac{3+\alpha-\alpha^2}{3(1-\alpha^2)} & -\frac{\alpha(2+\alpha)}{3(1-\alpha^2)} \end{pmatrix} + \begin{pmatrix} 0 & 0 & d \\ 0 & d & 0 \\ d & 0 & 0 \end{pmatrix}. \tag{3.16}$$

3.3 Constraining parameters from neutrino mixing

In this section, we discuss how the neutrino masses and mixing can be obtained from the m_ν mentioned above. Keeping in mind that m_ν^I can be diagonalized by U_{TB}, we first perform a rotation by U_{TB} on the explicit form of the light neutrino mass matrix obtained in Eq. (3.16) and the rotated m_ν is found to be

$$m_\nu' = U_{TB}^T m_\nu U_{TB} = \begin{pmatrix} -\frac{d}{2} - \frac{k}{(1+\alpha)} & 0 & \frac{\sqrt{3}d}{2} \\ 0 & d-k & 0 \\ \frac{\sqrt{3}d}{2} & 0 & \frac{d}{2} + \frac{k}{(1-\alpha)} \end{pmatrix}. \tag{3.17}$$

We note that a further rotation by U_1 (another unitary matrix) in the 13 plane in required to diagonalize the light neutrino mass matrix, $U_1^T m'_\nu U_1 = m_\nu^{\rm diag}$. With a form of U_1 as

$$U_1 = \begin{pmatrix} \cos\theta & 0 & \sin\theta e^{-i\psi} \\ 0 & 1 & 0 \\ -\sin\theta e^{i\psi} & 0 & \cos\theta \end{pmatrix}, \tag{3.18}$$

we have, $(U_{TB}U_1)^T m_\nu U_{TB} U_1 = {\rm diag}(m_1 e^{i\gamma_1}, m_2 e^{i\gamma_2}, m_3 e^{i\gamma_3})$, where $m_{i=1,2,3}$ are the real and positive eigenvalues and $\gamma_{i=1,2,3}$ are the phases associated to these mass eigenvalues. We can therefore extract the neutrino mixing matrix U_ν as,

$$U_\nu = U_{TB}U_1U_m = \begin{pmatrix} \sqrt{\frac{2}{3}}\cos\theta & \frac{1}{\sqrt{3}} & \sqrt{\frac{2}{3}}e^{-i\psi}\sin\theta \\ -\frac{\cos\theta}{\sqrt{6}} + \frac{e^{i\psi}\sin\theta}{\sqrt{2}} & \frac{1}{\sqrt{3}} & -\frac{\cos\theta}{\sqrt{2}} - \frac{e^{-i\psi}\sin\theta}{\sqrt{6}} \\ -\frac{\cos\theta}{\sqrt{6}} - \frac{e^{i\psi}\sin\theta}{\sqrt{2}} & \frac{1}{\sqrt{3}} & \frac{\cos\theta}{\sqrt{2}} - \frac{e^{-i\psi}\sin\theta}{\sqrt{6}} \end{pmatrix} U_m \tag{3.19}$$

where $U_m = {\rm diag}(1, e^{i\alpha_{21}/2}, e^{i\alpha_{31}/2})$ is the Majorana phase matrix with $\alpha_{21} = (\gamma_1 - \gamma_2)$ and $\alpha_{31} = (\gamma_1 - \gamma_3)$, one common phase being irrelevant. As the charged lepton mass matrix is a diagonal one, we can now compare this U_ν with the standard parametrization of lepton mixing matrix U_{PMNS}. The U_{PMNS} is therefore given by $U_{PMNS} = U_{\rm P}U_\nu$, where we need to multiply the U_ν matrix by a diagonal phase matrix $U_{\rm P}$ [127] from left as given by

$$U_P = {\rm diag}\left(1, 1 + \frac{i\sin\psi}{\cos\psi + \sqrt{3}\cot\theta}, 1 + \frac{i\sin\psi}{\cos\psi - \sqrt{3}\cot\theta}\right), \tag{3.20}$$

so that the U_{PMNS} excluding the Majorana phase matrix, can take the standard form where 23 and 33 elements are real as in Eq. (1.44). Hence we obtain the usual (in A_4 models) correlation [130] between the angles and CP violating Dirac phase δ as given by

$$\sin\theta_{13} = \sqrt{\frac{2}{3}}\,|\sin\theta|\,, \quad \sin^2\theta_{12} = \frac{1}{3(1 - \sin^2\theta_{13})}, \tag{3.21}$$

$$\sin^2\theta_{23} = \frac{1}{2} + \frac{1}{\sqrt{2}}\sin\theta_{13}\cos\delta, \quad \delta = \arg[(U_1)_{13}]. \tag{3.22}$$

The angle θ and phase ψ associated with U_1 can now be linked with the parameters involved in m_ν. For this we first rewrite the triplet contribution d as $d = |d|e^{i\phi_d}$ and define a parameter $\beta = |d|/k$ (hence β is real). This parameter indicates the relative size of the triplet contribution to the type-I contribution when $\alpha \leq 1$. As U_1 diagonalizes the m'_ν matrix, after some involved algebra, we finally get,

$$\tan 2\theta = \frac{\sqrt{3}}{\alpha}\frac{\left[1-\left(1-\alpha^2\right)\cos^2\phi_d\right]^{1/2}}{\frac{2}{\beta(1-\alpha^2)}+\cos\phi_d} \quad \text{and} \quad \tan\psi = (\tan\phi_d)/\alpha. \tag{3.23}$$

$\sin\theta$ may take positive or negative value depending on the choices of α, β as evident from the first relation in Eq. (3.23). For $\sin\theta > 0$, we find $\delta = \psi$ using $\delta = \arg[(U_1)_{13}$ and the second relation of Eq. (3.23).On the other hand for $\sin\theta < 0$; δ and ψ are related by $\delta = \psi \pm \pi$. Therefore in both these cases we obtain $\tan\psi = \tan\delta$ and hence

$$\tan\delta = (\tan\phi_d)/\alpha. \tag{3.24}$$

In our set-up, the source of this CP-violating Dirac phase δ is through the phase α_S associated with $\langle S\rangle$. Note that $\tan\delta$ is related with $\tan\phi_d$ and α as seen from Eq. (5.20). Now from the relation $d = |d|e^{i\phi_d}$ and using Eq. (3.10) and (3.15), we obtain ϕ_d satisfying

$$\tan\phi_d = \frac{(x_1 - x'_1)}{(x_1 + x'_1)}\tan\alpha_S, \tag{3.25}$$

where x_1 and x'_1 are the coupling involved in Eq. (3.9).

As seen from Eqs.(5.19) and (3.23), we conclude that the U_{PMNS} parameters θ_{13} and δ depend on the model parameters α, β and ϕ_d. Note that we expect terms a and b ($\alpha = b/a$) to be of similar order of magnitude as both originated from the tree level Lagrangian (see Eqs.(4.6) and (3.6)). We categorize $\alpha < 1$ as case A, while $\alpha > 1$ is with case B. The other parameter β basically represents the relative order of magnitude between the triplet contribution ($|d|$) and the type-I contribution (v^2y^2/a). Our framework produces the TBM mixing pattern to be generated solely by type-I seesaw and triplet contribution is present mainly to correct for the angle θ_{13} which is small compared to the other mixing angles. Therefore we consider that the triplet contribution is preferably the sub-dominant or at most comparable one. Therefore we expect the parameter β to be less than one.

Although we discuss what happens when $\beta > 1$ in some cases, we will restrict ourselves with $\beta < 1$ for the most of the analyses involved later in this work. In Fig.3.1 left panel, we study the variation of α and β in order to achieve the best fit value of $\sin^2\theta_{13} = 0.0234$ [5] while different values of δ are considered. In producing these plots, we have replaced

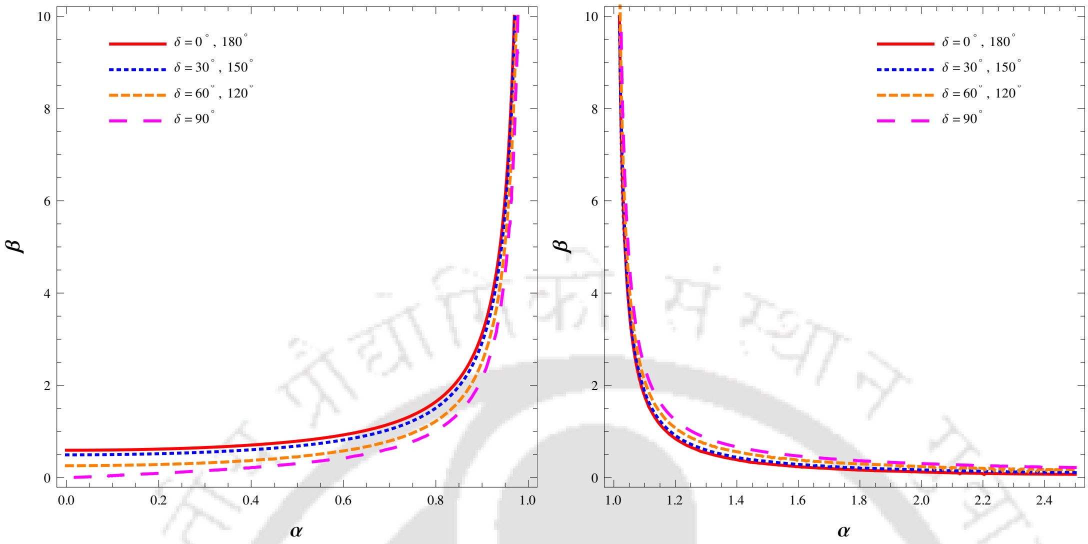

FIGURE 3.1: Contour plots for $\sin^2\theta_{13} = 0.0234$ in the $\alpha - \beta$ plane for various choices of δ as indicated inside the figure. Left panel is for (A) $\alpha < 1$ and right panel is with (B) $\alpha > 1$.

the ϕ_d dependence in terms of α and δ by employing the second equation in Eq. (3.23) as $\psi = \delta$. Similarly in the right panel of Fig.3.1, contour plots for $\sin^2\theta_{13} = 0.0234$ are depicted for $\alpha > 1$ with different values of δ. We find a typical contour plot for $\sin^2\theta_{13}$ with a specific δ value coincides with the one with other δ values obtained from $|\pi - \delta|$. For example, one particular contour plot for $\delta = 30^\circ$ is repeated for $\delta = 150^\circ, 210^\circ, 330^\circ$.

Diagonalizing m'_ν in Eq. (3.17), the light neutrino masses turn out to be,

$$m_1 = k\left[\left(\frac{\alpha}{\pm(1-\alpha^2)} - \frac{p}{k}\right)^2 + \left(\frac{q}{k}\right)^2\right]^{1/2}, \tag{3.26}$$

$$m_2 = k\left[1 + \beta^2 - 2\beta\cos\phi_d\right]^{1/2}, \tag{3.27}$$

$$m_3 = k\left[\left(\frac{\alpha}{\pm(1-\alpha^2)} + \frac{p}{k}\right)^2 + \left(\frac{q}{k}\right)^2\right]^{1/2}, \tag{3.28}$$

where p and q are defined as,

$$\left(\frac{p}{k}\right)^2 = \frac{1}{2}\left(\frac{A}{k^2} + \sqrt{\frac{A^2}{k^4} + \frac{B^2}{k^4}}\right) \quad , \quad \left(\frac{q}{k}\right)^2 = \frac{1}{2}\left(-\frac{A}{k^2} + \sqrt{\frac{A^2}{k^4} + \frac{B^2}{k^4}}\right); \tag{3.29}$$

$$\frac{A}{k^2} = \beta^2\cos 2\phi_d + \beta\frac{\cos\phi_d}{1-\alpha^2} + \frac{1}{(1-\alpha^2)^2} \quad , \quad \frac{B}{k^2} = \beta^2\sin 2\phi_d + \beta\frac{\sin\phi_d}{1-\alpha^2}. \tag{3.30}$$

The '+' sign in the expression of m_1 and m_3 is for $\alpha < 1$ (case A) where the '$-$' sign is associated with $\alpha > 1$ (case B). The Majorana phases in U_m (see Eq. (5.16)) are found to be

$$\alpha_{21} = \tan^{-1}\left[\frac{q/k}{p/k \pm \frac{\alpha}{(\alpha^2-1)}}\right] - \tan^{-1}\left[\frac{\beta\sin\phi_d}{\beta\cos\phi_d - 1}\right], \tag{3.31}$$

$$\alpha_{31} = \pi + \tan^{-1}\left[\frac{q/k}{p/k \pm \frac{\alpha}{(\alpha^2-1)}}\right] - \tan^{-1}\left[\frac{q/k}{p/k \pm \frac{\alpha}{(1-\alpha^2)}}\right]. \tag{3.32}$$

Note that the redefined parameters p/k and q/k are functions of α, β and ϕ_d, while the mass eigenvalues m_i, depend on k as well.

The parameters α, β and ϕ_d can now be constrained by the neutrino oscillation data. To have a more concrete discussion, we consider the ratio, r, defined by $r = \frac{\Delta m^2_\odot}{|\Delta m^2_{atm}|}$, with $\Delta m^2_\odot \equiv \Delta m^2_{21} = m_2^2 - m_1^2$ and $|\Delta m^2_{atm}| \equiv \Delta m^2_{31} = m_3^3 - m_1^2$ considering normal hierarchy. Following [5], the best fit values of $\Delta m^2_\odot = 7.6 \times 10^{-5}$ eV^2 and $|\Delta m^2_{atm}| = 2.48 \times 10^{-3}$ eV^2 are used for our analysis. Using Eqs.(5.23-5.25), we have an expression for r as,

$$r = \frac{\pm(1-\alpha^2)}{4\alpha}\frac{k}{p}\left[1 + \beta^2 - 2\beta\cos\phi_d - \left(\frac{\alpha}{\pm(1-\alpha^2)} - \frac{p}{k}\right)^2 - \left(\frac{q}{k}\right)^2\right]. \tag{3.33}$$

Here also, '+' corresponds to case A (*i.e.* with $\alpha < 1$) and '$-$' is for case B (*i.e.*, when $\alpha > 1$). Interestingly we note that r depends on α, β and ϕ_d. Therefore using this expression of r, we can now have a contour plot for $r = 0.03$ [4] in terms of α and β for specific choices of δ as we can replace the ϕ_d dependence in terms of α and δ through Eq. (5.20).For $\alpha < 1$, this is shown in Fig.3.2, left panel and a similar plot is made for $\alpha > 1$ in the right panel. Although we argue that it is more natural to consider β to be less than one, in this plot we allow larger values of β as a completeness. With this, for $\alpha < 1$ (case A) we see the appearance of two separate contours of $r = 0.03$ with $\delta = 30°$, one is for $\beta < 1$ and the other corresponds to $\beta > 1$. Similar plots are obtained for $\delta = 70°$ as well. However these isolated contours become a connected one once the value of δ increases, e.g. at $\delta = 80°$, it is shown in Fig.2, left panel. A similar pattern follows in case of $\alpha > 1$ case. Below we discuss the predictions of our model for case A (with $\alpha < 1$) and case B ($\alpha > 1$) separately.

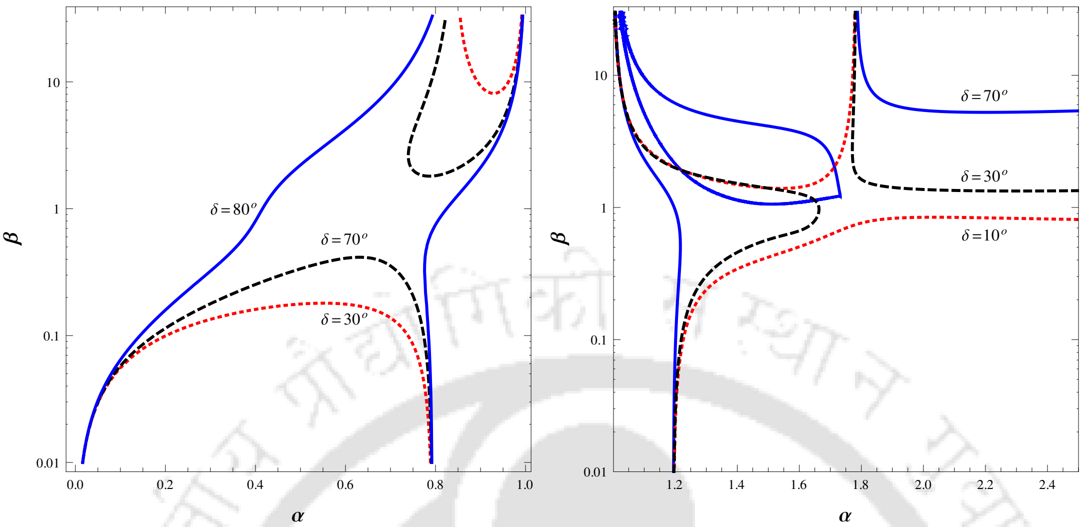

FIGURE 3.2: Contour plots for $r = 0.03$ are shown in the $\alpha - \beta$ plane for various choices of δ. Here, in the left panel (with $\alpha < 1$, case A) red (dotted), black (dashed) and blue (continuous) lines represent $\delta = 30°, 70°$ and $80°$ respectively. Similar contours are present for $|\pi - \delta|$ values of the CP violating Dirac phase. In the right panel (with $\alpha > 1$, case B) red (dotted), black (dashed) and blue (continuous) lines represent $\delta = 10°, 30°$ and $70°$ respectively.

3.3.1 Results for Case A

Note that we need to satisfy both the $\sin^2\theta_{13}$ as well as the value of r obtained from the neutrino oscillation experiments. For this reason, if we consider the two contour plots (one for $r = 0.03$ and the other for $\sin^2\theta_{13} = 0.0234$) together, then their intersection (denoted by $(\alpha,\ \beta)$) should indicate a simultaneous satisfaction of these experimental data for a specific choice of δ. This is exercised in Fig.3.3. In the left panel of Fig.3.3, contour plots of r and $\sin^2\theta_{13}$ are drawn in terms of α and β for two choices of δ= 20° and 40°. We find that there is no such solution for (α, β) which satisfy both r and $\sin^2\theta_{13}$ with $\alpha, \beta \lesssim 1$ in these cases. However there exists solution for α very close to one with a pretty large value of β as mentioned in Table 3. This solution as we expect is not a natural one, not only for a large value of β, but also for its very fine tuned situation. Note that α requires to be sufficiently close (and hence finely tuned) to one in this case. This situation can be understood from the fact that β being quite large (gg1), value of α has to be adjusted enough (see the involvement of the expression $\alpha/(1-\alpha^2)$ in Eq. (3.33)) so as to compete with the β dependent terms to get $r \sim 0.03$. Similarly variation of $\sin^2\theta_{13}$ is very sharp with respect to α (when close to 1) for large β. For example, a small change in α values

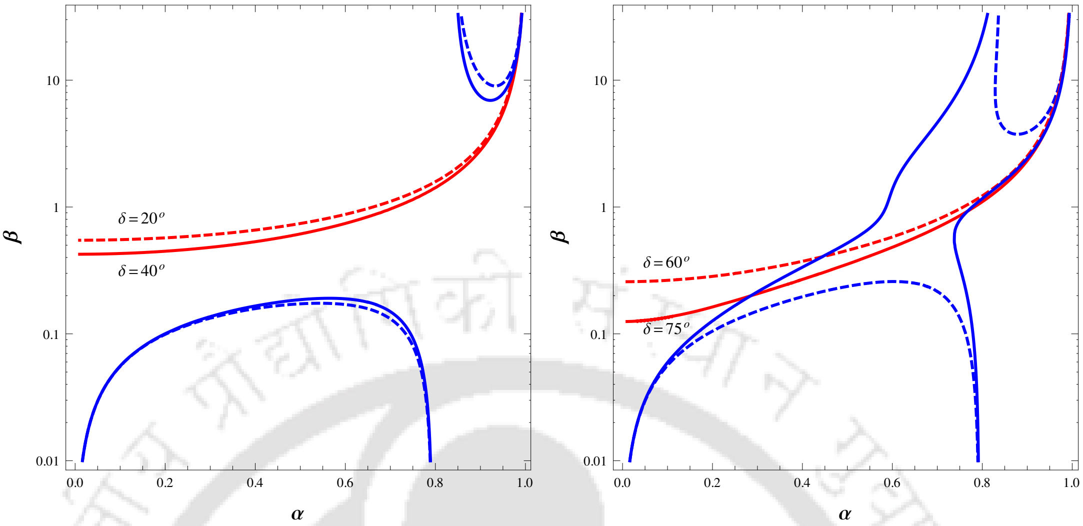

FIGURE 3.3: Contour plots for both $\sin^2\theta_{13} = 0.0234$ (shown in red-dashed and red-continuous lines) and $r = 0.03$ (shown in blue-dashed and blue-continuous lines) in the $\alpha - \beta$ plane for various choices of δ with $\alpha < 1$. In the left panel, dashed and continuous lines represent $\delta = 20°$ and $40°$ respectively, while in the right panel, dashed and continuous lines represent contour plots for $\delta = 60°$ and $75°$ respectively.

($\sim$ 1%) would induce a change in $\sin^2\theta_{13}$ by an amount of 15% near the intersection region.

However the situation changes dramatically as we proceed for higher values of δ as can be seen from Fig.3.3, right panel. This figure is for two choices of δ= 60° and 75°. We observe that with the increase of δ, the upper contour for r is extended toward downward direction and the lower one is pushed up, thereby providing a greater chance to have an intersection with the $\sin^2\theta_{13}$ contour. We also note that the portion of $\sin^2\theta_{13}$ contour for $\alpha < 1$ prefers a region with relatively small value of $\beta(< 1)$ as well. However a typical solution with both α and $\beta < 1$ appears when δ is closer to 75°. With this δ, we could see the lower and upper contours open up to form a connected one and we can have a solution for $(\alpha, \beta) \equiv (0.29, 0.2)$. In this case, there is one more intersection between the r and $\sin^2\theta_{13}$ contours with $\alpha, \beta < 1$ as given by (0.77, 0.93). When δ approaches 80° and up (till $\pi/2$) we have have solutions with $\alpha, \beta < 1$.

We have scanned the entire range of δ, from 0 to 2π and listed our findings in Table 3.2. For the δ values, we denote inside the first bracket those values of δ, for which the same set of solution points (α, β) are obtained. This is due to the fact that corresponding

δ	α	β	$\sum m_i$(eV)
$20^\circ(160^\circ, 200^\circ, 340^\circ)$	0.99	28.26	0.0714
$40^\circ(140^\circ, 220^\circ, 320^\circ)$	0.99	20.94	0.0709
$60^\circ(120^\circ, 240^\circ, 300^\circ)$	0.98	11.16	0.0701
$75^\circ(105^\circ, 255^\circ, 285^\circ)$	0.94 0.77 0.29	3.70 0.93 0.20	0.0691 0.0734 0.1333
$80^\circ(100^\circ, 260^\circ, 280^\circ)$	0.16	0.11	0.1835
$82^\circ(98^\circ, 262^\circ, 278^\circ)$	0.12	0.09	0.2137
$85^\circ(95^\circ, 265^\circ, 275^\circ)$	0.07	0.05	0.2827

TABLE 3.2: α, β values at the intersection points of the r and $\sin^2\theta_{13}$ contour plots are provided corresponding to different δ values. The sum of the light neutrino masses are also indicated in each case.

to a r or $\sin^2\theta_{13}$ contour plot for a typical δ between 0 and 2π, the same plot is also obtained for other $|\pi - \delta|$ values. Accepting the solutions for which $\alpha, \beta < 1$ (i.e. those are not fine tuned with large β), we find that the our setup then predicts an acceptable range of CP violating Dirac phase δ to be between $72^\circ - 82^\circ$, while the first quadrant is considered. For the whole range of δ between 0 and 2π, the allowed range therefore covers $72^\circ - 82^\circ$, $98^\circ - 108^\circ$, $252^\circ - 262^\circ$, $278^\circ - 288^\circ$. Note that δ between 83° and 90° (similarly regions of δ in other quadrants also) is ruled out from the constraints on the sum of the light neutrino mass mentioned in Table3.2. We will discuss about it shortly. Also the values of δs like 0, π, 2π are disallowed in our setup as they would not produce any CP violation which is the starting point of our scenario. Again $\delta = \pi/2, 3\pi/2$ are not favored as we have not obtained any solution of α, β that satisfied both r and $\sin^2\theta_{13}$. The same is true for the case with $\alpha > 1$.

We will now proceed to discuss the prediction of the model for the light neutrino masses and other relevant quantities in terms of the parameters involved in the set-up. For this, from now onward, we stick to the choice of $\delta = 80^\circ (\equiv 100^\circ, 260^\circ, 280^\circ)$ as a reference value for the Dirac CP violating phase. The r and $\sin^2\theta_{13}$ contours for this particular δ is shown separately in Fig.(3.4), left panel. In Fig.(3.4) right panel we put the $\sin^2\theta_{13}$ contours corresponding to the upper and lower values (detonated by red dotted lines) those are allowed by the 3σ range of $\sin^2\theta_{13}$. Only a section of r contour is also incorporated which encompasses the (α, β) solution points. This plot provides a range for (α, β) once the 3σ patch of $\sin^2\theta_{13}$ are considered. It starts from a set of values $(\sim 0.13, 0.09)$ (can be called a reference point P1) upto $(\sim 0.18, 0.14)$ (another reference

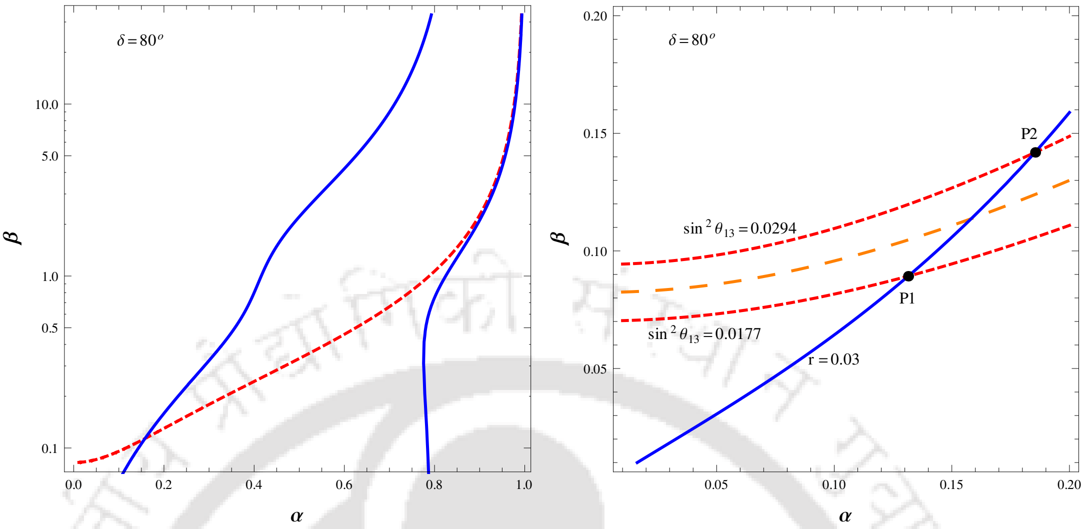

FIGURE 3.4: Left panel contains contour plots for best-fit values of r (indicated by blue-continuous lines) and $\sin^2\theta_{13}$ (indicated by red-dashed line) for $\delta = 80°$ in α-β plane with $\alpha < 1$. The right panel is for contour plot of r with its best fit value $r = 0.03$ (shown in blue-continuous line) and 3σ range of $\sin^2\theta_{13}$ (denoted by two red-dashed lines) along with the $\sin^2\theta_{12} = 0.0234$ contour (denoted by orange large-dashed line).

point P2). Note that there is always a one-to-one correspondence between the values of α and β, which falls on the line of r contour.

We have already noted that in the expression for r, parameters α, β and ϕ_d are present. Once we choose a specific δ, automatically it boils down to find α and β from Eq. (3.33). Although r is the ratio between $\Delta m^2_\odot$ and $|\Delta m^2_{atm}|$, we must also satisfy the mass-squared differences $\Delta m^2_\odot$ as well as $|\Delta m^2_{atm}|$ independently. For that we need to determine the value of the k parameter itself apart from its involvement in the ratio $\beta = |d|/k$ as evident from Eq. (5.23)-(5.25). For this purpose, with $\delta = 80°$ while moving from P1 to P2 along the r contour in the right panel of Fig.3.4, we find the values of α and correspondingly β which produce $r = 0.03$. Now using these values of (α, β), we can evaluate the values of k for each such set which satisfies $\Delta m^2_\odot = 7.6 \times 10^{-5}\text{eV}^2$. To obtain these values of k corresponding to (α, β) set, we employ Eqs.(5.23-5.24). The result is reflected in left panel of Fig.3.5, where we plot the required value of k in terms of its variation with α. In producing the plot, only a narrow range of α is considered which corresponds to the 3σ variation of $\sin^2\theta_{13}$ as obtained from Fig.(3.4), right panel (*i.e.* from P1 to P2). Although we plot it against α, each value of α is therefore accompanied by a unique value of β, as we just explain. Once the variation of k in terms of α is known, we plot the

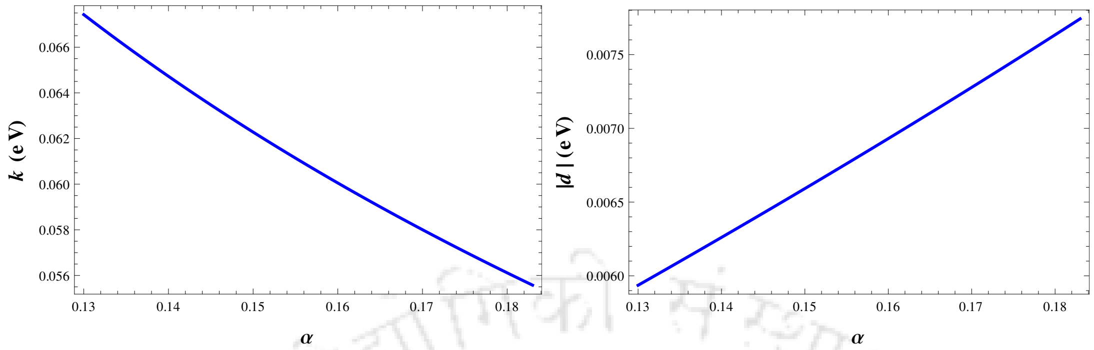

FIGURE 3.5: k vs α (left-panel) and $|d|$ vs α (right-panel) for $\delta = 80^\circ (\equiv 100^\circ, 260^\circ, 280^\circ)$.

variation of $|d|$ ($\beta = \beta k$) with α in Fig.3.5, right panel. Having the correlation between α and other parameters like β, k for a specific choice of δ is known, we are able to plot the individual light neutrino masses using Eqs.(5.23-5.25). This is done in Fig.3.6. The light neutrino masses satisfies normal mass hierarchy. We also incorporate the sum of light neutrino masses (Σm_i) to check its consistency with the cosmological limit set by Planck, $\Sigma m_i < 0.23$ eV [12]. In this particular case with $\delta = 80^\circ$ (also for $\delta = 100^\circ, 260^\circ, 280^\circ$), this limit is satisfied for the allowed range of α, it turns out that $\delta = 83^\circ$ and 97° (and similarly for $263^\circ - 277^\circ$) do not satisfy it as indicated in Table.3.2. One can check that indeed the light neutrino masses are mostly dominated by the type-I seesaw contribution. This can be seen from Eqs.(5.23-5.25) by setting $\beta = 0$. As an example, with $\delta = 80^\circ$ ($\alpha < 1$) case, m_3 is found to be 0.074 eV and the type-I contribution toward this mass is almost 0.07 eV. Similar condition holds for other range of δ values as well.

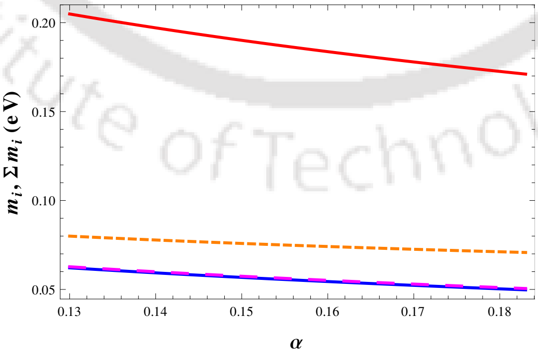

FIGURE 3.6: Light neutrino masses m_1 (blue-continuous line), m_2 (magenta-large dashed line), m_3 (orange-dashed line) and Σm_i (red continuous line) vs α for $\delta = 80^\circ (\equiv 100^\circ, 260^\circ, 280^\circ)$.

Now by using Eqs.(3.32-3.32), we estimate the Majorana phases[3] α_{21} and α_{31} for $\delta = 80°$, which appears in the effective neutrino mass parameter $|m_{ee}|$. $|m_{ee}|$ appears in evaluating the neutrinoless double beta decay and is given by[4],

$$|m_{ee}| = \left| m_1^2 c_{12}^2 c_{13}^2 + m_2^2 s_{12}^2 c_{13}^2 e^{i\alpha_{21}} + m_3^2 s_{13}^2 e^{i(\alpha_{31} - 2\delta)} \right|. \tag{3.34}$$

In Fig.3.7, we plot the prediction of $|m_{ee}|$ against α within its narrow range satisfying 3σ range of $\sin^2\theta_{13}$ with $\delta = 80°$. Here we obtain $0.050 \leq |m_{ee}| \leq 0.062$. This could be probed in future generation experiments providing a testable platform of the model itself.

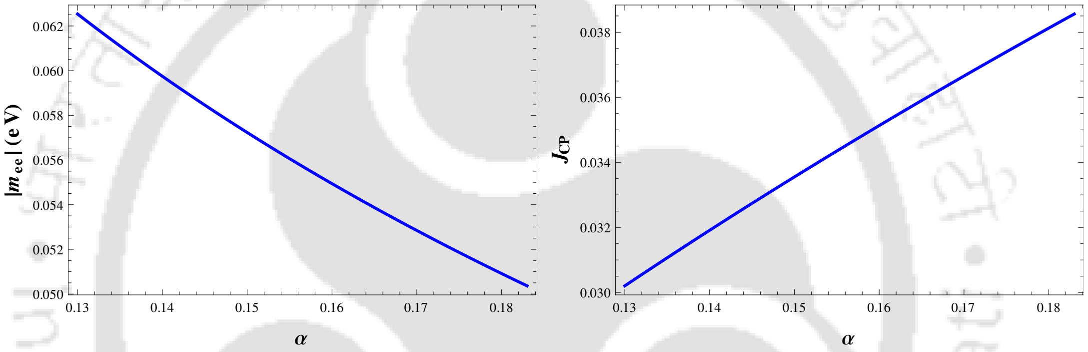

FIGURE 3.7: Effective neutrino mass parameter (left panel) and Jarlskog invariant (right panel) vs α for $\delta = 80°(100°, 260°, 280°)$.

It is known that presence of nonzero Dirac CP phase can trigger CP violation in neutrino oscillation at low energy. In standard parametrization, the magnitude of this CP violation can be estimated [4] through

$$\begin{aligned} J_{CP} &= \mathrm{Im}[U_{\mu 3} U_{e3}^* U_{e2} U_{\mu 2}^*] \\ &= \frac{1}{8} \cos\theta_{13} \sin 2\theta_{12} \sin 2\theta_{23} \sin 2\theta_{13} \sin\delta. \end{aligned} \tag{3.35}$$

As in our model, the unique source of δ is the CP violating phase α_S in S, it is interesting to see the prediction of our model towards J_{CP}. Using the expression of J_{CP} in Eq. (3.35) along with Eqs.(5.19) and (3.22) we estimate J_{CP} in our model as shown in Fig.3.7, right panel with $\delta = 80°$. Here also we include only that range of α which provides solutions corresponding to 3σ allowed range of $\sin^2\theta_{13}$. However we scanned the entire range of α

---

[3] The source of these phases are the phase ϕ_d only.

where the solutions exists for all allowed values of δ and find that J_{CP} in our model is predicted to be $0.03 < |J_{CP}| < 0.04$. This can be measured in future neutrino experiments.

3.3.2 Results for Case B

Similar to case A, we consider here the expression of r for $\alpha > 1$ from Eq. (3.33) to draw the contour plot for $r = 0.03$ in the $\alpha - \beta$ plane as shown in Fig.(3.8) while δ is fixed at different values. In the same plot we include the $\sin^2\theta_{13} = 0.0234$ contour as well to find the set of parameters (α, β) corresponding to a fixed δ which satisfies the best fit values of $\sin^2\theta_{13}$ and r. Once we restrict β to be below one, we find the solutions to exists for $\delta = 0° - 63°$, ($117° - 180°$, $180° - 243°$, $297° - 360°$) shown in Table 3.3. For δ's beyond 63° (when considered within $\pi/2$), the solutions exhibit βgg1 implying a fine tuned situation similar to case A. Note that α therefore falls in a narrow range $\simeq 1.2 - 1.4$ in order to satisfy both $\sin^2\theta_{13} = 0.0234$ and $r = 0.03$ considering all δ values. In Fig.(3.9), left panel, we find the intersection is at $(1.36, 0.53)$ for $\delta = 40° (\equiv 140°, 220°, 320°)$. Considering this δ as a reference for discussion, we further include the 3σ range of $\sin^2\theta_{13}$ in Fig.3.9, right panel. We find α to be varied between 1.35 and 1.39 while $\sin^2\theta_{13}$ changes from the

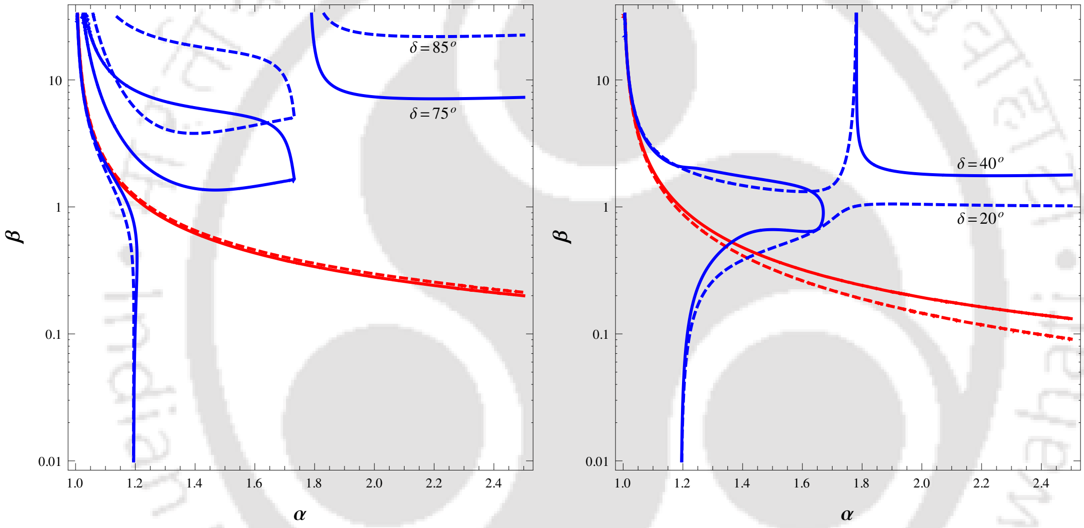

FIGURE 3.8: Contour plots for both $\sin^2\theta_{13} = 0.0234$ (shown in red-dashed and red-continuous lines) and $r = 0.03$ (shown in blue-dashed and blue-continuous lines) in the $\alpha - \beta$ plane for various choices of δ with $\alpha > 1$. In the left panel, dashed and continuous lines represent $\delta = 85°$ and 75° respectively, while in the right panel, dashed and continuous lines represent contour plots for $\delta = 20°$ and 40° respectively.

δ	α	β	$\sum m_i$(eV)
$10^\circ(170^\circ, 190^\circ, 350^\circ)$	1.43	0.36	0.0791
$30^\circ(150^\circ, 210^\circ, 330^\circ)$	1.39	0.45	0.0798
$40^\circ(140^\circ, 220^\circ, 320^\circ)$	1.36	0.53	0.0799
$50^\circ(130^\circ, 230^\circ, 310^\circ)$	1.32	0.64	0.0794
$60^\circ(120^\circ, 240^\circ, 300^\circ)$	1.26	0.83	0.0776
$70^\circ(110^\circ, 250^\circ, 290^\circ)$	1.17	1.13	0.0739
$73^\circ(107^\circ, 253^\circ, 287^\circ)$	1.07	3.02	0.0696

TABLE 3.3: Solutions for $\alpha(> 1)$ and β for various δ.

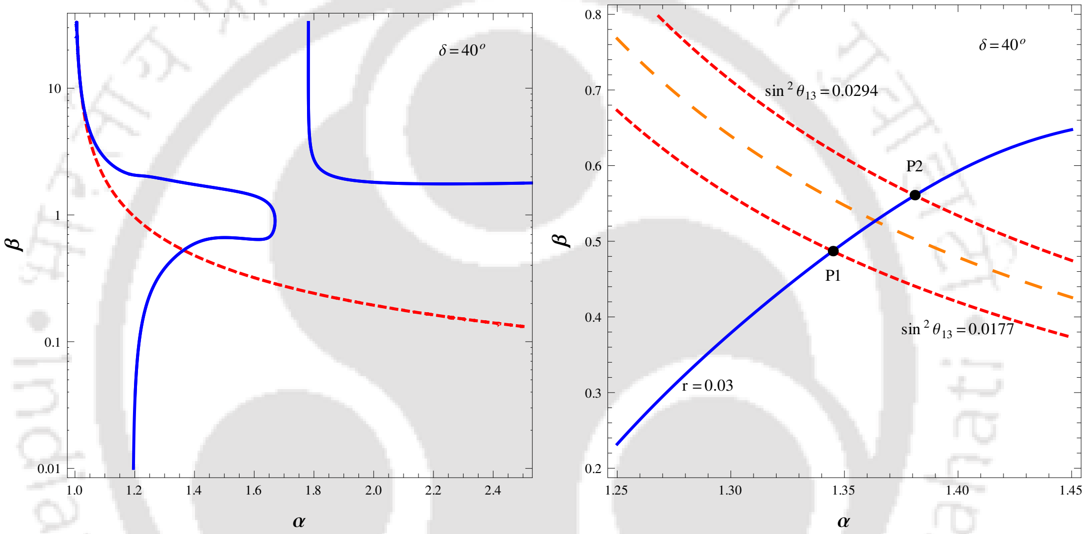

FIGURE 3.9: Left panel contains contour plots for best-fit values of r (indicated by blue-continuous lines) and $\sin^2\theta_{13}$ (indicated by red-dashed line) for $\delta = 40^\circ$ in α-β plane with $\alpha > 1$. The right panel is for contour plot of r with its best fit value $r = 0.03$ (shown in blue-continuous line) and 3σ range of $\sin^2\theta_{13}$ (denoted by two red-dashed lines) along with the $\sin^2\theta_{12} = 0.0234$ contour (denoted by orange large-dashed line)..

lower to the higher value, within 3σ limit. Within this range, we predict individual light neutrino masses and their sum. Here also we find normal hierarchy for them as seen from Fig.3.10. With $\alpha > 1$, we can check now that in obtaining the physical neutrino masses, type-I contribution dominates as in $\alpha < 1$ case also. For example, with $m_3 = 0.057$ eV, the type-I part provides ~ 0.062 eV (obtained by setting $\beta = 0$ in Eq. (5.25)) and hence the type-II contribution is almost one order of magnitude less compared to type-I contribution. For different δ-values, the Σm_i (corresponding to the best fit value of $\sin^2\theta_{13}$) are provided in Table 3.3. For showing the prediction of our model in terms

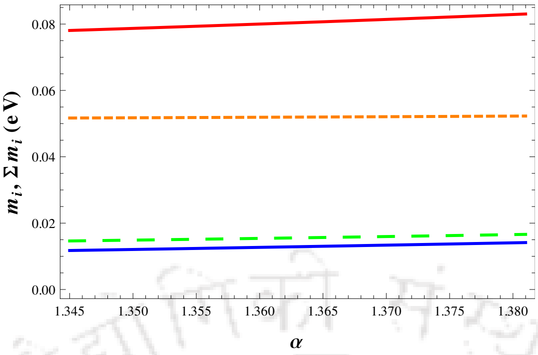

Figure 3.10: Light neutrino masses m_1 (blue-continuous line), m_2 (green-large dashed line), m_3 (orange-dashed line) and Σm_i (red continuous line) vs α for $\delta = 40°(\equiv 140°, 220°, 320°)$.

of other quantities like $|m_{ee}|$ and J_{CP}, the Fig.3.11,left and right panels are included. Considering all the δ values for which $\beta \leq 1$, we find $|J_{CP}|$ to be within $|J_{CP}| < 0.035$.

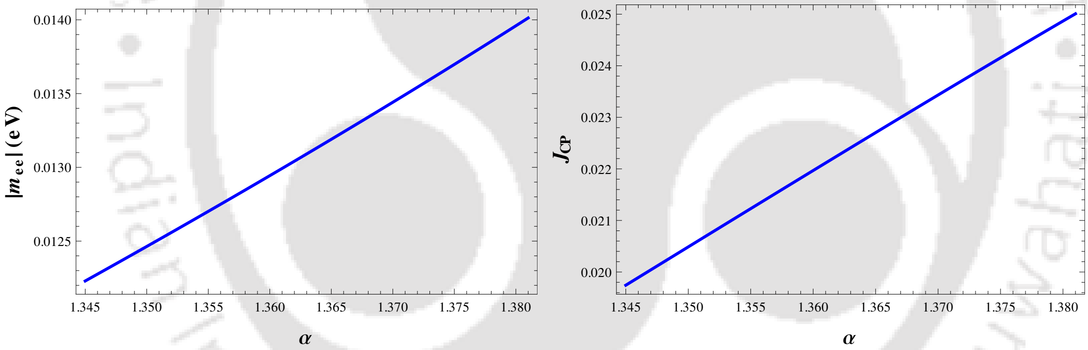

Figure 3.11: Effective neutrino mass parameter (left panel) and Jarlskog invariant (right panel) vs α for $\delta = 40°(140°, 220°, 320°)$ when $\alpha > 1$.

3.4 Leptogenesis

In a general type-II seesaw framework, leptogenesis can be successfully implemented through the decay of RH neutrinos [11] or from the decay of the triplet(s) involved [116, 191–194] or in a mixed scenario where both RH neutrino and the triplet(s) contribute [115, 124, 195–198]. In the present set-up, all the couplings involved in the pure type-I contribution are real and hence the neutrino Yukawa matrices and the RH neutrino mass matrices do not include any CP violating phase. Therefore CP asymmetry originated from the sole contribution of RH neutrinos is absent in our framework. As we have mentioned earlier, the source of CP violation is only present in the triplet contribution and that is through the vev of the S field. However as it is known[193, 199], a single $SU(2)_L$ triplet does not produce CP-asymmetry. Therefore there are two remaining possibilities to generate successful lepton asymmetry [115, 200]in the present context; (I) from the decay of the triplet where the one loop diagram involves the virtual RH neutrinos and (II) from the decay of the RH neutrinos where the one loop contribution involves the virtual triplet running in the loop. Provided the mass of the triplet is light compared to all the RH neutrinos (*i.e.*, $M_\Delta < M_{Ri}$), we consider option (I). Once the triplet is heavier than the RH neutrinos, we explore option (II).

First we consider option (I), *i.e.*, when $M_\Delta < M_{Ri}$. At tree level the scalar triplet can decay either into leptons or into two Higgs doublets, followed from the Lagrangian in Eq. (3.9) and (3.12). For $\Delta \longrightarrow LL$, the one loop diagram involves the virtual RH neutrinos running in the loop as shown in Fig.1.6. Interference of the tree level and the one loop results in the asymmetry parameter [115, 191, 201]

$$\epsilon_\Delta = 2\frac{\Gamma(\Delta^* \longrightarrow L + L) - \Gamma(\Delta \longrightarrow \bar{L} + \bar{L})}{\Gamma(\Delta^* \longrightarrow L + L) + \Gamma(\Delta \longrightarrow \bar{L} + \bar{L})}, \tag{3.36}$$

$$= \frac{1}{8\pi} \sum_k M_{Rk} \frac{\sum_{il} \mathrm{Im}[(\hat{Y}_D^*)_{ki} (\hat{Y}_D^*)_{kl} (Y_\Delta)_{il} \eta^*]}{\sum_{ij} |(Y_\Delta)_{ij}|^2 M_\Delta^2 + |\eta|^2} \log(1 + M_\Delta^2 / M_{Rk}^2). \tag{3.37}$$

Here i, j denote the flavor indices, $\hat{Y}_D = U_R^T Y_D$ in the basis where RH neutrino mass matrix is diagonal. Y_Δ, Y_D and expression of η can be obtained from Eqs.(3.6),(3.10) and (3.13). Masses of RH neutrinos can be expressed as

$$M_{R_1} = \frac{v^2 y^2}{k}(1 + \alpha), \tag{3.38}$$

$$M_{R_2} = \frac{v^2 y^2}{k}, \tag{3.39}$$

$$M_{R_3} = \left| \frac{v^2 y^2}{k}(1 - \alpha) \right|. \tag{3.40}$$

Therefore, in the limit when the scalar triplet is much lighter than the RH neutrinos, the asymmetry parameter in our model is estimated to be [115]

$$\epsilon_\Delta = -\frac{M_\Delta^2}{8\pi v^2}\frac{\alpha^2}{(1-\alpha^2)}\frac{k\mu\tilde{\omega}^3 v_S(x_1-x_1')\sin\alpha_S}{\left[3\tilde{\omega}^2\frac{v_S^2}{\Lambda^2}\left(x_1^2+x_1'^2+2x_1x_1'\cos 2\alpha_S\right)M_\Delta^2+(\mu\tilde{\omega}^2\Lambda)^2\right]}. \quad (3.41)$$

Here we denote $\tilde{\omega} = v_f/\Lambda$, where v_f is considered to be the common vev of all flavons except S-field's vev $\langle S\rangle = v_S e^{i\alpha_S}$. The associated phase α_S is the only source of CP-violation here. The total decay width of the triplet Δ (for $\Delta \rightarrow$ two leptons and $\Delta \rightarrow$ two scalar doublets) is given by

$$\Gamma_T = \Gamma_{\Delta^*\to LL} + \Gamma_{\Delta^*\to HH} \quad (3.42)$$

$$= \frac{M_\Delta}{8\pi}\left[\sum_{ij}|(Y_\Delta)_{ij}|^2 + \frac{|\eta|^2}{M_\Delta^2}\right]. \quad (3.43)$$

Note that there are few parameters in Eq. (3.41), *e.g.* α, k which already contributed in determining the mass and mixing for light neutrinos. Also ϕ_d is related with α_S by Eq. (3.25). In the previous section, we have found solutions for (α,β) that satisfy the best fit values of $\sin^2\theta_{13}$ and r for a specific choice of δ (the reference values $\delta = 80^\circ$ for $\alpha < 1$ and $\delta = 40^\circ$ for $\alpha > 1$). Then we can find the values of k and $|d|$ corresponding to that specific δ value. These set of $\alpha, |d|, k$ produce correct order of neutrino mass and mixing as we have already seen. Here to discuss the CP-asymmetry parameter ϵ_Δ, we therefore choose $\delta = 80^\circ(100^\circ, 260^\circ, 280^\circ)$ for $\alpha < 1$ and $\delta = 40^\circ(140^\circ, 220^\circ, 320^\circ)$ for $\alpha > 1$.

We further define $v_S/\Lambda = f\tilde{\omega}$ where f serves as a relative measure of the vevs. With this, the expression of ϵ_Δ takes the form

$$\epsilon_\Delta = -\frac{\alpha^2}{8\pi v^2(1-\alpha^2)}\frac{kf(x_1-x_1')\sin\alpha_S(\mu\Lambda/M_\Delta^2)}{\left[(3f^2/M_\Delta^2)\left(x_1^2+x_1'^2+2x_1x_1'\cos 2\alpha_S\right)+(\mu\Lambda/M_\Delta^2)^2\right]}, \quad (3.44)$$

which is $\tilde{\omega}$ independent. The expression for $|d|$ as obtained from Eq. 3.15 can be written as

$$|d| = 2fv^2\tilde{\omega}^4\frac{\mu\Lambda}{M_\Delta^2}(x_1+x_1')\cos\alpha_S\sec\phi_d. \quad (3.45)$$

Using Eq. (3.44), we obtain the contour plot for $\epsilon_\Delta = 10^{-6}, 10^{-7}, 10^{-8}$ with $\mu = 1, f = 0.1$, $x_1 = 0.5$ and $x_1' = 1$ which are shown in Fig.4.51, left panel. The electroweak vev is also inserted in the expression. In obtaining the plots we varied Λ above the

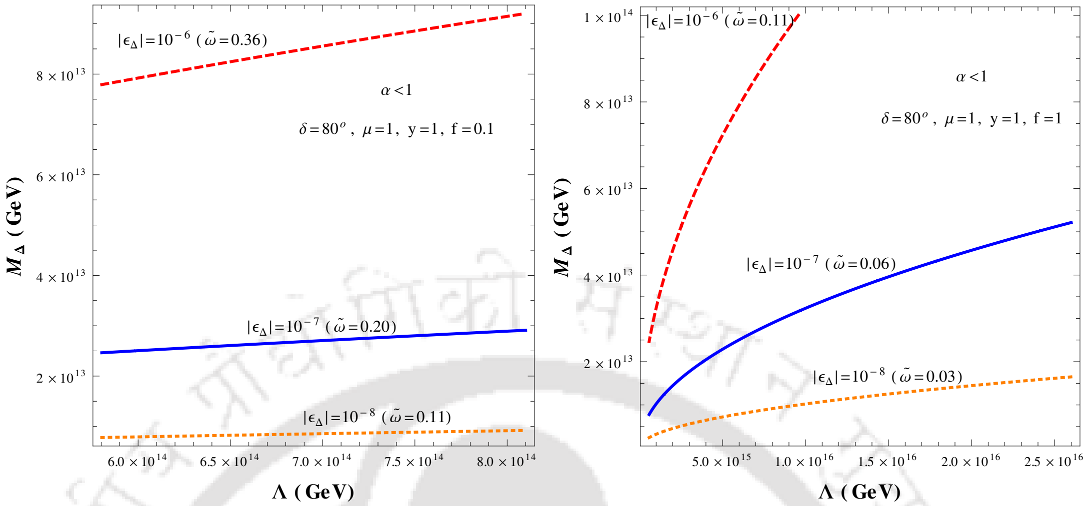

FIGURE 3.12: Contours corresponding to different values of ϵ_Δ in the $M_\Delta-\Lambda$ plane with$\alpha<1$. The choice of other parameters are provided inside the figures.

masses of RH neutrinos (Eqs. (3.38-3.40)). The variation of M_Δ is also restricted from above by the condition that we work in regime (I) where $M_\Delta<M_{R_{i=1,2,3}}$. Fig.4.51 is produced for a specific choice of $\delta=80°(100°,260°,280°)$ which corresponds to the solution ($\alpha=0.16,\beta=0.11$). The values of $|d|$ and k corresponding to this set of (α,β) are found to be 0.0068 eV and 0.06 eV respectively. Note that $M_\Delta<M_{Ri}$ restricts the choice of y in. We have chosen $y=1$ for the left panel of Fig.4.51. In order to keep $M_\Delta<M_{Ri}<\Lambda$, we find $M_\Delta\simeq10^{13-14}$ GeV would be the right choice for enough lepton asymmetry can be generated. As the values of α,k are fixed for generating the plots of Fig.4.51, the corresponding RH neutrino masses are found to be $M_{R_1}=5.8\times10^{14}$ GeV, $M_{R_2}=5.01\times10^{14}$ GeV and $M_{R_3}=4.22\times10^{14}$ GeV (with $y=1$) in this case following Eqs. (3.38-3.40).

Note that value of $\tilde{\omega}$ can be concluded from the expression of $|d|$ in Eq. (3.45), for a choice of Λ/M_Δ^2 which produces a ϵ_Δ contour. This is because corresponding to a specific choice of δ value, $|d|$ is uniquely determined for the solution point (α,β). Hence with fixed values of x_1,x_1',f,μ (with the same values to have the ϵ_Δ contour), $\tilde{\omega}$ can be evaluated from $|d|$ for a chosen Λ/M_Δ^2. It turns out that $\tilde{\omega}$ has a unique value for a specific ϵ_Δ for both the panels of Fig.4.51. For example, with $\epsilon_\Delta=10^{-7}$, we need $\tilde{\omega}=0.2$, while to have $\epsilon_\Delta=10^{-6}$, $\tilde{\omega}$ required to be 0.36. These $\tilde{\omega}$ values are provided in first bracket in each figure beside the ϵ_Δ value. The reason is the following. For the specified range of Λ

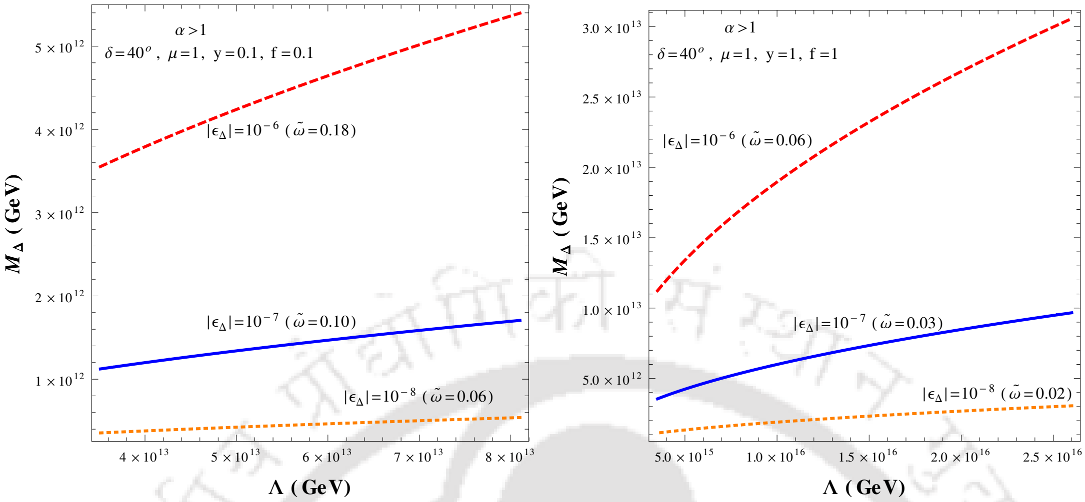

FIGURE 3.13: Contours corresponding to different values of ϵ_Δ in the $M_\Delta - \Lambda$ plane with $\alpha > 1$. The choice of other parameters are provided inside the figures.

(*i.e.* $M_\Delta < M_{Ri} < \Lambda$), it follows that[4] the first bracketed term in the denominator of Eq. (3.44) is almost negligible compared to the second term (with the choice of x_1, x_1', f, μ as mentioned before) and hence effectively

$$\epsilon_\Delta \simeq -\frac{\alpha^2}{8\pi v^2(1-\alpha^2)} kf(x_1 - x_1') \sin\alpha_S \frac{M_\Delta^2}{\mu\Lambda}. \tag{3.46}$$

Therefore for a typical choice of ϵ_Δ, Λ/M_Δ^2 is almost fixed and then $|d|$ expression in Eq. (3.46) tells that $\tilde{\omega}$ also is almost fixed. In the right panel of Fig.4.51, we take $y = 1, f = 1$ and draw the contours for ϵ_Δ while x_1, x_1', μ are fixed at their previous values considered for generating plots in the left panel. In this case, M_Δ turns out to be 10^{13-14} GeV.

Similarly, contours for ϵ_Δ are drawn in Fig.3.13 for $\alpha > 1$ case. Correspondingly, we have used solutions of ($\alpha = 1.36, \beta = 0.53$) and the values of $k = 0.02$ eV and $|d| = 0.01$ eV are taken for $\delta = 40^\circ$ (also for $140^\circ, 220^\circ, 320^\circ$). For left panel of Fig.3.13, $\mu = 1, y = 1$ and $f = 1$ are considered and we get somewhat lighter value of scalar $M_\Delta \sim 10^{13}$ GeV. In this case the RH neutrinos are with masses $M_{R_1} = 3.5 \times 10^{15}$ GeV, $M_{R_2} = 1.48 \times 10^{15}$ GeV and $M_{R_3} = 5.4 \times 10^{14}$ GeV and hence satisfying $M_\Delta < M_{Ri}$. For the right panel of Fig.3.13, y is considered as 0.1 and hence the RH neutrino masses are smaller compared to

---

[4] In principle, the operator $LHLH$ contributes in the present framework at a higher order, with $\frac{c_1}{\Lambda^2} LHLH\xi(\phi_S)$ term. However its contribution is suppressed compared to the type-I contribution by $\sim \tilde{\omega}^2 << 1$, with $c_1 \sim \mathcal{O}(1)$. It turns out that with the parameters specified in our discussion, it is also smaller (with $c_1 \sim \mathcal{O}(1)$) than the triplet contribution.

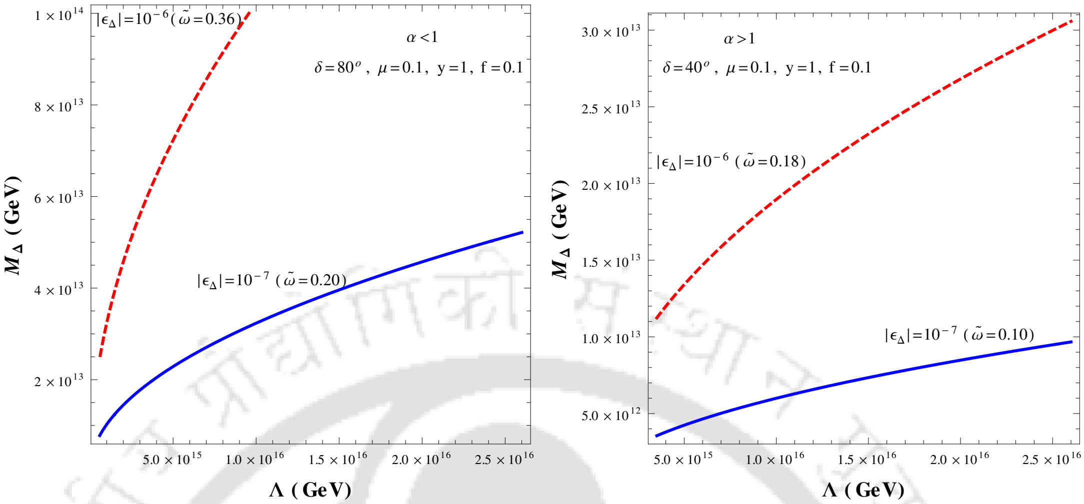

FIGURE 3.14: Contours corresponding different values of ϵ_Δ in the $M_\Delta - \Lambda$ plane for $\alpha < 1$ (left panel) and $\alpha > 1$ (right panel) with relatively small μ $(= 0.1)$. The choice of other parameters are provided inside the figures.

the left panel. However, they are still heavier (lightest RH neutrino mass, $M_{R_3} = 5.4\times10^{12}$ GeV) than the scalar triplet, $M_\Delta \sim 10^{12}$ GeV. In Fig.3.14 similar contour plots for ϵ_Δ are exercised with μ at somewhat lower values, fixed at $\mu = 0.1$ along with $f = 0.1$ for both $\alpha < 1$ (left panel) and $\alpha > 1$ (right panel). Corresponding to Fig.3.14, the masses of the RH neutrinos are $M_{R_1} = 5.8\times10^{14}$ GeV, $M_{R_2} = 5.01\times10^{14}$ GeV, $M_{R_3} = 4.22\times10^{14}$ GeV for $\alpha < 1$ (left panel) and $M_{R_1} = 3.5\times10^{15}$ GeV, $M_{R_2} = 1.48\times10^{15}$ GeV, $M_{R_3} = 5.4\times10^{14}$ GeV for $\alpha > 1$ (right panel).

So overall we have found that enough ϵ_Δ can be created so as to achieve the required lepton asymmetry through $\frac{n_L}{n_\gamma} = \epsilon_\Delta \frac{n_\Delta}{n_\gamma} D$ with $n_\Delta = n_{\Delta_0} + n_{\Delta_+} + n_{\Delta_{++}}$ is the total number density of the triplet and D is the efficiency factor. After converting it into baryon asymmetry by the sphaleron process, n_B/n_γ is given by $\frac{n_B}{n_\gamma} \simeq -0.03\epsilon_\Delta D$. D depends on the satisfaction of the out-of-equilibrium condition $(\Gamma_\Delta \leq H|_{T=M_\Delta})$. Being $SU(2)_L$ triplet, it also contains the gauge interactions. Hence the scattering like $\Delta\Delta \rightarrow$ SM particles can be crucial [202, 203]. In [115, 116, 193, 204, 205], it has been argued that even if the triplet mass (M_Δ) is much below 10^{14} GeV, the triplet leptogenesis mechanism considered here is not affected much by the gauge mediated scatterings. However the exact estimate of D requires to solve the Boltzmann equations in detail which is beyond the scope of the present work. However analysis toward evaluating D in this sort of framework (where a single triplet is present and RH neutrinos are in the loop

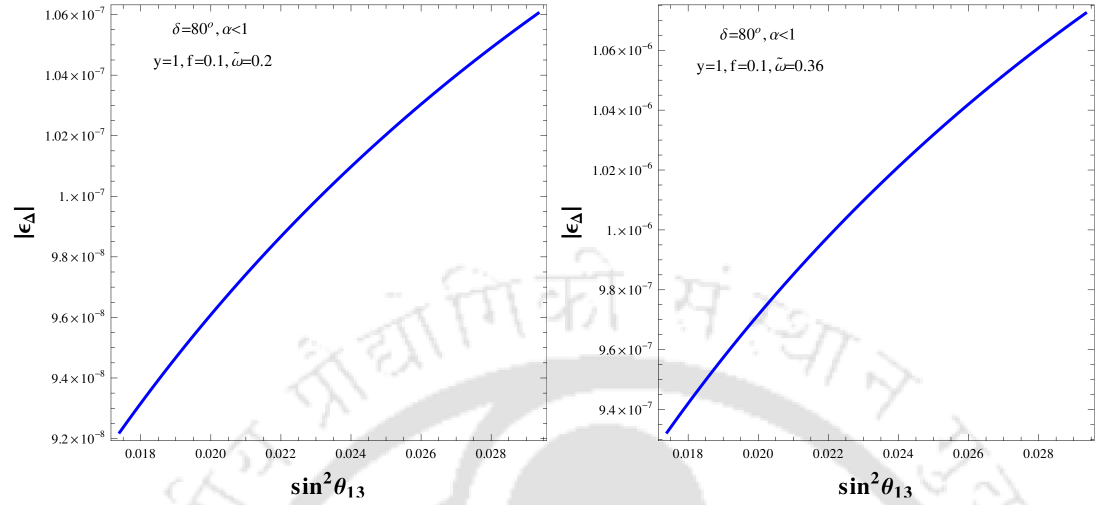

FIGURE 3.15: Variation of $|\epsilon_\Delta|$ with $\sin^2\theta_{13}$ for $\alpha < 1$. The left panel is with $\tilde{\omega} = 0.2$ while the right panel is with $\tilde{\omega} = 0.36$.

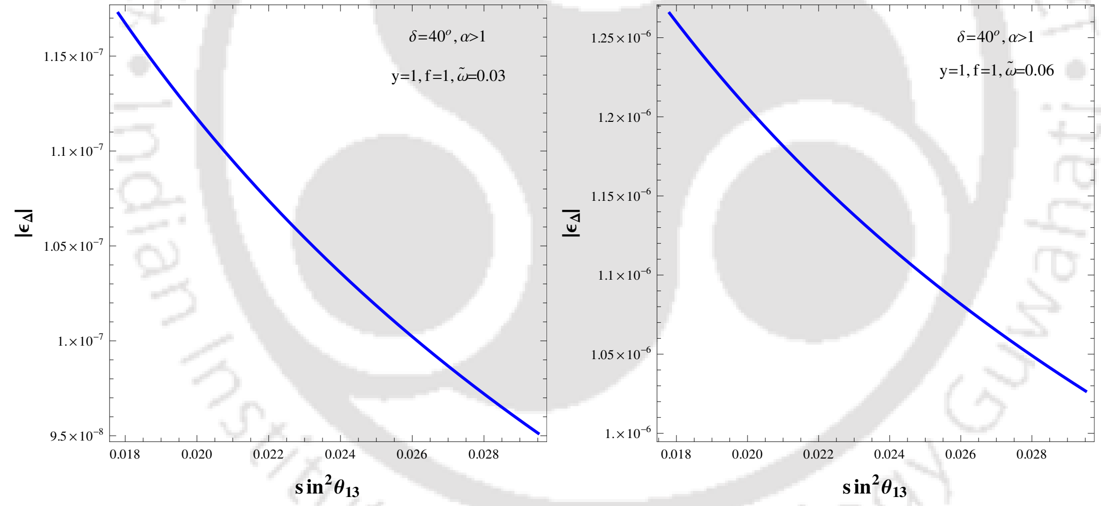

FIGURE 3.16: Variation of $|\epsilon_\Delta|$ with $\sin^2\theta_{13}$ for $\alpha > 1$. The left panel is with $\tilde{\omega} = 0.03$ while the right panel is with $\tilde{\omega} = 0.06$.

for generating ϵ_Δ) exits in [193]. Following [193], we note that with the effective type-II mass $\tilde{m}_\Delta \left(\equiv \sqrt{\mathrm{Tr}(m_\nu^{II\dagger} m_\nu^{II})}\right) \sim (0.01 - 0.02)$ eV, the efficiency D is of the order of 10^{-3}. In estimating[5] $\tilde{m}_\Delta$, we have considered all the parameters in a range (mentioned within

---

[5] It is possible to recast Eq. (3.37) as $\epsilon_\Delta = -\frac{1}{8\pi}\frac{M_\Delta}{v^2}\sqrt{B_L B_H}\frac{\mathrm{Tr}(m_\nu^{I\dagger} m_\nu^{II})}{\tilde{m}_\Delta}$ with the consideration $M_\Delta < M_{Rk}$. Here B_L and B_H are corresponding branching ratio's of decay of the triplet into two leptons and two scalar doublets.

Fig.4.51-3.13) so as to produce ϵ_Δ of order 10^{-6} as shown in Fig.4.51-3.13.

Now, using the approximated expression as given by Eq. (3.46) we can obtain variation of $|\epsilon_\Delta|$ against $\sin^2\theta_{13}$ as given in Fig.3.15 for $\alpha < 1$ and in Fig.3.16 with $\alpha > 1$. In doing so we have substituted $\mu\Lambda/M_\Delta^2$ from Eq. (3.45) in Eq. (3.46). Then as discussed in the previous section, using solutions of α, β for 3σ range of $\sin^2\theta_{13}$ with fixed δ value, we have obtained Fig.3.15 and Fig.3.16 for $\alpha < 1$ and $\alpha > 1$ respectively. Here Fig.3.15 for $\delta = 80^\circ (100^\circ, 260^\circ, 280^\circ)$ and Fig.3.16 with $\delta = 40^\circ (140^\circ, 220^\circ, 320^\circ)$.

It is interesting to note that within our present framework, neutrino oscillation data imposes an upper bound on the lepton asymmetry as seen from Fig.3.15 and 3.16 corresponding to the upper (lower) value of $\sin^2\theta_{13}$ within 3σ range for $\alpha < 1$ ($\alpha > 1$). Although a value of $|\epsilon_\Delta| = 10^{-7}$ as seen in Fig.3.15 seems to be quite restrictive for leptogenesis in the present context, a somewhat generous value of $|\epsilon_\Delta| = 10^{-6}$ can be obtained in our case by a mere change of $\tilde{\omega}$ from 0.2 to $\tilde{\omega} = 0.36$ as seen by comparing the left and right panel of Fig.3.15. Similar conclusions hold for $\alpha > 1$ case also as seen from Fig.3.16.

We now discuss the option II, when RH neutrinos are lighter than M_Δ. The one loop diagram involves here the virtual triplet (Δ) running in the loop as shown in Fig. 1.5. The contribution toward the CP-asymmetry parameter generated from the decay of the lightest neutrino is given by

$$\epsilon_{N_1} = -\frac{1}{8\pi v^2} M_{R_1} \frac{\sum_{il} \mathrm{Im}[(\hat{Y}_D)_{1i} (\hat{Y}_D)_{1l} (m_\nu^{II*})_{il}]}{\sum_i |(\hat{Y}_D)_{1i}|^2}, \tag{3.47}$$

$$= -\frac{M_{R_1}}{2} \frac{1}{8\pi v^2} |d| \sin\phi_d, \tag{3.48}$$

$$\epsilon_{N_2} = M_{R_2} \frac{1}{8\pi v^2} |d| \sin\phi_d \quad \text{and} \quad \epsilon_{N_3} = \pm \frac{M_{R_3}}{2} \frac{1}{8\pi v^2} |d| \sin\phi_d. \tag{3.49}$$

where we have used m_ν^{II} from Eq. (3.14). In the above, '+' and '−' sign stands for $\alpha > 1$ and $\alpha < 1$ cases respectively in computation of ϵ_{N_3}. Note that in the present scenario the RH neutrino masses are not entirely hierarchical, rather they are closely placed. therefore the total baryon asymmetry from the decay of the three RH neutrinos is to be estimated as $\left|\frac{n_B}{s}\right| = 1.48 \times 10^{-3} \sum_i \epsilon_{N_i} D_{N_i}$, where D_{N_i} is the respective efficiency factor. It turns out that with the same D_{N_i} for $i = 1, 2, 3$, $\sum_i \epsilon_{N_i} = 0$ as a result (using M_{R_i} from Eq. (3.40)) of the specific flavor structure considered. Therefore it is expected that the lepton asymmetry would be suppressed in this case. Also in this case $M_{R_i} < M_\Delta$, which can be obtained by considering smaller value of the Yukawa coupling y (as to generate the required $|d|$, specific values of α, β, k are already chosen). This could reduce the individual ϵ_{N_i}. We conclude this contribution (ϵ_N) as a subdominant to ϵ_Δ.

3.5 Chapter Summary

We this Chapter, have considered a flavor symmetric framework for generating light neutrino masses and mixing through type-II seesaw mechanism. In realizing it, we have introduced three SM singlet RH neutrinos, one $SU(2)_L$ triplet and few flavon fields. The RH neutrinos contribute to the type-I term, which guided by the $A_4 \times Z_4 \times Z_3$ symmetry of the model produces a TBM mixing pattern. Then we have shown that the typical flavor structure resulted from the model can generate nonzero θ_{13}. In this framework, all the couplings are considered to be real. The CP symmetry is violated spontaneously by the complex vev of a single SM singlet field, while other flavons have real vevs. Interestingly this particular field is involved only in the pure type-II term. Hence the triplet contribution not only generates the θ_{13}, it is also responsible for providing Dirac CP violating phase δ. Therefore the model has the potential to predict δ in terms of the parameters involved in neutrino masses and mixing. We have therefore studied the parameter space of the set-up considering that the triplet contribution is subdominant or at most comparable to the type-I term. The model indicates the values of δ to be in the range $72° - 82°$, $98° - 108°$, $252° - 262°$, $278° - 288°$ for $\alpha < 1$ and $\delta = 0° - 63°$, $117° - 180°$, $180° - 243°$, $297° - 360°$ for $\alpha > 1$. However $\delta = 0$ (and hence $\pi, 2\pi$) is disfavored in our scenario as in that case no CP violation would be present. Also $\delta = \pi/2, 3\pi/2$ are excluded here. These ranges can be tested in future neutrino experiments. We provide an estimate for the J_{CP}. The sum of the neutrino masses are also evaluated. It turns out that the scenario works with normal hierarchical masses of light neutrinos. We have also studied leptogenesis in this model. As the type-I contribution to the light neutrino mass does not involve any CP violating phase, RH neutrinos decay can not contribute to the lepton asymmetry in the conventional way. We have found the triplet decay with the virtual RH neutrino in the loop can produce enough lepton asymmetry.

Chapter 4

A_4 realization of inverse seesaw: neutrino masses, θ_{13} and leptonic non-unitarity

4.1 Introduction

In this Chapter we provide an A_4 based flavor symmetric scenario which accommodate s the inverse seesaw mechanism for explaining light neutrino masses and mixing. We find that the lepton mixing, in particular the TBM mixing pattern and its deviation through nonzero θ_{13}, is originated solely from the flavor structure of the lepton number violating contribution of the neutral lepton mass matrix. Here we discuss in detail how a nonzero value of θ_{13} is correlated with the other parameters in the framework and its impact on the Dirac CP phase δ. We also analyze the non-unitarity effects on lepton mixing matrix and its implication in terms of the lepton flavor violating decays, etc. The sucussion presented here is based on [266]

In Chapter 2 we have discussed that, the conventional type-I seesaw [34–36] tries to explain the smallness of neutrino mass by adding three right-handed (RH) neutrinos $N_{Ri=1,2,3}$ to the Standard Model (SM). They have Majorana mass M_R which is representative of the lepton number violation. With the Yukawa couplings of order unity, the left handed neutrinos can be light enough, $m_\nu \sim v^2/M_R$, provided the new physics scale

M_R is sufficiently high $\sim 10^{13}$ GeV or so. Though it suggests an interesting and natural explanation of why neutrinos are so light, such a high new physics scale is beyond the reach of present and future neutrino experiments.

Inverse seesaw [33, 45] on the other hand turns out to be a viable alternate scenario where the new physics scale responsible for neutrino mass generation can be brought down near TeV scale at the expense of involving additional fields (SM singlet fermions $S_{i=1,2,3}$). In presence of additional symmetry like a global $U(1)_{B-L}$, the corresponding neutral lepton 9×9 mass matrix takes the form

$$M_\nu = \begin{pmatrix} 0 & m_D & 0 \\ m_D^T & 0 & M \\ 0 & M^T & 0 \end{pmatrix}, \tag{4.1}$$

using the basis (ν_L^c, N_R, S). Note that at this level, neutrinos are massless. Once the lepton number violating term $\frac{1}{2}\overline{S^c}\mu S$ is introduced with $\mu << m_D < M$, the effective 3×3 light neutrino mass matrix is given by

$$m_\nu = m_D M^{-1} \mu (M^T)^{-1} m_D^T = F\mu F^T, \tag{4.2}$$

where $F = m_D M^{-1}$. Since the lepton number turns out to be only an approximate symmetry of nature, it is perhaps more natural to be broken by a small amount μ rather than by a large mass M_R as happened in case of type-I seesaw. Also note that the other mass scale M (say the new physics scale) in Eq. (4.1) can be as low as TeV since there exists a double suppression by this new physics scale through Eq.(4.2) and smallness of μ is then justified to produce correct amount of light neutrino mass.

In the light of recent measurement of nonzero θ_{13} [5, 79, 80] our aim to study the lepton mixing matrix in the inverse seesaw framework based on an A_4 flavor symmetry. In its minimal form, ref [206] discusses how a TBM pattern can be incorporated in an A_4 symmetric inverse seesaw scenario. They have shown (among one of the few possibilities discussed there) that if m_D, M and μ matrices all posses the following structure:

$$M_0 = \begin{pmatrix} X & 0 & 0 \\ 0 & Y & Z \\ 0 & Z & Y \end{pmatrix}, \tag{4.3}$$

the light neutrino mass matrix obtains a typical form, [134]

$$m_\nu = \begin{pmatrix} A & B & B \\ B & A+D & B-D \\ B & B-D & A+D \end{pmatrix}. \tag{4.4}$$

The diagonalizing matrix of the above form of m_ν is representative of the TBM mixing in the basis where charged lepton mass matrix is diagonal. In [265], authors have shown that in a S_4 based inverse seesaw, nonzero θ_{13} can be generated from the correction in the charged lepton sector. Few earlier attempts in realizing inverse seesaw in the framework of discrete flavor symmetries can be found in [208]. Here the construction is such that the charged lepton mass matrix becomes diagonal. Now with a simpler form for m_D and M (where $X = Z$ and $Y = 0$ in M_0), F in Eq. (4.2) becomes proportional to identity matrix and hence the structure of μ matrix coincides with that of m_ν. This means that μ matrix (and hence m_ν matrix also) of the form similar to M_0 would generate the TBM pattern of lepton mixing matrix. Therefore we finally adopt a μ matrix different from M_0 structure so as to accommodate the observed value of θ_{13}. It is interesting to note that in the inverse seesaw, μ matrix (the coefficient matrix of the $\overline{S^c}S$ term) being different from zero is the source of violation of the lepton number as stated earlier and now it also turns out that the same μ is also the source of non-zero θ_{13} as well as other mixings (the charged lepton mass matrix is diagonal) in our scenario. This is a salient feature of our model. We have then discussed the possible correlation between the Dirac CP phase (δ) with θ_{13} and other parameters involved. We have tried to address the smallness associated with the μ term by considering its origin from a higher dimensional operator. The A_4 symmetry along with other non-Abelian discrete symmetries like $Z_4 \times Z_3$ play important role. We have estimated the effective neutrino mass parameter associated with neutrinoless double beta decay [22, 23] and studied the correlation with δ as well.

Furthermore m_D being close to M, in general the inverse seesaw framework allows non-negligible mixing between the light and heavy neutrino states resulting non-unitarity contributions to the lepton flavor mixing. Since the flavor structure is completely known in our framework, we are then able to study the non-unitarity involved in the set-up and in turn constrain some of the parameters. Lepton flavor violating (LFV) decays also result from this non-unitarity effect. However it turns out in our scenario that branching ratio of those LFV decays are vanishingly small due to exact cancellation of elements involved followed from the particular flavor structure we have considered.

This Chapter is organized as follows. In the Section 4.2 below, we describe the construction of the model based on the symmetries of the framework. The detailed phenomenology constraining the parameters of the model from the available data of neutrino experiments takes place in Section 4.3 and 4.4. Section 4.5 is devoted in studying the non-unitarity effect and we comment on lepton flavor violating decays and additional contribution to neutrinoless double beta decay. Finally we conclude in Section 4.6.

4.2 The Model

In order to realize the usual inverse seesaw mechanism for the generation of light neutrino masses, we extend he SM particle content by introducing three RH neutrinos, $N_{R_{i=1,2,3}}$, and three other singlet fermions, $S_{i=1,2,3}$ as already mentioned. In addition few flavons (ϕ_S, ϕ_T, ξ, ξ', ρ) are included to understand the flavor structure of the lepton mixing. An additional global $U(1)_{B-L}$ symmetry is considered along with the flavor symmetry $A_4 \times Z_4 \times Z_3$. The field content of the model and their charges under the symmetry of the model (appropriate for the discussion) are mentioned in Table 4.1. Once the flavon fields get vev (along suitable directions), the desired structures of the mass matrices are generated as we will find below.

Fields	e_R	μ_R	τ_R	L	H	N_R	S	ϕ_S	ϕ_T	ξ	ξ'	ρ
A_4	1	$1'$	$1''$	3	1	3	3	3	3	1	$1'$	1
Z_4	$-i$	$-i$	$-i$	$-i$	1	$-i$	1	-1	1	-1	-1	i
Z_3	1	1	1	1	1	1	ω^2	1	1	1	1	ω
$B-L$	-1	-1	-1	-1	0	-1	1	-2	0	-2	-2	0

TABLE 4.1: Fields content and transformation properties under the symmetries imposed on the model.

The charged lepton Yukawa terms in the Lagrangian are given by[1],

$$\mathcal{L}_l = \frac{y_e}{\Lambda}(\bar{L}\phi_T)He_R + \frac{y_\mu}{\Lambda}(\bar{L}\phi_T)'H\mu_R + \frac{y_\tau}{\Lambda}(\bar{L}\phi_T)''H\tau_R, \tag{4.5}$$

---

[1] In Eq. (4.5), one can introduce a contribution like $\bar{L}\phi_T^\dagger He_R$. But such a term can be absorbed in the original contribution by a mere redefinition of the coupling.

to the leading order, where Λ represents the cut-off scale of the theory and y_e, y_μ and y_τ are the respective coupling constants. Terms within the first parenthesis describe the product of two A_4 triplets, which further contracts with A_4 singlets 1, $1''$ and $1'$ corresponding to e_R, μ_R and τ_R fields respectively to constitute a true A_4 singlet. Now we choose the vev of ϕ_T as $\langle\phi_T\rangle = v_T(1,0,0)$ [7] so that the charged lepton mass matrix turns out to be diagonal in the leading order and can be written as $M_l = v\frac{v_T}{\Lambda}\text{diag}\,(y_e, y_\mu, y_\tau)$.

The allowed terms in the neutrino sector invariant under the symmetries considered are given by:

$$\mathcal{L}_\nu = y_1 \bar{L}\widetilde{H}N_R + y_2\overline{N_R^c}S\rho + (\mu_1\xi\rho^2/\Lambda^2 + \mu_2\phi_S\rho^2/\Lambda^2)\overline{S^c}S + \mu_3\overline{S^c}S\xi'\rho^2/\Lambda^2, \tag{4.6}$$

where y_i, μ_i are the respective couplings. To construct the flavor structures we consider the flavons acquire vevs along $\langle\phi_S\rangle = v_S(1,1,1), \langle\xi\rangle = v_\xi, \langle\xi'\rangle = v_{\xi'}$ and $\langle\rho\rangle = v_\rho$. In appendix B, we have written the complete scalar potential invariant under $A_4 \times Z_4 \times Z_3$ and the additional global $U(1)_{B-L}$ symmetry. There we have argued that such choices of vev alignments are indeed possible. With such vev alignment Eq. (4.6) yields the following 9×9 mass matrix M_ν in the basis (ν_L^c, N_R, S)

$$M_\nu = \begin{pmatrix} 0 & m_D & 0 \\ m_D^T & 0 & M \\ 0 & M^T & \mu \end{pmatrix}. \tag{4.7}$$

The 3×3 mass matrices present in Eq. (4.7) are

$$m_D = y_1 v\begin{pmatrix} 1 & 0 & 0 \\ 0 & 0 & 1 \\ 0 & 1 & 0 \end{pmatrix}; M = y_2 v_\rho \begin{pmatrix} 1 & 0 & 0 \\ 0 & 0 & 1 \\ 0 & 1 & 0 \end{pmatrix} \quad \text{and} \tag{4.8}$$

$$\mu = \begin{pmatrix} a-2b/3 & b/3 & b/3 \\ b/3 & -2b/3 & a+b/3 \\ b/3 & a+b/3 & -2b/3 \end{pmatrix} + \begin{pmatrix} 0 & 0 & d \\ 0 & d & 0 \\ d & 0 & 0 \end{pmatrix}, \tag{4.9}$$

with $a = 2\mu_1 v_\xi v_\rho^2/\Lambda^2$, $b = -2\mu_2 v_S v_\rho^2/\Lambda^2$ and $d = 2\mu_3 v'_\xi v_\rho^2/\Lambda^2$. Note that μ term follows from a higher dimensional contribution and hence is expected to be naturally small compared to m_D and M.

4.3 Neutrino masses and Mixings

The specific flavor structure of the model ensures that (as evident from Eq. (4.2) and Eq. (4.8)) $F = m_D M^{-1} \propto \mathbb{I}$. Hence in our set-up, the effective light neutrino mass matrix becomes

$$m_\nu = F\mu F^T = \frac{v^2 y_1^2}{v_\rho y_2^2}\,\mu. \tag{4.10}$$

Eq. (4.10) clearly shows that the flavor structure of m_ν matrix is entirely dictated by that of μ. Such an interesting feature was also pointed out in [209], calling it screening mechanism in the context of double seesaw. Additionally we note here that μ serves the purpose of generating non-zero θ_{13} as well with a modification of its original TBM structure (similar to M_0 in Eq. (4.3)). This makes our model an interesting scenario to study, as the source of θ_{13} is connected with the lepton number violating parameter (μ). Now let us focus our attention to the μ matrix in Eq. (4.9). It is well known from the very specific structure of the first matrix of right hand side of Eq. (4.9) involving a, b only [7] that it leads to a TBM pattern of the lepton mixing matrix (as the charged lepton mass matrix is diagonal), given by Eq. (1.53) resulting $\theta_{13} = 0$. The second matrix in Eq. (4.9) breaks the TBM pattern and we expect a deviation of θ_{13} from zero. To find out the deviation and possible correlations between the mixing angles and parameters of the model, we first rotate m_ν from Eq. (4.10) by U_{TB} so as to get

$$\begin{aligned} m'_\nu &= U_{TB}^T m_\nu U_{TB}, \qquad (4.11)\\ &= \frac{v^2 y_1^2}{v_\rho^2 y_2^2}\begin{pmatrix} a-b-d/2 & 0 & \sqrt{3}d/2 \\ 0 & a+d & 0 \\ \sqrt{3}d/2 & 0 & -a-b+d/2 \end{pmatrix}. \qquad (4.12)\end{aligned}$$

As evident, a further rotation by U_1 (another unitary matrix) in the 13 plane will diagonalize the light neutrino mass matrix, *i.e.* $m_\nu^{diag} = U_1^T m'_\nu U_1$. The angle θ and phase ψ associated in U_1 are therefore related with the parameters a, b, d involved in ${m_\nu}^2$.

---

[2] The overall factor $\frac{y_1^2 v^2}{y_2^2 v_\rho^2}$ does not take part in determining the mixing angles and phases. However it would be important in determining the exact magnitude of light neutrino masses as we will see later.

Let us consider the form of U_1 as,

$$U_1 = \begin{pmatrix} \cos\theta & 0 & \sin\theta e^{-i\psi} \\ 0 & 1 & 0 \\ -\sin\theta e^{i\psi} & 0 & \cos\theta \end{pmatrix}, \tag{4.13}$$

where θ and ψ are the angle and phase respectively. The diagonalization of m_ν takes place through

$$(U_{TB}U_1)^T m_\nu U_{TB}U_1 = \text{diag}(m_1 e^{i\gamma_1}, m_2 e^{i\gamma_2}, m_3 e^{i\gamma_3}), \tag{4.14}$$

where $m_{i=1,2,3}$ are the real and positive eigenvalues and $\gamma_{i=1,2,3}$ are the phases extracted from the corresponding complex eigenvalues. We are now in a position to evaluate the effective light neutrino mixing U_ν such that $U_\nu^T m_\nu U_\nu = \text{diag}(m_1, m_2, m_3)$. The U_ν then becomes $U_\nu = U_{TB}U_1U_m$, where $U_m = \text{diag}(1, e^{i\alpha_{21}/2}, e^{i\alpha_{31}/2})$ is the Majorana phase matrix with $\alpha_{21} = (\gamma_1 - \gamma_2)$ and $\alpha_{31} = (\gamma_1 - \gamma_3)$, one common phase being irrelevant. Now this U_ν (charged lepton mass matrix being diagonal) can be compared with U_{PMNS} [4] which in its standard parametrization is given by Eq. (1.44).

We consider $a = |a|e^{i\phi_a}$, $b = |b|e^{i\phi_b}$ and $d = |d|e^{i\phi_d}$ (*i.e.* they are in general complex) the phases of which are indicated by $\phi_{a,b,d}$. For calculational purpose, we define parameters $|\alpha| = |b|/|a|$, $\beta| = |d|/|a|$ and the difference of phases by $\phi_{ba} = \phi_b - \phi_a$ and $\phi_{da} = \phi_d - \phi_a$. As U_1 diagonalizes the m'_ν matrix in Eq. (4.11), θ and ψ can be expressed in terms of a, b and d as,

$$\tan 2\theta = \frac{\sqrt{3}\beta\cos\phi_{da}}{(\beta\cos\phi_{da} - 2)\cos\psi + 2\alpha\sin\phi_{ba}\sin\psi}, \tag{4.15}$$

$$\tan\psi = \frac{\sin\phi_{da}}{\alpha\cos(\phi_{ba} - \phi_{da})}. \tag{4.16}$$

Comparing $U_\nu = U_{TB}U_1U_m$ with U_{PMNS} as in Eq.(1.44), we obtain the following expressions for θ_{13} and Dirac CP phase δ [149]

$$\sin\theta_{13} = \sqrt{\frac{2}{3}}|\sin\theta|, \quad \delta = \arg[(U_1)_{13}]. \tag{4.17}$$

These correlations are among the usual characteristics of the A_4 flavor symmetry [127, 129, 210, 211]. For $\sin\theta > 0$ (depending on the choices of α, β), the relation $\delta = \arg[(U_1)_{13}]$

implies $\delta = \psi$. Again if $\sin\theta < 0$, the relation becomes $\delta = \psi \pm \pi$. Hence for both the cases, we have $\tan\psi = \tan\delta$ and Eq. (5.18) becomes

$$\tan\delta = \frac{\sin\phi_{da}}{\alpha\cos(\phi_{ba} - \phi_{da})}. \tag{4.18}$$

Using Eq. (4.14), the complex light neutrino mass eigenvalues are evaluated as

$$m^c_{1,3} = \frac{v^2 y_1^2}{v_\rho^2 y_2^2}\left[-b \pm \sqrt{a^2 - ad + d^2}\right], \tag{4.19}$$

$$m^c_2 = \frac{v^2 y_1^2}{v_\rho^2 y_2^2}(a + d). \tag{4.20}$$

The real and positive mass eigenvalues (m_i) can be then extracted having the following expressions,

$$m_1 = k\left[(P - \alpha\cos\phi_{ba})^2 + (Q - \alpha\sin\phi_{ba})^2\right]^{1/2}, \tag{4.21}$$

$$m_2 = k\left[1 + \beta^2 + 2\beta\cos\phi_{da}\right]^{1/2}, \tag{4.22}$$

$$m_3 = k\left[(P + \alpha\cos\phi_{ba})^2 + (Q + \alpha\sin\phi_{ba})^2\right]^{1/2}, \tag{4.23}$$

where $k = |a|v^2|y_1|^2/v_\rho^2|y_2|^2$ and

$$P = \left[\frac{1}{2}(A + \sqrt{A^2 + B^2})\right]^{1/2}, \quad Q = \left[\frac{1}{2}(-A + \sqrt{A^2 + B^2})\right]^{1/2}, \tag{4.24}$$

$$A = 1 + \beta^2\cos 2\phi_{da} - \beta\cos\phi_{da}, \quad B = \beta^2\sin 2\phi_{da} - \beta\sin\phi_{da}. \tag{4.25}$$

The three phases associated with these mass eigenvalues are $\gamma_i = \phi_i + \phi_0$, where ϕ_0 is the overall phase for ay_1^2/y_2^2 and ϕ_i are given by

$$\begin{aligned}
\phi_1 &= \tan^{-1}\left(\frac{Q - \alpha\sin\phi_{ba}}{P - \alpha\cos\phi_{ba}}\right),\\
\phi_2 &= \tan^{-1}\left(\frac{\beta\sin\phi_{da}}{1 + \beta\cos\phi_{da}}\right),\\
\phi_3 &= \tan^{-1}\left(\frac{Q + \alpha\sin\phi_{ba}}{P + \alpha\cos\phi_{ba}}\right).
\end{aligned} \tag{4.26}$$

Note that the Majorana phases α_{21} and α_{31} depend on ϕ_i only.

4.4 Constraining parameters from neutrino data

Using Eqs.(5.23-5.25) one can define a ratio of solar to the atmospheric mass-squared differences as

$$r = \frac{\Delta m^2_\odot}{|\Delta m^2_{atm}|}, \tag{4.27}$$

with $\Delta m^2_\odot \equiv \Delta m^2_{21} = m^2_2 - m^2_1$ and $|\Delta m^2_{atm}| \equiv |\Delta m^2_{31}| = |m^2_3 - m^2_1|$. From the expressions above in Section 3, it is clear that neutrino mixing angle θ_{13}, Dirac CP phase δ, Majorana phases ($\alpha_{21} = \phi_1 - \phi_2$ and $\alpha_{31} = \phi_1 - \phi_3$) and ratio r are functions of four parameters, α, β, ϕ_{ba} and ϕ_{da}. The other two angles (θ_{23}, θ_{12}) are obtained from the comparison between U_ν and U_{PMNS}. Among these, $\theta_{13}, \theta_{23}, \theta_{12}$ and ratio r are precisely known from the neutrino oscillation data. Since δ (also the Majorana phases) is yet not be known from the experimental data, we perform the analysis for several choices of δ. Then the four parameters can be constrained using values of θ_{13}, r and δ once we keep one of them fixed. For convenience, we have divided our analysis into five cases: (i) Case A [$\phi_{ba} = \phi_{da} = 0$], (ii) Case B [$\phi_{ba} = 0$], (iii) Case C [$\phi_{da} = 0$], (iv) Case D [$\phi_{ba} = \phi_{da} = \phi$] and (v) the General Case.

Following [5], the best fit values of $\Delta m^2_\odot = 7.6 \times 10^{-5}$ eV^2 and $|\Delta m^2_{atm}| = 2.48 \times 10^{-3}$ eV^2 along with their 3σ ranges are used for our analysis. We have fixed r at 0.03. Though there exists another parameter k (see Eqs. (5.23-5.25)), this cancels out in the expression for r. The magnitude of k will be fixed in order to reproduce the solar or atmospheric mass square difference(s). Once this is also obtained, we essentially get the estimate of the absolute neutrino masses and Majorana phases. Expression for the effective neutrino mass parameter $|m_{ee}|$ appearing in the neutrinoless double beta decay is given by[4],

$$|m_{ee}| = \left| m_1 c^2_{12} c^2_{13} + m_2 s^2_{12} c^2_{13} e^{i\alpha_{21}} + m_3 s^2_{13} e^{i(\alpha_{31} - 2\delta)} \right|. \tag{4.28}$$

Hence we have a prediction for $|m_{ee}|$ for the allowed range of parameters. Note that in this analysis we should be able to find out values of $\alpha, \beta, k, \phi_{ba}, \phi_{da}$ and δ which are consistent with experimental data. However the scales involved as flavons vev, cut-off scale Λ, order of μ matrix (*i.e.* the magnitude of $|a|, |b|, |d|$) can not be determined, specifically here in this section. Latter while discussing the non-unitarity effects in Section 5, we would be able to set limits on those scales.

4.4.1 Case A: $[\phi_{ba} = \phi_{da} = 0]$

In this case, we make the simplest choice for the associated phases as $\phi_{ba} = \phi_{da} = 0$. Then Eq. (5.17 and 4.17) can be written as

$$\tan 2\theta = \frac{\sqrt{3}\beta}{(\beta - 2)} \quad \text{and} \quad \sin\theta_{13} = \sqrt{\frac{2}{3}}|\sin\theta|, \tag{4.29}$$

with $\tan\delta = 0$. Hence we note that $\sin\theta_{13}$ solely depends on β.

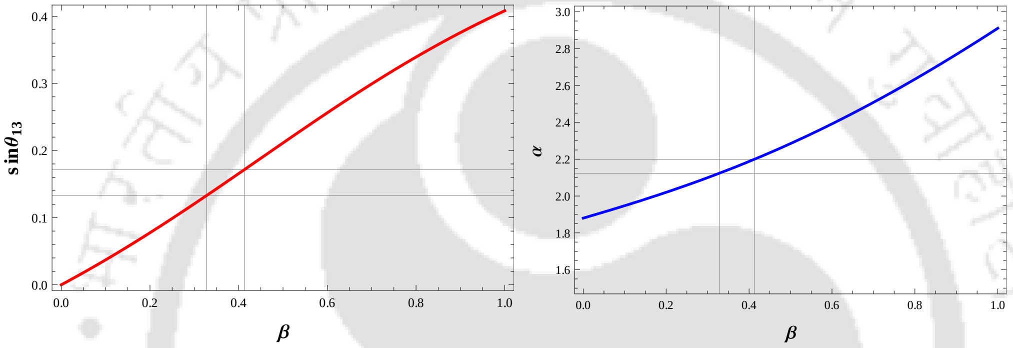

FIGURE 4.1: [Left panel] Plot for $\sin\theta_{13}$ vs β . Here 3σ range for $\sin\theta_{13}$ fixes β in the range 0.328-0.413. [Right panel] $r = 0.03$ contour in the α-β plane.

With $\beta = 0$ we get back the TBM pattern of neutrino mixing matrix. In Fig. 4.1 left panel, we plot the variation of $\sin\theta_{13}$ against β using Eq. (4.29) the 3σ range of $\sin\theta_{13}$ (between 0.133 and 0.177 as indicated by the two horizontal lines) predicts a range of β: $= 0.328 - 0.413$ (denoted by the vertical lines).

With $\phi_{ba} = \phi_{da} = 0$, expressions of absolute neutrino masses in Eq. (5.23-5.25) simplify into,

$$\begin{aligned} m_1 &= k\left|\sqrt{1+\beta^2-\beta} - \alpha\right|, && (4.30) \\ m_2 &= k\left[1+\beta\right], && (4.31) \\ m_3 &= k\left[\sqrt{1+\beta^2-\beta} + \alpha\right]. && (4.32) \end{aligned}$$

Thereby the ratio of solar to atmospheric mass-squared differences, r (as defined in Eq. (5.32)), now takes the form

$$r = \frac{1}{2} - \frac{\alpha^2 - 3\beta}{4\alpha\sqrt{1+\beta^2-\beta}}. \tag{4.33}$$

Note that this ratio depends upon both α and β. To understand this dependence in a better way, we draw the contour plot for $r = 0.03$ [4] in $\alpha - \beta$ plane as shown in Fig. 4.1 (right panel). We find that the allowed range of β from Fig. 4.1 (left panel) indicates a range of the other parameter α to be within (2.12 - 2.18) as seen from Fig. 4.1 (right panel). Note that contour plot of r provides a one to one correspondence between α and β values within this range. For example, the best fit values of $\sin\theta_{13}$ and r corresponds to $\alpha = 2.16$ and $\beta = 0.372$. So the sets of (α, β) values within this allowed range would be used for rest of our analysis in Case A. It is observed that θ_{12} and θ_{23} also fall within their 3σ value [5] for the entire allowed range of α and β.

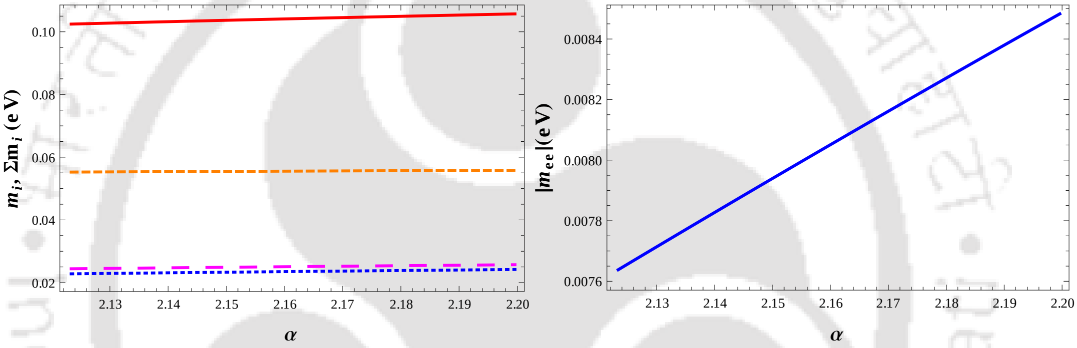

FIGURE 4.2: [Left panel] Absolute neutrino masses vs α (blue dotted, magenta large dashed, orange dashed and red continuous lines represent m_1, m_2, m_3 and $\sum m_i$ respectively); [Right panel] Plot for $|m_{ee}|$ vs α [Case A].

Parameters/Observables	Allowed Range
β	0.328-0.412
α	2.12-2.18
k (eV)	1.84×10^{-2} - 1.82×10^{-2}
$\sum m_i$ (eV)	0.102462 - 0.105713
$\lvert m_{ee}\rvert$ (eV)	0.0076-0.0085

TABLE 4.2: Range of $\beta, \alpha, k, \sum m_i$ and $|m_{ee}|$ for 3σ variation of $\sin\theta_{13}$ [Case A].

From Eq. (4.30-4.32) it is evident that along with α and β, individual absolute light neutrino masses depend also upon another parameter $k(= |a|v^2|y_1|^2/v_\rho^2|y_2|^2)$. Once we know the sets of (α, β) that produces $\sin\theta_{13}$ in the 3σ allowed range and $r = 0.03$, it is possible to determine k from the best fit values of solar (or atmospheric) mass square differences, $m_2^2 - m_1^2 = 7.6 \times 10^{-5}$ eV^2 ($|\Delta m^2_{atm}| = 2.48 \times 10^{-3}$ eV^2) [5]. Hence corresponding to a set (α, β), we can determine k. Doing so, we find the allowed range for

k turns out to be $(1.82-1.84)\times 10^{-2}$ eV. Using such a set of values of $(\alpha,\ \beta,\ k)$ we plot the sum of the light neutrino masses and effective mass parameter $|m_{ee}|$ for neutrinoless double beta decay in the left and right panels of Fig. 4.2 respectively. Our findings are summarized in Table 4.2 in terms of allowed ranges for parameters and observables.

4.4.2 Case B: $[\phi_{ba}=0]$

With $\phi_{ba}=0$, Eqs. (5.17) and (5.18) reduce into

$$\tan 2\theta = \frac{\sqrt{3}\beta\cos\phi_{da}}{(\beta\cos\phi_{da}-2)\cos\psi}, \quad \tan\delta = \frac{\tan\phi_{da}}{\alpha}. \tag{4.34}$$

As before, $\sin\theta_{13}$ can be obtained from the relation $\sin\theta_{13}=\sqrt{\frac{2}{3}}\,|\sin\theta|$. Using Eqs.(5.23-5.25), the ratio of solar to atmospheric mass squared differences in this case can be written as

$$r = \frac{1}{4\alpha P}\left[1+\beta^2+2\beta\cos\phi_{da}-(P-\alpha)^2-Q^2\right], \tag{4.35}$$

where P and Q are same as given in Eqs. (4.25).

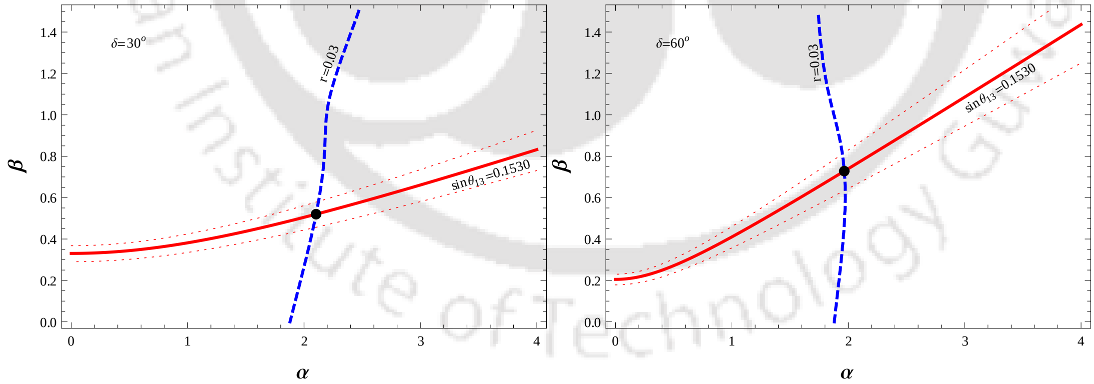

Figure 4.3: Contour plot for $r=0.03$ (dashed line) and $\sin\theta_{13}=0.153$ (continuous line) for $\delta=30°$ (left panel) and $\delta=60°$ (right panel) respectively. Red dotted lines represent a 3σ variation of $\sin\theta_{13}$ while black dots stand for intersection (solution) points for best fit values of $\sin\theta_{13}$ and r in both panels.

The above expressions show that $\sin\theta_{13}$ and r both are dependent on three parameters namely α,β and ϕ_{da} contrary to Case A where they depend only on two parameters α

δ	α	β	k (eV)	Σm_i (eV)	$\lvert m_{ee}\rvert$ (eV)
0°	2.162	0.372	0.0183	0.1042	0.0222
10°	2.155	0.393	0.0184	0.1047	0.0225
20°	2.136	0.448	0.0188	0.1065	0.0233
30°	2.103	0.521	0.0195	0.1093	0.0245
40°	2.060	0.596	0.0204	0.1128	0.0260
50°	2.011	0.666	0.0213	0.1162	0.0274
60°	1.965	0.728	0.0220	0.1182	0.0280
70°	1.928	0.782	0.0221	0.1179	0.0275
80°	1.901	0.827	0.0217	0.1152	0.0259
90°	1.879	0.859	0.0210	0.1109	0.0270

TABLE 4.3: Parameters satisfying neutrino oscillation data for various values of δ with $\phi_{ba} = 0$ [Case B].

and β. However if we choose a particular δ, we can replace ϕ_{da} dependence in terms of α by using the second relation from Eq.(4.34). Then if we draw contours of r and $\sin\theta_{13}$ in the α, β plane where a simultaneous satisfaction of best fit values of $\sin\theta_{13}$ and r provide solutions for α and β with that specific choice of δ. As an example, we have drawn contour plots for $\sin\theta_{13} = 0.153$ and $r = 0.03$ in Fig. 4.3 for $\delta = 30°$ (left panel) and $\delta = 60°$ (right panel) in $\alpha - \beta$ plane. Intersecting points between the $\sin\theta_{13}$ and r contours in these plots, denoted by black dots represent the set of solutions $(\alpha,\ \beta)$ satisfying neutrino oscillation data. θ_{12} and θ_{23} fall in the right range for the entire 3σ range of $\sin\theta_{13}$ considered. With each such set of solution points $(\alpha,\ \beta)$ for a fixed δ, we can compute the other parameter k in order to obtain the correct solar (or atmospheric) mass splitting. Here in Table 4.3 we have provided sets of values for (α, β, k) for various δ satisfying $\sin\theta_{13} = 0.153$ and $r = 0.03$ obtained from neutrino oscillation experiments.

It is to be noted that with a particular choice of δ, contour plots for both $\sin\theta_{13}$ and r are identical with the one obtained from $|\pi - \delta|$. Here in this set-up, scanning over all values of δ (with 3σ variation of $\sin\theta_{13}$ taken into account), sum of the three light neutrino masses and effective mass parameter are predicted to be in the range : 0.104 eV $\lesssim \Sigma m_i \lesssim 0.118$ eV and 0.022 eV $\lesssim |m_{ee}| \lesssim 0.028$ eV. These are mentioned in the two rightmost columns in Table 4.3.

4.4.3 Case C: $[\phi_{da} = 0]$

We consider here the other possibility of choosing one of the two phases as zero, *i.e.* $\phi_{da} = 0$. Then we have relations $\tan 2\theta = \frac{\sqrt{3}\beta}{(\beta-2)}$, $\sin\theta_{13} = \sqrt{\frac{2}{3}}|\sin\theta|$ with $\tan\delta = 0$. This coincides with Eq. (4.29) of Case A. Hence we can use the outcome of Fig. 4.1 (left panel) for specifying the range of α, β which reproduce the value of $\sin\theta_{13}$ (with in 3σ allowed range) and r respectively. With $\phi_{da} = 0$, the real and positive mass eigenvalues take the form

$$m_1 = k\left[(\sqrt{1+\beta^2}-\beta-\alpha\cos\phi_{ba})^2+(\alpha\sin\phi_{ba})^2\right]^{1/2}, \tag{4.36}$$

$$m_2 = k\,[1+\beta]\,, \tag{4.37}$$

$$m_3 = k\left[(\sqrt{1+\beta^2}-\beta+\alpha\cos\phi_{ba})^2+(\alpha\sin\phi_{ba})^2\right]^{1/2}. \tag{4.38}$$

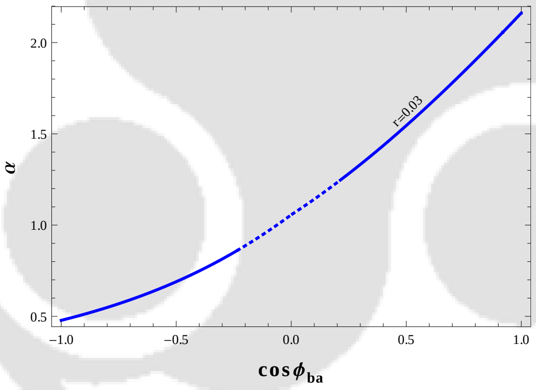

FIGURE 4.4: Contour plot for $r = 0.03$ in the $\alpha - \cos\phi_{ba}$ plane for $\phi_{ba} = 0$. The disallowed range of $\alpha, \cos\phi_{ba}$ is indicated by the dotted portion.

In this case, the ratio of solar to atmospheric mass-squared differences r, is related to the parameters by the relation,

$$r = \frac{3\beta-\alpha^2+2\alpha\cos\phi_{ba}\sqrt{1+\beta^2}-\beta}{4\alpha\sqrt{1+\beta^2}-\beta|\cos\phi_{ba}|}. \tag{4.39}$$

The Eq. (4.39) describes a relation between parameters α, β and ϕ_{ba}. We fix β at 0.372 which corresponds to the best fit value of $\sin\theta_{13} = 0.153$ as seen from Fig. 4.1 (left panel). Then $\cos\phi_{ba}$ and α correlation is addressed through a contour plot of $r = 0.03$ in Fig. 4.4

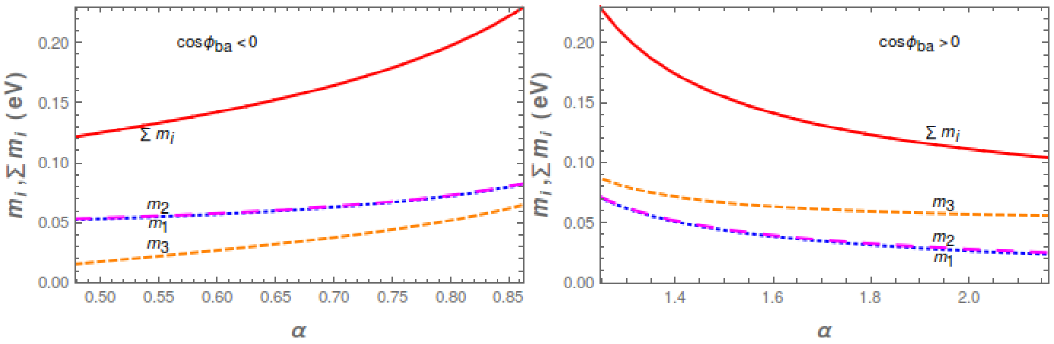

FIGURE 4.5: Absolute neutrino masses vs α (blue dotted, magenta large dashed, orange dashed and red continuous lines represent m_1, m_2, m_3 and $\sum m_i$ respectively). The left panel is for $\cos\phi_{ba} < 0$ and right panel is for $\cos\phi_{ba} > 0$.

using Eq. (4.39). We find for $-1 \leq \cos\phi_{ba} \leq 1$, α falls with the region $0.478 \leq \alpha \leq 2.162$. This range is further constrained once we use cosmological constraint on sum of the light neutrino masses to be below 0.23 eV [12]. This exclusion part is indicated by the dotted portion of the r contour in Fig. 4.4. Now in order to have an estimate of absolute neutrino masses, first we need to know the other parameter k. Corresponding to the fixed value of $\beta = 0.372$, we have sets of values of $(\cos\phi_{ba},\ \alpha)$ which leads to $r = 0.03$ from Fig.4.4. For each such set of $(\cos\phi_{ba},\ \alpha)$, we can have the corresponding k value in order to get the best fit value for solar mass squared difference, $m_2^2 - m_1^2 = 7.6 \times 10^{-5}$ eV^2, and obtain

$$k = \left[\frac{7.6 \times 10^{-5}}{4\alpha r\sqrt{1+\beta^2} - \beta|\cos\phi_{ba}|}\right]^{1/2}, \tag{4.40}$$

where the Eqs. (4.36, 4.39) are employed and $\beta = 0.372$ is taken. In Fig. 4.5 (left panel and right panel) we have plotted absolute neutrino masses (m_i) against α (with $\beta = 0.372$) where one to one correspondence between α and $\cos\phi_{ba}(< 0$ and $> 0)$ from Fig. 4.4 is taken into account. Here m_1, m_2, m_3 and $\sum m_i$ are denoted by blue dotted, magenta large dashed orange dashed and red continuous lines respectively. Note that $\cos\phi_{ba} < 0$ indicates the inverted hierarchy while $\cos\phi_{ba} > 0$ corresponds to the normal hierarchy for light neutrinos. We have found the prediction for $|m_{ee}|$ to be within $0.016\,\text{eV} < |m_{ee}| < 0.052\,\text{eV}$ for normal hierarchy and $0.047\,\text{eV} < |m_{ee}| < 0.066\,\text{eV}$ for inverted hierarchy considering the restricted variation of α ($0.478 \leqslant \alpha \leqslant 0.863$ for $\cos\phi_{ba} < 0$ and $1.247 \leqslant \alpha \leqslant 2.162$ for $\cos\phi_{ba} > 0$). Few of our findings are tabulated in Table 4.4.

α	$\cos\phi_{ba}$	k	$\sum m_i$	$\lvert m_{ee}\rvert$
1.904	0.8	0.0218 eV	0.1164 eV	0.0194 eV
0.814	-0.3	0.0544 eV	0.0231 eV	0.0604 eV

TABLE 4.4: Representative values of $k, \sum m_i$ and $|m_{ee}|$ in Case C.

4.4.4 Case D: $[\phi_{ba} = \phi_{da} = \phi_a]$

Now, if we consider $\phi_{ba} = \phi_{da} = \phi$, then Eqs. 5.17 and 5.18 can be written as

$$\tan 2\theta = \frac{\sqrt{3}\beta\cos\phi}{(\beta\cos\phi - 2)\cos\psi + 2\alpha\sin\phi\sin\psi}, \quad \tan\delta = \tan\psi = \frac{\sin\phi}{\alpha}. \tag{4.41}$$

and hence $\sin\theta_{13}$ again can be computed using the relation $\sin\theta_{13} = \sqrt{\frac{2}{3}}|\sin\theta|$. The real and positive mass eigenvalues now take the form

$$\begin{aligned} m_1 &= k\left[(P_D - \alpha\cos\phi)^2 + (Q_D - \alpha\sin\phi)^2\right]^{1/2}, \\ m_2 &= k\left[1 + \beta^2 + 2\beta\cos\phi\right]^{1/2}, \\ m_3 &= k\left[(P_D + \alpha\cos\phi)^2 + (Q_D + \alpha\sin\phi)^2\right]^{1/2}, \end{aligned}$$

with

$$P_D = \left[\frac{1}{2}\left(A_D + \sqrt{A_D^2 + B_D^2}\right)\right]^{1/2}, \quad Q_D = \left[\frac{1}{2}\left(-A_D + \sqrt{A_D^2 + B_D^2}\right)\right]^{1/2} \tag{4.42}$$

$$A_D = 1 + \beta^2\cos 2\phi - \beta\cos\phi, \quad B_D = \beta^2\sin 2\phi - \beta\sin\phi. \tag{4.43}$$

Using above expressions for light neutrino masses we can write the ratio of solar to atmospheric mass squared difference as

$$r = \frac{(1 + \beta^2 + 2\beta\cos\phi) - (P_D - \alpha\cos\phi)^2 - (Q_D - \alpha\sin\phi)^2}{4\alpha(P_D\cos\phi + Q_D\sin\phi)}. \tag{4.44}$$

Clearly just like Case B, here also both $\sin\theta_{13}$ and r both depends on α, β and the common phase ϕ. Following the same prescription as in Case B, one can draw contours for best fit values of $\sin\theta_{13}$ and r in the α, β plane. Intersecting points of these two contours then represent simultaneous solutions for both α and β for a particular value of δ. In Fig. 4.6 we have drawn such contours for $\delta = 30°$ (left panel) and $\delta = 60°$ (right panel) for demonstrative purpose. In this plot, black dots represent the intersecting points for $\sin\theta_{13} = 0.153$ and $r = 0.03$ contours and hence the solutions for α and β. Here we find that solutions satisfying neutrino oscillation data exist for all values of δ between 0° and 90° as given in Table 4.5. We find that the contour plots for both $\sin\theta_{13} = 0.1530$ and $r = 0.03$ with a specific δ value coincides (and hence the solutions for α, β) with the one with other δ values (in the range 0 to 2π) obtained from $|\pi - \delta|$.

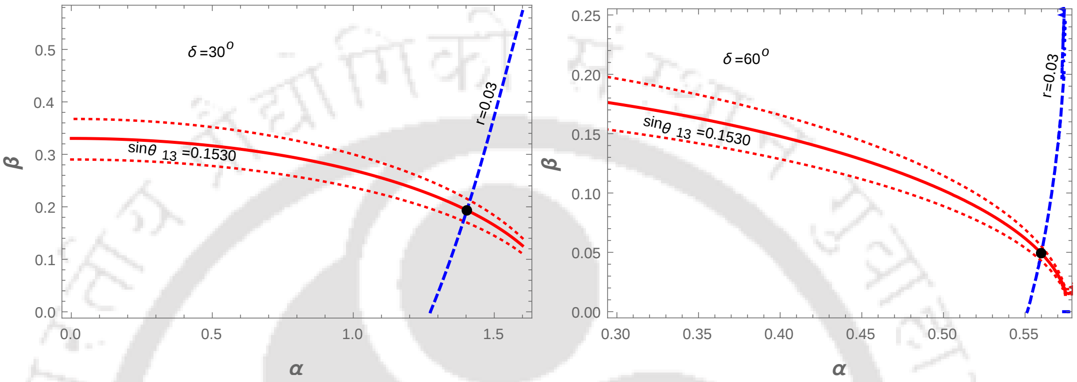

FIGURE 4.6: Contour plot for $r = 0.03$ (dashed line) and $\sin\theta_{13} = 0.153$ (continuous line) for $\delta = 30°$ (left panel) and $\delta = 60°$ (right panel) respectively. Red dotted lines represent a 3σ variation $\sin\theta_{13}$ and black dots stands for solution points for best fit values of $\sin\theta_{13}$ and r in both panels.

δ	α	β	k (eV)	Σm_i (eV)	$\lvert m_{ee}\rvert$ (eV)
0°	2.162	0.372	0.0183	0.1042	0.0220
10°	2.039	0.343	0.0194	0.1057	0.0221
20°	1.755	0.272	0.0223	0.1095	0.0214
30°	1.403	0.194	0.0273	0.1187	0.0225
40°	1.070	0.131	0.0354	0.1365	0.0319
50°	0.792	0.084	0.0472	0.1659	0.0447
60°	0.560	0.049	0.0658	0.2159	0.0641
62°	0.518	0.043	0.0701	0.2301	0.0694
70°	0.359	0.023	0.1011	0.3157	0.1000
80°	0.175	0.006	0.2027	0.6144	0.2022

TABLE 4.5: Parameters satisfying neutrino oscillation data for various values of δ with $\phi_{ba} = \phi_{ba} = \phi$ [Case D].

Following the same algorithm as described in Case B, in the last two column of Table 4.5 we have listed allowed values for sum of all three light neutrinos and effective mass parameter. Therefore varying δ between 0 to 2π, we find range of few quantities as 0.1042 eV $\lesssim \sum m_i \lesssim 0.6144$ eV and 0.0220 eV $\lesssim |m_{ee}| \lesssim 0.2022$ eV respectively. Therefore imposing the constraint $\sum m_i < 0.23$ eV on sum of all three light neutrinos coming from Planck [12], the allowed range for δ gets restricted and it finally lies in the range $0^\circ \leq \delta < 62^\circ$ (in terms of the full range $0^\circ - 360^\circ$, other allowed ranges are $128^\circ - 180^\circ$ and $180^\circ - 242^\circ$, $308^\circ - 360^\circ$). In this case only the normal hierarchy results as in Case A and B.

4.4.5 General Case

In the previous sub-sections, we have considered four different cases with specific choices for ϕ_{ba} and/or ϕ_{da} for our analysis on neutrino masses and mixing. Here we discuss the most general case where we allow the variation of ϕ_{ba} and ϕ_{da} for their entire range between 0 and 2π. For this purpose, we employ Eqs. (5.17-4.17) in order to analyze the mixing angles. On the other hand, the ratio of solar to the atmospheric mass-squared differences r, defined in Eq. (5.32), can also be computed once we use the general expressions for absolute neutrino masses given in Eq. (5.23-5.25).

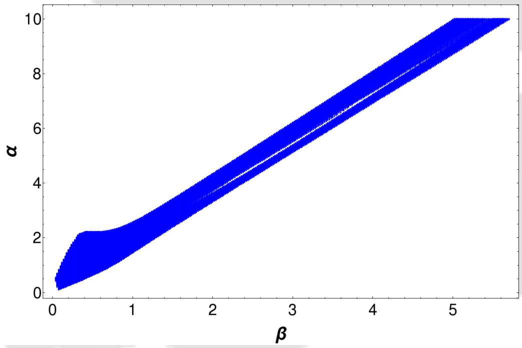

FIGURE 4.7: Allowed range (represented by the blue patch) of α and β in order to satisfy 3σ range of $\sin\theta_{13}$ and r. The phases $\phi_{ba,da}$ are allowed to vary within 0 to 2π.

Now using the 3σ allowed ranges for θ_{13} and r [5], we represent the allowed regions for α and β in Fig. 4.7 represented by the blue patch. Here ϕ_{ba} and ϕ_{da} are allowed to vary within their full range (0 to 2π). However it turns out that only a portion of this entire range can actually satisfy the required θ_{13} and r through Eqs. (5.17-4.17) along with the range of $\alpha - \beta$ depicted in Fig. 4.7. This is shown in Fig. 4.8 in the $\phi_{ba} - \phi_{da}$ plane. Knowing the allowed range of α, β and their correlation with phases ϕ_{ba}, ϕ_{da}, we plot in Fig. 4.9 the prediction of the model in terms of sum of the three light neutrino masses ($\sum m_i$) in the left panel and effective mass parameter for neutrinoless double beta decay ($|m_{ee}|$) in the right panel as functions of β. In the left panel of Fig. 4.9, the horizontal

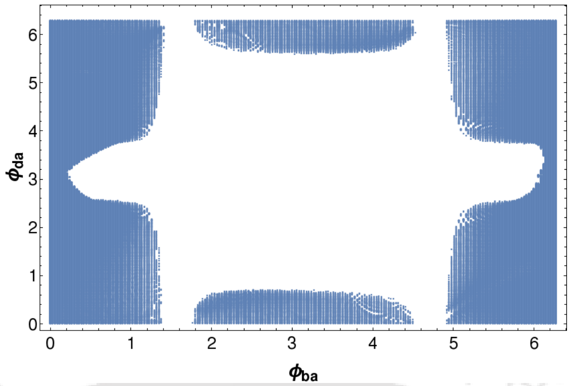

FIGURE 4.8: Allowed ranges of ϕ_{ba} and ϕ_{da} in order to produce $\sin\theta_{13}$ in the 3σ range, correct r, satisfying $\sum m_i < 0.23$ eV.

orange patch represents the excluded region by the upper bound on sum of the absolute neutrino masses $\sum m_i \leq 0.23$ eV, whereas in the right panel of the same figure we have already included this additional constraint to plot $|m_{ee}|$. Finally in Fig. 4.10, we show the allowed range of the Dirac CP phase δ against the range of β (allowed) where we consider simultaneously the corresponding allowed range of α, ϕ_{ba} and ϕ_{da} following Figs. 4.7-4.9.

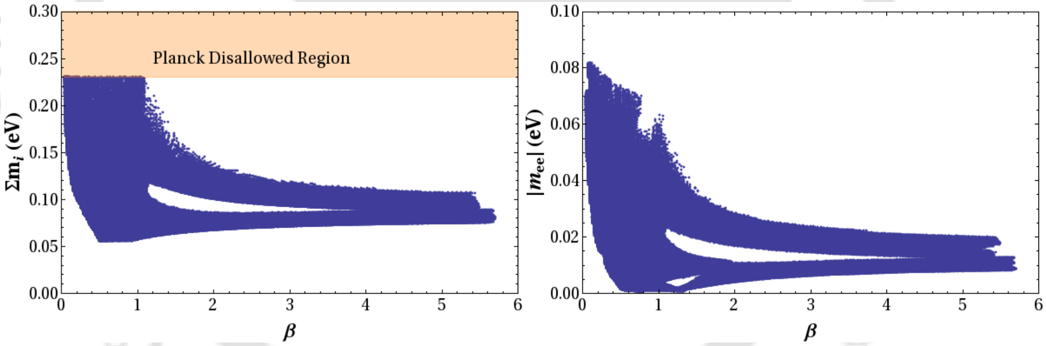

FIGURE 4.9: [Left panel] $\sum m_i$ vs β which satisfy 3σ range of $\sin\theta_{13}$ and r. Horizontal orange patch represents the excluded region from the upper bound on sum of all the three light neutrino masses ($\sum m_i < 0.23$ eV). [Right panel] $|m_{ee}|$ vs β satisfying $\sum m_i < 0.23$ eV. In both the panels α, ϕ_{ba} and ϕ_{da} vary according to Figs. 4.7-4.8.

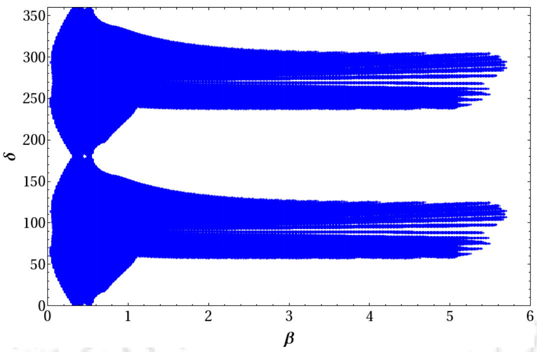

FIGURE 4.10: Dirac CP phase δ vs β satisfying constraints from 3σ range of $\sin\theta_{13}$ and r (with $\sum m_i < 0.23$ eV). Here both ϕ_{ba} and ϕ_{da} varies between $0 - 2\pi$.

4.5 Non-unitary effect

In Section 3, we have determined the neutrino mixing matrix U_ν and identify it with the U_{PMNS} (charged lepton mass matrix being diagonal) as it diagonalizes the effective light neutrino mass matrix m_ν through the unitary transformation $U_\nu^T m_\nu U_\nu =$ diag(m_1, m_2, m_3). However the U_{PMNS} should receive a correction over U_ν as the heavy states carries an admixture with the light neutrinos [212]. To clarify, suppose V_ν is the diagonalizing matrix which makes M_ν into the block diagonal form first, *i.e.*

$$V_\nu^T M_\nu V_\nu = \begin{pmatrix} m_{\nu_{light}3\times3} & 0_{3\times6} \\ 0_{6\times3} & m_{\nu_{heavy}6\times6} \end{pmatrix}. \tag{4.45}$$

At this point the light neutrino mass matrix $m_{\nu_{light}} \simeq -m_\nu = -m_D M^{-1}\mu(M^T)^{-1}m_D^T$ and the other one is given by

$$m_{\nu_{heavy}} \simeq \begin{pmatrix} 0 & M^T \\ M & \mu \end{pmatrix}, \tag{4.46}$$

in the lowest order [46]. Let U be the matrix of the form

$$U = \begin{pmatrix} U_\nu & 0 \\ 0 & U_h \end{pmatrix}, \tag{4.47}$$

which will do the individual diagonalization, *i.e.* U_ν and U_h are expected to diagonalize $m_{\nu_{light}}$ and $m_{\nu_{heavy}}$ respectively (remember that U_ν is the diagonalizing matrix of m_ν as already discussed in Section 3). So finally $W = V_\nu U$ diagonalizes the entire 9×9 matrix M_ν such that $W^T M_\nu W = \mathrm{diag}(m_{i=1,2,3}, m_{N_{k=1,2,..,6}})$. One can decompose W as follows:

$$W = \begin{pmatrix} W_{3\times3} & W_{3\times6} \\ W_{6\times3} & W_{6\times6} \end{pmatrix}, \tag{4.48}$$

where the block $W_{3\times3}$ is the leading order replacement of U_{PMNS} matrix which is non-unitary [213**?**]. It is shown [213, 215] that $W_{3\times3} \simeq (\mathbb{I} - \frac{1}{2}FF^\dagger)U_\nu$, where the non unitary effect is parametrized by

$$\eta = \frac{1}{2}FF^\dagger, \tag{4.49}$$

with $F = m_D M^{-1}$ as defined before. The present bound on η (at 90% C.L.) can be summarized as [214]

$$|\eta| < \begin{pmatrix} 2.0\times10^{-3} & 3.5\times10^{-5} & 8.0\times10^{-3} \\ 3.5\times10^{-5} & 8.0\times10^{-4} & 5.1\times10^{-3} \\ 8.0\times10^{-3} & 5.1\times10^{-3} & 2.7\times10^{-3} \end{pmatrix}. \tag{4.50}$$

In our case F is proportional to identity as mentioned before and so as η. In the present framework η turns out to satisfy $|\eta| = \frac{v^2|y_1|^2}{2v_\rho^2|y_2|^2}\mathbb{I} = C_1\mathbb{I}$ say, and hence the above bound on η can be translated into

$$C_1 \; < \; 8.0\times10^{-4}, \tag{4.51}$$

where $C_1 = v^2|y_1|^2/2v_\rho^2|y_2|^2$. Using this bound, we can now estimate the scales involved in our scenario, *i.e.* v_ρ, Λ etc. For simplicity we assume all the flavons have the same vevs v_f. Then C_1 is given by $\lambda v^2/2v_f^2$ where $\lambda = |y_1|^2/|y_2|^2$. Hence the common flavon vev v_f is bounded by

$$v_f \; > \; 6.15\sqrt{\lambda} \;\; \mathrm{TeV}, \tag{4.52}$$

which follows from Eq.(4.51).

4.5.1 Determining the scales (v_f, Λ) involved in the set-up

Note that the parameter k defined in Section 3 can be written as

$$k = \frac{\lambda v^2}{v_f^2}|a| = 2\lambda|\mu_1|\frac{v_f v^2}{\Lambda^2}, \qquad (4.53)$$

once the common flavon vev v_f is assumed and $a = 2\mu_1 v_f^3/\Lambda^2$ is inserted. As we already have an estimate for the range of k for all cases (A, B, C and D), we can use that input on k to study the correlation between v_f and Λ for various choices of λ while $|\mu_1|$ is fixed, say at unity. This correction however satisfy Eq. (4.52) and we discuss it below case by case.

4.5.1.1 Case A: $[\phi_{ba} = \phi_{da} = 0]$

In this case, we have found $k = 0.0183$ eV corresponding to the set of parameters α, β ($\alpha = 2.16, \beta = 0.372$) which produces the best fit value of $\sin\theta_{13} = 0.1530$ and $r = 0.03$ so as to have the solar and atmospheric mass squared splittings 7.6×10^{-5} eV^2 and 2.48×10^{-3} eV^2 respectively via Eqs. (4.30-4.32). Now using this particular value of k, we employ Eq.(4.53) to have an estimate of v_f and Λ once the couplings λ and $|\mu_1|$ are fixed. In Fig. 4.11, we plot the contour lines for $k = 0.0183$ eV in the $v_f - \Lambda$ plane for different choices of λ. Here $|\mu_1|$ is assumed to be unity for simplicity. Following Eq. (4.52), the $v_f - \Lambda$ correlation gets further constrained. Depending on the specific choices of λ, the lower

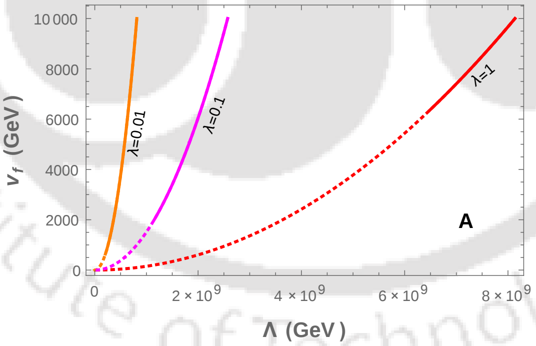

FIGURE 4.11: Contour plots for $k = 0.0183$ eV in the $v_f - \Lambda$ plane (using Eq. (4.53)) for $\phi_{ba} = \phi_{da} = 0$ (and $|\mu_1| = 1$). The dotted portion in each curve indicates the excluded part in view of Eq. (4.52). Here the orange, magenta and red line stands for λ= 0.01, 0.1 and 1 respectively.

	$\lambda = 0.01$	$\lambda = 0.1$	$\lambda = 1$
Λ in GeV (for $C_1 = 7.5 \times 10^{-4}$)	2.06×10^8	1.16×10^9	6.48×10^9
Λ in GeV (for $C_1 = 4 \times 10^{-4}$)	2.40×10^8	1.35×10^9	7.59×10^9

TABLE 4.6: Cutoff scale Λ for different C_1 (with $\phi_{da} = \phi_{ba} = 0$) when $\lambda = 0.01$, 0.1 and 1.

bound on v_f is obtained through Eq. (4.52). The portion of each k contour line which does not satisfy Eq.(4.52) is indicated by the dotted segment. Note that corresponding to a specific choice of the non-unitarity parameter η, v_f would fixed through $C_1 = \frac{\lambda v^2}{2v_f^2}$ (for fixed λ) which then indicates a particular Λ. In Table 4.6, we provide some such specific choices of Λ corresponding to different choice of η. We find that with λ small enough, the cut-off scale can also be lowered $\sim$ TeV.

4.5.1.2 Case B: $[\phi_{ba} = 0]$

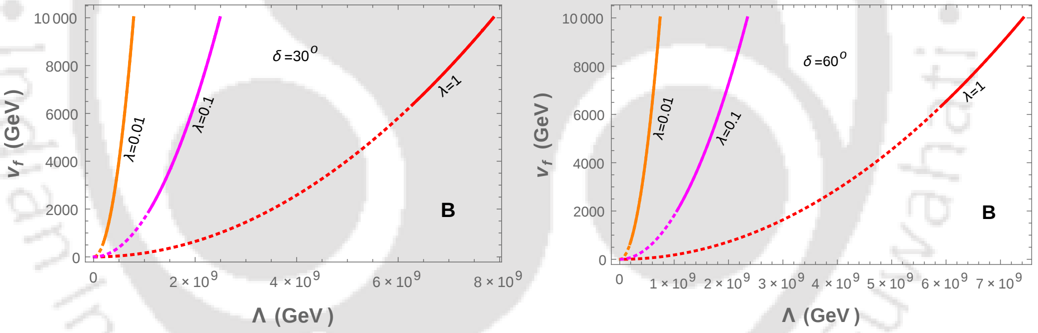

FIGURE 4.12: [Left panel] Contour plot for $k = 0.0195$ eV in the $v_f - \Lambda$ plane for $\phi_{ba} = 0$ and $\delta = 30°$. [Right panel] Contour plot for $k = 0.0220$ eV in the $v_f - \Lambda$ plane for $\phi_{ba} = 0$ and $\delta = 60°$. In both the panels orange, magenta and red lines stand for λ= 0.01, 0.1 and 1 respectively.

	$C_1 = 7.5 \times 10^{-4}$			$C_1 = 4 \times 10^{-4}$		
	$\lambda = 0.01$	$\lambda = 0.1$	$\lambda = 1$	$\lambda = 0.01$	$\lambda = 0.1$	$\lambda = 1$
Λ in GeV ($\delta = 30°$)	1.98×10^8	1.12×10^9	6.3×10^9	2.32×10^8	1.31×10^9	7.34×10^9
Λ in GeV ($\delta = 60°$)	1.89×10^8	1.05×10^9	5.9×10^9	2.19×10^8	1.23×10^9	6.92×10^9

TABLE 4.7: Cutoff scale Λ for different C_1 (with $\phi_{ba} = 0$) and λ (= 0.01, 0.1 and 1).

In Section 4.4 we have seen that for $\phi_{ba} = 0$, r and $\sin\theta_{13}$ depend not only on α, β, but also on the choice of Dirac CP phase δ. We have already listed our finding toward this dependency in Table 4.3. Corresponding to each δ, we have sets of (α, β) and k from

Table 4.3. Now for a fixed δ and k we can study the correlation of v_f and Λ in a similar way as described in Case A above. In Fig. 4.12, we have studied this correlation for two different choices for $\delta = 30^\circ$, $k = 0.0195$ eV (left panel) and $\delta = 60^\circ$, $k = 0.0220$ eV (right panel). We consider $|\mu_1| = 1$ and choices for $\lambda = |y_1|^2/|y_2|^2 = 0.01$ (orange line), 0.1 (magenta line) and 1 (red line) in both panels are shown. Since k (see Table 4.3) does not change much with the change of δ, correlation between v_f and Λ remains almost unaltered as seen from the two panels of Fig. 4.12. The dotted section of each contour line in Fig. 4.12 represents the excluded part in view of Eq. (4.52). With some specific choices of C_1 (satisfying Eq. (4.51)) we have listed the corresponding scale Λ in Table 4.7.

4.5.1.3 Case C: $[\phi_{da} = 0]$

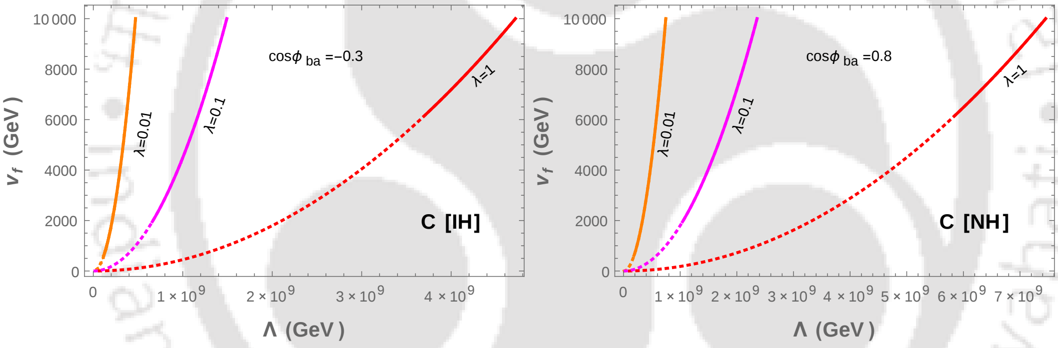

FIGURE 4.13: [Left panel] Contour plot for $k = 0.0544$ eV in the $v_f - \Lambda$ plane for $\phi_{da} = 0$ and $\cos\phi_{ba} = -0.3$ ($\alpha = 0.814$) [IH: Inverted hierarchy]. [Right panel] Contour plot for $k = 0.0218$ GeV in the $v_f - \Lambda$ plane for $\phi_{ba} = 0$ and $\cos\phi_{ba} = 0.8$ ($\alpha = 1.904$) [NH: Normal hierarchy]. In both the panels orange, magenta and red lines stand for λ= 0.01, 0.1 and 1 respectively.

In this case, as we conclude from Fig. 4.4, the range of α is restricted as $0.478 < \alpha < 0.863$ for $\cos\phi_{ba} < 0$ and $1.247 < \alpha < 2.162$ for $\cos\phi_{ba} > 0$. We have found that $\cos\phi_{ba} < 0$ represents inverted hierarchy while $\cos\phi_{ba} > 0$ stands for normal hierarchy. Here δ turns out to be zero. Therefore for a specific value of α (and hence also for $\cos\phi_{ba}$) we obtain the corresponding value of k as mentioned in Table 4.4. Using that particular k, we draw contour plot of k in v_f-Λ plane in Fig. 4.13 where Eq. (4.53) is employed. Left panel of Fig. 4.13 is for inverted hierarchy of light neutrinos and right panel represents the case of normal hierarchy. Using the non-unitarity constraints through Eq. (4.52), similar to Case A and Case B, here also we indicate the disallowed portion of v_f-Λ correlation. Considering some specific choice of C_1, we provide sample values of Λ in Table 4.8.

	$C_1 = 7.5 \times 10^{-4}$			$C_1 = 4 \times 10^{-4}$		
	$\lambda = 0.01$	$\lambda = 0.1$	$\lambda = 1$	$\lambda = 0.01$	$\lambda = 0.1$	$\lambda = 1$
Λ in GeV ($\cos\phi_{ba} = -0.3$)	1.19×10^8	6.69×10^8	3.76×10^9	1.40×10^8	7.82×10^8	4.40×10^9
Λ in GeV ($\cos\phi_{ba} = 0.8$)	1.88×10^8	1.06×10^9	5.94×10^9	2.20×10^8	1.24×10^9	6.95×10^8

TABLE 4.8: Cutoff scale Λ for different C_1 and $\cos\phi_{ba}$ (with $\phi_{da} = 0$) when λ= 0.01, 0.1 and 1.

4.5.1.4 Case D: $[\phi_{ba} = \phi_{da} = \phi]$

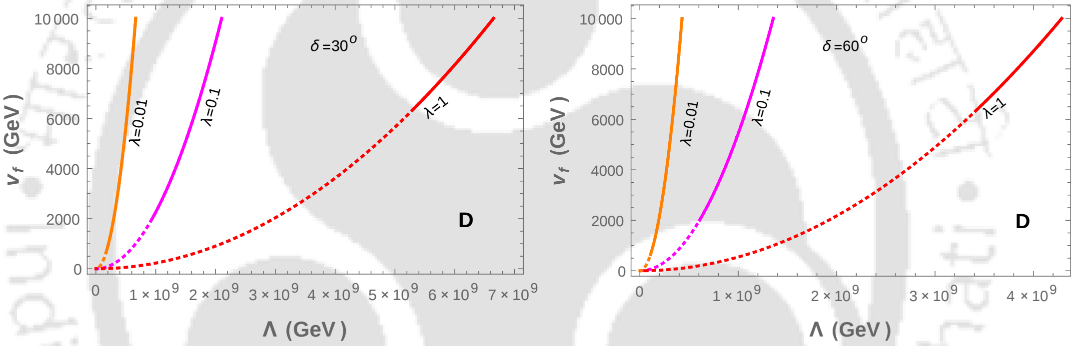

FIGURE 4.14: [Left panel] Contour plot for $k = 0.0274$ eV in the $v_f - \Lambda$ plane for $\phi_{ba} = \phi_{da} = \phi$ and $\delta = 30°$. [Right panel] Contour plot for $k = 0.0658$ eV in the $v_f - \Lambda$ plane for $\phi_{ba} = \phi_{da} = \phi$ and $\delta = 60°$. In both the panels orange, magenta and red lines stand for λ= 0.01, 0.1 and 1 respectively.

With the consideration $\phi_{ba} = \phi_{da} = \phi$, we have already discussed in the previous section that α, β $\sin\theta_{13}$ and r are correlated with the choice of δ. We have listed α, β as well as k for different allowed values of δ in Table 4.5. As discussed before, here also we can plot the dependency of $v_f - \Lambda$ using Eq. (4.53) and estimate the allowed regions for v_f and Λ employing Eq. (4.52). In Fig. 4.14 we have plotted this dependency for various choice of λ with $\delta = 30°$ (left panel) and $\delta = 60°$ (right panel). In both of these panels orange, magenta and red lines stand for $\lambda = 0.01, 0.1$ and 1 respectively. Following this we have listed few representative values of Λ in Table 4.9.

	$C_1 = 7.5 \times 10^{-4}$			$C_1 = 4 \times 10^{-4}$		
	$\lambda = 0.01$	$\lambda = 0.1$	$\lambda = 1$	$\lambda = 0.01$	$\lambda = 0.1$	$\lambda = 1$
Λ in GeV ($\delta = 30°$)	1.68×10^8	9.48×10^8	5.30×10^9	1.96×10^8	1.10×10^9	6.20×10^9
Λ in GeV ($\delta = 60°$)	1.08×10^8	6.08×10^8	3.42×10^9	1.26×10^8	7.11×10^8	4.00×10^9

TABLE 4.9: Cutoff scale Λ for different C_1 and δ (with $\phi_{ba} = \phi_{da} = \phi$) when λ= 0.01, 0.1 and 1.

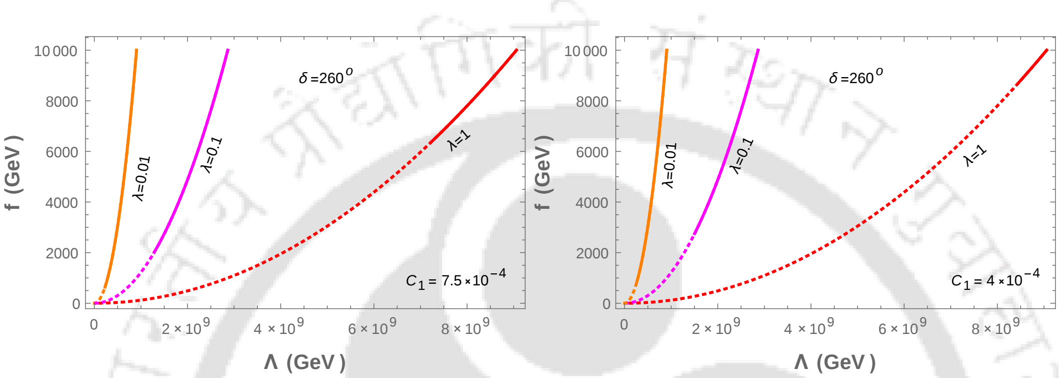

FIGURE 4.15: Contour plot for $k = 0.0147$ eV in the $v_f - \Lambda$ plane where $\alpha = 2.25, \beta = 1, \phi_{ba} = 0.5$ and $\phi_{da} = 2$ and with $C_1 = 7.5 \times 10^{-4}$ (left panel) and $C_1 = 4 \times 10^{-4}$ (right panel). In both the panels orange, magenta and red lines stand for λ= 0.01, 0.1 and 1 respectively.

4.5.1.5 General Case

From our previous analysis in section 4.4, we choose a particular value of $\delta = 260°$ for this general case (a value close to recent hint [5, 80? , 81]) to study the scales v_f, Λ. The set of parameters that would correspond to this value of δ are found to be $\alpha = 2.25, \beta = 1, \phi_{ba} = 0.5$ and $\phi_{da} = 2$ which satisfy constrains imposed from mixing angles, r and $\sum m_i < 0.23$ eV. Here k is found to be 0.0147 eV in order to have adequate solar and atmospheric splittings. Using this k through Eq. (4.53), we then obtain the contour plot of v_f against λ as shown in Fig. 4.15 for different choices of λ. The dotted portion in each curve indicates the excluded part in view of Eq. (4.52) with $C_1 = 7.5 \times 10^{-4}$ (left panel) and $C_1 = 4 \times 10^{-4}$ (right panel). These numerical estimates are summarized in Table 4.10.

	$\lambda = 0.01$	$\lambda = 0.1$	$\lambda = 1$
Λ in GeV (for $C_1 = 7.5 \times 10^{-4}$)	2.29×10^8	1.28×10^9	7.22×10^9
Λ in GeV (for $C_1 = 4 \times 10^{-4}$)	2.68×10^8	1.50×10^9	8.45×10^9

TABLE 4.10: Cutoff scale Λ for different C_1 with $\delta = 260°$ (with $\alpha = 2.25, \beta = 1, \phi_{ba} = 0.5$ and $\phi_{da} = 2$) and λ= 0.01, 0.1 and 1.

4.5.2 Lepton flavor violation

In view of the presence of this non-unitarity effect, the neutrino states ($\nu_{\alpha L}$ with $\alpha = e, \mu, \tau$) appearing in the SM charged current interaction Lagrangian now can be written as,

$$\nu_{\alpha L} = [(1 - C_1)\, U_\nu]_{\alpha i}\; \nu_i + [\mathcal{K}]_{\alpha j}\; N_j, \tag{4.54}$$

where the matrix $W_{3\times6}$ (see Eq. (4.48)) is conventionally denoted by $\mathcal{K}$. $\nu_{i=1,2,3}$ and $N_{j=4,5,...9}$ are the light and heavy neutrino mass eigenstates respectively. Then in a basis where charged leptons are diagonal (as in our case), the charged current interactions have contributions involving three light neutrinos ν_i and six heavy neutrinos N_j as

$$-\mathcal{L}_{CC} \;=\; \frac{g}{\sqrt{2}} \bar{l}_\alpha \gamma^\mu \left\{[(1 - C_1)\, U_\nu]_{\alpha i}\; \nu_i + [\mathcal{K}]_{\alpha j}\; N_j\right\} W_\mu^- + \text{h.c.}. \tag{4.55}$$

These nine neutrino states can therefore mediate lepton flavor violating decays like $l_\alpha \to l_\beta \gamma$ in one loop ($e.g$ $\mu \longrightarrow e\gamma$). Resulting branching ratio for such processes (in the limit $m_\beta \to 0$) now can be written as [217, 218, 220–226],

$$\mathrm{BR}(L_\alpha \to L_\beta \gamma) \simeq \frac{\alpha_W^3 \sin^2\theta_W m_{l_\alpha}^5}{256\pi^2 m_W^4 \Gamma_{l_\alpha}} \left| \sum_{j=1}^{3} [(1 - C_1)\, U_\nu]^*_{\alpha j} [(1 - C_1)\, U_\nu]_{\beta k j} I_\gamma \left(\frac{m_{\nu_j}^2}{m_W^2}\right) \right. \\ \left. + \sum_{l=4}^{9} \mathcal{K}^*_{\alpha l} \mathcal{K}_{\beta l} I_\gamma \left(\frac{m_{N_l}^2}{m_W^2}\right) \right|^2, \tag{4.56}$$

where

$$I_\gamma\,(x) = \frac{10 - 43x + 78x^2 - 49x^3 + 18x^3 \ln x + 4x^4}{12(1-x)^4}, \text{ with } x = \frac{m_{\nu,N}^2}{m_W^2}. \tag{4.57}$$

Here $\alpha_W = g^2/4\pi$, with g as the weak coupling, θ_W is electroweak mixing angle, m_W is $W^\pm$ boson mass and Γ_{l_α} is the total decay width of the decaying charged lepton l_α.

Current upper bound for the branching ratio of the LFV decays are [4] (at 90% CL)

$$\mathrm{BR}(\mu \longrightarrow e\gamma) < 5.7 \times 10^{-13}, \tag{4.58}$$

$$\mathrm{BR}(\tau \longrightarrow e\gamma) < 3.3 \times 10^{-8}, \tag{4.59}$$

$$\mathrm{BR}(\tau \longrightarrow \mu\gamma) < 4.4 \times 10^{-8}. \tag{4.60}$$

Another important lepton flavor violating decay $\mu \to eee$ is also worthy to mention and details of computation of branching ratio calculation can be found in [217, 218]. Current upper limit for this decay is $\mathrm{BR}(\mu \longrightarrow eee) < 1.0 \times 10^{-12}$ (90% CL) [4].

Since the flavor structure of the neutrino mass matrix is already fixed in our present scenario (from the A_4 and additional symmetry consideration), it would provide some concrete understanding for the LFV processes in this inverse seesaw model. Both the $W_{3\times3} = (1 - C_1)\, U_\nu$ and $W_{3\times6} = \mathcal{K}$ matrices play the instrumental role here. Remember that, U_ν is the diagonalizing matrix for the light neutrinos, defined by $U_\nu = U_{TB}U_1U_m$ as discussed in section 4.3. Hence this can be obtained in terms of $\alpha, \beta, k, \phi_{ba}$ and ϕ_{da}. The non-unitary parmeter C_1 is required to satisfy, $C_1 = \lambda v^2/2v_f^2 < 8 \times 10^{-4}$ as discussed earlier. Therefore we can completely evaluate $W_{3\times3} = (1 - C_1)\, U_\nu$, once a specific value of C_1 is chosen.

On the other hand the rectangular matrix $\mathcal{K}$ is approximately given by [215, 216]

$$\mathcal{K} \simeq (-F\mu M^{-1}, F)U_h, \tag{4.61}$$

where U_h is the diagonalizing matrix of $m_{\nu_{heavy}}$ given in Eq. (4.46). As previously mentioned, $F = m_D M^{-1}$ in our scenario is proportional to identity matrix of order 3×3, *i.e.* $F = \frac{y_1 v}{y_2 v_f}\mathbb{I}_{3\times3} = f_1\mathbb{I}_{3\times3}$. Hence, the matrix $\mathcal{K}$ turns out to be

$$\mathcal{K} = (-f_1\mu M^{-1}, f_1\mathbb{I}_{3\times3})U_h. \tag{4.62}$$

Using Eqs. (4.8) and (4.9), we find

$$\mu M^{-1} = \frac{a}{y_2 v_f}\begin{pmatrix} 1-\frac{2}{3}\alpha e^{i\phi_{ba}} & \frac{1}{3}\alpha e^{i\phi_{ba}}+\beta e^{i\phi_{da}} & \frac{1}{3}\alpha e^{i\phi_{ba}} \\ \frac{1}{3}\alpha e^{i\phi_{ba}} & 1+\frac{1}{3}\alpha e^{i\phi_{ba}} & -\frac{2}{3}\alpha e^{i\phi_{ba}}+\beta e^{i\phi_{da}} \\ \frac{1}{3}\alpha e^{i\phi_{ba}}+\beta e^{i\phi_{da}} & -\frac{2}{3}\alpha e^{i\phi_{ba}} & 1+\frac{1}{3}\alpha e^{i\phi_{ba}}. \end{pmatrix}, \tag{4.63}$$

where we have used the explicit flavor structure of μ and M.

We now proceed to find out the form of U_h, the diagonalizing matrix of $m_{\nu_{heavy}}$. Note that the $m_{\nu_{heavy}}$ matrix can first be block diagonalized by V_0 as

$$m'_{\nu_{heavy}} = (V_0)^T m_{\nu_{heavy}} V_0 \simeq \begin{pmatrix} -M+\mu/2 & 0 \\ 0 & M+\mu/2 \end{pmatrix}, \tag{4.64}$$

where V_0 is given by (in our scenario both μ and M are symmetric matrices)

$$V_0 \simeq \frac{1}{\sqrt{2}} \begin{pmatrix} \mathbb{I}+\frac{\mu M^{-1}}{4} & \mathbb{I}-\frac{\mu M^{-1}}{4} \\ -\mathbb{I}+\frac{\mu M^{-1}}{4} & \mathbb{I}+\frac{\mu M^{-1}}{4} \end{pmatrix}. \tag{4.65}$$

Here we have neglected the terms involving higher orders in μM^{-1} as expected in inverse seesaw scenario in general. Now the upper $(-M+\mu/2)$ and lower $(M+\mu/2)$ block matrices of $m'_{\nu_{heavy}}$ carry the form of μ matrix itself (or m_ν). The presence of M just redefines the previous parameter a by $a_{1,2} = a/2 \mp y_2 v_f$ (see Eq. (4.8) and (4.9)). Therefore we can follow the similar prescription for diagonalizing these blocks as we did in case of m_ν diagonalization. Hence $m'_{\nu_{heavy}}$ can further be diagonalized by $V^T m'_{\nu_{heavy}} V$ with

$$V = \begin{pmatrix} U_{TB}.V_1(\theta_1,\psi_1) & 0 \\ 0 & U_{TB}.V_2(\theta_2,\psi_2) \end{pmatrix}, \tag{4.66}$$

where V_i has the form similar to U_1, *i.e.*

$$V_i = \begin{pmatrix} \cos\theta_i & 0 & \sin\theta_i e^{-i\psi_i} \\ 0 & 1 & 0 \\ -\sin\theta_i e^{i\psi_i} & 0 & \cos\theta_i \end{pmatrix}. \tag{4.67}$$

Therefore the diagonalizing matrix of $m_{\nu_{heavy}}$ can be written as

$$U_h \simeq \frac{1}{\sqrt{2}} \begin{pmatrix} \mathbb{I}+\frac{\mu M^{-1}}{4} & \mathbb{I}-\frac{\mu M^{-1}}{4} \\ -\mathbb{I}+\frac{\mu M^{-1}}{4} & \mathbb{I}+\frac{\mu M^{-1}}{4} \end{pmatrix} \begin{pmatrix} U_{TB}.V_1(\theta_1,\psi_1) & 0 \\ 0 & U_{TB}.V_2(\theta_2,\psi_1) \end{pmatrix}. \tag{4.68}$$

In order to find U_h, we use μM^{-1} as obtained in Eq. (4.63). Furthermore, we get $\theta_{1,2}$ and $\psi_{1,2}$ appearing in $V_{1,2}$ as discussed earlier. Hence following the same way as in Eq.

(5.17) and Eq. (5.18) we find

$$\tan 2\theta_i = \frac{\sqrt{3}\beta_i \cos\phi_{da}}{(\beta_i \cos\phi_{da} - 2)\cos\psi_i + 2\alpha_i \sin\phi_{ba}\sin\psi_i}, \tag{4.69}$$

$$\tan\psi_i = \frac{\sin\phi_{da}}{\alpha_i \cos(\phi_{ba} - \phi_{da})}, \tag{4.70}$$

with $i = 1, 2$ and we use the definition of α_i and β_i as,

$$\alpha_{1,2} = \frac{|b|}{|a| \mp 2|y_2|v_f} \text{ and } \beta_{1,2} = \frac{|d|}{|a| \mp 2|y_2|v_f}. \tag{4.71}$$

For simplicity we discard phase difference between y_2 and a, and set $\phi_{y_2 a} = 0$.

Note that from our understanding in Sections 4.3-4.4, we can have estimates over the parameters α, β, k along with the phases ϕ_{ba}, ϕ_{da} in order to satisfy $\sin\theta_{13}$, other mixing angles, r, individual solar and atmospheric splittings, also to be consistent with the upper bound on sum of the light neutrino masses. Specific choice of C_1 enables us to compute magnitude of the flavon vev v_f and hence $|a|$ from Eq. (4.53). With all these values in hand we can finally evaluate parameters $\theta_i, \psi_i, \alpha_i$ and β_i appearing in U_h. Here we consider [3] $|y_2| = 1$. Now following the analytic expressions in Eqs. (4.61-4.63), (4.66-4.71), we can estimate $W_{3\times3}$ and $\mathcal{K}$ and hence the corresponding contribution to the branching ratio (see Eq. (4.56)). Due to particular flavor structures of the matrices μ as well as m_D and M, we find $W_{3\times3}$ and $\mathcal{K}$ are such that this scenario predicts vanishingly small branching ratio ($\sim 10^{-35}$) for LFV decays.

In addition, we have performed the evaluation numerically also. In order to evaluate it, we need to diagonalize the entire 9×9 neutrino mass matrix M_ν. Since the neutrino mixings are entirely dictated by the flavor structure of μ matrix, we could have find the entire M_ν numerically with the choices of α, β, k along with the phases ϕ_{ba}, ϕ_{da} as done in cases A, B, C, D and the general case. However to compute m_D and M, we need consider to $|y_1|$ and $|y_2|$ separately (for example, to have $\lambda = 1$, we assume $|y_1| = |y_2| = 1$). Then following Eq. (4.7), we can entirely construct the M_ν matrix numerically. Then with the help of Mathematica[4], we are able to find the diagonalizing matrix W (and hence $\mathcal{K}$ matrix also) and have estimate over the LFV decays. It turns out that the numerical

---

[3] A common phase ϕ_0 as described in the discussion above Eq. (4.26) in Section 4.3, is irrelevant for neutrino phenomenology and hence we put it at zero. We also set phases of f_1 and a/y_2 to zero.

[4] We also use Takagi factorization [219] to find W.

estimate coinsides with our analytical evaluation of vanishingly small branching ratios for LFV decays to a good extent.

4.5.3 Neutrinoless double beta decay and contribution of heavy neutrinos

We note that in addition to the standard contribution to the effective mass parameter involved in neutrinoless double beta decay as described in Section 4.3, there will be additional contribution due the presence of mixing between light and heavy neutrinos (*i.e.* with nonzero $W_{3\times6}$). Hence the half life associated with neutrinoless double beta can be expressed as [229, 230, 232, 233]

$$(T^{0\nu}_{1/2})^{-1} = \mathcal{G}^{0\nu}\left|\frac{\mathcal{M}_\nu}{m_e}\right|^2\left|\sum_{i=1}^{3}(W_{3\times3})^2_{ei}m_i + < q^2 > \sum_{i=1}^{6}(W_{3\times6})^2_{ei}m_N^{-1}\right|^2 \tag{4.72}$$

where $\mathcal{G}^{0\nu}$ is the phase space factor and $< q^2 >= -m_e m_p \mathcal{M}_\nu/\mathcal{M}_N = -(182\ \mathrm{MeV}^2)$ [229]. Here m_e is the mass of electron, m_p is the mass of proton, $\mathcal{M}_\nu$ is the nuclear matrix element for light neutrino states and $\mathcal{M}_N$ is nuclear matrix element for heavy neutrino states. Here the first and second contribution in Eq. (4.72) is due to the light and heavy neutrinos respectively. We already have an estimate for the first contribution (with $W_{3\times3} \simeq (1-\eta)\,U_\nu$) as provided in several tables of Section 4, which turns out to be of order $\sim 10^{-2}$ eV. Now with some specific choice of λ and $|y_2|$, we can determine the W matrix numerically as discussed in the previous subsection where information on other parameters α, β, k *etc.* are taken from Section 4 (different cases). Then we evaluate numerically the $\mathcal{K}$ (*i.e.* $W_{3\times6}$). In order to maximize this contribution, we consider lowest value of v_f which is allowed from Eq. (4.52). It turns out then that the second contribution remains sub-dominant ($\sim 10^{-6}$ eV or less) compared to the first contribution of Eq. (4.72). The smallness of the second term can also be understood from our finding for $\mathcal{K}$ as $\mathcal{K}_{ei} = f\,(U_h)_{4i}$. A naive estimate for this contribution (to $|m_{ee}|$) therefore is of order $\frac{\lambda}{y_2}v^2\langle q^2\rangle/v_f^3$. The using the lowest possible v_f consistent with Eq. (4.52), the estimate indicates that this contribution is essentially small compared to the first contribution. So the effective mass involved in the neutrinoless double beta decay process is mostly unaffected with the presence of heavy neutrinos in the present set-up.

4.6 Conclusion

In this present work, we have considered an inverse seesaw framework embedded in a flavor symmetric environment in order to study whether it can accommodate the neutrino masses and mixing as suggested from present experimental data, particularly in view of nonzero θ_{13}. We employ an $A_4 \times Z_4 \times Z_3$ discrete symmetry which is concocted with a global $B-L$ symmetry. We note that the flavor structure of light neutrino mass matrix is essentially dictated by that of the μ matrix itself, which is the matrix containing the lepton number breaking contribution in the inverse seesaw scenario. The flavor structure of μ matrix is generated when the flavons have vevs. We notice that the typical structure of this matrix can lead to a lepton mixing consistent with neutrino data where the charged lepton mass matrix is found to be diagonal in the framework. In doing this analysis, we have studied the correlation between different parameters of the model and their dependence on the neutrino parameters such as mass-squared differences, mixing angles etc., evaluated from experimental results. Dependency on the Dirac CP violating phase is also studied.

Since there exists a small mixing between light and heavy neutrino states in the framework, we have also checked the non-unitarity effects in our set-up which contribute to LFV processes, neutrinoless double beta decay etc.. We have found that owing to the typical flavor structure of the neutrino mass matrix here, the effective contribution of it to the LFV processes and neutrinoless double beta decays are vanishingly small. It can be noted that the μ matrix results from the breaking of a flavon which carries charge under the global $U(1)_{B-L}$. Hence we expect to have Goldstone boson or majoron (J) [292]. It may open Higgs boson decay channel ($H \to JJ$) and demands extensive analysis in the context of current and future LHC data. Discussions in this direction can be found in [227, 228]. Particularly current 13 TeV run of LHC will be important for such analysis. However further discussion in this regard is beyond the scope of the present study. Since the new physics scale in the present set-up is around few TeV, collider aspects of such a scenario turns out to be intersting and discussion in this direction can be found in [234, 235].

Chapter 5

Flavor origin of dark matter, nonzero θ_{13} and Dirac CP phase δ

5.1 Introduction

In this present work, we propose a minimal extension of the SM by including a $U(1)$ flavor symmetry to establish a correlation between the relic abundance of dark matter and non-zero value of $\sin\theta_{13}$. The analysis presented here is based on [258, 259]. Apart from matter-anti matter asymmetry of the universe, the origin and nature of dark matter is still elusive to us. Understanding the energy budget of the universe suggests that only 5% is made up of ordinary baryonic matter while dark energy and dark matter constitute about 69% and 26% respectively. Therefore almost 95% of our universe is still unknown to us, however can not be explained in the context of SM. There are several evidences in favor of dark matter, for example

(i) Galactic rotation curves [236]

(ii) Gravitational lensing [237–239]

(iii) Bullet clusters [240]

(iv) Cosmic Microwave Background Radiation (CMBR) [12, 92] etc., which have established the existence of dark matter in our universe. The current bound on the relic abundance for a dark matter candidate is [12, 256],

$$0.1175 \leq \Omega_{\rm DM}h^2 \leq 0.1219\,. \tag{5.1}$$

All these evidences in favor of dark matter are purely from their gravitational influences and so far we have no strong evidence for non-gravitational interaction of a dark matter. Therefore understanding its characteristics is a challenging task in particle cosmology. Till date true nature of DM is unknown to us, however several cosmological and astronomical observations point out towards few possible characteristics. For example a potential dark matter candidate possibly have the following properties: they are neutral, long lived or stable, weakly interacting, should have small self-interactions etc. Over the years there are many proposed dark matter candidates and their masses vary in a wide range. This zoo of possible dark matter candidates includes: axions, gravitinos, neutralinos, sneutrinos, sterile neutrinos, Majorons, etc. Out of all the dark matter candidates considered in the literature, Weakly Interacting Massive Particles (WIMPs) are very common. As its name suggests, they have weak cross section and mass around electroweak scale [242]. The primary reason for incorporating this WIMP hypothesis is that with these characteristics of a dark matter candidate, one can easily reproduce observed relic density. This is known as "WIMP miracle". Also WIMPs naturally appear in various extensions of SM scenarios, for example sneutrinos and neutralinos are typical WIMPs in many supersymmetric theories. Most importantly they can be probed by various satellite and laboratory experiments [243]. The complete relic density of a dark matter (say, ψ_1) with mass M_1 can be approximately written as [244]

$$\Omega_{\psi_1}h^2 = \frac{1.09\times10^9~\text{GeV}^{-1}}{g_\star^{1/2}M_{PL}}\frac{1}{J(x_f)}\,, \tag{5.2}$$

where $J(x_f)$ is given by

$$J(x_f) = \int_{x_f}^{\infty}\frac{\langle\sigma v\rangle_{eff}}{x^2}\,dx\,. \tag{5.3}$$

Here M_{PL} is the Planck scale, $\langle\sigma v\rangle_{eff}$ is the thermal average of dark matter cross sections, $x_f = \frac{M_1}{T_f}$ with T_f as the freeze out temperature and $g_\star$ is the total number of effectively relativistic degrees of freedom at the time of freeze-out. Current bound on this dark matter relic abundance is given by Eq. (5.1).

Form the discussions presented in the previous chapters, we are at a stage to say that ideas of masive neutrinos and dark matter emerges from concrete experimental evidences. We are also convinced that some BSM new physics phenomenons might explain theses sectors. Enormous efforts have been given to explain these sectors separately, but one can always ask the question: *is there are any connection between neutrinos and dark matter, the two seemingly uncorrelated sectors?* Initially, back in 1970, SM neutrinos were postulated as a dark matter candidate [245], however it is found that they can only have a sub-dominant contribution. Hence SM particle content is often extended to accommodate dark matter candidates and establish a connection with neutrinos. In a wider sense, this can be achieved in two possible ways: first, a dark matter candidate can be introduced such way that they play an important role in neutrino mass generation. This can be done either incorporating sterile neutrinos in the framework or generating neutrino mass radiativly where dark matters appear in the loop [246]. For a detailed discussion on dark matter and radiative neutrino mass, see [247–249]. Secondly, in an another approach, dark matter candidate can be associated with SM symmetries. Here neutrinos are generally related to the dark matter via the symmetries on the neutrino sector. Neutrino mixing patterns and quantum number of the additional symmetries turns out to be connected with dark matter sector. For example, global and gauged $U(1)$ symmetries can be introduced to serve this purpose[250]. We have discussed earlier that non-Abelian discrete flavor symmetries plays an important role in determining the neutrino masses and mixing. Here in this chapter we study one such interplay between dark matter sector and neutrino sector incorporating flavor symmetry.

Flavor symmetries are often used to explore many unsolved issues within and beyond the SM of particle physics. For example, a global $U(1)$ flavor symmetry was proposed a long ago to explain the quark mass hierarchy and Cabibbo mixing angle [82]. Subsequently many flavor symmetric frameworks have been adopted to explain neutrino masses and mixings in the lepton sector. As illustrated in the earlier chapters, a TBM lepton mixing generated from a discrete flavor symmetry such as A_4 attracts a lot of attention [7] due to its simplicity and predictive nature. However the main drawback of these analyses was that it predicts vanishing reactor mixing angle θ_{13} which is against the recent robust observation of $\theta_{13} \approx 9°$ [5, 79, 80] by DOUBLE CHOOZ [75], Daya Bay [76], RENO [78] and T2K [81] experiments. Hence, a modification of the TBM structure of lepton mixing is required.

In this work we consider the existence of a dark sector [260] consisting of vector-like fermions which are charged under an additional $U(1)$ flavor symmetry. Specifically, we consider a vector-like SM singlet fermion (χ^0) and a $SU(2)_L$ doublet fermion (ψ) which are odd under the remnant $\mathcal{Z}_2$ symmetry generated from the broken $U(1)$. The neutral components mix to give rise a fermionic DM (ψ_1). Note that in the simplest case, a singlet fermion (χ^0) can generate a Higgs portal interaction by dimension five operator suppressed by the new physics scale as $(\overline{\chi^0}\chi^0 H^\dagger H)/\Lambda$. However, as we argue, that the new physics scale (Λ) involved in the theory has to generate the required neutrino mass as well and thus making it very high. As a result, the annihilation rate of DM becomes too small which in turn make the relic density over abundant. On the other hand, a vector-like fermion doublet (ψ) suffers from a large annihilation cross-section to SM through Z mediation and is never enough to produce the required density. It is only through the mixing of these two that can produce correct relic density as we demonstrate here. We also assume the existence of a TBM neutrino mixing pattern (in a basis where charged leptons are diagonal) based on A_4 symmetry. The interaction between the dark and the lepton sector of the SM is mediated by flavon fields charged under the $U(1)$ and/or A_4. These flavons also take part in producing additional interactions involving lepton and Higgs doublets. The $U(1)$ symmetry, once allowed to be broken by the vacuum expectation value (vev) of a flavon, generates a non-zero $\sin\theta_{13}$ after the electroweak symmetry breaking (and when A_4 breaks too). In Fig. 5.1 we presented a schematic diagram of our framework. We show that the non-zero value of $\sin\theta_{13}$ is proportional to the strength of Higgs portal coupling of DM giving rise to the correct relic density. In other words, the precise value of $\sin\theta_{13}$ and DM relic density can fix the charge of dark matter under $U(1)$ flavor symmetry. Indeed

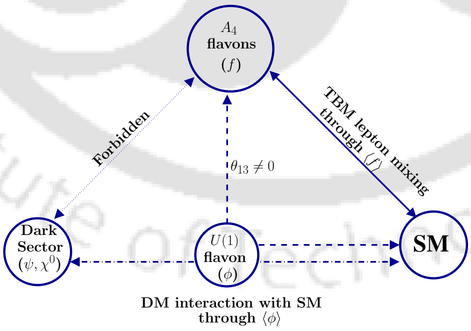

FIGURE 5.1: Nonzero values of $\sin\theta_{13}$ predict Higgs portal couplings of DM via a $U(1)$ flavor symmetry: a schematic presentation.

it is true for the Dirac CP violating phase $\delta = 0$ as shown in our previous work [258]. However, we have found here that the non-zero values of δ plays an important role for the determination of DM charge under $U(1)$ flavor symmetry. Although the current allowed range of δ $(0^\circ - 360^\circ)$ can significantly increase the uncertainty in the determination of DM flavor charge (compared to $\delta = 0$ scenario), a future measurement of δ would be important in fixing the charge. In [258], we have assumed a prevailing TBM pattern and here in this work we provide an explicit construction of that too. We also show that the effective Higgs portal coupling of the vector-like leptonic DM can be tested at future direct search experiments, such as Xenon1T [261] and at the Large Hadron Collider (LHC) [260, 262, 263].

The Chapter is arranged as follows. In section 5.2 we discuss the relevant model for correlating non-zero $\sin\theta_{13}$ to Higgs portal coupling of DM which gives correct relic density. In section 5.3 and 5.4, we obtain the constraints on model parameters from neutrino masses and mixing and relic abundance of dark matter respectively. In section 5.5, we obtain the correlation between the non-zero $\sin\theta_{13}$ and Higgs portal coupling of dark matter and conclude in section 5.6.

5.2 Structure of the model

In this section, we describe the field content and symmetries involved. We consider an effective field theory approach for realizing the neutrino masses and mixing while trying to connect it with the DM sector as well. The set-up includes the interaction between these two sectors which has the potential to generate adequate θ_{13}, and hence a deviation of TBM mixing happens, to match with the experimental observation while satisfying the constraints from relic density and direct search of DM.

5.2.1 Neutrino Sector

The basic set-up relies on the A_4 symmetric construction of the Lagrangian associated with neutrino mass term [7]. Based on the construction by Altarelli-Feruglio (AF) model [7] (for generating TBM mixing), we have extended the flavon sector and symmetry of the model. The SM doublet leptons (ℓ) transform as triplet under the A_4 symmetry while

Field	e_R	μ_R	τ_R	ℓ	H	ψ	χ^o	ϕ_S	ϕ_T	ξ	η	ϕ
$SU(2)_L$	1	1	1	2	2	2	1	1	1	1	1	1
A_4	1	$1''$	$1'$	3	1	1	1	3	3	1	$1'$	1
Z_3	ω	ω	ω	ω	1	1	1	ω	1	ω	ω	1
Z_2	-1	-1	-1	1	1	-1	-1	1	-1	1	1	1
$U(1)$	0	0	0	0	0	q_1	q_2	0	0	0	$-x$	x

TABLE 5.1: Fields content and transformation properties under the symmetries imposed on the model. Here $nx = q_1 - q_2$ (justified from Eq.(5.10)), n will be determined later.

the singlet charged leptons: e_R, μ_R and τ_R transform as $1, 1^{''}$ and $1^{'}$ respectively under A_4. The flavon fields and their charges (along with the SM fields) are described in Table 5.1. The flavons ϕ_S, ϕ_T and ξ break the A_4 flavor symmetry by acquiring vevs in suitable directions. Note that here ϕ_S and ϕ_T transform as A_4 triplets but the flavon ξ and the SM Higgs doublet (H) transform as a singlet under A_4. So the contribution to the effective neutrino mass matrix coming through the higher dimensional operator respecting the symmetries considered can be written as

$$-\mathcal{L}_{\nu_0} = (\ell H \ell H)(y_1 \xi - y_2 \phi_S)/\Lambda^2\,, \tag{5.4}$$

where Λ is the cut off scale of the theory and y_1, y_2 represents respective coupling constant. The scalar fields break the flavor symmetry when acquire vevs along[1] $\langle \phi_S \rangle = (v_S, 0, 0)$, $\langle \phi_T \rangle = v_T(1, 1, 1)$, $\langle \xi \rangle = v_\xi$ and $\langle H \rangle = v$. As a result we obtain the light neutrino mass matrix as

$$(m_\nu)_0 = \begin{pmatrix} a - 2b/3 & b/3 & b/3 \\ b/3 & -2b/3 & a + b/3 \\ b/3 & a + b/3 & -2b/3 \end{pmatrix}, \tag{5.5}$$

where $a = y_1(v^2/\Lambda)\epsilon$ and $b = y_2(v^2/\Lambda)\epsilon$, with $\epsilon = v_\xi/\Lambda = v_S/\Lambda$ is considered without loss of generality as any prefactor (due to the mismatch of vevs) can be absorbed in the definition of y_2. The above mass matrix can be diagonalized by the TBM mixing matrix matrix [6] given by Eq. (1.53). The relevant contribution to charged leptons (considering charges from Table 5.1) can be obtained via

$$\mathcal{L}_l = \frac{y_e}{\Lambda}(\bar{\ell}\phi_T)He_R + \frac{y_\mu}{\Lambda}(\bar{\ell}\phi_T)'H\mu_R + \frac{y_\tau}{\Lambda}(\bar{\ell}\phi_T)''H\tau_R\,, \tag{5.6}$$

---

[1] The chosen vev alignments of ϕ_S and ϕ_T can be obtained by minimizing the potential involving them along a similar line followed in [7, 127, 264, 265].

which yields the diagonal mass matrix:

$$M_l = \begin{pmatrix} y_e v \frac{v_T}{\Lambda} & 0 & 0 \\ 0 & y_\mu v \frac{v_T}{\Lambda} & 0 \\ 0 & 0 & y_\tau v \frac{v_T}{\Lambda} \end{pmatrix}. \tag{5.7}$$

Note that this is the leading order contribution (and is proportional to $1/\Lambda$) in the charged lepton mass matrix. Due to the symmetry of the model as described in Table 5.1 (including the $U(1)$ symmetry to be discussed later) there will be no term proportional to $1/\Lambda^2$. Therefore no contribution to the lepton mixing matrix originated from the charged lepton sector up to $1/\Lambda^2$ is present. Here it is worthy to mention that the dimension-5 operator $\ell H \ell H/\Lambda$ is forbidden due to the Z_3 symmetry specified in Table 5.1. This additional symmetry also forbids the dimension-6 operator $\ell H \ell H(\phi_T + \phi_T^\dagger)/\Lambda^2$. The $U(1)$ flavor symmetry considered here does not allow terms involving ϕ, η (such as: $\ell H \ell H(\phi+\eta)/\Lambda^2$) as discussed (where ϕ and η are charged under $U(1)$ but the SM particles are not). Therefore, Eq. (5.4) is the only relevant term up to $1/\Lambda^2$ order contributing to the neutrino mass matrix $(m_\nu)_0$ ensuring its TBM structure as in Eq. (5.5). Note that these kind of structure of the neutrino mass matrix of $(m_\nu)_0$ can also be obtained in a A_4 based set-up either in a type-I, II or inverse seesaw framework [117, 149, 180, 266].

The immediate consequence of TBM mixing as given in Eq. (**??**) is that it implies $\sin^2\theta_{12} = 1/3$, $\sin^2\theta_{23} = 1/2$ and $\sin\theta_{13} = 0$. Now to explain the current experimental observation on θ_{13} we consider an operator of order $1/\Lambda^3$:

$$-\delta\mathcal{L}_\nu = y_3 \frac{(\ell H \ell H)\phi\eta}{\Lambda^3}, \tag{5.8}$$

where we have introduced two other SM singlet flavon fields ϕ and η which carry equal and opposite charges under the $U(1)$ symmetry but transform as 1 and $1'$ under A_4 respectively. The $U(1)$ charge assignment to these two flavons also ensures that ϕ and η do not take part in $(m_\nu)_0$. Thus, after flavor and electroweak symmetry breaking this term contributes to the light neutrino mass matrix as follows:

$$\delta m_\nu = \begin{pmatrix} 0 & 0 & d \\ 0 & d & 0 \\ d & 0 & 0 \end{pmatrix}, \tag{5.9}$$

where $d = y_3(v^2/\Lambda)\epsilon^2$ with $\epsilon = \langle\phi\rangle/\Lambda \equiv \langle\eta\rangle/\Lambda$. This typical flavor structure of the additional contribution in the neutrino mass matrix follows from the involvement of η field, which transforms as $1'$ under A_4 [117, 125]. This δm_ν can indeed generate the $\theta_{13} \neq 0$ in the same line as in [117, 149, 266]. Note that the choice of Z_2 symmetry presented in Table 5.1 also forbids the contributions to neutrino mass matrix proportional to $1/\Lambda^3$ (involving terms like $\ell H \ell H \phi_S \phi_T, \ell H \ell H \xi \phi_T, \ell H \ell H \phi_S \phi_T^\dagger$ and $\ell H \ell H \xi \phi_T^\dagger$) and thus ensuring Eq. (5.9) is the only contribution responsible for breaking the TBM mixing.

5.2.2 Dark sector and its interaction with neutrino sector

The dark sector associated with the present construction consists of a vector-like $SU(2)_L$ doublet $\psi^T = (\psi^0, \psi^-)$ and a neutral singlet fermion χ^0 [260], which are odd under the Z_2 symmetry as has already been mentioned in Table 5.1. These fermions are charged under an additional $U(1)$ flavor symmetry, but neutral under the existing symmetry in the neutrino sector (say the non-Abelian A_4 and additional discrete symmetries required). Note that all the SM fields and the additional flavons in the neutrino sector except ϕ are neutral under this additional $U(1)$ symmetry. Since ψ and χ^0 are vector-like fermions, they can have bare masses, M_ψ and M_χ, which are not protected by the SM symmetry. The effective Lagrangian, invariant under the symmetries considered, describing the interaction between the dark and the SM sector is then given by:

$$\mathcal{L}_{\rm int} = \left(\frac{\phi}{\Lambda}\right)^n \overline{\psi}\widetilde{H}\chi^0, \tag{5.10}$$

where n is not fixed at this stage. The above term is allowed provided the $U(1)$ charge of ϕ^n is compensated by ψ and χ^0 *i.e.* $nx = q_1 - q_2$. We will fix it later from phenomenological point of view.

When ϕ acquires a vev, the $U(1)$ symmetry breaks down and an effective Yukawa interaction is generated between the SM and the DM sectors. After electroweak symmetry is broken, the DM emerges as an admixture of the neutral component of the vector-like fermions ψ, *i.e.* ψ^0, and χ^0. The Lagrangian describing the DM sector and the interaction as a whole reads as

$$-\mathcal{L}_{\rm Yuk} \supset M_\psi \overline{\psi}\psi + M_\chi \overline{\chi^0}\chi^0 + \left[Y\overline{\psi}\widetilde{H}\chi^0 + {\rm h.c.}\right], \tag{5.11}$$

where the effective Yukawa connecting the dark sector to the SM Higgs reads as $Y = \epsilon^n = \left(\frac{\langle\phi\rangle}{\Lambda}\right)^n$. We have already argued in introduction about our construction of dark matter sector. The idea of introducing vector-like fermions in the dark sector is also motivated by the fact that we expect a replication of the SM Yukawa type interaction to be present in the dark sector as well. Here the ϕ field plays the role of the messenger field similar to the one considered in [267]. See also [268–278] for some earlier efforts to relate A_4 flavor symmetry to DM. Note that the vev of the ϕ field is also instrumental in producing the term d to the neutrino mass matrix along with the vev of η. Since the d-term is responsible for generation of nonzero θ_{13} (will be discussed in the next section) a connection between non-zero $\sin\theta_{13}$ and DM interaction becomes correlated in our set-up.

A discussion about other possible terms allowed by the symmetries considered would be pertinent here. Terms like $\overline{\psi}\psi H^\dagger H/\Lambda$ and $\overline{\chi^0}\chi^0 H^\dagger H/\Lambda$ are actually allowed in the present set-up. However it turns out that their role is less significant compared to the other terms present. The reason is the following: firstly they could contribute to bare mass terms of ψ and χ^0 fields. However these contribution being proportional to v^2/Λ are insignificant as compared to M_ψ and M_χ. Similar conclusion holds for the Yukawa term as well. Secondly, they could take part in the DM annihilation. However as we will see, there also they do not have significant contribution because of the Λ suppression.

5.3 Phenomenology of the neutrino sector

Combining Eqs. (5.5) and (5.9), we get the light neutrino mass matrix as $m_\nu = (m_\nu)_0 + \delta m_\nu$. We have already seen that $(m_\nu)_0$ can be diagonalized by U_{TB} alone. Hence including δm_ν, rotation by U_{TB} results into the following structure of neutrino mass matrix:

$$m'_\nu = U_{TB}^T m_\nu U_{TB}, \tag{5.12}$$

$$= \begin{pmatrix} a-b-d/2 & 0 & \sqrt{3}d/2 \\ 0 & a+d & 0 \\ \sqrt{3}d/2 & 0 & -a-b+d/2 \end{pmatrix}. \tag{5.13}$$

So an additional rotation (by the U_1 matrix given below) is required to diagonalize m_ν,

$$(U_{TB}U_1)^T m_\nu (U_{TB}U_1) = \text{diag}(m_1 e^{i\gamma_1}, m_2 e^{i\gamma_2}, m_3 e^{i\gamma_3}) \tag{5.14}$$

where

$$U_1 = \begin{pmatrix} \cos\theta_\nu & 0 & \sin\theta_\nu e^{-i\varphi} \\ 0 & 1 & 0 \\ -\sin\theta_\nu e^{i\varphi} & 0 & \cos\theta_\nu \end{pmatrix}. \tag{5.15}$$

Here $m_{i=1,2,3}$ are the real and positive eigenvalues and $\gamma_{i=1,2,3}$ are the phases associated to these mass eigenvalues. We can therefore extract the neutrino mixing matrix U_ν as,

$$U_\nu = U_{TB}U_1U_m = \begin{pmatrix} \sqrt{\frac{2}{3}}\cos\theta_\nu & \frac{1}{\sqrt{3}} & \sqrt{\frac{2}{3}}e^{-i\varphi}\sin\theta_\nu \\ -\frac{\cos\theta_\nu}{\sqrt{6}} + \frac{e^{i\varphi}\sin\theta_\nu}{\sqrt{2}} & \frac{1}{\sqrt{3}} & -\frac{\cos\theta_\nu}{\sqrt{2}} - \frac{e^{-i\varphi}\sin\theta_\nu}{\sqrt{6}} \\ -\frac{\cos\theta_\nu}{\sqrt{6}} - \frac{e^{i\varphi}\sin\theta_\nu}{\sqrt{2}} & \frac{1}{\sqrt{3}} & \frac{\cos\theta_\nu}{\sqrt{2}} - \frac{e^{-i\varphi}\sin\theta_\nu}{\sqrt{6}} \end{pmatrix} U_m\,, \tag{5.16}$$

where $U_m = \text{diag}(1, e^{i\alpha_{21}/2}, e^{i\alpha_{31}/2})$ is the Majorana phase matrix with $\alpha_{21} = (\gamma_1 - \gamma_2)$ and $\alpha_{31} = (\gamma_1 - \gamma_3)$, one common phase being irrelevant. The angle θ_ν and phase φ associated in U_1 can now be linked with the parameters: a, b, d involved in m_ν through Eq. (5.13).

Note that the parameters: a, b and d are all in general complex quantities. We define the phases associated with a, b, d as ϕ_a, ϕ_b and ϕ_d respectively. Also for simplifying the analysis, we consider $|y_1| = |y_3| = y$ and $|y_2| = k$. With these, θ_ν and φ can be expressed in terms of the parameters involved in the effective light neutrino mass matrix m'_ν as:

$$\tan 2\theta_\nu = \frac{\sqrt{3}\epsilon\cos\phi_{db}}{(\epsilon\cos\phi_{db} - 2\cos\phi_{ab})\cos\varphi}, \tag{5.17}$$

$$\tan\varphi = \frac{y}{k}\frac{\sin(\phi_{db} - \phi_{ab})}{\cos\phi_{db}}. \tag{5.18}$$

where $\phi_{ab} = \phi_a - \phi_b$ and $\phi_{db} = \phi_d - \phi_b$. Then comparing the standard U_{PMNS} parametrization and neutrino mixing matrix $U_\nu (= U_{TBM}U_1U_m)$ we obtain

$$\sin\theta_{13} = \sqrt{\frac{2}{3}}\,|\sin\theta_\nu|\,, \quad \delta = \arg[(U_1)_{13}]. \tag{5.19}$$

From Eq. (5.17) and (5.18) it is clear that, $\sin\theta_\nu$ may take positive or negative value depending on the choices of ϵ and y/k. For $\sin\theta_\nu > 0$, we find $\delta = \varphi$ using $\delta = \arg[(U_1)_{13}]$. On the other hand for $\sin\theta_\nu < 0$; δ and φ are related by $\delta = \varphi \pm \pi$. Therefore in both these cases we obtain $\tan\varphi = \tan\delta$ and hence Eq. (5.18) leads to

$$\tan\delta = \frac{y}{k}\frac{\sin(\phi_{db} - \phi_{ab})}{\cos\phi_{db}}. \tag{5.20}$$

The other two mixing angles follow the standard correlation with θ_{13} in A_4 models [127, 134].

Using Eq. (5.14), the complex light neutrino mass eigenvalues are evaluated as

$$\begin{aligned} m^c_{1,3} &= \left[-b \pm \sqrt{a^2 - ad + d^2}\right], & (5.21)\\ m^c_2 &= (a + d). & (5.22) \end{aligned}$$

Correspondingly the real and positive mass eigenvalues of light neutrinos are determined as

$$\begin{aligned} m_1 &= \alpha\frac{y}{k}\left[\left(P - \frac{k}{y}\right)^2 + Q^2\right]^{1/2}, & (5.23)\\ m_2 &= \alpha\frac{y}{k}\left[1 + \epsilon^2 + 2\epsilon\cos(\phi_{ab} - \phi_{db})\right]^{1/2}, & (5.24)\\ m_3 &= \alpha\frac{y}{k}\left[\left(P + \frac{k}{y}\right)^2 + Q^2\right]^{1/2}, & (5.25) \end{aligned}$$

where

$$\alpha = \frac{k}{\Lambda}v^2\epsilon, \quad P = \left[\frac{1}{2}(A + \sqrt{A^2 + B^2})\right]^{1/2} \text{ and } Q = \left[\frac{1}{2}(-A + \sqrt{A^2 + B^2})\right]^{1/2}, \tag{5.26}$$

with

$$\begin{aligned} A &= (\cos 2\phi_{ab} + \epsilon^2\cos 2\phi_{db} - \epsilon\cos(\phi_{ab} + \phi_{db})), & (5.27)\\ B &= (\sin 2\phi_{ab} + \epsilon^2\sin 2\phi_{db} - \epsilon\sin(\phi_{ab} + \phi_{db})). & (5.28) \end{aligned}$$

Also, phases (γ_i) associated with each mass eigenvalues can be expressed as

$$\begin{aligned}\gamma_1 &= \phi_b + \tan^{-1}\left(\frac{Q}{P - \frac{k}{y}}\right), &(5.29)\\ \gamma_2 &= \phi_b + \tan^{-1}\left(\frac{\sin\phi_{ab} + \epsilon\sin\phi_{db}}{\cos\phi_{ab} + \epsilon\cos\phi_{db}}\right), &(5.30)\\ \gamma_3 &= \pi + \phi_b + \tan^{-1}\left(\frac{Q}{P + \frac{k}{y}}\right). &(5.31)\end{aligned}$$

Using the above expressions of absolute neutrino masses, we define the ratio of solar to atmospheric mass-squared differences as r,

$$r = \frac{\Delta m^2_{\odot}}{|\Delta m^2_{atm}|}, \tag{5.32}$$

with $\Delta m^2_{\odot} \equiv \Delta m^2_{21} = m^2_2 - m^2_1$ and $|\Delta m^2_{atm}| \equiv |\Delta m^2_{31}| = |m^3_3 - m^2_1|$. Then it turns out that both r and θ_{13} depends on $\epsilon, y/k$ and the relative phases: ϕ_{ab}, ϕ_{db}. The Dirac CP phase δ is also a function of these parameters only. As values of r and θ_{13} are precisely known from neutrino oscillation data, it would be interesting to constrain the parameter space of $\epsilon, y/k$ and the relative phases which can be useful in predicting δ. However analysis with all these four parameters is difficult to perform. So, below we categorize few cases depending on some specific choices of relative phases. In doing the analysis, following [5], the best fit values of $\Delta m^2_{\odot} = 7.6 \times 10^{-5}$ eV^2 and $|\Delta m^2_{atm}| = 2.48 \times 10^{-3}$ eV^2 are used for our analysis. r and $\sin\theta_{13}$ are taken as 0.03 and 0.1530 (best fit value [5]) respectively.

5.3.1 Case A : $\phi_{ab} = \phi_{db} = 0$

Here we make the simplest choice for the phases, $\phi_{ab} = \phi_{db} = 0$. Then the Eq. (5.17) becomes function of ϵ alone [117] as:

$$\tan 2\theta_\nu = \frac{\sqrt{3}\epsilon}{\epsilon - 2}. \tag{5.33}$$

Hence $\sin\theta_{13}$ depends only on ϵ where following Eq. (5.20), the Dirac CP phase is zero or π. The ϵ dependence of $\sin\theta_{13}$ is represented in Fig. 5.2. The horizontal patch in Fig. 5.2 denotes the allowed 3σ range of $\sin\theta_{13}$ ($\equiv$ 0.1330-0.1715) [5] which is in turn restrict the range of ϵ parameter (between 0.328 and 0.4125) denoted by the vertical patch in the same figure. Note that the interaction strength of DM with the SM particles depends on $\epsilon^n \equiv Y$. Therefore we find that the size of $\sin\theta_{13}$ is intimately related with the Higgs portal coupling of DM. This is the most significant observation of this paper. With the above mentioned range of ϵ, obtained from Fig. 5.2, the two other mixing angles θ_{12} and θ_{23} are found to be within the 3σ range.

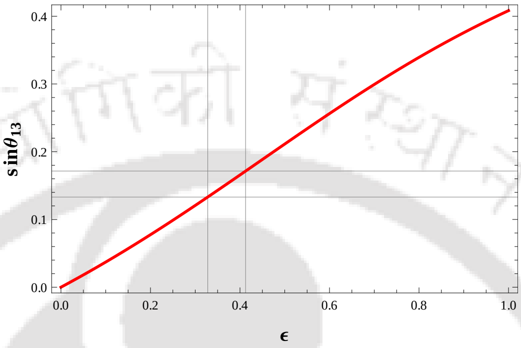

FIGURE 5.2: Plot of $\sin\theta_{13}$ against ϵ. 3σ range [5] of $\sin\theta_{13}$ (indicated by the horizontal lines) fixes ϵ in the range: 0.328-0.4125 (indicated by vertical lines).

Expressions for the real and positive mass eigenvalues are obtained from Eq. (5.23-5.25) and can be written as

$$m_1 = \alpha\frac{y}{k}\left|\sqrt{1-\epsilon+\epsilon^2}-k/y\right|, \tag{5.34}$$

$$m_2 = \alpha\frac{y}{k}\left[1+\epsilon\right], \tag{5.35}$$

$$m_3 = \alpha\frac{y}{k}\left[\sqrt{1-\epsilon+\epsilon^2}+k/y\right]. \tag{5.36}$$

With the above mass eigenvalues, one can write the ratio of solar to atmospheric mass-squared differences as defined in Eq. (5.32) as:

$$r = \frac{3\epsilon\frac{y}{k}-\frac{k}{y}+2\sqrt{1-\epsilon+\epsilon^2}}{4\sqrt{1-\epsilon+\epsilon^2}}. \tag{5.37}$$

From Fig. 5.2, we have fixed ϵ range corresponding to 3σ range of $\sin\theta_{13}$. Now, to satisfy $r = 0.03$ [5], we vary the ratio of the coupling constants, y/k, against ϵ using Eq. (5.32) and (5.34-5.36). The result is presented in Fig. 5.3. The vertical patch there represents allowed region for ϵ fixed from Fig. 5.2 which determines the range of y/k to be within 0.471-0.455. After obtaining ϵ and the ratio y/k, we can now find the factor k/Λ (within

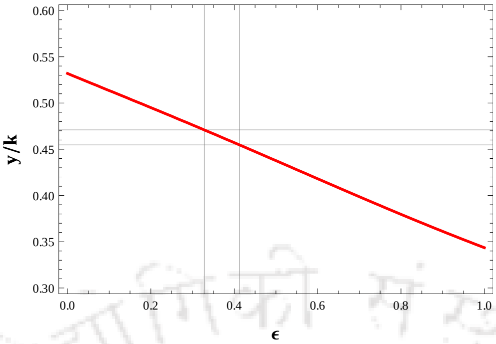

FIGURE 5.3: Contour plot of $r = 0.03$ in $y/k - \epsilon$ plane. The vertical lines represent the allowed range for ϵ (0.328-0.4125) corresponding to 3σ range of $\sin\theta_{13}$ which restricts the ratio y/k between 0.471 to 0.455 indicated by horizontal lines.

α) in order to satisfy the solar mass-squared difference $\Delta m^2_{\odot} = m^2_2 - m^2_1 = 7.6 \times 10^{-5}$ eV^2 [5]. Using Eq. (5.34) and (5.35) we find this factor to be

$$\frac{k}{\Lambda} = \frac{1}{v^2\epsilon\frac{y}{k}}\sqrt{\frac{\Delta m^2_{\odot}}{\left[3\epsilon - \left(\frac{k}{y}\right)^2 + 2\frac{k}{y}\sqrt{1+\epsilon^2} - \epsilon\right]}}. \tag{5.38}$$

Considering the 3σ variation of $\sin\theta_{13}$, it falls within 1.97×10^{-15} GeV^{-1} to 1.60×10^{-15} GeV^{-1} with $v = 246$ GeV. Once we know about all parameters involved like $\epsilon, y/k, k/\Lambda$

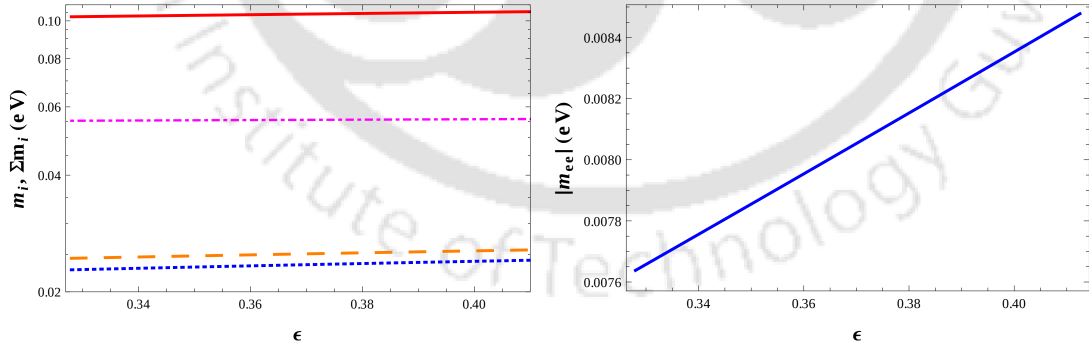

FIGURE 5.4: Left: Individual absolute neutrino masses (m_1- blue dotted line, m_2- orange dashed line, m_3- magenta dot-dashed line) and their sum (continuous red line) against ϵ (0.328-0.4125) corresponding to 3σ range of $\sin\theta_{13}$. Right: Effective neutrino mass parameter (continuous blues line) against ϵ (0.328-0.4125) corresponding to 3σ range of $\sin\theta_{13}$.

with the specific choice of the phases (in this case $\phi_{ab} = \phi_{db} = 0$), it is straightforward

Parameters/Observable	Allowed Range
ϵ	0.328-0.4125
k/Λ (GeV^{-1})	1.97×10^{-15} - 1.60×10^{-15}
Σm_i (eV)	0.102 - 0.106
$\lvert m_{ee}\rvert$ (eV)	0.00764-0.00848

TABLE 5.2: Range of $\epsilon, k/\Lambda, \Sigma m_i, |m_{ee}|$ for 3σ range of $\sin\theta_{13}$ with $\phi_{ab} = \phi_{db} = 0$.

to determine absolute neutrino masses and effective neutrino mass parameter involved in neutrinoless double beta decay using

$$|m_{ee}| = \left|m_1^2 c_{12}^2 c_{13}^2 + m_2^2 s_{12}^2 c_{13}^2 e^{i\alpha_{21}} + m_3^2 s_{13}^2 e^{i(\alpha_{31}-2\delta)}\right| \tag{5.39}$$

as shown in Fig. 5.4. We also have listed the summary of the predictions of these quantities in Table 5.2.

5.3.2 Case B : $\phi_{db} = 0$

Now we consider the case: $\phi_{db} = 0$. Then the relations for θ_ν and δ take the form

$$\tan 2\theta_\nu = \frac{\sqrt{3}\epsilon}{(\epsilon - 2\cos\phi_{ab})\cos\varphi}, \tag{5.40}$$

$$\tan\delta = -\frac{y}{k}\sin\phi_{ab}\,. \tag{5.41}$$

So from Eqs. (5.19, 5.40-5.41) and since $\tan\delta = \tan\varphi$, it is clear that unlike the Case A, here $\sin\theta_{13}$ depends not only on ϵ and y/k but also on the phase present in the theory, *i.e.* ϕ_{ab}. Therefore there would exist a one to one correspondence between ϵ and y/k in order to produce a specific value of $\sin\theta_{13}$ once a particular choice of δ has been made.

Now, with $\phi_{db} = 0$, absolute neutrino masses given in Eq. (5.23-5.25) are reduced to

$$m_1 = \alpha\frac{y}{k}\left[(P_1 - \frac{k}{y})^2 + Q_1^2\right]^{1/2}, \tag{5.42}$$

$$m_2 = \alpha\frac{y}{k}\left[1 + \epsilon^2 + 2\epsilon\cos\phi_{ab}\right]^{1/2}, \tag{5.43}$$

$$m_3 = \alpha\frac{y}{k}\left[(P_1 + \frac{k}{y})^2 + Q_1^2\right]^{1/2}, \tag{5.44}$$

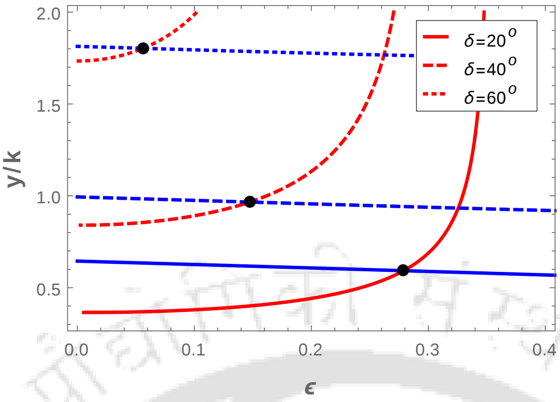

FIGURE 5.5: Contour plots for both $\sin\theta_{13} = 0.1530$ (shown in red continuous, dashed and dotted lines) and $r = 0.03$ (shown in blue continuous, dashed and dotted lines) for $\delta = 20°, \delta = 40°$ and $\delta = 60°$ respectively in ϵ-y/k plane. Black dots on each intersection represents solution for ϵ and y/k corresponding to each δ for $\phi_{db} = 0$.

with

$$P_1 = \left[\frac{1}{2}(A_1 + \sqrt{A_1^2 + B_1^2})\right]^{1/2}, \; Q_1 = \left[\frac{1}{2}(-A_1 + \sqrt{A_1^2 + B_1^2})\right]^{1/2}, \tag{5.45}$$

$$A_1 = \left(\epsilon^2 + \cos 2\phi_{ab} - \epsilon\cos\phi_{ab}\right) \text{ and } B_1 = \left(\sin 2\phi_{ab} - \epsilon\sin\phi_{ab}\right). \tag{5.46}$$

The ratio of solar to atmospheric neutrino mass-squared differences takes the form

$$r = \frac{1}{4P_1\frac{k}{y}}\left[(1 + \epsilon^2 + 2\epsilon\cos\phi_{ab}) - \left(P_1 - \frac{k}{y}\right)^2 - Q_1^2\right]. \tag{5.47}$$

Clearly, one finds that ϵ and y/k are the only parameters involved in both $\sin\theta_{13}$ and r once δ values are taken as input. Therefore, those values of ϵ and y/k are allowed which simultaneously satisfy data obtained for $\sin\theta_{13}$ and r from neutrino oscillation experiments. Here we have considered the best fit values from [5] and drawn contour plots for $\sin\theta_{13} = 0.1530$ and $r = 0.03$. Intersection of these contours then represents solutions for ϵ and y/k. Note that $\delta = 0$ case corresponds to the results obtained in Case A.

In Fig. 5.5, we have plotted typical contours obtained for $\sin\theta_{13} = 0.1530$ (red lines) and $r = 0.03$ (blue lines) for $\delta = 20°, \delta = 40°$ and $\delta = 60°$ respectively in ϵ-y/k plane. The intersecting points are denoted by black dots and represent the solution points for ϵ

and y/k. In Table 5.3 we have listed estimations for ϵ and y/k for different δ values. Just like the previous case, after obtaining ϵ and y/k, we can find the factor k/Λ using the fact that it has to produce correct solar mass-squared difference $\Delta m^2_\odot = m_2^2 - m_1^2 = 7.6 \times 10^{-5}$ eV^2 [5]. For this, we employ Eq. (5.42) and (5.43). All these findings are mentioned in Table 5.3 including sum of the absolute masses (Σm_i) of all three light neutrinos and effective neutrino mass parameter involved in neutrinoless double beta decay ($|m_{ee}|$) for different considerations of leptonic CP phase δ. In this analysis we observe that, for various values of δ between 0° to 360° there are certain points where same set of solutions for ϵ and y/k are repeated ($e.g.$ solutions with δ is repeated for $|\pi - \delta|$). We should also employ the upper bound of sum of all three light neutrino masses ($\Sigma m_i < 0.23$ eV) coming from cosmological observation by Planck [**?**]. Once this is included, we note that some of the δ values need to be discarded as the corresponding sum of the masses exceeds 0.23 eV as seen from Table 5.3. We therefore conclude that the allowed values for δ are: between $0° - 61°$ (and also $119° - 180°$, $180° - 241°$ and $299° - 360°$).

δ	ϵ	y/k	k/Λ (10^{-15} GeV^{-1})	Σm_i (eV)	$\lvert m_{ee}\rvert$ (eV)
0°	0.372	0.463	1.756	0.1042	0.0222
10°	0.343	0.496	1.910	0.1068	0.0236
20°	0.279	0.592	2.361	0.1143	0.0274
30°	0.209	0.745	3.140	0.1267	0.0331
40°	0.147	0.966	4.405	0.1454	0.0409
50°	0.096	1.288	6.610	0.1743	0.0516
60°	0.056	1.803	11.10	0.2230	0.0682
61°	0.053	1.873	11.80	0.2298	0.0704
70°	0.026	2.798	23.22	0.3210	0.1002
80°	0.007	5.743	85.42	0.6173	0.1952

TABLE 5.3: Estimated values of various parameters and observables satisfying neutrino oscillation data for different values of δ with $\phi_{db} = 0$.

5.3.3 Case C : $\phi_{ab} = 0$

When $\phi_{ab} = 0$, relations for θ_ν and δ take the form

$$\tan 2\theta_\nu = \frac{\sqrt{3}\epsilon \cos\phi_{db}}{(\epsilon \cos\phi_{db} - 2)\cos\varphi}, \tag{5.48}$$

$$\tan\delta = \frac{y}{k}\tan\phi_{ab}. \tag{5.49}$$

Here also $\sin\theta_{13}$ depends on $\epsilon, y/k$ and the phase involved ϕ_{db}. The real and positive mass eigenvalues can be written as

$$m_1 = \alpha\frac{y}{k}\left[(P_2 - \frac{k}{y})^2 + Q_2^2\right]^{1/2}, \tag{5.50}$$

$$m_2 = \alpha\frac{y}{k}\left[1 + \epsilon^2 + 2\epsilon\cos\phi_{db}\right]^{1/2}, \tag{5.51}$$

$$m_3 = \alpha\frac{y}{k}\left[(P_2 + \frac{k}{y})^2 + Q_2^2\right]^{1/2}, \tag{5.52}$$

with

$$P_2 = \left[\frac{1}{2}(A_2 + \sqrt{A_2^2 + B_2^2})\right]^{1/2}, \; Q_2 = \left[\frac{1}{2}(-A_2 + \sqrt{A_2^2 + B_2^2})\right]^{1/2}, \tag{5.53}$$

where

$$A_2 = \left(1 + \epsilon^2\cos 2\phi_{db} - \epsilon\cos\phi_{db}\right) \text{ and } B_2 = \left(\epsilon^2\sin 2\phi_{db} - \epsilon\sin\phi_{db}\right). \tag{5.54}$$

The ratio of solar to atmospheric neutrino mass-squared differences takes the form

$$r = \frac{y/k}{4P_2}\left[(1 + \epsilon^2 + 2\epsilon\cos\phi_{db}) - (P_2 - k/y)^2 - Q_2^2\right]. \tag{5.55}$$

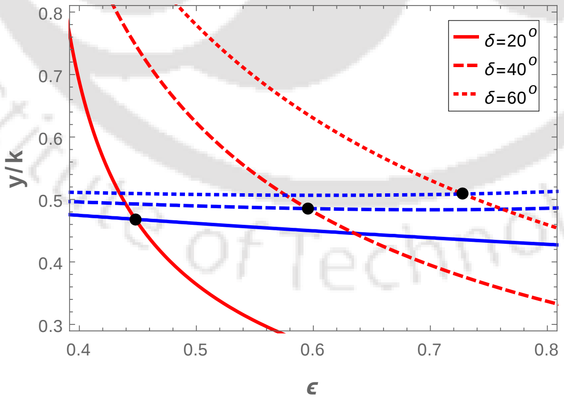

FIGURE 5.6: Contour plots for both $\sin\theta_{13} = 0.1530$ (shown in red continuous, dashed and dotted lines) and $r = 0.03$ (shown in blue continuous, dashed and dotted lines) for $\delta = 20°, \delta = 40°$ and $\delta = 60°$ respectively in ϵ-y/k plane. Black dots on each intersection represents solution for ϵ and y/k corresponding to each δ for $\phi_{ab} = 0$.

We then scan the parameter space for ϵ and y/k for various choices of δ so as to have $r = 0.03$ and $\sin\theta_{13} = 0.153$. In Fig. 5.6, we provide contour plots for $\sin\theta_{13} = 0.1530$ (red lines) and $r = 0.03$ (blue lines) for $\delta = 20°, \delta = 40°$ and $\delta = 60°$. The intersection between $\sin\theta_{13}$ and r contours indicate the simultaneous satisfaction of them. Hence the intersections are indicated by black dots with which a pair of $\epsilon, y/k$ are attached. Similar to the previous two cases, here we estimate the k/Λ for each such pair of $\epsilon, y/k$ with a specific δ. This in turn provide an estimate of Σm_i and effective mass parameter $|m_{ee}|$ depending on the choice of δ. We provide these outcomes in Table 5.4.

δ	ϵ	y/k	k/Λ (10^{-15} GeV^{-1})	Σm_i (eV)	$\lvert m_{ee}\rvert$ (eV)
0°	0.372	0.463	1.756	0.1042	0.0222
10°	0.393	0.464	1.670	0.1048	0.0225
20°	0.448	0.468	1.480	0.1065	0.0233
30°	0.520	0.475	1.300	0.1093	0.0245
40°	0.595	0.485	1.167	0.1128	0.0260
50°	0.666	0.497	1.065	0.1162	0.0273
60°	0.728	0.509	0.981	0.1182	0.0280
70°	0.782	0.519	0.901	0.1179	0.0275
80°	0.827	0.526	0.826	0.1152	0.0259

TABLE 5.4: Estimated values of various parameters and observables satisfying neutrino oscillation data for different values of δ with $\phi_{ab} = 0$.

5.3.4 Case D : $\phi_{ab} = \phi_{db} = \beta$

With $\phi_{ab} = \phi_{db} = \beta$, the mixing angle θ_ν turns out to be function of ϵ only and is given by

$$\tan 2\theta_\nu = \frac{\sqrt{3}\epsilon}{\epsilon - 2}, \tag{5.56}$$

while $\tan\delta$ becomes zero. Note that the expressions for the mixing angle θ_ν and δ are identical to the ones obtained in Case A. Therefore we use the constraint on ϵ obtained from Fig. 5.2 in order to satisfy 3σ allowed range of $\sin\theta_{13}$. However the expressions for real and positive mass eigenvalues involve the common phase β and can be written as (following Eqs. (5.23-5.25))

$$m_1 = \alpha\frac{y}{k}\left[\left(\sqrt{1-\epsilon+\epsilon^2}\cos\beta-\frac{k}{y}\right)^2+\left(\sqrt{1-\epsilon+\epsilon^2}\sin\beta\right)^2\right]^{1/2}, \quad (5.57)$$

$$m_2 = \alpha\frac{y}{k}\left[1+\epsilon\right], \quad (5.58)$$

$$m_3 = \alpha\frac{y}{k}\left[\left(\sqrt{1-\epsilon+\epsilon^2}\cos\beta+\frac{k}{y}\right)^2+\left(\sqrt{1-\epsilon+\epsilon^2}\sin\beta\right)^2\right]^{1/2}. \quad (5.59)$$

Then following our approach for finding the range of parameters which would satisfy the oscillation parameters obtained from experimental data, we define the ratio of solar to atmospheric mass-squared differences as defined in Eq. (5.32) as

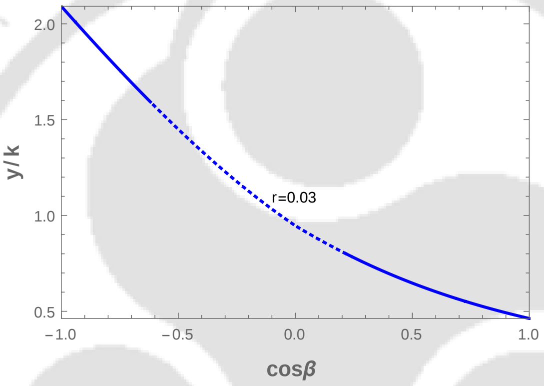

FIGURE 5.7: Contour plot for $r = 0.03$ in the $y/k - \cos\beta$ plane for $\phi_{db} = \phi_{ab} = \beta$. The disallowed range of $y/k, \cos\beta$ is indicated by the dotted portion.

$$r = \frac{3\epsilon\frac{y}{k}-\frac{k}{y}+2\cos\beta\sqrt{1-\epsilon+\epsilon^2}}{4|\cos\beta|\sqrt{1-\epsilon+\epsilon^2}}. \quad (5.60)$$

From Fig. 5.2 we fix $\epsilon = 0.372$ which would produce the best fit value of $\sin\theta_{13}$. Then, using the ratio of solar to atmospheric mass squared difference as given in Eq. (5.60), we can constrain y/k and $\cos\beta$. Here we plot $r = 0.03$ contour in the y/k-$\cos\beta$ plane as shown in Fig. 5.7. For $-1 \leq \cos\beta \leq 1$. We observe that y/k falls within the range: $0.463 \leq \ y/k \leq 2.091$. Thus Fig. 5.7 establishes a correlation between y/k and $\cos\beta$. Now to find absolute neutrino masses we need to obtain k/Λ first. We can find k/Λ from the best fit value for solar mass squared difference, $m_2^2 - m_1^2 = 7.6 \times 10^{-5}$ eV^2, and is

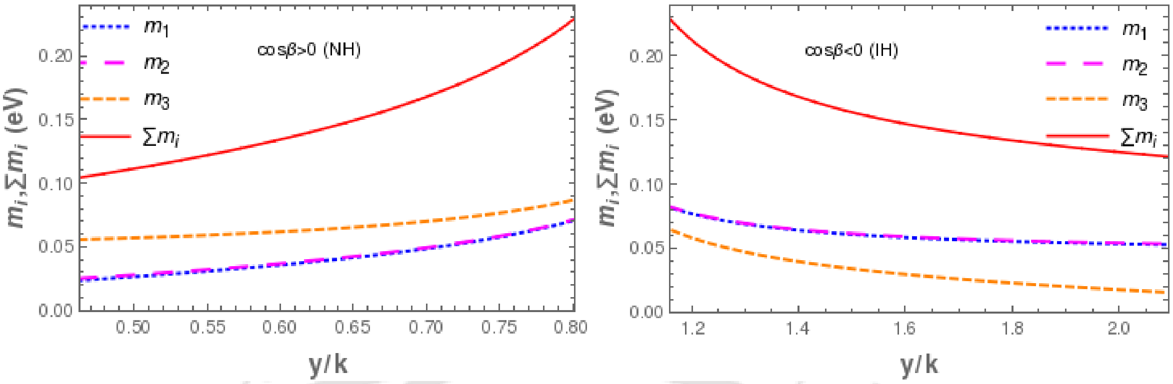

FIGURE 5.8: Absolute neutrino masses vs y/k (blue dotted, magenta large-dashed, orange dashed and red continuous lines represent m_1, m_2, m_3 and $\sum m_i$ respectively). The left panel is for $\cos\beta > 0$ and right panel is for $\cos\beta < 0$.

given by

$$\left(\frac{k}{\Lambda}\right)^2 = \frac{\Delta m^2_{\odot}}{4r(v^2\epsilon)^2 y/k|\cos\beta|\sqrt{1+\epsilon^2}-\epsilon}. \tag{5.61}$$

We have used Eq. (5.57-5.59) to obtain the above equation. Once ϵ is fixed at 0.372 and following Fig. 5.7 we know y/k and corresponding $\cos\beta$ (to have $r = 0.03$), we can use Eq. (5.61) to have an estimate for k/Λ. Now by knowing k/Λ, we have plotted absolute masses for light neutrinos in Fig. 5.8 by using Eq. (5.57-5.59). Here the left (right) panel is for $\cos\beta > 0 (< 0)$ and indicates normal (inverted) hierarchy for light neutrino masses. In Fig. 5.8, absolute neutrino masses m_1, m_2, m_3 and $\sum m_i$ are denoted by blue dotted, magenta large-dashed, orange dashed and red continuous lines respectively. Note that here we have plotted sum of the three absolute light neutrino masses consistent with the recent observation made by PLANCK, *i.e.* $\sum m_i \leq 0.23$ eV [**?**]. If we impose this constraint on the sum of absolute masses of the three light neutrinos, then the allowed region for y/k gets further constrained. The dotted portion in Fig. 5.7 represents this excluded part. Therefore the allowed region for y/k then turns out to be $0.463 \leqslant y/k \leqslant 0.802$ for $\cos\beta > 0$ (normal hierarchy) and $1.159 \leqslant y/k \leqslant 2.091$ for $\cos\beta < 0$ (inverted hierarchy). Finally in this case, the prediction for $|m_{ee}|$ found to be within 0.022 eV $< |m_{ee}| <$ 0.039 eV for normal hierarchy and 0.016 eV $< |m_{ee}| <$ 0.035 eV for inverted hierarchy.

5.4 Phenomenology of DM Sector

The dark sector consists of two vector-like fermions: a fermion doublet ψ and a singlet χ. The corresponding Lagrangian respecting the $U(1)$ and other discrete symmetries is provided in Eq. (5.11). At this stage we can remind ourselves about the minimality of the construction in terms of choice of constituents of the dark sector. Note that a vector-like singlet fermion alone can not have a coupling with the SM sector at the renormalizable level and thereby its relic density is expected to be over abundant (originated from interaction suppressed by the new physics scale Λ). On the contrary, a vector-like fermion doublet alone can have significant annihilation cross section from its gauge interaction with the SM sector and thereby we would expect the corresponding dark matter relic density to be under-abundant unless the DM mass is exorbitantly high. Hence we can naturally ask the question whether involvement of a singlet and a doublet vector-like fermions can lead to the dark matter relic density at an acceptable level. It then crucially depends on the mixing term between the singlet and the doublet fermions, *i.e.* on $m_D = Yv$. We expect a rich phenomenology out of it particularly because the coupling Y depends on the parameter ϵ through $Y = \epsilon^n$ where ϵ plays an important role in the neutrino physics as evident from our discussion in the previous section. We aim to restrict n phenomenologically.

The electroweak phase transition along with the $U(1)$ breaking give rise to the following mass matrix in the basis (χ^0, ψ^0)

$$\mathcal{M} = \begin{pmatrix} M_\chi & m_D \\ \\ m_D & M_\psi \end{pmatrix}. \tag{5.62}$$

We obtain mass eigenstates ψ_1 and ψ_2 with masses M_1 and M_2 respectively after diagonalization of the above matrix as

$$\begin{aligned} \psi_1 &= \cos\theta_d \chi^0 + \sin\theta_d \psi^0, \\ \psi_2 &= \cos\theta_d \psi^0 - \sin\theta_d \chi^0\,, \end{aligned} \tag{5.63}$$

where $\tan 2\theta_d = 2m_D/(M_\psi - M_\chi)$. We will work in the regime where $m_D << M_\psi, M_\chi$. This choice would be argued soon. However this is not unnatural as the dark matter is expected to interact weakly. In this limit, the mass eigenvalues are found to be

$$\begin{aligned} M_1 &\approx M_\chi - \frac{m_D^2}{M_\psi - M_\chi}, \\ M_2 &\approx M_\psi + \frac{m_D^2}{M_\psi - M_\chi}. \end{aligned} \tag{5.64}$$

In this small mixing limit, we can write $M_\psi - M_\chi \simeq M_2 - M_1 = \Delta M$. Therefore the mixing angle θ_d can be approximately represented by

$$\sin 2\theta_d \simeq \frac{2Yv}{\Delta M}\,. \tag{5.65}$$

Then as evident from Eqs. (5.63), ψ_1 is dominantly the singlet having a small admixture with the doublet. We assume it to be the lightest between the two (*i.e.* $M_1 < M_2$) and forms the DM component of the universe. In the physical spectrum, we also have a charged fermion $\psi^+(\psi^-)$ with mass $M^+(M^-) = M_1 \sin^2\theta_d + M_2 \cos^2\theta_d$. In the limit $\theta_d \to 0$, $M^\pm = M_2 = M_\psi$. In this section, we will discuss the relic density of dark matter as a function of Y. Although Y represents Yukawa coupling of the DM with SM Higgs, in presence of a singlet and doublet fermions, Y is also a function of the mixing angle $\sin\theta_d$ as well as the mass splitting (ΔM as in Eq. (5.65)) which crucially controls DM phenomenology as we demonstrate in the following discussion.

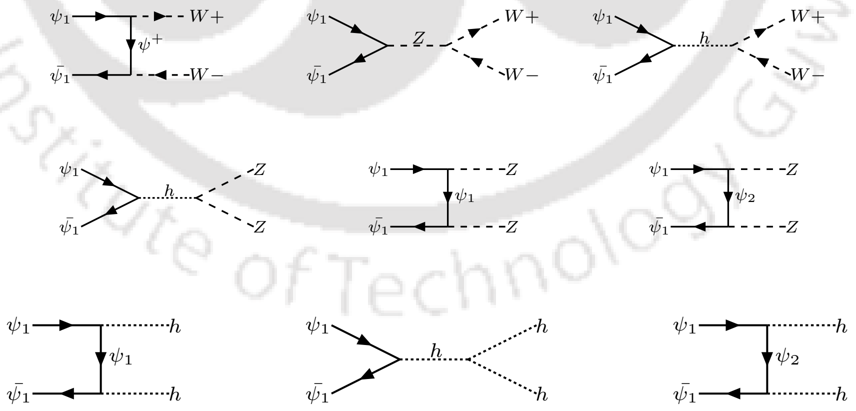

FIGURE 5.9: Dominant Annihilation processes to Higgs and Gauge boson final states.

Note that ψ_0 being the gauge doublet, it carries the gauge interactions and hence, the physical mass eigenstates including the DM have the following interaction with Z, W

bosons as :

$$\frac{g}{\sqrt{2}}\overline{\psi_0}\gamma^\mu W^+_\mu \psi^- + \text{h.c.} \rightarrow \frac{g\sin\theta_d}{\sqrt{2}}\overline{\psi_1}\gamma^\mu W^+_\mu \psi^- + \frac{g\cos\theta_d}{\sqrt{2}}\overline{\psi_2}\gamma^\mu W^+_\mu \psi^- + \text{h.c.}\,, \tag{5.66}$$

$$\frac{g}{2\cos\theta_w}\overline{\psi_0}\gamma^\mu Z_\mu \psi_0 \rightarrow \frac{g}{2\cos\theta_w}\Big(\sin^2\theta_d\overline{\psi_1}\gamma^\mu Z_\mu\psi_1 + \sin\theta_d\cos\theta_d(\overline{\psi_1}\gamma^\mu Z_\mu\psi_2 + \overline{\psi_2}\gamma^\mu Z_\mu\psi_1) + \cos^2\theta_d\overline{\psi_2}\gamma^\mu Z_\mu\psi_2\Big)\,. \tag{5.67}$$

The relic density of the dark matter (ψ_1) is mainly dictated by annihilations through (i) $\overline{\psi_1}\psi_1 \rightarrow W^+W^-, ZZ$ through $SU(2)_L$ gauge coupling and (ii) $\overline{\psi_1}\psi_1 \rightarrow hh$ through Yukawa coupling introduced in Eq. (5.10). The relevant processes are indicated in Fig. 5.9. The other possible channels are mainly co-annihilation of ψ_1 with ψ_2 (see Fig. 5.10), ψ_1 with $\psi^\pm$ (see Fig. 5.11) and annihilations of $\psi^\pm$ (see Fig. 5.12) which would dominantly contribute to relic density in a large region of parameter space [260, 279–282] as can be seen once we proceed further. At this stage we can argue on our choice of making θ_d small, or in other words why the mixing with doublet is necessary to be small for the model to provide a DM with viable relic density. This is because the larger is the doublet content in DM ψ_1, the annihilation goes up significantly in particular through $\psi_1\overline{\psi_1} \rightarrow W^+W^-$

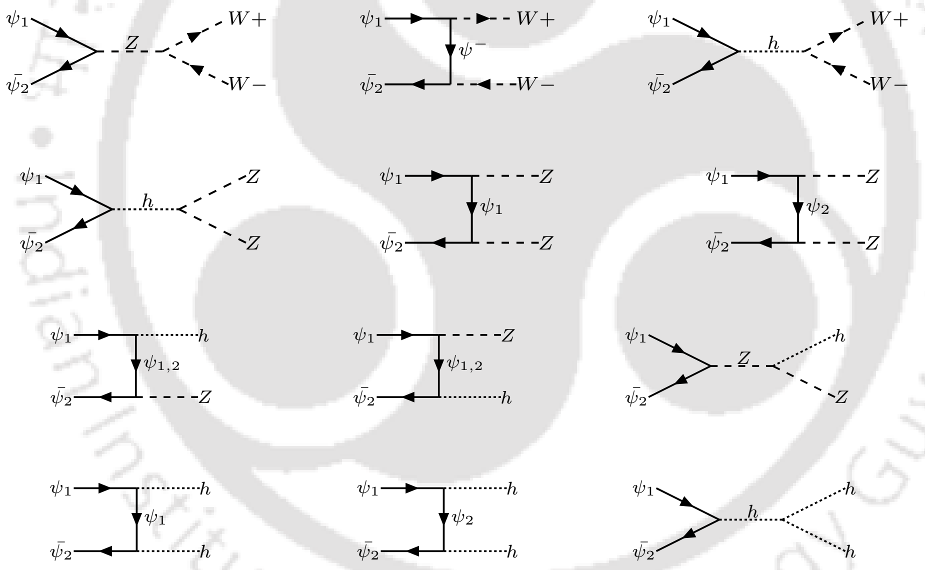

FIGURE 5.10: Dominant Co-Annihilations $\psi_1\bar{\psi}_2$ to Higgs and Gauge boson final states.

through Z and hence yielding a very small relic density. So in the small mixing limit, ψ_2 is dominantly a doublet having a mixture of minor singlet component. This implies that ψ_2 mass is required to be larger than 45 GeV in order not to be in conflict with the invisible Z-boson decay width.

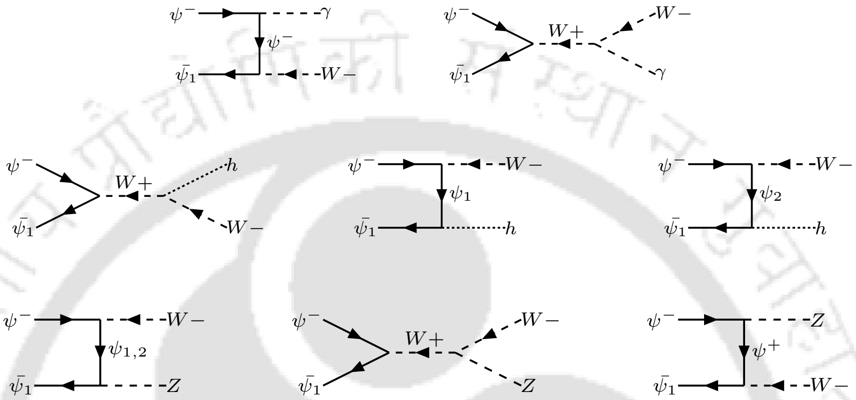

FIGURE 5.11: Dominant Co-Annihilation $\bar{\psi_1}\psi^-$ to Higgs and gauge boson final states.

The relic density of the ψ_1 DM with mass M_1 can be given by Eq. (5.2), where $\langle\sigma|v|\rangle_{eff}$

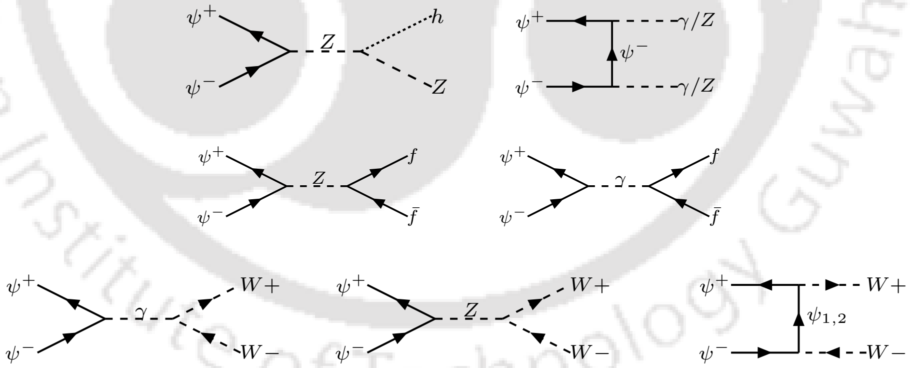

FIGURE 5.12: Dominant Co-Annihilation processes of $\psi^+\psi^- \rightarrow$ SM particles where f represents SM fermions.

is the thermal average of dark matter annihilation cross sections including contributions from co-annihilations as follows[2]:

$$\begin{aligned}\langle\sigma|v|\rangle_{eff} =& \frac{g_1^2}{g_{eff}^2}\sigma(\overline{\psi_1}\psi_1) + 2\frac{g_1 g_2}{g_{eff}^2}\sigma(\overline{\psi_1}\psi_2)(1+\Delta)^{3/2}exp(-x\Delta)\\ &+ 2\frac{g_1 g_3}{g_{eff}^2}\sigma(\overline{\psi_1}\psi^-)(1+\Delta)^{3/2}exp(-x\Delta)\\ &+ 2\frac{g_2 g_3}{g_{eff}^2}\sigma(\overline{\psi_2}\psi^-)(1+\Delta)^{3}exp(-2x\Delta) + \frac{g_2 g_2}{g_{eff}^2}\sigma(\overline{\psi_2}\psi_2)(1+\Delta)^{3}exp(-2x\Delta)\\ &+ \frac{g_3 g_3}{g_{eff}^2}\sigma(\psi^+\psi^-)(1+\Delta)^{3}exp(-2x\Delta)\,. \end{aligned} \tag{5.68}$$

In the above equation g_1,g_2 and g_3 are the spin degrees of freedom for ψ_1, ψ_2 and ψ^- respectively. Since these are spin half particles, all g's are 2. The freeze-out of ψ_1 is parameterised by $x_f = \frac{M_1}{T_f}$, where T_f is the freeze out temperature. Δ depicts the mass splitting ratio as $\Delta = \frac{M_2-M_1}{M_1} = \frac{\Delta M}{M_1}$, where M_2 stands for the mass of both ψ_2 and $\psi^\pm$. The effective degrees of freedom g_{eff} in Eq. (5.68) is given by

$$g_{eff} = g1 + g_2(1+\Delta)^{3/2}exp(-x\Delta) + g_3(1+\Delta)^{3/2}exp(-x\Delta)\,. \tag{5.69}$$

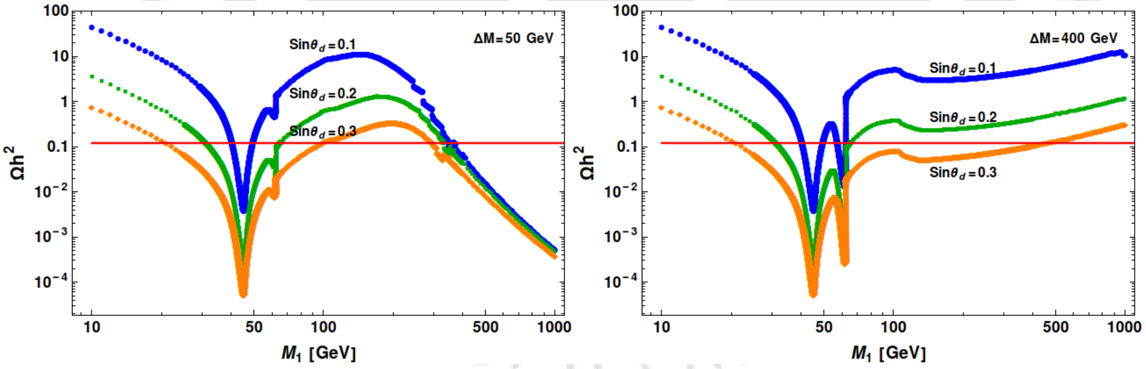

FIGURE 5.13: Relic density vs DM mass M_1 (in GeV) for different choices of $\sin\theta_d = \{0.1, 0.2, 0.3\}$ with $\Delta M = 50$ GeV [left] (corresponding to $Y = \{0.02, 0.04, 0.058\}$ with blue, green, orange respectively) and $\Delta M = 400$ GeV [right] (corresponding to $Y = \{0.16, 0.32, 0.46\}$ with Blue, Green, Orange respectively). Horizontal lines define the correct relic density.

---

[2] If M_2 is very close to M_1 then ψ_2 decay to ψ_1 should contribute to relic density. However the parameter space scan that we have performed with $\Delta M \gtrsim$ GeV, excludes such possibility.

As it turns out from the above discussion, the dark-sector phenomenology in our set-up is mainly dictated by three parameters $\sin\theta_d, M_1$ and ΔM. However we will keep on changing $\sin\theta_d$ and/or ΔM dependence with Y wherever required using Eq.(5.65). In the following we use the code `MicrOmegas` [283] to find the allowed region of correct relic abundance for our DM candidate ψ_1 satisfying PLANCK constraints [256**?**] as in Eq. (5.1).

In Fig. 5.13 we plot relic density versus DM mass M_1 for different choices of $\sin\theta_d = 0.1, 0.2$ and 0.3 (represented by blue, green and orange dotted lines respectively) while keeping the mass difference ΔM fixed at 50 GeV in the left panel and at $\Delta M = 400$ GeV in the right panel. The choice of various $\sin\theta_d$ can be translated into different values of Y as well, through Eq. (5.65) since ΔM is kept fixed. Then it is equivalent to say that the blue, green and orange dotted lines in the left panel ($\Delta M = 50$ GeV) represent Y= 0.02, 0.04, 0.058 respectively. In a similar way, the blue, green and orange dotted lines in the right panel ($\Delta M = 400$ GeV) represent $Y = 0.16, 0.32, 0.46$ respectively. We infer that as the mixing increases or in other words Y increases (ΔM is fixed), the doublet component starts to dominate (see Eq. (5.65)) and hence give larger cross-section which leads to a smaller DM abundance for a particular M_1. The second important point to note is the presence of Z resonance at $M_1 = M_Z/2 \sim 45$ GeV and a Higgs resonance at $M_1 = M_H/2 \sim 63$ GeV where relic density drops sharply due to increase in annihilation cross-section. We can also see that with larger ΔM, *i.e.* with larger Y (as $\sin\theta_d$ is fixed) in the right hand side, the Higgs resonance is more prominent for obvious reasons. Relic density for these chosen parameters are satisfied across the Z resonance window and H resonance window (more prominent for larger ΔM on the right panel). For small $\Delta M = 50$ GeV (left panel of Fig. 5.13), relic density drops beyond DM mass of 300 GeV. This is due to co-annihilation channels start contributing $\overline{\psi_2}\psi_1 \to SM$ or $\overline{\psi^+}\psi_1 \to SM$ and we find that the relic density is satisfied for DM mass $\sim$ 400 GeV. This is however not seen in the right panel where we have larger ΔM. This is because with the large mass gap, co-annihilation doesn't contribute significantly due to Boltzmann suppression for DM masses upto TeV. That is why with larger ΔM (right panel of Fig. 5.13), there is no point for DM mass beyond 100 GeV associated with smaller $\sin\theta_d$ values like 0.1, 0.2, where relic density constraint is satisfied. With larger $\sin\theta_d = 0.3$ one can satisfy relic density without the aid of co-annihilation for $M_1 \sim 500$ GeV. We also note a small drop in relic density on the right panel in particular, when WW and ZZ channels open up for annihilation.

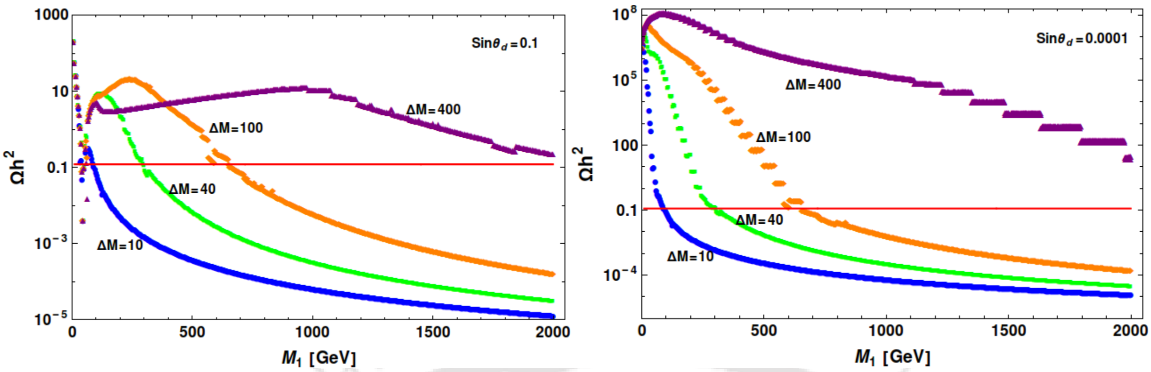

FIGURE 5.14: Left: Ωh^2 versus Dark matter mass M_1 (in GeV) for $\sin\theta_d = 0.1$ with different choices of $\Delta M = \{10, 40, 100, 400\}$ GeV described by { blue, green, orange, purple respectively}. Right: Same as left panel but with different $\sin\theta_d = 0.0001$. Horizontal lines indicate correct relic density.

In order to show the effect of co-annihilations more closely, we draw Fig. 5.14, where one can see the ΔM dependency on relic density for a specific choice of mixing angle. In the left panel we choose $\sin\theta_d = 0.1$ and that in the right panel for $\sin\theta_d = 0.0001$. The slices with constant ΔM is shown for $\Delta M = \{10, 40, 100, 400\}$ GeV in blue, green, orange, purple lines respectively. We note here, that with larger ΔM, annihilation cross-section increases due to enhancement in Yukawa coupling ($Y \propto \Delta M$ as $\sin\theta_d$ is fixed). However, co-annihilation decreases due to increase in ΔM as $\sigma \propto e^{-\Delta M/M_1}$ specifically for a particular DM mass. Hence the larger is ΔM the smaller is co-annihilation and the larger is the relic density. This is clearly visible in both the panels of Fig. 5.14. In particular, when $\sin\theta_d$ is small, the effect of co-annihilation is pronounced as contribution from annihilation cross section is less dominant. This is the case shown in the right panel of Fig. 5.14. Hence the bigger is ΔM, the larger is the required DM mass to satisfy relic density for a given mixing angle $\sin\theta_d$. This is evident from the plot with $\Delta M = 400$ GeV.

For extremely small mixing angle, say $\sin\theta_d = 0.0001$ (shown on the right panel of Fig. 5.14), the annihilation of $\bar{\psi}_1\psi_1, \bar{\psi}_1\psi_2 \to SM$ particles are highly suppressed. As a result the dominant contribution to relic density arises from $\psi_2\psi^{\pm}, \psi^{+}\psi^{-} \to$ SM particles. This is an interesting consequence of our model. In this case we get a lower limit of the singlet-doublet mixing angle by assuming that the $\psi_2, \psi^{\pm}$ particles decay to ψ_1 before the latter freezes out from the thermal bath [260]. If the mass splitting between ψ^{-} and ψ_1

is larger than $W^{\pm}$-boson mass, then ψ^- decay preferably occurs through the two body process: $\psi^- \to \psi_1 + W^-$. However, if the mass splitting between ψ^- and ψ_1 is less than $W^{\pm}$ boson mass, then ψ^- decays through three body process, say $\psi^- \to \psi_1 \ell^- \overline{\nu_\ell}$. For the latter case, we get a stronger lower bound on the mixing angle than for two body decay. For the above mentioned channel, the three body decay width of ψ^- is given by [260]:

$$\Gamma = \frac{G_F^2 sin^2\theta_d}{24\pi^3} M_2^5 I \tag{5.70}$$

where G_F is the Fermi coupling constant and I is given as:

$$I = \frac{1}{4}\lambda^{1/2}(1, a^2, b^2) F_1(a,b) + 6F_2(a,b) \ln\left(\frac{2a}{1 + a^2 - b^2 - \lambda^{1/2}(1, a^2, b^2)}\right) . \tag{5.71}$$

In the above Equation $F_1(a,b)$ and $F_2(a,b)$ are two polynomials of $a = M_1/M_2$ and $b = m_\ell/M_2$, where m_ℓ is the charged lepton mass. Up to $\mathcal{O}(b^2)$, these two polynomials are given by

$$\begin{aligned} F_1(a,b) &= \left(a^6 - 2a^5 - 7a^4(1+b^2) + 10a^3(b^2-2) + a^2(12b^2-7) + (3b^2-1)\right) \\ F_2(a,b) &= \left(a^5 + a^4 + a^3(1-2b^2)\right) . \end{aligned} \tag{5.72}$$

In Eq. (5.71), $\lambda^{1/2} = \sqrt{1 + a^4 + b^4 - 2a^2 - 2b^2 - 2a^2b^2}$ defines the phase space. In the limit $b = m_\ell/M_2 \to 1 - a = \Delta M/M_2$, $\lambda^{1/2}$ goes to zero and hence $I \to 0$. The life time of ψ^- is then given by $\tau \equiv \Gamma^{-1}$. Now to compare the life time of ψ^- with DM freeze out epoch, we assume that the freeze out temperature of DM is $T_f = M_1/20$. Since the DM freezes out during radiation dominated era, the corresponding time of DM freeze-out is given by :

$$t_f = 0.301 g_\star^{-1/2} \frac{m_{\rm pl}}{T_f^2} , \tag{5.73}$$

where $g_\star$ is the effective massless degrees of freedom at a temperature T_f and $m_{\rm pl}$ is the Planck mass. Demanding that ψ^- should decay before the DM freezes out (i.e. $\tau \lesssim t$) we get

$$\sin\theta_d \gtrsim 1.1789 \times 10^{-5} \left(\frac{1.375 \times 10^{-5}}{I}\right)^{1/2} \left(\frac{200\text{GeV}}{M_2}\right)^{5/2} \left(\frac{g_\star}{106.75}\right)^{1/4} \left(\frac{M_1}{180\text{GeV}}\right) . \tag{5.74}$$

Notice that the lower bound on the mixing angle depends on the mass of ψ^- and ψ_1.

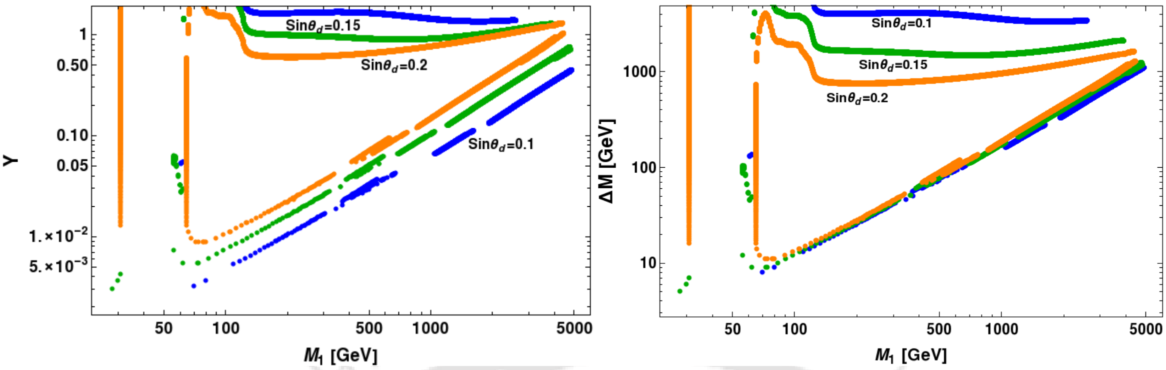

FIGURE 5.15: Left: Y versus M_1 (in GeV) for correct relic density (Eq. 5.1). $\sin\theta_d =$ 0.1, 0.2, 0.15 (blue, green and orange respectively) has been chosen, while ΔM vary arbitrarily. Right: Same plot in $M_1 - \Delta M$ plane.

In Fig. 5.15 (left), we plot Y versus M_1 to produce correct relic density with $\sin\theta_d = \{0.1,\ 0.15,\ 0.2\}$ (blue, orange, green respectively). In order to be consistent with Eq. (5.65), ΔM has to be adjusted accordingly. It points out a relatively wide DM mass range satisfy the relic density constraint. Main features that emerge out of this figure are as follows: (i) Firstly, there exist a lower DM mass region where Z and H resonances occur. Relic density is easily satisfied in this region for all possible moderate choices of $\sin\theta_d$, independent of Y or ΔM as is seen on the left hand side vertical lines (in both the plots). For large $\sin\theta_d$ this is more prominent as both Z and H mediation is enhanced with larger mixing. (ii) The other point is to note that there are two regions for each $\sin\theta_d$ value which satisfy relic density; one at the below, where Y (on the left) and ΔM (on the right panel) increase with larger DM mass to satisfy relic density. This region is dominantly contributed from co-annihilations as the small Y is not enough to produce annihilations required for relic density. While there is a second region with larger Y (on left) and larger ΔM (on right), more insensitive to DM mass, where relic density is satisfied by appropriate annihilation cross-section, not aided by co-annihilations. Both of these regions (annihilation and co-annihilation domination) meet at some large DM mass $\sim$ 5000 GeV, more clearly visible from the right panel plot. Points above the 'correct annihilation lines' (for specific $\sin\theta_d$) provide more than required annihilation and hence those are under abundant regions. Similarly just below those, the annihilation will not be enough to produce correct density and hence are over abundant regions. Points below the correct co-annihilation regions produce more co-annihilations than required and hence depict under abundant regions.

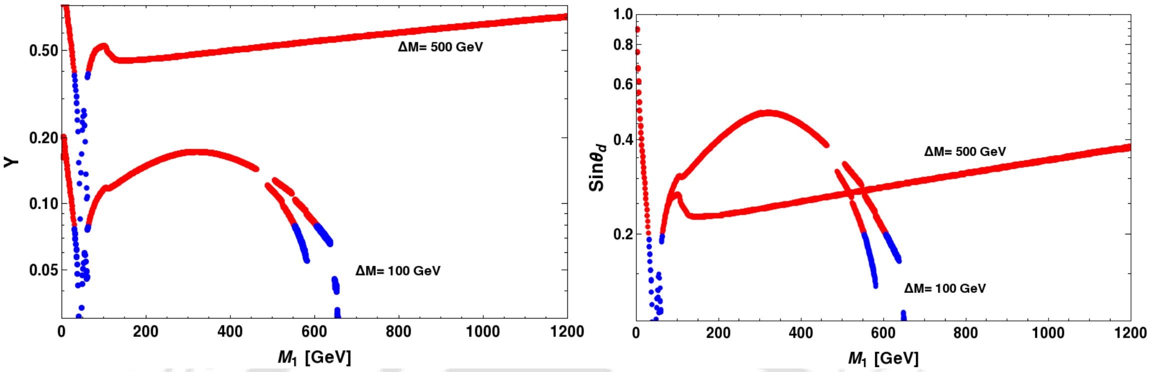

FIGURE 5.16: Left: Y versus M_1 (in GeV) for correct relic density (within the range given by Eq. (5.1)) with fixed ΔM at 100, 500 GeV, while $\sin\theta_d$ is allowed to vary. Right: Same plot in $M_1 - \sin\theta_d$ plane. In both panels, blue dots are the allowed points for small $\sin\theta_d$ to satisfy the Y, ΔM abundance via Eq. (5.65).

The other possible correlation in this model for correct relic density can be drawn between DM mass (M_1) and the mixing angle ($\sin\theta_d$) for fixed ΔM. This is shown in Fig. 5.16 both in $M_1 - Y$ plane (on the left) or in $M_1 - \sin\theta_d$ plane (on the right). For illustration, we choose two widely different values of mass difference: $\Delta M = 100$ GeV and $\Delta M = 500$ GeV. This is clearly understood that with larger ΔM, a larger Y is favored for a specific DM mass in order to satisfy the correct relic abundance. With $\Delta M = 100$ GeV we also note that Y drops substantially around $M_1 \sim 500$ GeV. This is because around this value, co-annihilation process starts contributing and hence it requires a further drop in Y (in terms of mixing angle θ_d) to obtain right relic density which is clearly visible in the right side of Fig. 5.16 as well. Here we would like to draw the attention that the right relic density line has a split when co-annihilation starts dominating. This is due to the fact that there are two different co-annihilations that occur here with ψ_2 and $\psi^{\pm}$. There exist a slight mass difference between these particles and the DM mass is adjusted to either of them to effectively co-annihilate and produce right relic density. For $\Delta M = 500$ GeV, this phenomena of co-annihilation occurs at a very large DM mass and can't be seen from the plot. Resonance drops both in $Y - M_1$ and $\sin\theta_d - M_1$ plots can be observed for $M_1 \sim M_H/2$ and $M_1 \sim M_Z/2$. We also note that beyond $\sin\theta_d \geq 0.2$ as shown by the red points in Fig. 5.16 break small θ_d limit as has been assumed in Eq. (5.65) and hence discarded within this approximation.

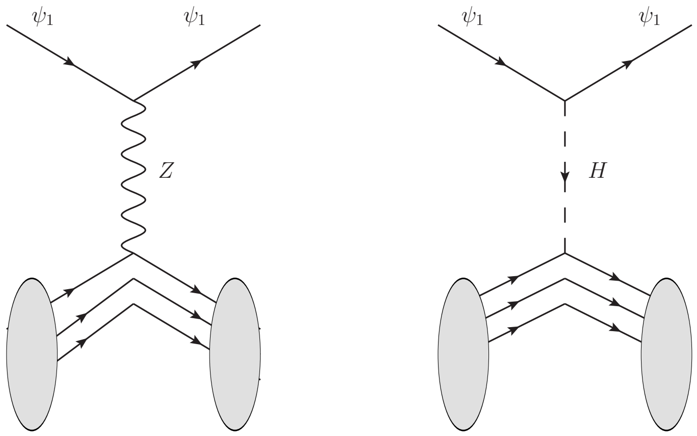

FIGURE 5.17: Feynman diagrams for DM to interact with Nucleon.

Non-observation of DMs in direct search experiments tend to put a stringent bound on WIMP DM parameter space. Direct search interactions for ψ_1 has two different channels, through Z and H mediation as shown in Fig. 5.17, where the one through Z mediation dominates over H mediated interaction because of $SU(2)$ gauge coupling. The cross-section per nucleon for Z mediation is given by [284, 285]

$$\sigma_{\rm SI}^{Z} = \frac{1}{\pi A^2}\mu_r^2|\mathcal{M}|^2 \tag{5.75}$$

where $\mu_r = M_1 m_n/(M_1 + m_n) \approx m_n$ is the reduced mass, m_n is the mass of nucleon (proton or neutron), A is the mass number of the target nucleus and $\mathcal{M}$ is the amplitude for Z-mediated DM-nucleon cross-section

$$\mathcal{M} = \sqrt{2}G_F[Z(f_p/f_n) + (A - Z)]f_n \sin^2\theta_d\,, \tag{5.76}$$

f_p and f_n are the interaction strengths of DM with proton and neutron respectively and Z is the atomic number of the target nucleus. Using $f_n \simeq 1/3$ [286–289], we obtain direct search cross-section per nucleon to be

$$\sigma_{\rm SI}^{Z} \simeq 3.75 \times 10^{-39}{\rm cm}^2 \sin^4\theta_d\,. \tag{5.77}$$

Higgs mediated cross-section depends on can be written as

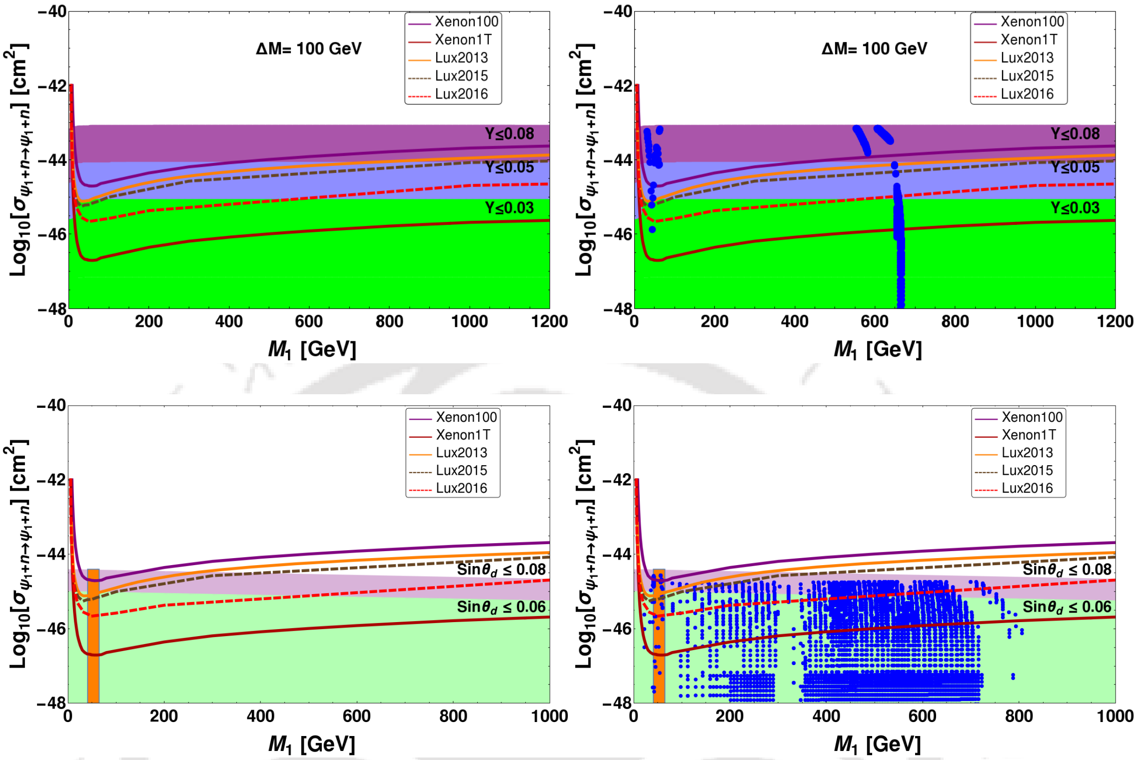

FIGURE 5.18: Spin independent direct search cross-section as a function of DM mass. Upper Left Panel: Different Y ranges are indicated Y : $\{0.001-0.03\}$ (green), Y : $\{0.03-0.05\}$ (blue) and Y : $\{0.05-0.08\}$ (purple). $\Delta M = 100$ GeV is used for the scan. Upper Right Panel: Same as left, additional blue dots represent points which satisfy relic density constraint. Lower left panel: Allowed ranges of $\sin\theta_d \leq 0.06, 0.08$ (light green and lilac regions respectively) are shown. Here ΔM varies arbitrarily upto 1.1 TeV. Lower right panel is same as the lower left panel having blue dots representative of points which satisfy relic density constraint. The resonance region is separately indicated in orange. Constraints from Xenon100, Lux 2013, 2015, 2016 data and predictions of Xenon1T are presented.

$$\sigma^h_{\rm SI} = \frac{1}{\pi A^2}\mu_r^2 \left[Z f_p + (A-Z) f_n\right]^2 \tag{5.78}$$

where the effective interaction strengths of DM with proton and neutron are given by:

$$f_{p,n} = \sum_{q=u,d,s} f^{(p.n)}_{Tq}\alpha_q \frac{m_{(p,n)}}{m_q} + \frac{2}{27} f^{(p,n)}_{TG} \sum_{q=c,t,b} \alpha_q \frac{m_{p.n}}{m_q} \tag{5.79}$$

with

$$\alpha_q = \frac{Y \sin 2\theta_d}{M_h^2}\left(\frac{m_q}{v}\right) . \tag{5.80}$$

We compute the direct search cross-section with both diagrams using `MicrOmegas` [283]. It turns out that the most stringent constraint on the model and hence on the portal coupling Y ($\lesssim \sin 2\theta_d \Delta M/(2v)$) comes from the direct search of DM from updated LUX data [290] as demonstrated in Fig. 5.18. We show the correct region of direct search allowed parameter space in two ways: in upper panel we choose a specific ΔM and vary $\sin\theta_d$ to evaluate spin independent direct search cross-section and show the constraints in terms of Y. On the upper right panel, we also show the relic density allowed points through blue dots for this particular choice of ΔM. In the bottom panel of Fig. 5.18, instead of choosing a specific ΔM, we vary it arbitrarily upto 1.1 TeV and point out the direct search constraints in terms of mixing angle $\sin\theta_d$. On the right bottom panel, we also show the relic density allowed points through blue dots. Restricting direct search cross-section to experimental limit actually puts a stringent bound on mixing angle $\sin\theta_d$ to tame Z-mediated diagram in particular. We see that the bound from LUX, constraints the coupling: $Y \sim 0.03$ for DM masses $\gtrsim 600$ GeV (green regions in the upper panel of Fig. 5.18). The Yukawa coupling needs to be even smaller for small DM mass for example, $M_1 \simeq 200$ GeV. The resonance region is exempted from this constraint for obvious reasons. The annihilation cross-section is enhanced due to s-channel contribution and to tame it to right relic density, one needs much smaller values of mixing angle, which sharply drops the direct search cross-section. Though large couplings are allowed by correct relic density, they are highly disfavored by the direct DM search at terrestrial experiments. From the top right figure, we also see that correct relic density points for a specific ΔM lies in the vicinity of a specific DM mass ~ 700 GeV where co-annihilation plays the crucial role for correct relic density and that doesn't contribute to direct search cross-section at all, so that the blue points yield very small direct search cross-sections. This can easily be extended for other choices of ΔM, where there exist a specific DM mass at which co-annihilation plays a crucial role to yield right relic density, which doesn't contribute to direct search and thus can have very small direct search cross-section as is seen from the right bottom figure. Note also that direct search constraints are less dependent on ΔM as to the mixing angle, which plays otherwise a crucial role in the relic abundance of DM. In bottom panel, we show the parameter space satisfied by relic density constraint for $\sin\theta_d \leq 0.08, 0.06$ (lilac and green regions respectively) to direct search constraints. The direct search tightly constraints the mixing angle to $\sin\theta_d \leq 0.08$, allowing DM masses as heavy as 900 GeV. Tighter constraint in mixing angle, for example, $\sin\theta_d \leq 0.06$, allows smaller DM mass ≥ 500 GeV as can be seen from the cross-over of LUX constraint with relic density allowed parameter space.

In summary, the dark sector phenomenology with the inclusion of vector-like fermions provides a simple extension to SM, with a rich phenomenology with a large region of allowed parameter space from relic density constraints. Direct search on the other hand constrains the mixing to a small value ≤ 0.08, allowing co-annihilation to play a dominant part to keep the model alive. We will focus on the correlations to non-zero θ_{13} and DM in the following section with the results obtained from above analysis. Note that the $U(1)$ symmetry being global, its spontaneous breaking would lead to potentially dangerous Goldstone boson ($G = \text{Im}\phi$). The problem however can be evaded by gauging the symmetry. Additionally if we assume the corresponding gauge boson to be sufficiently heavy, its existence will not modify our results of the dark matter phenomenology. Another way out is to provide tiny mass to the Goldstone by introducing an explicit symmetry breaking term in the Lagrangian. In this case however the most significant coupling of the Goldstone with Higgs appears through $\lambda_{12}\phi^\dagger\phi H^\dagger H$ coupling. Hence it contributes (considering $m_G \ell^+\ell^- m_h/2$) to the invisible decay of the SM Higgs boson [292], $\Gamma_{h\to G\ G} \sim \frac{1}{32\pi}[m_h^3/\langle\phi\rangle]\sin^2\alpha$, where α signifies the mixing between the states (H,ϕ) and the physical Higgs fields (h, H') resulting (H' is the heavy Higgs) from non-zero λ_{12}. In the limit of λ_{12} to zero, α vanishes. Using the present limit on the branching ratio of Higgs invisible decay [293, 294] , the coupling λ_{12} (involved in the definition of mixing angle α) is expected to be small $(\ell^+\ell^- 1)$. If we assume a very small value of λ_{12}, $\sim 10^{-8}$ or even smaller, then it can be shown that the Goldstone can never be in thermal equilibrium [295] and hence they can not contribute to the primordial abundance through freeze out mechanism [3] and we may basically ignore its presence for our purpose.

We can now put together all the constraints for a specific choice of $\sin\theta_d = 0.06$ into the plane of $M_1 - M_2$ to show the allowed parameter space of the model. This is what

---

[3] In this case, the other option could be [296] the freeze-in mechanism [297]. It requires a detailed study and is at present beyond the scope of current analysis.

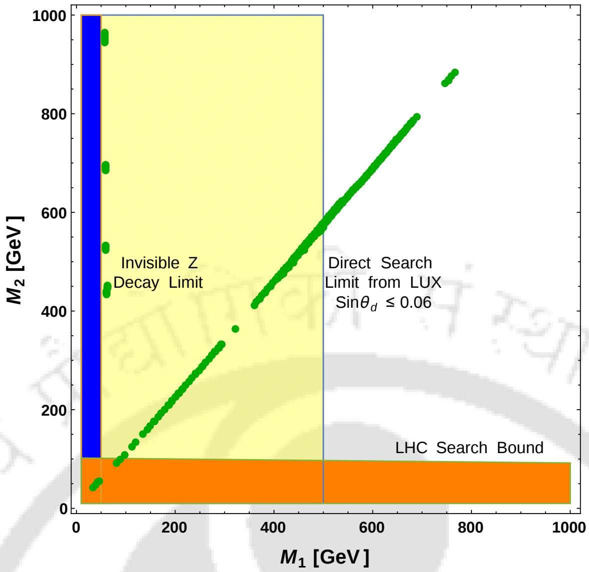

FIGURE 5.19: Summary of all constraints in $M_1 - M_2$ parameter space from relic density with $\sin\theta_d = 0.06$ (green dots), direct search (Yellow region is forbidden by updated LUX with $\sin\theta_d \sim 0.06$), invisible Z-decay (blue region is forbidden) and collider (LHC) search limit (orange region is disallowed with an over estimation for $\sin\theta_d = 0.1$).

we have done in Fig. 5.19 following

$$\begin{aligned}
\text{Inv Z decay : } \mathrm{M}_1 &< \frac{\mathrm{M_z}}{2} \sim 45\ \text{GeV} \rightarrow \sin\theta_d \lesssim 0.00125 \\
\text{Inv H decay : } \mathrm{M}_1 &< \frac{\mathrm{M_h}}{2} \sim 63\ \text{GeV} \rightarrow \sin\theta_d \lesssim 0.1 \\
\text{Relic Density : } \mathrm{M}_2 &\lesssim \mathrm{M}_1 + 100\ \text{GeV for } \sin\theta_d \lesssim 0.1 \\
\text{Direct Search : } \mathrm{M}_1 &\geq 500\ \text{GeV for } \sin\theta_d \sim 0.06 \\
\text{Collider Bound : } \mathrm{M}_2 &\simeq \mathrm{M}^{\pm} \geq 101\ \text{GeV for } \sin\theta_d \sim 0.06.
\end{aligned}$$

We choose $\sin\theta_d = 0.06$ as a reference value as it satisfies all of the constraints discussed here. We see that a sizable part of the DM parameter space is allowed shown by the green dotted points, excepting for the direct search bound shown by yellow band, a blue band disfavored by the Invisible Z decay and orange band disfavored by direct collider search data [291]. One should also note here that if we choose a smaller $\sin\theta_d$ to illustrate the case, a larger DM mass region is allowed by direct search constraint. Green dotted points show relic density allowed regions of the model in $M_1 - M_2$ plane. We note here that for $\sin\theta_d < 0.1$, only co-annihilation can provide with right relic density, hence is independent of the choices $\sin\theta_d \sim 0.1$ or ~ 0.06 as has been chosen in Fig. 5.19.

5.5 Correlation between Dark and Neutrino Sectors

As stated before, our description of the DM sector is composed of a vector like $SU(2)_L$ doublet and a neutral singlet fermions which interact with the SM sector via Eq. (5.10). We have seen in the previous section the importance of the effective coupling Y in determining the mixing between the singlet and doublet components of DM (see Eq. (5.65)). This mixing in turn plays the crucial role in realizing the correct relic density as well as involved in the direct search cross section (see Eqs. (5.2) and (5.75, 5.78)). Note that this effective coupling Y is generated from the vev of the flavon ϕ through $Y = \epsilon^n$, where the n is the unknown $U(1)$ charge assigned to ϕ. However this vev alone does not appear separately in our dark matter analysis. On the other hand, we have noted earlier the involvement of ϵ parameter in the neutrino phenomenology, in particular in producing θ_{13} in the correct ballpark. So we observe that the allowed value of nonzero θ_{13} and the Higgs portal coupling of a vector like dark matter can indeed be obtainable from a $U(1)$ flavor extension of the SM. In this section we aim to fix the charge n from combining the results of neutrino as well as the dark matter analyses. This complementarity between the neutrino and the DM sector will be clear as we proceed below in summarizing constraints on ϵ and Y obtained from neutrino and DM analyses respectively.

Section 5.3 was devoted to neutrino phenomenology, where we have discussed four different cases. In case A, we find that the parameter ϵ is clearly determined to be within the range $0.328 - 0.413$ in order to keep $\sin\theta_{13}$ in agreement with experimental data (see Fig. 5.2). In cases B and C however, this correlation between ϵ and θ_{13} is not that transparent as it depends also on the CP phase δ. Combining all the phenomenological constraints (*e.g.* on $\sum_i m_{\nu_i}$), we have provided the range of ϵ in Table 5.3 and 5.4 for cases B and C respectively. The range of ϵ corresponding to case D is similar to case A. On the other hand, the information on Y is embedded in the relic density and direct detection cross section.

In the left upper panel of Fig. 5.18, we plot the direct search cross-section against dark matter mass M_1 for a fixed choice of $\Delta M = 100$ GeV. In this plot, we indicate regions

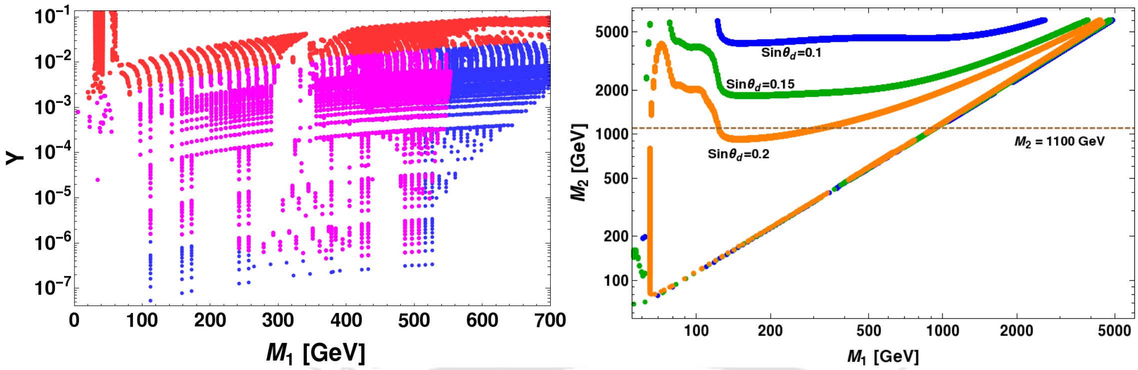

FIGURE 5.20: Left Panel: Y vs M_1 scatter plot for correct relic density (Eq. 5.1). Here $\sin\theta_d$ (10^{-6}-0.2) and ΔM (1-1100 GeV) varies simultaneously. The top red points are disallowed by Lux 2016 direct search constraint. Both magenta and blue dots simultaneously satisfies relic density and Lux 2016 direct search constraints. The magenta dots additionally satisfies the condition $\Delta M < M_W$. Right Panel: M_1 versus M_2 (in GeV) for correct relic density. $\sin\theta_d = 0.1,\ 0.2,\ 0.15$ (blue, green and orange respectively) has been chosen, while ΔM varies. The left panel is consistent with this plot upto $M_2 = 1.1$ TeV as marked by the horizontal dashed line in this plot.

allowed by direct search experimental limits. Since each point in the region allowed by direct search correspond to a specific relic density, once we incorporate both the relic density and direct search limit by LUX 2016, we find the allowed region is narrowed down as shown in the right upper panel of Fig. 5.18 (indicated by blue patch).

Similarly the left lower panel (left and right) of Fig. 5.18 shows the allowed (by both relic density and LUX 2016) region of parameter space where variation of M_2 is restricted up to 1.1 TeV with $\sin\theta_d \leq 0.2$. We find that an uper limit on $\sin\theta_d$ is prevailing from this plot. Combining relic density constraint and direct search limits, we find the allowed region indicated by blue dots in the right lower panel of Fig. 5.18. In order to obtain limits on Y while ΔM and $\sin\theta_d$ are varied, we have provided a scatter plot of Y versus M_1 in Fig. 5.20. In producing this plot, we have varied M_2 (up to 1.1 TeV), $10^{-7} < \sin\theta_d < 0.2$. Here red dots correspond to those points which are disallowed by LUX 2016 even if these satisfy the relic density constraint. The blue patch indicates the region allowed by both the relic density and LUX 2016 data having $\Delta M > m_W$. For $\Delta M < m_W$, we use a lower limit on $\sin\theta_d$ obtained from Eq. (5.74). Hence the points in magenta satisfy the above $\sin\theta_d$ constraint and represent the allowed region by relic density and direct search limits. From this plot we can clearly see the upper limit of Y is almost 0.03 while the lower limit of it can be very small, $\sim 10^{-7}$. Note that the Y region limited by the choice of upper value of $M_2 = 1.1$ TeV is consistent with our earlier plot in Fig. 5.15 with fixed $\sin\theta_d$ values. For elaboration purpose, we provide the figure in the right panel of Fig. 5.20, which is the same plot as Fig. 5.15 except that it is now plotted in terms of M_2 vs. M_1. The narrow patch for a fixed $\sin\theta_d$ becomes wider as we varied $\sin\theta_d$ as well. The horizontal dashed line indicates our consideration of keeping the variation of M_2 within 1.1 TeV.

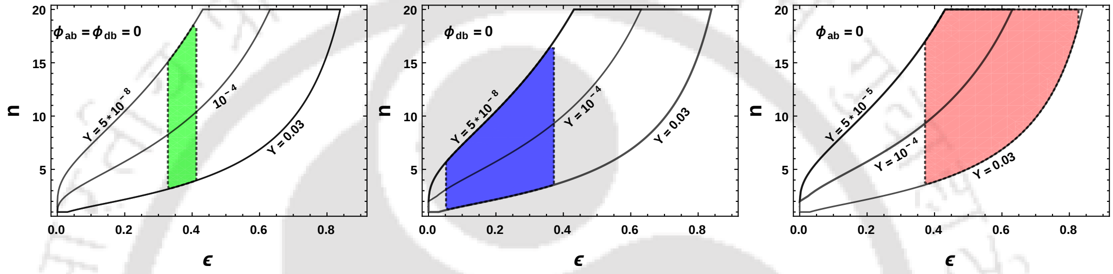

FIGURE 5.21: n vs ϵ to generate different values of $Y = \epsilon^n$ for (a) $\phi_{db} = \phi_{ab} = 0$ (left), (b) $\phi_{db} = 0$ (middle) and (c) $\phi_{ab} = 0$ (right).

We summarize here these constraints on ϵ and $Y = \epsilon^n$ to determine the unknown flavor charge n of the dark matter in our scenario. It is shown in Fig. 5.21. Colored patch in each plot corresponds to the allowed range of ϵ obtained in section 5.3 for Cases A(D), B and C. In the left-most panel of Fig. 5.21, we have shown the allowed values of n where the CP-violating phases are taken to be zero corresponding to Case A. As the direct search of DM restricts the Y values to be $Y \lesssim 0.03$, we get $n \gtrsim 2$. Different contour lines with different Y values are shown in the figure. A similar conclusion holds for the other case (Case D) with $\phi_{db} = \phi_{ab} = \beta$. On the other hand, if $\phi_{ab} \neq \phi_{db}$ then a larger range of n values are expected to be allowed. In particular, by setting $\phi_{db} = 0$ and $\phi_{ab} \neq 0$ (as shown in middle panel of Fig. 5.21) we see that lower limit on n starts from 1. On the other hand, if $\phi_{ab} = 0$ and $\phi_{db} \neq 0$ (as shown in the right panel of Fig. 5.21) then n can take values starting from 3. Thus we conclude that the non-zero values of phases introduce more uncertainty in specifying n. The future measurements of Dirac CP phase δ and a more stringent constraints from Direct search experiments would reduce this uncertainty in n.

5.6 Conclusions

In this Chapter we have explored a $U(1)$ flavor extension of the SM in order to establish a possible correlation between the SM sector (more specifically neutrino sector) and the DM one, in particular between the reactor lepton mixing angle $\sin\theta_{13}$ and the interaction of dark matter with SM Higgs. To start with, we have considered a tri-bimaximal mixing pattern (*i.e.* with $\theta_{13} = 0$) for the lepton mixing matrix originated from a typical flavor structure of the neutrino mass matrix guided by the non-Abelian flavor symmetry, where the charged lepton mass matrix is found to be diagonal. In its simplest version, we achieve the TBM structure of the neutrino mass matrix by assuming an $A_4 \times Z_3$ symmetry where the effective dimension six operators involving A_4 flavons contributes to Majorana masses for light neutrinos. The symmetry forbids the usual dimension five operator. On the other hand, the dark sector consists of two vector-like fermions, one is a $SU(2)_L$ doublet and the other one is a SM gauge singlet. In addition we assume the existence of a $U(1)$ flavor symmetry under which the DM fields as well as two flavons, ϕ and η, are charged. It is interesting to note that with the vector-like fermions present in the dark sector, there exists a replica of SM Yukawa interaction in the dark sector which involves flavon ϕ. The $U(1)$ symmetry of the model was broken at a high scale by the vev of that flavon field ϕ to a remnant $\mathcal{Z}_2$ under which the dark sector particles are odd. As a result the lightest odd particles becomes a viable candidate of dark matter. Moreover, a higher dimensional operator involving ϕ and η constitutes a correction to the TBM pattern of the neutrino mass matrix which leads to a non-zero value of $\sin\theta_{13}$. The involvement of ϕ ensures that $B - L$ breaking vev is also involved in this correction term. As a result we are able to show that the non-zero value of $\sin\theta_{13}$ is proportional to the Higgs portal coupling, $Y = (\phi/\Lambda)^n \equiv \epsilon^n$, of the dark matter which gives rise to correct relic density measured by WMAP and PLANCK and consistent with direct DM search bound from LUX. Finally it is interesting to note that Y, on one hand is related to the mixing in the neutrino sector, while it also crucially controlled by the mixing involved in the dark sector. We also find that the current allowed values of $\sin\theta_{13}$ indicates the $U(1)$ charge of DM $\gtrsim 1$ which can be probed at the future direct DM search experiments such as Xenon-1T. The next to lightest stable particle (NLSP) is a charged fermion which can be searched at the LHC [262, 263]. In the limit of small $\sin\theta_d$, the NLSP can give rise to a displaced vertex at LHC, a rather unique signature of the model discussed in ref. [260]. We argue that this is a minimal extension to SM to accommodate DM and non-zero $\sin\theta_{13}$ by using a flavor symmetric approach.

Chapter 6

Summary and Conclusions

The SM of particle physics, in spite of being one of the most profound theory of the nature, still can't completely explain the physics of neutrino mass and mixing. Interestingly, by incorporating additional symmetries, the observed pattern of neutrino mixing can be explained, providing a clue for the long standing flavor puzzle. In this regards, non-Abelian discrete flavor symmetries are considered to be most suitable for studies of neutrino mixing for their simplicity and economic nature. Prior to 2012, it was speculated that neutrino mixing follows a particular pattern, known as TBM mixing where the mixing angle θ_{13} turns out to be zero. However with smoking gun evidence for nonzero θ_{13} ($8^\circ - 9^\circ$) from various experiments like Daya Bay, RENO, Double Chooz, TBM mixing in neutrino sector is ruled out. Hence we need an urgent inspection to the models based on discrete flavor symmetries to accommodate nonzero θ_{13}. Apart from neutrino mixing, the mystery of mater-antimatter asymmetry in our universe and nature of dark matter is yet to be unveiled. Neutrino physics here can play an important role in connecting all these phenomenons. Standing at this situation we can ask the question: *Non-Abelian discrete symmetries which was well studied in explaining TBM pattern of neutrino mixing, can we still explain nonzero θ_{13} in such scenarios and does the involvement of flavor symmetries play any role in explaining mater-antimatter asymmetry and dark matter present in our universe?* Hence in this thesis we explore various extensions of SM, to generate nonzero θ_{13} by deviating from TBM mixing in the context of A_4 non-Abelian discrete symmetry and study various phenomenology associated with neutrino physics. We further extend our analysis to study the role nonzero θ_{13} in explaining leptogenesis and dark matter, with the involvement of flavor symmetry in it. In this chapter, we present a brief summary of the works carried out in this thesis, whereas in Section 2.6, Section 3.5, Section 4.6, Section 5.6 we have presented a detailed summery of all our works separately at the end of Chapter 2, Chapter 3, Chapter 4 and Chapter 5.

In Chapter 1, we first present a detailed motivation of our work followed some preliminaries on SM, physics of neutrino mass, mixing and oscillation. Here we also present some basic understanding of A_4 discrete group. We end this chapter by giving an introductory idea of the matter-antimatter asymmetry in our universe.

In Chapter 2, we first consider a type-I seesaw scenario based upon $A_4 \times Z_3$ discrete flavor symmetry to explain neutrino masses and mixing. Here we extend the particle content of the exiting AF model by adding one flavon, ξ', which contributes in the RH neutrino mass matrix. We show that this minimal modification is sufficient in generation of nonzero θ_{13} and the observed range of this mixing angle restricts the parameter space of the framework (with δ=0). Here our predictions for sum of absolute mass of the light neutrinos are 0.07 eV to 0.1 eV for NH and 0.13 eV to 0.23 eV for IH respectively. Here we also obtain an exclusive sum rule for the three light neutrinos which can be verified by the upcoming experiments. Interestingly the Majorana phases present in the set-up also get constrained, whose involvement in the lepton asymmetry parameter is extremely important. An estimation for the effective mass parameter appearing in the neutrinoless double beta decay is also given. The tree level framework of such models always predicts vanishing CP-asymmetry due to special flavor structure of the Yukawa coupling. Hence we show that a next-to-leading order contribution in the same coupling can successfully generate the observed matter-antimatter asymmetry (produced from the out-of-equilibrium decay of RH neutrinos present in this type-I seesaw framework) and further study its correlation with nonzero θ_{13}. It is worthy to mention here that, in such scenario, even if we consider the Dirac CP phase to be zero, observed baryon asymmetry can still be generated.

Next in Chapter 3, we study the interplay between the two terms present in a general type-I+II seesaw scenario in explaining neutrino masses and mixing when SM particle content is extended by three RH neutrinos and only one $SU(2)_L$ scalar triplet. Here the pure type-I contribution, respecting $A_4 \times Z_4 \times Z_3$ symmetry, explains TBM mixing whereas the type-II triggers the deviation from TBM mixing to generate nonzero θ_{13}. Interestingly a flavon present in this type-II contribution spontaneously violates CP symmetry hence magnitude of its vev contributes in the generation of nonzero θ_{13} and acting as the only source of CP violation in the theory (*i.e.* source of Dirac CP phase, Majorana CP phase and CP violation required for matter-antimatter asymmetry) when all the Yukawa couplings and other vevs are considered to be real. In this set-up a value close to resent hint $\sim 270^\circ$ for Dirac CP phase δ can be found although the model excludes the exact equality $\delta = 90^\circ, 270^\circ$. We also make predictions for sum of absolute mass of the light neutrinos, effective mass parameter appearing in the neutrinoless double beta decay and J_{CP} in this set-up. Finally we find that the triplet decaying with the virtual RH neutrino in the loop plays the most crucial role in explaining lepton asymmetry and role of nonzero θ_{13} in the lepton asymmetry parameter is also studied.

In Chapter 4, we worked in an inverse seesaw framework guided by $A_4 \times Z_4 \times Z_3$ discrete flavor symmetry, associated with a global $B - L$ symmetry, to study generation of nonzero θ_{13}. The striking feature in this scenario is that the flavor structure of the lepton number violating contribution (μ matrix, originated from $\overline{S^c}S$ contribution) in inverse seesaw fully dictates the light neutrino mass matrix hence gives rise to nonzero θ_{13} as well as complete neutrino masses and mixing. Here we also study the predictions for absolute neutrino masses as well as neutrinoless double beta decay. We also perform an complete parameter space scanning and find all the predictions for Dirac CP phase satisfying observed neutrino oscillation data. Potential mixing between the light and heavy neutrino states in this set-up, gives rise to the non-unitarity and we study its effects in LFV processes, neutrinoless double beta decay etc.. Here depending upon the magnitude of this non-unitarity effect we draw a correlation between vev of the A_4 flavons involved in the model with the cut-off scale of the theory and typical mass scale for the heavy neutrinos present can also be obtained. We find that due to the underlying flavor structure of the neutrino mass matrix involved here, the effective contribution to the LFV processes is vanishingly small and contribution due the presence of heavy neutrino states in neutrinoless double beta decays is also very negligible.

In the previous chapters, it is established that the discrete flavor symmetric scenarios can beautifully explain TBM mixing as well as its deviation to generate observed nonzero θ_{13}. Moving one step futher, in Chapter 5, we adopt an $U(1)$ flavor symmetric extension of the SM to draw a possible correlation between the dark matter sector and neutrino sector of SM. Here we proposed a framework, guided by $A_4 \times Z_3$ symmetry, which ensures TBM mixing in lepton sector in the first instance. Now a flavon (ϕ) charged under this global $U(1)$ flavor symmetry appears in both neutrino mass term (originated from and proportional to the conventional dimension five $\ell H \ell H$ operator) and also in the dark matter Yukawa like coupling with Higgs. Therefore breaking of the global $U(1)$ flavor symmetry to a remnant $\mathcal{Z}_2$ symmetry (as under this symmetry the dark matters are odd) ensures the stability of the dark matter and generates adequate θ_{13}, hence provides a unique connection between the dark matter sector and neutrino sector. Here the dark matter sector consists of two vector-like fermions, one is a $SU(2)_L$ doublet and the other one is a SM gauge singlet. Such a choice replicates the Yukawa interaction in the dark matter sector as well and the lightest neutral particle originated from their mixing gives rise to viable dark matter candidate. It is also worthy to mention here that the involvement of only one of these two particles alone can not satisfy the observed relic density and direct search constraints. Here we show that the non-zero value of θ_{13} is proportional to the Higgs portal coupling, $Y = (\phi/\Lambda)^n \equiv \epsilon^n$, of the dark matter which satisfies correct relic density PLANCK and consistent with direct DM search bound from LUX. Therefore the coupling Y, controlled by the mixing in the neutrino sector, is also crucially restricted by the mixing involved in the dark sector (between doublet and singlet fields). Here we observe that current allowed values of θ_{13} indicates the $U(1)$ charge of DM $\gtrsim 1$ which can be probed at the future direct DM search experiments such as Xenon-1T and involvement of non zero Dirac CP phase δ introduces lots of uncertainty in specifying this charge. Therefore a future measurement of δ will put a stringent constraints from direct search experiments, which will minimize this uncertainty in the $U(1)$ flavor charge of DM.

In conclusion, in this thesis we have studied various seesaw models based on discrete flavor symmetry to explore the interplay between physics of neutrino mass, mixing (and associated phenomenology) and various aspects of particle cosmology. The fate of these models crucially depends upon current and future neutrino (and dark matter) experiments of various type, starting from absolute neutrino mass (and effective mass parameter) measurement to measurement of CP violation in neutrino sector. In some models we have specific sum rule for absolute neutrino masses and hierarchy dependence of the model predictions which increases the chance of distinguishing these class of models. CP violation is an essential ingredient of our universe. Several state of the art experiments are already running to measure the CP violation in lepton sector. Therefore future measurement of this CP phase is going to put a stringent constrains on these models. In this thesis we have some interesting results on δ in the study of spontaneous CP violation in a general type-II seesaw. We also provide a unique connection between the neutrino and dark matter in the context of recent measurement of nonzero θ_{13}. There we have also stressed upon the case with nonzero δ. Future dark matter direct search and CP violation measurement experiments will further test the viability of these models.

Although lot of efforts were given in the past to draw connection between neutrino physics and cosmology and the subject is quite vast, here we have tried to readdress few issues particularly after precise measurement of θ_{13}. We attempted to study the subject in a coherent manner but there are several unanswered questions, hence well equipped ideas are needed to address those issues. Here we just mention some future directions as probable continuation beyond this thesis work. All the models in this thesis were constructed in such a way that the charged lepton sector always turned out to be diagonal. Therefore in such class of models, if charged lepton sector is not diagonal it also can lead to deviation from TBM mixing to generate nonzero θ_{13}. It would be also interesting to study other non-Abelian symmetries like $S_4, \Delta(27)$. Further, it will be interesting to study both lepton and quark mixing in a common platform particularly involving recent measurement of nonzero θ_{13}. In the coming years neutrino oscillation experiments are likely to measure the octant of the mixing angle θ_{23}, and neutrino mass hierarchy. Therefore it will be interesting to study models which lead to precise prediction for these parameters. Collider aspects of the flavons involved in discrete flavor symmetric models, particularly in low energy seesaw scenarios may be an interesting topic to explore. In future if CP violation in lepton sector is accurately measured it is worth studying its possible implication from flavor symmetry.

Appendix A

Vaccum Alignments in Chapter 2:

In our model driving part of the LO superpotential, invariant under $A_4 \times Z_3$ with $R = 2$, can be written as

$$w_d = M(\phi_0^T \phi_T) + g(\phi_0^T \phi_T \phi_T) + \phi_0^S (g_1 \phi_S \phi_S + g_2 \phi_S \xi + g_3 \phi_S \xi') + \xi_0 (g_4 \phi_S \phi_S + g_5 \xi \xi). \quad (A.1)$$

Equations which give vacuum structure of ϕ_T are given by:

$$\begin{aligned}
\frac{\partial w}{\partial \phi_{01}^T} &= M\phi_{T1} + \frac{2g}{3}\left(\phi_{T1}^2 - \phi_{T2}\phi_{T3}\right) = 0, \\
\frac{\partial w}{\partial \phi_{02}^T} &= M\phi_{T1} + \frac{2g}{3}\left(\phi_{T2}^2 - \phi_{T1}\phi_{T3}\right) = 0, \\
\frac{\partial w}{\partial \phi_{03}^T} &= M\phi_{T1} + \frac{2g}{3}\left(\phi_{T3}^2 - \phi_{T1}\phi_{T2}\right) = 0. \qquad (A.2)
\end{aligned}$$

Solution of these equations can be given by: $\langle \phi_T \rangle = (v_T, 0, 0)$ where $v_T = -\frac{3M}{2g}$. Again, equations responsible for vacuum alignments of ϕ_S, ξ and ξ' are:

$$\frac{\partial w}{\partial \phi_{01}^S} = \frac{2g_1}{3}\left(\phi_{S1}^2 - \phi_{S2}\phi_{S3}\right) + g_2 \xi \phi_{S1} + g_3 \xi' \phi_{S3} = 0$$

$$\frac{\partial w}{\partial \phi^S_{02}} = \frac{2g_1}{3}\left(\phi^2_{S2} - \phi_{S1}\phi_{S3}\right) + g_2\xi\phi_{S3} + g_3\xi'\phi_{S2} = 0$$

$$\frac{\partial w}{\partial \phi^S_{03}} = \frac{2g_1}{3}\left(\phi^2_{S3} - \phi_{S1}\phi_{S2}\right) + g_2\xi\phi_{S2} + g_3\xi'\phi_{S1} = 0$$

$$\frac{\partial w}{\partial \xi_0} = g_4(\phi^2_{S1} + 2\phi_{S2}\phi_{S3}) + g_5\xi\xi = 0 \tag{A.3}$$

From these equations we obtain $\langle\phi_S\rangle = (v_S, v_S, v_S), \langle\xi\rangle = u$ and $\langle\xi'\rangle = u' \neq 0$ with $v_s^2 = \frac{-g_5 u^2}{3g_4}$ and $u' = \frac{-g_2 u}{g_3}$. Note that NLO correction terms with $1/\Lambda$ suppression involving ξ' in the superpotential w_d are absent and so the vevs of the flavon fields remain unchanged.

Appendix B

Vacuum Alignments in Chapter 3:

The most general renormalizable potential involving all the flavons of our set-up which is invariant under $A_4 \times Z_4 \times Z_3$ and respecting $U(1)_{B-L}$ can be written as

$$V = V(H)+V(\phi_S)+V(\phi_T)+V(\xi)+V(\xi')+V(\rho)+V(H,\phi_S,\phi_T,\xi,\xi',\rho)+V(\phi_S,\phi_T,\xi,\xi',\rho)$$

where

$$V(H) = \mu_H^2 H^\dagger H + \lambda_H (H^\dagger H)(H^\dagger H) \tag{B.1}$$

$$\begin{aligned} V(\phi_S) = {} & \mu_S^2 ({\phi_S}^\dagger \phi_S)_1 + \lambda_1^S ({\phi_S}^\dagger \phi_S)_1 ({\phi_S}^\dagger \phi_S)_1 + \lambda_2^S ({\phi_S}^\dagger \phi_S)_{1'} ({\phi_S}^\dagger \phi_S)_{1''} \\ & \lambda_3^S ({\phi_S}^\dagger \phi_S)_{3S} ({\phi_S}^\dagger \phi_S)_{3S} + \lambda_4^S ({\phi_S}^\dagger \phi_S)_{3A} ({\phi_S}^\dagger \phi_S)_{3A} \\ & +\lambda_5^S ({\phi_S}^\dagger \phi_S)_{3S} ({\phi_S}^\dagger \phi_S)_{3A} \end{aligned} \tag{B.2}$$

$$\begin{aligned} V(\phi_T) = {} & \mu_T^2 ({\phi_T}^\dagger \phi_T)_1 + \lambda_T^1 ({\phi_T}^\dagger \phi_T)_1 ({\phi_T}^\dagger \phi_T)_1 + \lambda_T^2 ({\phi_T}^\dagger \phi_T)_{1'} ({\phi_T}^\dagger \phi_T)_{1''} \\ & +\lambda_T^3 ({\phi_T}^\dagger \phi_T)_{3S} ({\phi_T}^\dagger \phi_T)_{3S} + \lambda_T^4 ({\phi_T}^\dagger \phi_T)_{3A} ({\phi_T}^\dagger \phi_T)_{3A} \\ & +\lambda_T^4 ({\phi_T}^\dagger \phi_T)_{3S} ({\phi_T}^\dagger \phi_T)_{3A} \end{aligned} \tag{B.3}$$

$$V(\xi) = \mu_\xi^2 \xi^\dagger \xi + \lambda_\xi (\xi^\dagger \xi)(\xi^\dagger \xi) \tag{B.4}$$

$$V(\xi') = \mu_{\xi'}^2 {\xi'}^\dagger \xi' + \lambda_{\xi'} ({\xi'}^\dagger \xi')({\xi'}^\dagger \xi') \tag{B.5}$$

$$V(\rho) = \mu_\rho^2 \rho^\dagger \rho + \lambda_\rho (\rho^\dagger \rho)(\rho^\dagger \rho) \tag{B.6}$$

$$\begin{aligned} V(H,\phi_S,\phi_T,\xi,\xi',\rho) = {} & \lambda_{HS} (H^\dagger H)({\phi_S}^\dagger \phi_S)_1 + \lambda_{HT} (H^\dagger H)({\phi_T}^\dagger \phi_T)_1 \\ & +\lambda_{H\xi} (H^\dagger H)(\xi^\dagger \xi) + \lambda_{H\rho} (H^\dagger H)(\rho^\dagger \rho) + \lambda_{H\xi'} (H^\dagger H)({\xi'}^\dagger \xi') \end{aligned} \tag{B.7}$$

$$
\begin{aligned}
V(\phi_S,\phi_T,\xi,\xi',\rho) \;=\;& k_{11}(\phi_T\phi_T)_{3S}\phi_T + k_{12}(\phi_T\phi_T)_{3A}\phi_T + k_{31}(\phi_S^\dagger\phi_S)_{3S}\phi_T + k_{32}(\phi_S^\dagger\phi_S)_{3A}\phi_T \\
&+k_4(\phi_S\phi_T)_1\xi^\dagger + k_5(\phi_S\phi_T)_{1'}\xi'^\dagger + k_6(\phi_S^\dagger\phi_T)_1\xi + k_7(\phi_S^\dagger\phi_T)_{1''}\xi' \\
&+k_8(\phi_S\phi_T^\dagger)_1\xi^\dagger + k_9(\phi_S\phi_T^\dagger)_{1'}\xi'^\dagger + k_{10}(\phi_S^\dagger\phi_T^\dagger)_1\xi + k'_{10}(\phi_S^\dagger\phi_T^\dagger)_{1''}\xi' \\
&+\lambda^1_{ST}({\phi_S}^\dagger\phi_S)_1({\phi_T}^\dagger\phi_T)_1 + \lambda^2_{ST}({\phi_S}^\dagger\phi_S)_{1'}({\phi_T}^\dagger\phi_T)_{1''} \\
&+\lambda^{22}_{ST}({\phi_S}^\dagger\phi_S)_{1''}({\phi_T}^\dagger\phi_T)_{1'} + \lambda^3_{ST}({\phi_S}^\dagger\phi_S)_{3S}({\phi_T}^\dagger\phi_T)_{3S} \\
&+\lambda^4_{ST}({\phi_S}^\dagger\phi_S)_{3A}({\phi_T}^\dagger\phi_T)_{3A} + \lambda^5_{ST}({\phi_S}^\dagger\phi_S)_{3S}({\phi_T}^\dagger\phi_T)_{3A} \\
&+\lambda^6_{ST}({\phi_S}^\dagger\phi_S)_{3A}({\phi_T}^\dagger\phi_T)_{3S} + \lambda'^1_{ST}({\phi_S}^\dagger\phi_T)_1({\phi_T}^\dagger\phi_S)_1 \\
&+\lambda'^2_{ST}({\phi_S}^\dagger\phi_T)_{1'}({\phi_T}^\dagger\phi_S)_{1''} + \lambda'^{22}_{ST}({\phi_S}^\dagger\phi_T)_{1''}({\phi_T}^\dagger\phi_S)_{1'} \\
&+\lambda'^3_{ST}({\phi_S}^\dagger\phi_T)_{3S}({\phi_T}^\dagger\phi_S)_{3S} + \lambda'^4_{ST}({\phi_S}^\dagger\phi_T)_{3A}({\phi_T}^\dagger\phi_S)_{3A} \\
&+\lambda'^5_{ST}({\phi_S}^\dagger\phi_T)_{3S}({\phi_T}^\dagger\phi_S)_{3A} + \lambda'^6_{ST}({\phi_S}^\dagger\phi_T)_{3A}({\phi_T}^\dagger\phi_S)_{3S} \\
&+\lambda_{S\xi}({\phi_S}^\dagger\phi_S)_1(\xi^\dagger\xi) + \lambda'_{S\xi}({\phi_S}^\dagger\xi)(\xi^\dagger\phi_S) \\
&+\lambda_{S\xi'}({\phi_S}^\dagger\phi_S)_1({\xi'}^\dagger\xi')_1 + \lambda'_{S\xi'}({\phi_S}^\dagger\xi')({\xi'}^\dagger\phi_S) \\
&+\lambda_{S\rho}({\phi_S}^\dagger\phi_S)_1(\rho^\dagger\rho) + \lambda'_{S\rho}({\phi_S}^\dagger\rho)(\rho^\dagger\phi_S) \\
&+\lambda_{T\xi}({\phi_T}^\dagger\phi_T)_1(\xi^\dagger\xi) + \lambda'_{T\xi}({\phi_T}^\dagger\xi)(\xi^\dagger\phi_T) \\
&+\lambda_{T\xi'}({\phi_T}^\dagger\phi_T)_1({\xi'}^\dagger\xi')_1 + \lambda'_{T\xi'}({\phi_T}^\dagger\xi')({\xi'}^\dagger\phi_T) \\
&+\lambda_{T\rho}({\phi_T}^\dagger\phi_T)_1(\rho^\dagger\rho) + \lambda'_{T\rho}({\phi_T}^\dagger\rho)(\rho^\dagger\phi_T) \\
&+\lambda_{\xi\rho}(\xi^\dagger\xi)(\rho^\dagger\rho) + \lambda'_{\xi\rho}(\xi^\dagger\rho)(\rho^\dagger\xi) + \lambda_{\xi\xi'}(\xi\xi^\dagger)_1(\xi'\xi'^\dagger)_1 \\
&+\lambda_{\xi'\rho}(\xi'\xi'^\dagger)(\rho^\dagger\rho) + \lambda'_{\xi'\rho}(\xi'\rho^\dagger)({\xi'}^\dagger\rho) \\
&+\lambda_{S\xi\xi'}({\phi_S}^\dagger\phi_S)_{1''}(\xi^\dagger\xi')_{1'} + \lambda_{T\xi\xi'}({\phi_T}^\dagger\phi_T)_{1''}(\xi^\dagger\xi')_{1'} \\
&+\lambda^2_{S\xi\xi'}({\phi_S}^\dagger\phi_S)_{1'}(\xi\xi'^\dagger)_{1''} + \lambda^2_{T\xi\xi'}({\phi_T}^\dagger\phi_T)_{1'}(\xi\xi'^\dagger)_{1''} \\
&+\lambda^1_{SS\xi}({\phi_S}^\dagger\phi_S)_{3S}(\phi_S\xi^\dagger) + \lambda^2_{SS\xi}({\phi_S}^\dagger\phi_S)_{3A}(\phi_S\xi^\dagger) \\
&+\lambda^1_{SS\xi'}({\phi_S}^\dagger\phi_S)_{3S}(\phi_S\xi'^\dagger) + \lambda^2_{SS\xi'}({\phi_S}^\dagger\phi_S)_{3A}(\phi_S\xi'^\dagger) \\
&+\lambda^1_{TS\xi}({\phi_T}^\dagger\phi_T)_{3S}(\phi_S\xi^\dagger) + \lambda^2_{TS\xi}({\phi_T}^\dagger\phi_T)_{3A}(\phi_S\xi^\dagger) \\
&+\lambda^1_{TS\xi'}({\phi_T}^\dagger\phi_T)_{3S}(\phi_S\xi'^\dagger) + \lambda^2_{TS\xi'}({\phi_T}^\dagger\phi_T)_{3A}(\phi_S\xi'^\dagger) \\
&+\lambda^{11}_{SS\xi}({\phi_S}^\dagger\phi_S)_{3S}({\phi_S}^\dagger\xi) + \lambda^{22}_{SS\xi}({\phi_S}^\dagger\phi_S)_{3A}({\phi_S}^\dagger\xi) \\
&+\lambda^{11}_{SS\xi'}({\phi_S}^\dagger\phi_S)_{3S}({\phi_S}^\dagger\xi') + \lambda^{22}_{SS\xi'}({\phi_S}^\dagger\phi_S)_{3A}({\phi_S}^\dagger\xi') \\
&+\lambda^{11}_{TS\xi}({\phi_T}^\dagger\phi_T)_{3S}({\phi_S}^\dagger\xi) + \lambda^{22}_{TS\xi}({\phi_T}^\dagger\phi_T)_{3A}({\phi_S}^\dagger\xi) \\
&+\lambda^{11}_{TS\xi'}({\phi_T}^\dagger\phi_T)_{3S}({\phi_S}^\dagger\xi') + \lambda^{22}_{TS\xi'}({\phi_T}^\dagger\phi_T)_{3A}({\phi_S}^\dagger\xi'). \qquad \text{(B.8)}
\end{aligned}
$$

Here the explicit multiplication of A_4 are taken into account. In general this potential involves several free parameters. These plenty free parameters should naturally allow therefore the required vev alignment of the flavons we considered, $\langle\phi_S\rangle = v_S(1,1,1)$, $\langle\phi_T\rangle = v_T(1,0,0)$, $\langle\xi\rangle = v_\xi$, $\langle\xi'\rangle = v_{\xi'}$, $\langle\rho\rangle = v_\rho$. For example, with a particular choice like the followings[1]

$$\begin{aligned}
[3\lambda_{HS}v^2 + 3\lambda_{HT}v^2 + \lambda_{H\xi}v^2 + \lambda_{H\xi'}v^2 + \lambda_{H\rho}v^2 - 3\mu_S^2 - 3\mu_T^2 - \mu_\xi^2 - \mu_{\xi'}^2 - \mu_\rho^2] \sim 1\ \text{GeV}^2 \\
[2k_{11} + k_4 + k_5 + k_6 + k_7 + k_8 + k_9 + k_{10} + k'_{10}] \sim -\,1\ \text{GeV} \\
\big[9(\lambda_1^S + \lambda_2^S) + (3\lambda_{ST}^1 + \lambda_{ST}^{22} + \lambda_{ST}^{\prime 1} + \lambda_{ST}^{\prime 2} + \lambda_{ST}^{\prime 22} + 6\lambda_{ST}^{\prime 3} + 2\lambda_{ST}^{\prime 4}) + \\
(3\lambda_{S\xi} + 3\lambda'_{S\xi}) + (3\lambda_{S\xi'} + 3\lambda'_{S\xi'}) + (9\lambda_1^T + 4\lambda_3^T) + (3\lambda_{S\rho} + 3\lambda'_{S\rho}) \\
(\lambda_{\xi\rho} + \lambda'_{\xi\rho}) + \lambda_\rho + (\lambda_{T\xi'} + \lambda'_{T\xi'}) + (\lambda_{\xi'\rho} + \lambda'_{\xi'\rho}) + 2\lambda_{TS\xi}^{11} + 3\lambda_{S\xi\xi'}^2\big] \sim\ 0.00075\,.
\end{aligned}$$

can actually lead to a common vev $v_S = v_T = v_\xi = v_{\xi'} = v_\rho \sim 1$ TeV along the required direction.

---

[1] Along the specified vev directions, terms involving the couplings $\lambda_{3,4,5}^S$, $\lambda_{2,4,5}^T$, $k_{12,31,32}$ λ_{ST}^2, λ_{ST}^{22}, λ_{ST}^3, λ_{ST}^4, λ_{ST}^5, λ_{ST}^6, $\lambda_{ST}^{\prime 5}$, $\lambda_{ST}^{\prime 6}$, $\lambda'_{T\xi'}$,$\lambda_{T\xi\xi'}$, $\lambda_{T\xi\xi'}^2$, $\lambda_{SS\xi}^1$, $\lambda_{SS\xi}^2$, $\lambda_{SS\xi'}^1$, $\lambda_{SS\xi'}^2$, $\lambda_{TS\xi}^2$, $\lambda_{TS\xi'}^1$, $\lambda_{TS\xi'}^2$ $\lambda_{SS\xi}^{11}$, $\lambda_{SS\xi}^{22}$, $\lambda_{SS\xi'}^{11}$, $\lambda_{SS\xi'}^{22}$, $\lambda_{TS\xi}^{22}$, $\lambda_{TS\xi'}^{11}$ and $\lambda_{TS\xi'}^{22}$ do not contribute.

Bibliography

[1] G. Aad *et al.* [ATLAS Collaboration], Phys. Lett. B **716**, 1 (2012) [arXiv:1207.7214 [hep-ex]].

[2] S. Chatrchyan *et al.* [CMS Collaboration], Phys. Lett. B **716**, 30 (2012) [arXiv:1207.7235 [hep-ex]].

[3] S. Fukuda *et al.* [Super-Kamiokande Collaboration], Phys. Lett. B **539**, 179 (2002) [hep-ex/0205075]; P. Adamson *et al.* [MINOS Collaboration], Phys. Rev. Lett. **106**, 181801 (2011) [arXiv:1103.0340 [hep-ex]]; T. Araki *et al.* [KamLAND Collaboration], Phys. Rev. Lett. **94**, 081801 (2005) [hep-ex/0406035].

[4] K. A. Olive *et al.* [Particle Data Group Collaboration], Chin. Phys. C **38**, 090001 (2014).

[5] D. V. Forero, M. Tortola and J. W. F. Valle, Phys. Rev. D **90**, no. 9, 093006 (2014) [arXiv:1405.7540 [hep-ph]].

[6] P. F. Harrison, D. H. Perkins and W. G. Scott, Phys. Lett. B **458**, 79 (1999) [hep-ph/9904297].

[7] G. Altarelli and F. Feruglio, Nucl. Phys. B **741**, 215 (2006) [hep-ph/0512103].

[8] R. N. Mohapatra and A. Y. Smirnov, Ann. Rev. Nucl. Part. Sci. **56**, 569 (2006) [hep-ph/0603118].

[9] T. Schwetz, M. A. Tortola and J. W. F. Valle, New J. Phys. **10**, 113011 (2008) [arXiv:0808.2016 [hep-ph]].

[10] M. Fukugita and T. Yanagida, Phys. Lett. B **174**, 45 (1986).

[11] For a review, see S. Davidson, E. Nardi and Y. Nir, Phys. Rept. **466**, 105 (2008) [arXiv:0802.2962 [hep-ph]].

[12] P. A. R. Ade *et al.* [Planck Collaboration], arXiv:1303.5076 [astro-ph.CO].

[13] N. Cabibbo, Phys. Rev. Lett. **10**, 531 (1963).

[14] M. Kobayashi and T. Maskawa, Prog. Theor. Phys. **49**, 652 (1973).

[15] L. L. Chau and W. Y. Keung, Phys. Rev. Lett. **53**, 1802 (1984).

[16] Z. Maki, M. Nakagawa and S. Sakata, Prog. Theor. Phys. **28**, 870 (1962).

[17] C. Kraus *et al.*, Eur. Phys. J. C **40**, 447 (2005) [hep-ex/0412056].

[18] V. M. Lobashev *et al.*, Phys. Lett. B **460**, 227 (1999).

[19] K. Eitel, Nucl. Phys. Proc. Suppl. **143**, 197 (2005).

[20] Image taken from: *https://cuore.lngs.infn.it/en/about/physics*

[21] F. T. Avignone, III, S. R. Elliott and J. Engel, Rev. Mod. Phys. **80**, 481 (2008) [arXiv:0708.1033 [nucl-ex]].

[22] K. Asakura *et al.* [KamLAND-Zen Collaboration], AIP Conf. Proc. **1666**, 170003 (2015) [arXiv:1409.0077 [physics.ins-det]].

[23] J. B. Albert *et al.* [EXO-200 Collaboration], Nature **510**, 229 (2014) [arXiv:1402.6956 [nucl-ex]].

[24] S. Weinberg, Phys. Rev. Lett. **43**, 1566 (1979).

[25] A. Zee, Phys. Lett. **93B**, 389 (1980) Erratum: [Phys. Lett. **95B**, 461 (1980)].

[26] T. P. Cheng and L. F. Li, Phys. Rev. D **22**, 2860 (1980).

[27] S. T. Petcov, Phys. Lett. **115B**, 401 (1982).

[28] K. S. Babu, Phys. Lett. B **203**, 132 (1988).

[29] L. J. Hall and M. Suzuki, Nucl. Phys. B **231**, 419 (1984).

[30] Y. Grossman and H. E. Haber, Phys. Rev. Lett. **78**, 3438 (1997) [hep-ph/9702421].

[31] N. Arkani-Hamed, S. Dimopoulos and G. R. Dvali, Phys. Lett. B **429**, 263 (1998) [hep-ph/9803315].

[32] K. R. Dienes, E. Dudas and T. Gherghetta, Nucl. Phys. B **557**, 25 (1999) [hep-ph/9811428].

[33] R. N. Mohapatra and J. W. F. Valle, Phys. Rev. D **34**, 1642 (1986).

[34] P. Minkowski, Phys. Lett. B **67**, 421 (1977).

[35] M. Gell-Mann, P. Ramond and R. Slansky, Conf. Proc. C **790927**, 315 (1979) [arXiv:1306.4669 [hep-th]].

[36] R. N. Mohapatra and G. Senjanovic, Phys. Rev. Lett. **44**, 912 (1980).

[37] T. Yanagida, Prog. Theor. Phys. **64**, 1103 (1980).

[38] J. Schechter and J. W. F. Valle, Phys. Rev. D **25**, 774 (1982).

[39] K. S. Babu and R. N. Mohapatra, Phys. Rev. Lett. **70**, 2845 (1993) [hep-ph/9209215].

[40] M. Magg and C. Wetterich, Phys. Lett. B **94**, 61 (1980).

[41] G. Lazarides, Q. Shafi and C. Wetterich, Nucl. Phys. B **181**, 287 (1981).

[42] R. N. Mohapatra and G. Senjanovic, Phys. Rev. D **23**, 165 (1981).

[43] J. Schechter and J. W. F. Valle, Phys. Rev. D **22**, 2227 (1980).

[44] R. Foot, H. Lew, X. G. He and G. C. Joshi, Z. Phys. C **44**, 441 (1989).

[45] R. N. Mohapatra, Phys. Rev. Lett. **56**, 561 (1986).

[46] M. C. Gonzalez-Garcia and J. W. F. Valle, Phys. Lett. B **216**, 360 (1989).

[47] G. 't Hooft, NATO Sci. Ser. B **59**, 135 (1980).

[48] L. M. Brown, Phys. Today **31N9**, 23 (1978).

[49] E. Fermi, Nuovo Cim. **11**, 1 (1934).

[50] C. L. Cowan, F. Reines, F. B. Harrison, H. W. Kruse and A. D. McGuire, Science **124**, 103 (1956).

[51] G. Danby, J. M. Gaillard, K. A. Goulianos, L. M. Lederman, N. B. Mistry, M. Schwartz and J. Steinberger, Phys. Rev. Lett. **9**, 36 (1962).

[52] T. Patzak [DONUT Collaboration], Europhys. News **32**, 56 (2001).

[53] J. Beringer *et al.* [Particle Data Group Collaboration], Phys. Rev. D **86**, 010001 (2012).

[54] H. A. Bethe, Phys. Rev. **55**, 434 (1939).

[55] R. Davis, Jr., D. S. Harmer and K. C. Hoffman, Phys. Rev. Lett. **20**, 1205 (1968).

[56] J. N. Bahcall, N. A. Bahcall and G. Shaviv, Phys. Rev. Lett. **20**, 1209 (1968).

[57] K. S. Hirata *et al.* [Kamiokande-II Collaboration], Phys. Lett. B **205**, 416 (1988).

[58] R. Becker-Szendy *et al.*, Phys. Rev. D **46**, 3720 (1992).

[59] B. Pontecorvo, Sov. Phys. JETP **26**, 984 (1968) [Zh. Eksp. Teor. Fiz. **53**, 1717 (1967)].

[60] P. Anselmann *et al.* [GALLEX Collaboration], Phys. Lett. B **327**, 377 (1994).

[61] J. N. Abdurashitov *et al.* [SAGE Collaboration], Phys. Rev. C **60**, 055801 (1999) [astro-ph/9907113].

[62] Q. R. Ahmad *et al.* [SNO Collaboration], Phys. Rev. Lett. **87**, 071301 (2001) [nucl-ex/0106015].

[63] S. Fukuda *et al.* [Super-Kamiokande Collaboration], Phys. Rev. Lett. **86**, 5651 (2001) [hep-ex/0103032].

[64] K. Eguchi *et al.* [KamLAND Collaboration], Phys. Rev. Lett. **90**, 021802 (2003) [hep-ex/0212021].

[65] M. H. Ahn *et al.* [K2K Collaboration], Phys. Rev. Lett. **90**, 041801 (2003) [hep-ex/0212007].

[66] D. G. Michael *et al.* [MINOS Collaboration], Phys. Rev. Lett. **97**, 191801 (2006) [hep-ex/0607088].

[67] K. Abe *et al.* [T2K Collaboration], Phys. Rev. Lett. **107**, 041801 (2011) [arXiv:1106.2822 [hep-ex]].

[68] A. de Gouvea, J. Jenkins and B. Kayser, Phys. Rev. D **71**, 113009 (2005) [hep-ph/0503079].

[69] Y. Fukuda *et al.* [Super-Kamiokande Collaboration], Phys. Rev. Lett. **81**, 1562 (1998) [hep-ex/9807003].

[70] M. Apollonio *et al.* [CHOOZ Collaboration], Phys. Lett. B **420**, 397 (1998) [hep-ex/9711002].

[71] M. Apollonio *et al.* [CHOOZ Collaboration], Phys. Lett. B **466**, 415 (1999) [hep-ex/9907037].

[72] M. Apollonio *et al.* [CHOOZ Collaboration], Eur. Phys. J. C **27**, 331 (2003) [hep-ex/0301017].

[73] F. Boehm *et al.*, Phys. Rev. D **64**, 112001 (2001) [hep-ex/0107009].

[74] Y. Abe *et al.* [Double Chooz Collaboration], Phys. Rev. D **86**, 052008 (2012) [arXiv:1207.6632 [hep-ex]].

[75] Y. Abe *et al.* [Double Chooz Collaboration], Phys. Rev. Lett. **108**, 131801 (2012) [arXiv:1112.6353 [hep-ex]].

[76] F. P. An *et al.* [Daya Bay Collaboration], Phys. Rev. Lett. **108**, 171803 (2012) [arXiv:1203.1669 [hep-ex]].

[77] F. P. An *et al.* [Daya Bay Collaboration], Chin. Phys. C **37**, 011001 (2013) [arXiv:1210.6327 [hep-ex]].

[78] J. K. Ahn *et al.* [RENO Collaboration], Phys. Rev. Lett. **108**, 191802 (2012) [arXiv:1204.0626 [hep-ex]].

[79] M. C. Gonzalez-Garcia, M. Maltoni and T. Schwetz, JHEP **1411**, 052 (2014) [arXiv:1409.5439 [hep-ph]].

[80] F. Capozzi, G. L. Fogli, E. Lisi, A. Marrone, D. Montanino and A. Palazzo, Phys. Rev. D **89**, no. 9, 093018 (2014) [arXiv:1312.2878 [hep-ph]].

[81] K. Abe *et al.* [T2K Collaboration], Phys. Rev. Lett. **112**, 061802 (2014) [arXiv:1311.4750 [hep-ex]].

[82] C. D. Froggatt and H. B. Nielsen, Nucl. Phys. B **147**, 277 (1979).

[83] H. Ishimori, T. Kobayashi, H. Ohki, Y. Shimizu, H. Okada and M. Tanimoto, Prog. Theor. Phys. Suppl. **183**, 1 (2010) [arXiv:1003.3552 [hep-th]].

[84] G. Altarelli, F. Feruglio and Y. Lin, Nucl. Phys. B **775**, 31 (2007) [hep-ph/0610165].

[85] A. Adulpravitchai, A. Blum and M. Lindner, JHEP **0907**, 053 (2009) [arXiv:0906.0468 [hep-ph]].

[86] T. Kobayashi, S. Raby and R. J. Zhang, Nucl. Phys. B **704**, 3 (2005) [hep-ph/0409098].

[87] T. Kobayashi, H. P. Nilles, F. Ploger, S. Raby and M. Ratz, Nucl. Phys. B **768**, 135 (2007) [hep-ph/0611020].

[88] P. Ko, T. Kobayashi, J. h. Park and S. Raby, Phys. Rev. D **76**, 035005 (2007) Erratum: [Phys. Rev. D **76**, 059901 (2007)] [arXiv:0704.2807 [hep-ph]].

[89] H. Abe, K. S. Choi, T. Kobayashi and H. Ohki, Nucl. Phys. B **820**, 317 (2009) [arXiv:0904.2631 [hep-ph]].

[90] H. Abe, K. S. Choi, T. Kobayashi and H. Ohki, Phys. Rev. D **80**, 126006 (2009) [arXiv:0907.5274 [hep-th]].

[91] H. Abe, K. S. Choi, T. Kobayashi and H. Ohki, Phys. Rev. D **81**, 126003 (2010) [arXiv:1001.1788 [hep-th]].

[92] C. L. Bennett *et al.* [WMAP Collaboration], Astrophys. J. Suppl. **208**, 20 (2013) [arXiv:1212.5225 [astro-ph.CO]].

[93] A. D. Sakharov, Pisma Zh. Eksp. Teor. Fiz. **5**, 32 (1967) [JETP Lett. **5**, 24 (1967)] [Sov. Phys. Usp. **34**, 392 (1991)] [Usp. Fiz. Nauk **161**, 61 (1991)].

[94] M. B. Gavela, P. Hernandez, J. Orloff and O. Pene, Mod. Phys. Lett. A **9**, 795 (1994) [hep-ph/9312215].

[95] P. Huet and E. Sather, Phys. Rev. D **51**, 379 (1995) [hep-ph/9404302].

[96] M. Trodden, Rev. Mod. Phys. **71**, 1463 (1999) [hep-ph/9803479].

[97] M. Yoshimura, Phys. Rev. Lett. **41**, 281 (1978) Erratum: [Phys. Rev. Lett. **42**, 746 (1979)].

[98] I. Affleck and M. Dine, Nucl. Phys. B **249**, 361 (1985).

[99] V. A. Rubakov and M. E. Shaposhnikov, Usp. Fiz. Nauk **166**, 493 (1996) [Phys. Usp. **39**, 461 (1996)] [hep-ph/9603208].

[100] A. Riotto and M. Trodden, Ann. Rev. Nucl. Part. Sci. **49**, 35 (1999) [hep-ph/9901362].

[101] G. 't Hooft, Phys. Rev. D **14**, 3432 (1976) Erratum: [Phys. Rev. D **18**, 2199 (1978)].

[102] N. S. Manton, Phys. Rev. D **28**, 2019 (1983).

[103] F. R. Klinkhamer and N. S. Manton, Phys. Rev. D **30**, 2212 (1984).

[104] C. Hagedorn, E. Molinaro and S. T. Petcov, JHEP **0909**, 115 (2009) [arXiv:0908.0240 [hep-ph]].

[105] S. Pascoli, S. T. Petcov and A. Riotto, Phys. Rev. D **75**, 083511 (2007) [hep-ph/0609125].

[106] S. Blanchet, P. Di Bari and G. G. Raffelt, JCAP **0703**, 012 (2007) [hep-ph/0611337].

[107] S. Davidson, J. Garayoa, F. Palorini and N. Rius, JHEP **0809**, 053 (2008) [arXiv:0806.2832 [hep-ph]].

[108] M. Flanz, E. A. Paschos and U. Sarkar, Phys. Lett. B **345**, 248 (1995) [Erratum-ibid. B **382**, 447 (1996)] [hep-ph/9411366].

[109] L. Covi, E. Roulet and F. Vissani, Phys. Lett. B **384**, 169 (1996) [hep-ph/9605319].

[110] M. Plumacher, Z. Phys. C **74**, 549 (1997) [hep-ph/9604229].

[111] W. Buchmuller and M. Plumacher, Phys. Lett. B **431**, 354 (1998) [hep-ph/9710460].

[112] W. Buchmuller, P. Di Bari and M. Plumacher, Annals Phys. **315**, 305 (2005) [hep-ph/0401240].

[113] G. F. Giudice, A. Notari, M. Raidal, A. Riotto and A. Strumia, Nucl. Phys. B **685**, 89 (2004) [hep-ph/0310123].

[114] A. Pilaftsis, Phys. Rev. D **56**, 5431 (1997) [hep-ph/9707235]; A. Pilaftsis and T. E. J. Underwood, Nucl. Phys. B **692**, 303 (2004) [hep-ph/0309342].

[115] T. Hambye and G. Senjanovic, Phys. Lett. B **582**, 73 (2004) [hep-ph/0307237].

[116] T. Hambye, E. Ma and U. Sarkar, Nucl. Phys. B **602**, 23 (2001) [hep-ph/0011192]; Chapter 1

[117] B. Karmakar and A. Sil, Phys. Rev. D **91**, 013004 (2015) [arXiv:1407.5826 [hep-ph]].

[118] S. F. King and C. Luhn, Rept. Prog. Phys. **76**, 056201 (2013) [arXiv:1301.1340 [hep-ph]].

[119] E. Ma, Phys. Rev. D **70**, 031901 (2004) [hep-ph/0404199].

[120] G. Altarelli and F. Feruglio, Nucl. Phys. B **720**, 64 (2005) [hep-ph/0504165].

[121] K. S. Babu, E. Ma and J. W. F. Valle, Phys. Lett. B **552**, 207 (2003) [hep-ph/0206292]; B. Adhikary, B. Brahmachari, A. Ghosal, E. Ma and M. K. Parida, Phys. Lett. B **638**, 345 (2006) [hep-ph/0603059]; M. Honda and M. Tanimoto, Prog. Theor. Phys. **119**, 583 (2008) [arXiv:0801.0181 [hep-ph]].

[122] B. Brahmachari, S. Choubey and M. Mitra, Phys. Rev. D **77**, 073008 (2008) [Erratum-ibid. D **77**, 119901 (2008)] [arXiv:0801.3554 [hep-ph]].

[123] Y. Lin, Nucl. Phys. B **813**, 91 (2009) [arXiv:0804.2867 [hep-ph]]; S. F. King, Phys. Lett. B **675**, 347 (2009) [arXiv:0903.3199 [hep-ph]]; G. C. Branco, R. Gonzalez Felipe, M. N. Rebelo and H. Serodio, Phys. Rev. D **79**, 093008 (2009) [arXiv:0904.3076 [hep-ph]]; Y. Lin, Nucl. Phys. B **824**, 95 (2010) [arXiv:0905.3534 [hep-ph]]; S. Morisi and E. Peinado, Phys. Rev. D **80**, 113011 (2009) [arXiv:0910.4389 [hep-ph]]; Y. H. Ahn and C. -S. Chen, Phys. Rev. D **81**, 105013 (2010) [arXiv:1001.2869 [hep-ph]]; J. Barry and W. Rodejohann, Phys. Rev. D **81**, 093002 (2010) [Erratum-ibid. D **81**, 119901 (2010)] [arXiv:1003.2385 [hep-ph]]; Y. H. Ahn, arXiv:1006.2953 [hep-ph]; I. de Medeiros Varzielas and L. Merlo, JHEP **1102**, 062 (2011) [arXiv:1011.6662 [hep-ph]]; Y. H. Ahn, H. -Y. Cheng and S. Oh, Phys. Rev. D **83**, 076012 (2011) [arXiv:1102.0879 [hep-ph]].

[124] D. Aristizabal Sierra, F. Bazzocchi, I. de Medeiros Varzielas, L. Merlo and S. Morisi, Nucl. Phys. B **827**, 34 (2010) [arXiv:0908.0907 [hep-ph]];

[125] Y. Shimizu, M. Tanimoto and A. Watanabe, Prog. Theor. Phys. **126**, 81 (2011) [arXiv:1105.2929 [hep-ph]].

[126] E. Ma and D. Wegman, Phys. Rev. Lett. **107**, 061803 (2011) [arXiv:1106.4269 [hep-ph]].

[127] S. F. King and C. Luhn, JHEP **1109**, 042 (2011) [arXiv:1107.5332 [hep-ph]].

[128] Y. H. Ahn, H. -Y. Cheng and S. Oh, Phys. Rev. D **84**, 113007 (2011) [arXiv:1107.4549 [hep-ph]]; S. Antusch, S. F. King, C. Luhn and M. Spinrath, Nucl. Phys. B **856**, 328 (2012) [arXiv:1108.4278 [hep-ph]]; G. -J. Ding and D. Meloni, Nucl. Phys. B **855**, 21 (2012) [arXiv:1108.2733 [hep-ph]]; S. F. King and C. Luhn, JHEP **1203**, 036 (2012) [arXiv:1112.1959 [hep-ph]]; Y. H. Ahn and H. Okada, Phys. Rev. D **85**, 073010 (2012) [arXiv:1201.4436 [hep-ph]]; Y. H. Ahn and S. K. Kang, Phys. Rev. D **86**, 093003 (2012) [arXiv:1203.4185 [hep-ph]]; H. Ishimori and E. Ma, Phys. Rev. D **86**, 045030 (2012) [arXiv:1205.0075 [hep-ph]].

[129] G. Altarelli, F. Feruglio, L. Merlo and E. Stamou, JHEP **1208**, 021 (2012) [arXiv:1205.4670 [hep-ph]].

[130] G. Altarelli, F. Feruglio and L. Merlo, Fortsch. Phys. **61**, 507 (2013) [arXiv:1205.5133 [hep-ph]];

[131] E. Ma, A. Natale and A. Rashed, Int. J. Mod. Phys. A **27**, 1250134 (2012) [arXiv:1206.1570 [hep-ph]]; Y. H. Ahn, S. Baek and P. Gondolo, Phys. Rev. D **86**, 053004 (2012) [arXiv:1207.1229 [hep-ph]]; Y. BenTov, X. -G. He and A. Zee, JHEP **1212**, 093 (2012) [arXiv:1208.1062 [hep-ph]]; E. Ma, Phys. Rev. D **86**, 117301 (2012) [arXiv:1209.3374 [hep-ph]]; M. -C. Chen, J. Huang, J. -M. O'Bryan, A. M. Wijangco and F. Yu, JHEP **1302**, 021 (2013) [arXiv:1210.6982 [hep-ph]]; M. Holthausen, M. Lindner and M. A. Schmidt, Phys. Rev. D **87**, no. 3, 033006 (2013) [arXiv:1211.5143 [hep-ph]]; I. de Medeiros Varzielas and D. Pidt, JHEP **1303**, 065 (2013) [arXiv:1211.5370 [hep-ph]]; N. Memenga, W. Rodejohann and H. Zhang, Phys. Rev. D **87**, 053021 (2013) [arXiv:1301.2963 [hep-ph]]; S. Antusch, S. F. King and M. Spinrath, Phys. Rev. D **87**, no. 9, 096018 (2013) [arXiv:1301.6764 [hep-ph]]; S. F. King, S. Morisi, E. Peinado and J. W. F. Valle, Phys. Lett. B **724**, 68 (2013) [arXiv:1301.7065 [hep-ph]]; A. Kadosh, JHEP **1306**, 114 (2013) [arXiv:1303.2645 [hep-ph]]; M. Borah, B. Sharma and M. K. Das,

arXiv:1304.0164 [hep-ph]; Y. H. Ahn, S. K. Kang and C. S. Kim, Phys. Rev. D **87**, no. 11, 113012 (2013) [arXiv:1304.0921 [hep-ph]]; S. F. King, Phys. Lett. B **724**, 92 (2013) [arXiv:1305.4846 [hep-ph]]; S. Antusch, C. Gross, V. Maurer and C. Sluka, Nucl. Phys. B **877**, 772 (2013) [arXiv:1305.6612 [hep-ph]]; S. Morisi, D. V. Forero, J. C. Romo and J. W. F. Valle, Phys. Rev. D **88**, no. 1, 016003 (2013) [arXiv:1305.6774 [hep-ph]]; P. M. Ferreira, L. Lavoura and P. O. Ludl, Phys. Lett. B **726**, 767 (2013) [arXiv:1306.1500 [hep-ph]]; S. Antusch and D. Nolde, JCAP **1310**, 028 (2013) [arXiv:1306.3501 [hep-ph]]; S. Antusch, C. Gross, V. Maurer and C. Sluka, Nucl. Phys. B **879**, 19 (2014) [arXiv:1306.3984 [hep-ph]]; Y. H. Ahn and S. Baek, Phys. Rev. D **88**, no. 3, 036017 (2013) [arXiv:1306.4138 [hep-ph]]; D. Borah, Nucl. Phys. B **876**, 575 (2013) [arXiv:1307.2426]; G. -J. Ding, S. F. King and A. J. Stuart, JHEP **1312**, 006 (2013) [arXiv:1307.4212]; A. E. Carcamo Hernandez, I. de Medeiros Varzielas, S. G. Kovalenko, H. Pas and I. Schmidt, Phys. Rev. D **88**, no. 7, 076014 (2013) [arXiv:1307.6499 [hep-ph]]; Y. Zhao and P. -F. Zhang, arXiv:1402.5834 [hep-ph]; Y. Grossman and W. H. Ng, arXiv:1404.1413 [hep-ph]; D. Aristizabal Sierra and I. de Medeiros Varzielas, JHEP **1407**, 042 (2014) [arXiv:1404.2529 [hep-ph]]; V. V. Vien and H. N. Long, arXiv:1405.4665 [hep-ph].

[132] E. E. Jenkins and A. V. Manohar, Phys. Lett. B **668**, 210 (2008) [arXiv:0807.4176 [hep-ph]].

[133] I. K. Cooper, S. F. King and C. Luhn, Nucl. Phys. B **859**, 159 (2012) [arXiv:1110.5676 [hep-ph]].

[134] G. Altarelli and F. Feruglio, Rev. Mod. Phys. **82**, 2701 (2010) [arXiv:1002.0211 [hep-ph]].

[135] B. Adhikary and A. Ghosal, Phys. Rev. D **78**, 073007 (2008) [arXiv:0803.3582 [hep-ph]]; S. -F. Ge, H. -J. He and F. -R. Yin, JCAP **1005**, 017 (2010) [arXiv:1001.0940 [hep-ph]].

[136] G. Altarelli and D. Meloni, J. Phys. G **36**, 085005 (2009) [arXiv:0905.0620 [hep-ph]].

[137] S. Fukuda *et al.* [Super-Kamiokande Collaboration], Phys. Lett. B **539**, 179 (2002) [hep-ex/0205075]; Y. Ashie *et al.* [Super-Kamiokande Collaboration], Phys. Rev.

D **71**, 112005 (2005) [hep-ex/0501064]. P. Adamson *et al.* [MINOS Collaboration], Phys. Rev. Lett. **106**, 181801 (2011) [arXiv:1103.0340 [hep-ex]]. T. Araki *et al.* [KamLAND Collaboration], Phys. Rev. Lett. **94**, 081801 (2005) [hep-ex/0406035].

[138] S. M. Bilenky, J. Hosek and S. T. Petcov, Phys. Lett. B **94**, 495 (1980); P. Langacker, S. T. Petcov, G. Steigman and S. Toshev, Nucl. Phys. B **282**, 589 (1987).

[139] J. Barry and W. Rodejohann, Nucl. Phys. B **842**, 33 (2011) [arXiv:1007.5217 [hep-ph]]; S. F. King, A. Merle and A. J. Stuart, JHEP **1312**, 005 (2013) [arXiv:1307.2901 [hep-ph]].

[140] S. -F. Ge, D. A. Dicus and W. W. Repko, Phys. Lett. B **702**, 220 (2011) [arXiv:1104.0602 [hep-ph]]; S. -F. Ge, D. A. Dicus and W. W. Repko, Phys. Rev. Lett. **108**, 041801 (2012) [arXiv:1108.0964 [hep-ph]]; D. Hernandez and A. Y. .Smirnov, Phys. Rev. D **86**, 053014 (2012) [arXiv:1204.0445 [hep-ph]].

[141] S. M. Bilenky and C. Giunti, Mod. Phys. Lett. A **27**, 1230015 (2012) [arXiv:1203.5250 [hep-ph]].

[142] Y. Huang and B. -Q. Ma, arXiv:1407.4357 [hep-ph].

[143] J. A. Harvey and M. S. Turner, Phys. Rev. D **42**, 3344 (1990).

[144] G. Engelhard, Y. Grossman and Y. Nir, JHEP **0707**, 029 (2007) [hep-ph/0702151 [HEP-PH]].

[145] G. Engelhard, Y. Grossman, E. Nardi and Y. Nir, Phys. Rev. Lett. **99**, 081802 (2007) [hep-ph/0612187].

[146] S. T. Petcov, S. Profumo, Y. Takanishi and C. E. Yaguna, Nucl. Phys. B **676**, 453 (2004) [hep-ph/0306195].

[147] S. T. Petcov, W. Rodejohann, T. Shindou and Y. Takanishi, Nucl. Phys. B **739**, 208 (2006) [hep-ph/0510404].

[148] A. Djouadi and J. Quevillon, JHEP **1310**, 028 (2013) [arXiv:1304.1787 [hep-ph]].

[149] B. Karmakar and A. Sil, Phys. Rev. D **93**, no. 1, 013006 (2016) [arXiv:1509.07090 [hep-ph]].

[150] J. H. Christenson, J. W. Cronin, V. L. Fitch and R. Turlay, Phys. Rev. Lett. **13**, 138 (1964).

[151] B. Aubert *et al.* [BaBar Collaboration], Phys. Rev. Lett. **86**, 2515 (2001) [hep-ex/0102030].

[152] K. Abe *et al.* [Belle Collaboration], Phys. Rev. Lett. **87**, 091802 (2001) [hep-ex/0107061].

[153] A. S. Joshipura and E. A. Paschos, hep-ph/9906498.

[154] A. S. Joshipura, E. A. Paschos and W. Rodejohann, Nucl. Phys. B **611**, 227 (2001) [hep-ph/0104228].

[155] B. Bajc, G. Senjanovic and F. Vissani, Phys. Rev. Lett. **90**, 051802 (2003) [hep-ph/0210207].

[156] S. Antusch and S. F. King, Nucl. Phys. B **705**, 239 (2005) [hep-ph/0402121].

[157] S. Antusch and S. F. King, Phys. Lett. B **597**, 199 (2004) [hep-ph/0405093].

[158] N. Sahu and S. U. Sankar, Phys. Rev. D **71**, 013006 (2005) [hep-ph/0406065].

[159] W. Rodejohann and Z. z. Xing, Phys. Lett. B **601**, 176 (2004) [hep-ph/0408195].

[160] S. L. Chen, M. Frigerio and E. Ma, Nucl. Phys. B **724**, 423 (2005) [hep-ph/0504181].

[161] S. Bertolini and M. Malinsky, Phys. Rev. D **72**, 055021 (2005) [hep-ph/0504241].

[162] E. K. Akhmedov and M. Frigerio, JHEP **0701**, 043 (2007) [hep-ph/0609046].

[163] W. Rodejohann, Phys. Rev. D **70**, 073010 (2004) [hep-ph/0403236].

[164] P. H. Gu, H. Zhang and S. Zhou, Phys. Rev. D **74**, 076002 (2006) [hep-ph/0606302].

[165] A. Abada, P. Hosteins, F. X. Josse-Michaux and S. Lavignac, Nucl. Phys. B **809**, 183 (2009) [arXiv:0808.2058 [hep-ph]].

[166] D. Borah and M. K. Das, Phys. Rev. D **90**, no. 1, 015006 (2014) [arXiv:1303.1758 [hep-ph]].

[167] D. Borah, Int. J. Mod. Phys. A **29**, 1450108 (2014) [arXiv:1403.7636 [hep-ph]].

[168] M. Borah, D. Borah, M. K. Das and S. Patra, Phys. Rev. D **90**, no. 9, 095020 (2014) [arXiv:1408.3191 [hep-ph]].

[169] R. Kalita, D. Borah and M. K. Das, Nucl. Phys. B **894**, 307 (2015) [arXiv:1412.8333 [hep-ph]].

[170] S. Pramanick and A. Raychaudhuri, arXiv:1508.02330 [hep-ph].

[171] T. D. Lee, Phys. Rev. D **8**, 1226 (1973).

[172] A. E. Nelson, Phys. Lett. B **136**, 387 (1984).

[173] S. M. Barr, Phys. Rev. Lett. **53**, 329 (1984).

[174] J. A. Harvey, P. Ramond and D. B. Reiss, Phys. Lett. B **92**, 309 (1980).

[175] J. A. Harvey, D. B. Reiss and P. Ramond, Nucl. Phys. B **199**, 223 (1982).

[176] G. C. Branco, Phys. Rev. D **22**, 2901 (1980).

[177] L. Bento and G. C. Branco, Phys. Lett. B **245**, 599 (1990).

[178] L. Bento, G. C. Branco and P. A. Parada, Phys. Lett. B **267**, 95 (1991).

[179] G. C. Branco, P. A. Parada and M. N. Rebelo, hep-ph/0307119.

[180] G. C. Branco, R. Gonzalez Felipe, F. R. Joaquim and H. Serodio, Phys. Rev. D **86**, 076008 (2012) [arXiv:1203.2646 [hep-ph]].

[181] G. C. Branco, T. Morozumi, B. M. Nobre and M. N. Rebelo, Nucl. Phys. B **617**, 475 (2001) [hep-ph/0107164].

[182] T. Araki and H. Ishida, PTEP **2014**, no. 1, 013B01 (2014) [arXiv:1211.4452 [hep-ph]].

[183] Y. H. Ahn, S. K. Kang and C. S. Kim, Phys. Rev. D **87**, no. 11, 113012 (2013) [arXiv:1304.0921 [hep-ph]].

[184] J. E. Kim and S. Nam, arXiv:1506.08491 [hep-ph].

[185] Y. Achiman, Phys. Lett. B **599**, 75 (2004) [hep-ph/0403309].

[186] Y. Achiman, Phys. Lett. B **653**, 325 (2007) [hep-ph/0703215].

[187] M. Frank, Phys. Rev. D **70**, 036004 (2004).

[188] M. C. Chen and K. T. Mahanthappa, with spontaneous CP violation," Phys. Rev. D **71**, 035001 (2005) [hep-ph/0411158].

[189] N. Sahu and S. U. Sankar, Nucl. Phys. B **724**, 329 (2005) [hep-ph/0501069].

[190] W. Chao, S. Luo and Z. z. Xing, Phys. Lett. B **659**, 281 (2008) [arXiv:0704.3838 [hep-ph]].

[191] P. J. O'Donnell and U. Sarkar, Phys. Rev. D **49**, 2118 (1994) [hep-ph/9307279].

[192] E. Ma and U. Sarkar, Phys. Rev. Lett. **80**, 5716 (1998) [hep-ph/9802445];

[193] T. Hambye, M. Raidal and A. Strumia, Phys. Lett. B **632**, 667 (2006) [hep-ph/0510008].

[194] G. C. Branco, R. G. Felipe and F. R. Joaquim, Rev. Mod. Phys. **84**, 515 (2012) [arXiv:1111.5332 [hep-ph]].

[195] S. Antusch, Phys. Rev. D **76**, 023512 (2007) [arXiv:0704.1591 [hep-ph]].

[196] E. K. Akhmedov and W. Rodejohann, JHEP **0806**, 106 (2008) [arXiv:0803.2417 [hep-ph]].

[197] D. Aristizabal Sierra and I. de Medeiros Varzielas, Fortsch. Phys. **61**, 645 (2013) [arXiv:1205.6134 [hep-ph]].

[198] D. Aristizabal Sierra, F. Bazzocchi and I. de Medeiros Varzielas, Nucl. Phys. B **858**, 196 (2012) [arXiv:1112.1843 [hep-ph]].

[199] T. Hambye, New J. Phys. **14**, 125014 (2012) [arXiv:1212.2888 [hep-ph]].

[200] D. Aristizabal Sierra, M. Dhen and T. Hambye, JCAP **1408**, 003 (2014) [arXiv:1401.4347 [hep-ph]].

[201] G. Lazarides and Q. Shafi, Phys. Rev. D **58**, 071702 (1998) [hep-ph/9803397].

[202] J. N. Fry, K. A. Olive and M. S. Turner, Phys. Rev. D **22**, 2977 (1980).

[203] E. Ma, S. Sarkar and U. Sarkar, Phys. Lett. B **458**, 73 (1999) [hep-ph/9812276].

[204] T. Hambye, hep-ph/0412053.

[205] T. Hambye, Y. Lin, A. Notari, M. Papucci and A. Strumia, Nucl. Phys. B **695**, 169 (2004) [hep-ph/0312203].

[206] M. Hirsch, S. Morisi and J. W. F. Valle, Phys. Lett. B **679**, 454 (2009) [arXiv:0905.3056 [hep-ph]].

[207] L. Dorame, S. Morisi, E. Peinado, J. W. F. Valle and A. D. Rojas, Phys. Rev. D **86**, 056001 (2012) [arXiv:1203.0155 [hep-ph]].

[208] M. Abbas, S. Khalil, A. Rashed and A. Sil, Phys. Rev. D **93**, no. 1, 013018 (2016) [arXiv:1508.03727 [hep-ph]]; S. Fraser, E. Ma and O. Popov, Phys. Lett. B **737**, 280 (2014) doi:10.1016/j.physletb.2014.08.069 [arXiv:1408.4785 [hep-ph]]; E. Ma and R. Srivastava, Mod. Phys. Lett. A **30**, no. 26, 1530020 (2015) doi:10.1142/S0217732315300207 [arXiv:1504.00111 [hep-ph]]; A. Mukherjee and M. K. Das, Nucl. Phys. B **913**, 643 (2016) doi:10.1016/j.nuclphysb.2016.10.008 [arXiv:1512.02384 [hep-ph]].

[209] M. Lindner, M. A. Schmidt and A. Y. Smirnov, JHEP **0507**, 048 (2005) [hep-ph/0505067].

[210] X. G. He and A. Zee, Phys. Lett. B **645**, 427 (2007) [hep-ph/0607163].

[211] C. H. Albright and W. Rodejohann, Eur. Phys. J. C **62**, 599 (2009) [arXiv:0812.0436 [hep-ph]].

[212] S. Antusch, C. Biggio, E. Fernandez-Martinez, M. B. Gavela and J. Lopez-Pavon, JHEP **0610**, 084 (2006) [hep-ph/0607020].

[213] K. Kanaya, Prog. Theor. Phys. **64**, 2278 (1980).

[214] S. Antusch, J. P. Baumann and E. Fernandez-Martinez, Nucl. Phys. B **810**, 369 (2009) [arXiv:0807.1003 [hep-ph]].

[215] P. S. B. Dev and R. N. Mohapatra, Phys. Rev. D **81**, 013001 (2010) [arXiv:0910.3924 [hep-ph]].

[216] A. G. Dias, C. A. de S.Pires, P. S. Rodrigues da Silva and A. Sampieri, Phys. Rev. D **86**, 035007 (2012) [arXiv:1206.2590].

[217] A. Ilakovac and A. Pilaftsis, Nucl. Phys. B **437**, 491 (1995) [hep-ph/9403398].

[218] R. Alonso, M. Dhen, M. B. Gavela and T. Hambye, JHEP **1301**, 118 (2013) [arXiv:1209.2679 [hep-ph]].

[219] T. Hahn, physics/0607103.

[220] R. Lal Awasthi and M. K. Parida, Phys. Rev. D **86**, 093004 (2012) [arXiv:1112.1826 [hep-ph]].

[221] M. K. Parida, R. L. Awasthi and P. K. Sahu, JHEP **1501**, 045 (2015) [arXiv:1401.1412 [hep-ph]].

[222] M. K. Parida and B. P. Nayak, arXiv:1607.07236 [hep-ph].

[223] S. M. Bilenky, S. T. Petcov and B. Pontecorvo, Phys. Lett. **67B**, 309 (1977).

[224] B. He, T. P. Cheng and L. F. Li, Phys. Lett. B **553**, 277 (2003) [hep-ph/0209175].

[225] D. V. Forero, S. Morisi, M. Tortola and J. W. F. Valle, JHEP **1109**, 142 (2011) [arXiv:1107.6009 [hep-ph]].

[226] L. Delle Rose, C. Marzo and A. Urbano, JHEP **1512**, 050 (2015) [arXiv:1506.03360 [hep-ph]].

[227] C. Bonilla, J. W. F. Valle and J. C. Romo, Phys. Rev. D **91**, no. 11, 113015 (2015) [arXiv:1502.01649 [hep-ph]].

[228] C. Bonilla, R. M. Fonseca and J. W. F. Valle, Phys. Lett. B **756**, 345 (2016) [arXiv:1506.04031 [hep-ph]].

[229] M. Mitra, G. Senjanovic and F. Vissani, Nucl. Phys. B **856**, 26 (2012) [arXiv:1108.0004 [hep-ph]].

[230] J. Chakrabortty, H. Z. Devi, S. Goswami and S. Patra, JHEP **1208**, 008 (2012) [arXiv:1204.2527 [hep-ph]].

[231] A. S. Joshipura and J. W. F. Valle, Nucl. Phys. B **397**, 105 (1993). A. S. Joshipura and S. D. Rindani, Phys. Rev. Lett. **69**, 3269 (1992). J. C. Romao, F. de Campos and J. W. F. Valle, Phys. Lett. B **292**, 329 (1992) [hep-ph/9207269].

[232] V. Tello, M. Nemevsek, F. Nesti, G. Senjanovic and F. Vissani, Phys. Rev. Lett. **106**, 151801 (2011) [arXiv:1011.3522 [hep-ph]].

[233] S. Khan, S. Goswami and S. Roy, Phys. Rev. D **89**, no. 7, 073021 (2014) [arXiv:1212.3694 [hep-ph]].

[234] P. S. Bhupal Dev, R. Franceschini and R. N. Mohapatra, Phys. Rev. D **86**, 093010 (2012) [arXiv:1207.2756 [hep-ph]].

[235] A. Das, P. S. Bhupal Dev and N. Okada, Phys. Lett. B **735**, 364 (2014) [arXiv:1405.0177 [hep-ph]].

[236] A. Borriello and P. Salucci, Mon. Not. Roy. Astron. Soc. **323**, 285 (2001) [astro-ph/0001082].

[237] H. Hoekstra, H. Yee and M. Gladders, New Astron. Rev. **46**, 767 (2002) [astro-ph/0205205].

[238] R. B. Metcalf, L. A. Moustakas, A. J. Bunker and I. R. Parry, Astrophys. J. **607**, 43 (2004) [astro-ph/0309738].

[239] L. A. Moustakas and R. B. Metcalf, Mon. Not. Roy. Astron. Soc. **339**, 607 (2003) [astro-ph/0206176].

[240] D. Clowe, M. Bradac, A. H. Gonzalez, M. Markevitch, S. W. Randall, C. Jones and D. Zaritsky, Astrophys. J. **648**, L109 (2006) [astro-ph/0608407].

[241] P. A. R. Ade *et al.* [Planck Collaboration], Astron. Astrophys. **594**, A13 (2016) [arXiv:1502.01589 [astro-ph.CO]].

[242] G. Steigman and M. S. Turner, Nucl. Phys. B **253**, 375 (1985).

[243] G. Bertone, D. Hooper and J. Silk, Phys. Rept. **405**, 279 (2005) [hep-ph/0404175].

[244] K. Griest and D. Seckel, Phys. Rev. D **43**, 3191 (1991).

[245] R. Cowsik and J. McClelland, Phys. Rev. Lett. **29**, 669 (1972).

[246] J. Kubo, E. Ma and D. Suematsu, Phys. Lett. B **642**, 18 (2006) [hep-ph/0604114].

[247] D. Restrepo, O. Zapata and C. E. Yaguna, JHEP **1311**, 011 (2013) [arXiv:1308.3655 [hep-ph]].

[248] M. Lindner, D. Schmidt and T. Schwetz, Phys. Lett. B **705**, 324 (2011) [arXiv:1105.4626 [hep-ph]].

[249] S. S. C. Law and K. L. McDonald, JHEP **1309**, 092 (2013) [arXiv:1305.6467 [hep-ph]].

[250] N. Okada and O. Seto, Phys. Rev. D **82**, 023507 (2010) [arXiv:1002.2525 [hep-ph]].

[251] S. Fukuda *et al.* [Super-Kamiokande Collaboration], Phys. Lett. B **539**, 179 (2002) [hep-ex/0205075].

[252] Y. Ashie *et al.* [Super-Kamiokande Collaboration], Phys. Rev. D **71**, 112005 (2005) [hep-ex/0501064].

[253] P. Adamson *et al.* [MINOS Collaboration], Phys. Rev. Lett. **106**, 181801 (2011) [arXiv:1103.0340 [hep-ex]].

[254] T. Araki *et al.* [KamLAND Collaboration], Phys. Rev. Lett. **94**, 081801 (2005) [hep-ex/0406035].

[255] G. Hinshaw *et al.* [WMAP Collaboration], Astrophys. J. Suppl. **208**, 19 (2013) [arXiv:1212.5226 [astro-ph.CO]].

[256] P. A. R. Ade *et al.* [Planck Collaboration], Astron. Astrophys. **594**, A13 (2016) doi:10.1051/0004-6361/201525830 [arXiv:1502.01589 [astro-ph.CO]].

[257] G. Bertone, D. Hooper and J. Silk, Phys. Rept. 405, 279 (2005), arXiv:hep-ph/0404175.

[258] S. Bhattacharya, B. Karmakar, N. Sahu and A. Sil, Phys. Rev. D **93**, no. 11, 115041 (2016) [arXiv:1603.04776 [hep-ph]].

[259] S. Bhattacharya, B. Karmakar, N. Sahu and A. Sil, JHEP **1705**, 068 (2017) [arXiv:1611.07419 [hep-ph]].

[260] S. Bhattacharya, N. Sahoo and N. Sahu, Phys. Rev. D **93**, no. 11, 115040 (2016) [arXiv:1510.02760 [hep-ph]].

[261] E. Aprile *et al.* [XENON Collaboration], [arXiv:1512.07501 [physics.ins-det]].

[262] C. Arina, R. N. Mohapatra and N. Sahu, Phys. Lett. B **720** (2013) 130 [arXiv:1211.0435 [hep-ph]].

[263] C. Arina, J. O. Gong and N. Sahu, Nucl. Phys. B **865**, 430 (2012) [arXiv:1206.0009 [hep-ph]].

[264] M. Holthausen, M. Lindner and M. A. Schmidt, Phys. Rev. D **87**, no. 3, 033006 (2013) [arXiv:1211.5143 [hep-ph]].

[265] L. Dorame, S. Morisi, E. Peinado, J. W. F. Valle and A. D. Rojas, Phys. Rev. D **86**, 056001 (2012) [arXiv:1203.0155 [hep-ph]].

[266] B. Karmakar and A. Sil, arXiv:1610.01909 [hep-ph].

[267] L. Calibbi, A. Crivellin and B. Zaldvar, Phys. Rev. D **92**, no. 1, 016004 (2015) [arXiv:1501.07268 [hep-ph]].

[268] M. Hirsch, S. Morisi, E. Peinado and J. W. F. Valle, Phys. Rev. D **82**, 116003 (2010) [arXiv:1007.0871 [hep-ph]].

[269] M. S. Boucenna, M. Hirsch, S. Morisi, E. Peinado, M. Taoso and J. W. F. Valle, JHEP **1105**, 037 (2011) [arXiv:1101.2874 [hep-ph]]

[270] R. de Adelhart Toorop, F. Bazzocchi and S. Morisi, Nucl. Phys. B **856**, 670 (2012) [arXiv:1104.5676 [hep-ph]].

[271] Y. Hamada, T. Kobayashi, A. Ogasahara, Y. Omura, F. Takayama and D. Yasuhara, JHEP **1410**, 183 (2014) [arXiv:1405.3592 [hep-ph]].

[272] W. C. Huang, JHEP **1411**, 083 (2014) [arXiv:1405.5886 [hep-ph]].

[273] M. Lattanzi, R. A. Lineros and M. Taoso, New J. Phys. **16**, no. 12, 125012 (2014) [arXiv:1406.0004 [hep-ph]].

[274] I. de Medeiros Varzielas, O. Fischer and V. Maurer, JHEP **1508**, 080 (2015) [arXiv:1504.03955 [hep-ph]].

[275] E. Ma, Phys. Lett. B **754**, 114 (2016) [arXiv:1506.06658 [hep-ph]].

[276] I. Medeiros Varzielas and O. Fischer, JHEP **1601**, 160 (2016) [arXiv:1512.00869 [hep-ph]].

[277] A. Mukherjee and M. K. Das, Nucl. Phys. B **913**, 643 (2016) [arXiv:1512.02384 [hep-ph]].

[278] J. M. Lamprea and E. Peinado, arXiv:1603.02190 [hep-ph].

[279] K. Griest and D. Seckel, Phys. Rev. **D 43**, 3191 (1991); A. Chatterjee and N. Sahu, Phys. Rev. D **90**, no. 9, 095021 (2014) [arXiv:1407.3030 [hep-ph]].

[280] G. Cynolter and E. Lendvai, Eur. Phys. J. C **58**, 463 (2008) [arXiv:0804.4080 [hep-ph]].

[281] T. Cohen, J. Kearney, A. Pierce and D. Tucker-Smith, Phys. Rev. D **85**, 075003 (2012) [arXiv:1109.2604 [hep-ph]].

[282] C. Cheung and D. Sanford, JCAP **1402**, 011 (2014) [arXiv:1311.5896 [hep-ph]].

[283] G. Belanger, F. Boudjema, A. Pukhov and A. Semenov, Comput. Phys. Commun. **180**, 747 (2009) [arXiv:0803.2360 [hep-ph]].

[284] M. W. Goodman and E. Witten, Phys. Rev. D **31**, 3059 (1985).

[285] R. Essig, Phys. Rev. D **78**, 015004 (2008) [arXiv:0710.1668 [hep-ph]].

[286] R. Koch, Z. Phys. C **15**, 161 (1982),

[287] J. Gasser, H. Leutwyler and M. E. Sainio, Phys. Lett. B **253**, 260 (1991).

[288] M. M. Pavan, I. I. Strakovsky, R. L. Workman and R. A. Arndt, PiN Newslett. **16**, 110 (2002) [hep-ph/0111066].

[289] A. Bottino, F. Donato, N. Fornengo and S. Scopel, Phys. Rev. D **78**, 083520 (2008) [arXiv:0806.4099 [hep-ph]].

[290] D. S. Akerib *et al.*, arXiv:1608.07648 [astro-ph.CO].

[291] K. A. Olive *et al.* [Particle Data Group Collaboration], Chin. Phys. C **38**, 090001 (2014).

[292] A. S. Joshipura and J. W. F. Valle, Nucl. Phys. B **397**, 105 (1993).

[293] G. Aad *et al.* [ATLAS Collaboration], JHEP **1601**, 172 (2016) doi:10.1007/JHEP01(2016)172 [arXiv:1508.07869 [hep-ex]].

[294] V. Khachatryan *et al.* [CMS Collaboration], JHEP **1702**, 135 (2017) doi:10.1007/JHEP02(2017)135 [arXiv:1610.09218 [hep-ex]].

[295] C. P. Burgess, M. Pospelov and T. ter Veldhuis, Nucl. Phys. B **619**, 709 (2001) doi:10.1016/S0550-3213(01)00513-2 [hep-ph/0011335].

[296] M. Frigerio, T. Hambye and E. Masso, Phys. Rev. X **1**, 021026 (2011) doi:10.1103/PhysRevX.1.021026 [arXiv:1107.4564 [hep-ph]].

[297] L. J. Hall, K. Jedamzik, J. March-Russell and S. M. West, JHEP **1003**, 080 (2010) doi:10.1007/JHEP03(2010)080 [arXiv:0911.1120 [hep-ph]].